Abstract

Title of thesis: MECHANICAL DESIGN OF A ROBOTIC ARM EXOSKELETON FOR SHOULDER REHABILITATION

Michael Scott Liszka, Master of Science, 2006

Thesis directed by: Professor David L. Akin
Department of Aerospace Engineering

Traditional shoulder therapy techniques involve the physical therapist controlling and measuring forces on the patient's arm to work particular muscles. The imprecise nature of this leads to inconsistent exercises and inaccurate measurements of patient progress. Some research has shown that robotic devices can be valuable in a physical therapy setting, but most of these mechanisms do not have enough degrees of freedom in the shoulder joint to be useful in shoulder therapy, nor are they able to apply forces along the arm limbs. Based upon the shortcomings of traditional physical therapy robots and low force exoskeletons designed for virtual reality applications, requirements were generated for a robotic arm exoskeleton designed specifically for rehabilitation. Various kinematic designs were explored and compared until a final design emerged. Options for actuation were discussed, and the selection process for actuator components was detailed. Sensors were addressed in their role in the control and safety architecture. A mechanical analysis was performed on the final design to determine various properties, such as torque output,

range of motion, and frequency response. Finally, a list of future work was compiled based on the final design's deficiencies.

MECHANICAL DESIGN OF A ROBOT ARM EXOSKELETON FOR SHOULDER REHABILITATION

by

Michael Scott Liszka

Thesis submitted to the Faculty of the Graduate School of the
University of Maryland, College park in partial fulfillment
of the requirements for the degree of
Master of Science
2006

Advisory Committee:

Professor David L. Akin, Chair
Research Associate Craig R. Carignan
Professor Norman M. Wereley

Acknowledgements

Although my name is on the title page, there are many others whose have made significant contributions to this project. Dave Akin, who is the director of the Space Systems Laboratory (SSL) where this research was performed, has created a wonderful environment that made this research possible. As principle investigator for this project, Craig Carignan provided direction not only for the project as a whole, but also for my thesis. He spent countless hours helping me edit my drafts, and every red mark was greatly appreciated. Brian Roberts and Stephen Roderick gave helpful advice about graduate life at the SSL, and did not hesitate to give me a little external motivation for thesis writing. As the only full-time mechanical engineer in the SSL, Walter Franklin Smith III was a mentor to me. Much of what I know about mechanical design is due in no small part to his guidance. I would also like to recognize the rest of the faculty, staff, and students of the SSL for their continued support whenever it was needed. Lastly, I would like to thank my parents for their constant encouragement and their perpetual belief in me.

Without sponsors, none of this research would have been possible. The MGA exoskeleton project was sponsored through the Georgetown University Imaging Science and Information Systems (ISIS) Center and the U.S. Army Medical Research and Materiel Command (grant number W81XWH-04-1-0078).

Table of Contents

List of Tables

List of Figures

Chapter 1 Introduction

The shoulder is the most mobile joint in the human body. While this joint is normally modeled as a single ball-and-socket connection, in reality it is a complex series of joints packaged in a compact volume. Movement of the clavicle, scapula, and humerus all contribute to the rotation and translation of the shoulder (Figure 1). Due to the complexity and mobility of the shoulder, it is the joint in the upper extremity most prone to injury. While injury to the shoulder girdle can usually be treated with physical therapy, traditional therapy techniques are limited in their ability to control the motion of the shoulder and to accurately measure the joint stresses imposed by exercise.

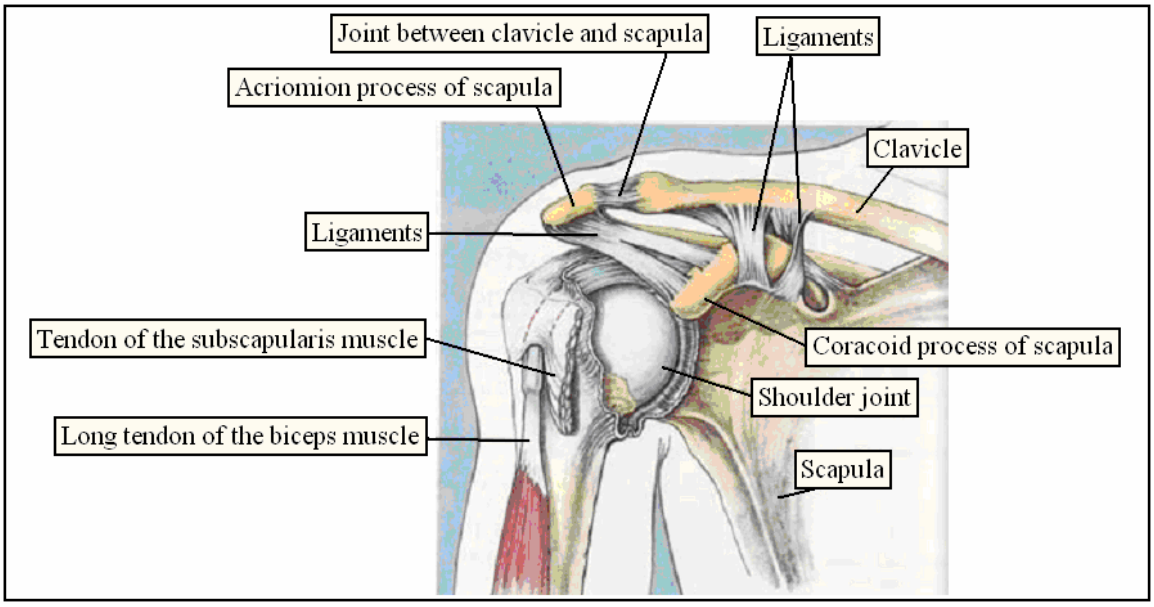

Figure 1: Anatomy of the human shoulder (adapted from [25])

The development and use of robotic manipulators as rehabilitative tools is a relatively new occurrence. While many of these devices have shown the utility of robotics in this setting, they generally lack the ability to exercise the full range of motion of the human arm, thus limiting their usefulness. Robotic arm exoskeletons have many properties well suited for rehabilitation, but have thus far been primarily used as haptic (force) devices for virtual reality (VR) applications. A robotic arm exoskeleton designed specifically for therapy applications could have the range of motion, strength, and sensing capability to be a significant aid in shoulder rehabilitation.

The aim of this project is to develop the mechanical design and produce the physical implementation of a robotic arm exoskeleton that has the capability of assisting a physical therapy patient in shoulder rehabilitation exercises without significantly limiting the scope of the rehabilitation program.

This thesis includes the mechanical design of the robotic manipulator as well as the verification of that design as meeting the initial project requirements. Although software and electronics are an essential component of any robotic device, they will not be discussed here except with regard to their direct impact on the mechanical design. Also, the evaluation of the exoskeleton for its therapeutic capabilities will not be considered.

Chapter 2 will discuss previous work in arm exoskeleton design, in both their capabilities and limitations. Some advantages exoskeletons have over traditional physical therapy techniques will be addressed, along with a review of virtual reality applications of

exoskeletons. Chapter 3 will outline the project requirements, broken down into kinematics, torque and force, control, and safety. Chapter 4 will detail the kinematic design of each of the three joint groups as well as address the adjustability of the exoskeleton. Chapter 5 will cover how motor and transmission components were chosen to satisfy the requirements set forth in Chapter 0. Chapter 6 will go over the selection of components for the sensor and safety system. Chapter 7 will provide a mechanical analysis of the capabilities and mechanical properties of the final design of the exoskeleton. Conclusions and future work will be discussed in Chapter 8.

Chapter 2 Previous Work

Exoskeletons have several advantages over traditional physical therapy techniques and other robotic rehabilitation devices. Unlike other techniques, an exoskeleton envelops the arm and contacts it in several locations. In this way, it can target particular muscles or muscle groups for movement or exercise. Although a physical therapist can do this by choosing an appropriate exercise motion, it can be done to a much higher degree of accuracy with an exoskeleton. The joint angles and contact forces can be precisely measured, and therefore precisely controlled. In addition, the strength of the human patient can be measured via the sensors in the manipulator, allowing for direct measurement of the patient's progress. While most robotic devices can also measure strength and orientation, non-exoskeletons have difficulty reproducing a human's range of motion. In any type of physical therapy, it is important to exercise the entire range of motion so that full functionality is eventually returned to the affected muscles. An exoskeleton's joints are located at the same location as a human's joints, so the range of motion is much more closely matched.

Like any type of exercise, shoulder physical therapy depends on repetition of certain motions. With traditional physical therapy techniques, the therapist is often directly involved in providing assistance or resistance to these motions. Often, a physical therapist will work with several patients simultaneously, which can fatigue the therapist. A robotic

system does not have this limitation whatsoever. While exoskeletons seem very well suited for therapy applications, they have primary been used for virtual reality applications thus far. Since much research has already been done on exoskeletons in this field, it would be valuable to review this information.

2.1 Previous Work in Virtual Reality Applications

Most robotic exoskeletons developed thus far have been for virtual reality (VR) applications. Several arm exoskeletons that have been built to date are listed in Table 1. The table lists the number of joints, power source, mass, and the shoulder type. If the exoskeleton is portable, then the mass of the backpack and exoskeleton are each given. Four different shoulder types appear based upon the sequence of rotations in the shoulder.

In order to simulate contact with virtual objects, these devices need to have a relatively high control bandwidth. In most cases, this constraint led to the use of electric motors to power the arm, although some exoskeletons use hydraulics. While these actuators can be controlled at a high frequency, they generally have a low power-to-weight-ratio. For VR applications, this is not necessarily a problem since contact with a virtual environment does not require full human strength. The only exoskeleton that approaches human strength is the hydraulically powered Sarcos Dextrous Arm Master [16], which was developed as a force-reflecting master arm for teleoperation applications. While it is the strongest exoskeleton built to-date, it is also the heaviest.

Table 1: Arm exoskeleton prototypes

Device	# of DOFs	Power *	Mass (kg) †	Shoulder kinematics ‡
EXOS [6]	5	E	82/1.8	FAR
Dex [16]	7	H	20.9	FAR
Sensor [22]	7	E	6	FAR
GIA [3], [19]	5	E	10	AFR
ATHD [10]	7	E	?/2.3	BSR
MB [27]	7	0	?/15	ZLR
FreFlex [32]	7	E	?	AFR
pMA [31]	7	P	2	FAR
Salford [7]	9	0	?/0.75	AFR
L-EXOS [13]	5	E	11	AFR
ESA [30]	16	E	10	FAR

* E-electric, H-hydraulic, P-pneumatic, 0-unactuated
† Backpack/Arm (from first shoulder joint)
‡ FAR (flexion-abduction-rotation), AFR (abduction, flexion, rotation), ZLR (azimuth-elevation-roll), BSR (ball and socket rotation)

Although the MB Exoskeleton [27] is a passive device, it has many features that are important to an arm exoskeleton intended for rehabilitation. It has a generous range of motion and it has adjustable link lengths to accommodate differently sized people. In addition, it is also lightweight and portable, although much of the reduced weight can be attributed to the lack of motors.

The only exoskeleton developed so far that specifically accommodates translation of the glenohumeral (GH) joint (labeled as "shoulder joint" in Figure 1) is the ESA Exoskeleton [30], being built for the European Space Agency for VR applications. This design has six degrees of freedom in the shoulder, only three of which are active. While this does not

limit motion in the shoulder, neither does it fully actuate it, making it incapable of producing all of the forces necessary for shoulder rehabilitation.

The Motorized Upper Limb Orthotic System (MULOS) [18] was developed as an assistive arm exoskeleton, but not as an exercise machine. Although it does not allow for scapulo-thoracic motion, it does have several features that could be useful in any arm exoskeleton intended for shoulder rehabilitation. Its shoulder kinematics offer a larger usable workspace, and it incorporates a torque limiting device in the actuators to protect the user from spastic motion.

2.2 Current Development in Rehabilitation Robotics

A few arm exoskeletons are being developed as orthotic devices. At the University of Washington [29], an exoskeleton is being designed as a strength amplifier, and it uses processed surface electromyography signals as one of the primary inputs to the control system. Like MULOS, this system does not allow for translation of the GH joint. In addition, its link lengths are not adjustable, due to the nature of its cable driven joints.

A true rehabilitation exoskeleton, RUPERT is being built to help stroke survivors regain the ability to reach and grasp objects [14]. The device is meant to be comfortably worn, so it uses pneumatic muscle actuators to reduce weight. However, using this type of actuation makes it unsuitable for VR applications because the low static stiffness of the actuators significantly decreases the natural frequency of the manipulator. In addition,

RUPERT does not come close to matching the number of degrees of freedom in the human arm, and would therefore be severely limited in its use as a therapeutic device.

Chapter 3 Requirements

Based upon comparison with existing physical therapy devices, along with discussions with physical therapists, a list of requirements and constraints was compiled for this project. These can be broken down into kinematic (geometric), force/torque, control, and safety requirements. Each of these is separately discussed below.

3.1 Kinematics

One of the core features behind this project is the manipulator's kinematics. Not only must it allow the user to move throughout most of the human arm's natural workspace, but it also must allow for scapula movement. The former concern dictates that the manipulator shoulder must have three degrees of freedom (DOFs) to mimic the human shoulder's ball and socket joint. Additionally, there must be one DOF in the elbow. No other actuated DOFs are required because joints distal of the elbow have negligible affect on muscles in the shoulder. However, a passive DOF is desired in the forearm roll so that the user can roll his or her forearm to a comfortable position. Lastly, the desire for scapula movement drove the need for an additional degree of freedom. Although scapula movement is described by more than one DOF, elevation and depression are much more important than protraction and retraction (forward and backward). Another reason to approximate scapula motion as one DOF is to reduce the complexity of the shoulder joint, which already has many DOFs crowded into a small volume. The resulting

exoskeleton therefore has one active DOF in the scapula, three in the shoulder, one in the elbow, and one passive DOF in the forearm.

The arrangement of these degrees of freedom is also very important. As with any serial manipulator, singularities must be considered. A singularity occurs when two rotational axes become aligned and the manipulator temporarily loses a degree of freedom. Most robotic controllers will command joint speeds approaching infinity as the manipulator approaches a singularity because the determinant of the Jacobian approaches zero. Therefore, it is important to avoid these locations in the workspace. For the exoskeleton, singularities cannot be eliminated, but they can be moved. Therefore, the exoskeleton should be designed so that singularities do not occur in the operating workspace.

Although the kinematics allow for full range of motion, joint limits also play a critical role in determining the actual workspace volume. In some cases, it is desired to have a small joint range. An example of this is in the human elbow, where the arm can move from being straight out to making an approximate 40-degree angle between the upper and lower arm. If the actuator paired with this joint has a range beyond the natural range of the arm, then it has the potential of injuring the arm by hyper-extending or hyper-flexing the human elbow. The situation in the shoulder is much less straightforward. Here, three 1-DOF actuators are arranged in such a way as to mimic the 3-DOF ball-and-socket of the natural shoulder. While both setups have three DOFs, they are not mechanically equivalent. Making the manipulator's workspace match the human shoulder's workspace is an exercise in compromise. The glenohumeral joint has a large range of motion,

restricted most significantly by the geometry of the ball and socket and also by the structure of the muscles and tendons surrounding the joint. The manipulator's overall joint range is affected most significantly by the joint configuration and by possible collisions between each of the three 1-DOF actuators and the links connecting the actuators to each other. All of these factors must be considered while attempting to match the exoskeleton's workspace to the human arm workspace.

3.2 Torque and Force

In addition to matching the manipulator's workspace to a human's workspace, another desire is to match the manipulator's strength to the human's strength. In physical therapy of the shoulder, the therapist may try to resist the patient's arm movements as a way of giving the patient some strength training. Naturally, it makes sense for the manipulator to be as strong as the average human. However, mass and control bandwidth constraints indicated that such a requirement would be too ambitious. Thus, the loaded torque capacity (i.e. gravity effects included) of the exoskeleton should be at least half of the unloaded torque capacity (i.e. gravity effects not included) of the average human. Because the manipulator might eventually be mounted on an electric wheelchair, it should also be able to share the same power source: a 24-volt battery (two 12-volt batteries in series). Therefore, 24-volt windings should be used for the motors.

3.3 Control

The control strategy for the exoskeleton requires a certain amount of data feedback. All of the joints angles for both passive and active DOFs must be measured. In addition, the reaction forces between the manipulator and the human must be measured in at least as many degrees of freedom as there are kinematic degrees of freedom within the exoskeleton.

Since the exoskeleton will partly be used as a haptic device, it must possess the control bandwidth to simulate contact with virtual objects. One of the implications of this can be seen in the necessary precision of the joint angle sensors. In order to meet the bandwidth requirement, the joint angles must be measured accurately to within 1.31 milli-degrees. Past experience with the RANGER robotic arm shows that resolution poorer than this will result in substandard operation of the manipulator. As will be discussed in Chapter 0, the need for relatively high control bandwidth also forced the use of electric motors and mechanical transmissions in the actuators over use of other types of motion generation such as pneumatic actuators.

3.4 Safety

One of the drawbacks of traditional methods of shoulder therapy is the inability to precisely gauge progress. This information can be obtained by utilizing the sensors mentioned in the previous section. Data taken from these sensors should show any progress made by the human arm in terms of strength and range of motion. Because these

sensors are the primary input to the controller, safety requirements dictate that they must be single fault redundant. In this way, if two redundant sensors do not agree, then one of them must be giving a false reading. The software can then take the appropriate action, whether it be cutting power to the exoskeleton or just pausing any motion. Without redundancy in the sensors, a malfunctioning sensor cannot be directly detected and could cause undesired function of the manipulator. In addition to redundant sensors, safety also dictates that the PT patient and the device operator should have a method of quickly stopping the manipulator at any given moment.

A significant proportion of the population of patients expected to use this device are those who have suffered a stroke. These individuals have lost a great deal of control of their muscles, and are often subject to spastic motion. If a spastic joint's movement is restricted, then it or its controlling muscles are more likely to be injured. Therefore, as a safety measure, the MGA exoskeleton should have a feature that allows the elbow to flex freely during the event of a muscle spasm. Along the same lines, the exoskeleton should also be simple and quick to doff in case of an emergency. This means that the arm should not be restrained through rigid attachments, but strapped using Velcro ® or other quick release mechanisms.

For reference, Figure 2 shows the degrees of freedom in the human arm, and Table 2 shows a summary of the project requirements.

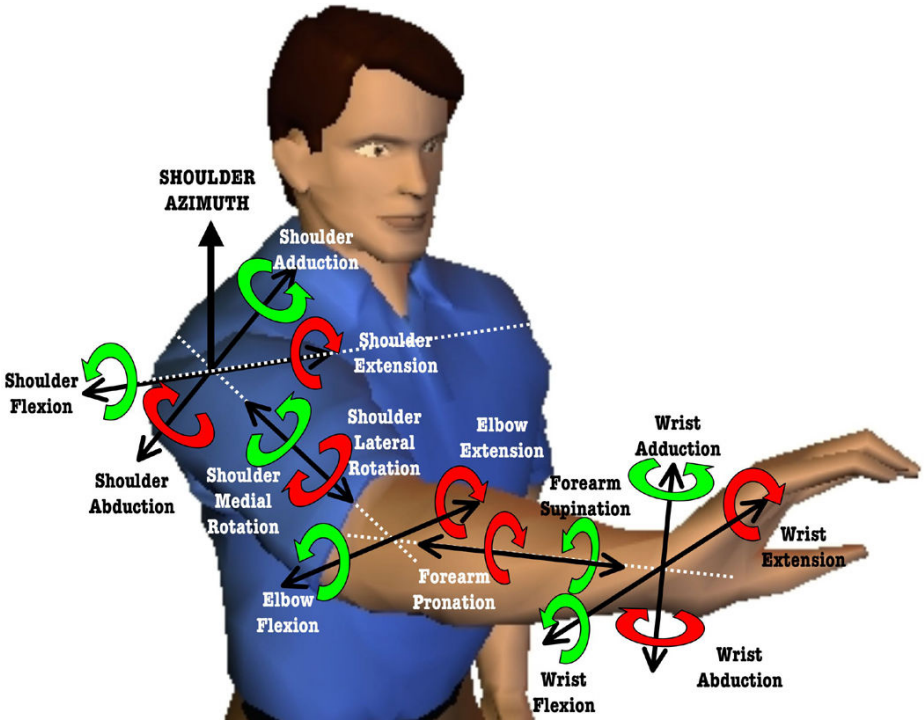

Figure 2: Degrees of freedom in the human arm

Table 2: Exoskeleton requirements and constraints

Requirement	Constraints
Allow for arm movement	
Scapula elevation/depression	Joint range > 30°
Shoulder abduction/adduction	Joint range > 134/48° [11]
Shoulder flexion/extension	Joint range > 61/188° [11]
Shoulder medial/lateral rotation	Joint range > 97/34° [11]
Elbow flexion/extension	Joint range > 142/0° [11]
Forearm supination/pronation	Joint range > 90/85° [11]
Measure exoskeleton orientation	Angle measurement accuracy < 1.31 milli-degrees Measuring device must be single-fault tolerant
Transmit forces to the user's arm	
Provide torque for scapula elevation/depression	Torque capability > 62.5 Nm
Provide torque for shoulder	Torque capability > 62.5 Nm
Provide torque for elbow elevation/depression	Torque capability > 36.25 Nm
Transmit no forces during user spasm	
Sense when the event occurs	Sensor must be single-fault tolerant
Forces must be able to be controlled at > 10 Hz	
Measure forces transmitted to the arm	Measuring device must be single-fault tolerant
Adjust to differing human arm dimension	Consider 5th to 95th percentile human dimensions
Allow for quick donning and doffing	
Allow for quick shutdown of the device	
Allow for device portability	Total mass should be less than 15 kg
Provide power to device	Power must be drawn from a 24 V source

Chapter 4 Kinematic Design

This chapter will describe the kinematic design process, including the construction of three rapid prototypes to validate movement. During the design phase, the location of certain degrees of freedom was easier to determine than others. The elbow, for example, is a single DOF that must be replicated in the manipulator. In order for the manipulator to move smoothly with the arm, the arm's elbow axis and the manipulator's elbow axis must be collinear. The same logic applies to the forearm roll DOF. However, other DOFs were not so straight-forward. The human shoulder is a ball-and-socket joint, which can be kinematically approximated in a number of different ways. The elevation and depression of the GH joint is prescribed by synchronous motion of the scapula and clavicle, which produces very complex movement. The following sections describe how degrees of freedom in the exoskeleton were matched to degrees of freedom in the human arm.

4.1 Scapula

The shoulder complex, which includes the scapula, clavicle, and humerus, contains eleven degrees of freedom. However, these DOFs are not all independent, so the pose of the glenoid can in fact be described by four degrees of freedom. Moesland et al. (2003) have shown that the motion of the GH joint in the frontal plane can be expressed by only two arm parameters [20]. Although the GH joint can be independently translated (e.g. shoulder shrug), the motion that is significant to this project is the coordinated motion

between the arm and the shoulder complex. Figure 3 shows the motion of the GH joint in the frontal plane as the arm is abducted. The blue circles, which represent the actual data, account for abduction angles from zero degrees (arm straight down, left-most data point) to 180 degrees (arm straight up, right-most data point), and the data has been normalized such that the displacements are zero when the arm is abducted 90 degrees. The dotted blue line shows the progression of the movement, but is not intended to imply actual data. The red curve is a least-squares fit of the data to a circle [9], found by minimizing the following objective function:

$$F = \sum_{i=1}^{n} \left(r_i - \bar{r} \right)^2 \tag{1}$$

where r_i is the geometric distance between the i^{th} data point and the center of the least-squares circles, and $\bar{r}$ is the radius of the least-squares circle. Here, the circle radius is about 71 mm.

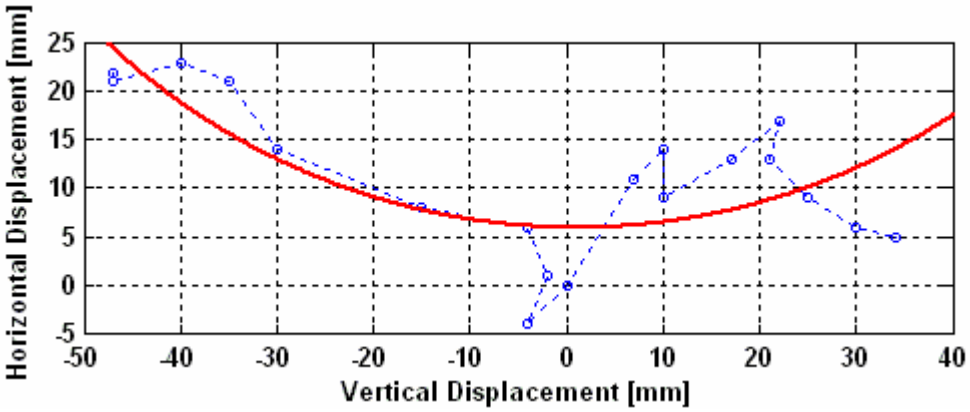

Figure 3: Motion of GH joint in frontal plane during arm abduction (data adapted from [20])

Although the least-squares circle is far from a perfect fit, it shows that a single rotary joint can roughly approximate the primary motion of the shoulder complex. Since the motion occurs in the frontal plane, the axis of the joint would have to be perpendicular to

that plane. Through this brief analysis, it has been shown that the four DOFs of the glenoid can be approximated by a single rotational degree of freedom.

4.2 Shoulder

The configuration of the DOFs in the exoskeleton shoulder is open to many more solutions. As discussed before, the glenohumeral joint is a ball-and-socket joint, capable of abduction/adduction, flexion/extension, and medial/lateral rotation.

For a serial manipulator to replicate this motion, three serially connected rotational joints with mutually intersecting axes are needed. In order to maximize the theoretical workspace of the tool tip (not accounting for physical joint limits), the following relationships between the joint axes must be upheld:

$$\frac{\pi}{2} - \theta_3 \leq \theta_2 \leq \frac{\pi}{2} + \theta_3 \tag{2}$$

$$\pi - \theta_2 - \theta_3 \leq \theta_1 \leq \theta_2 + \theta_3 \tag{3}$$

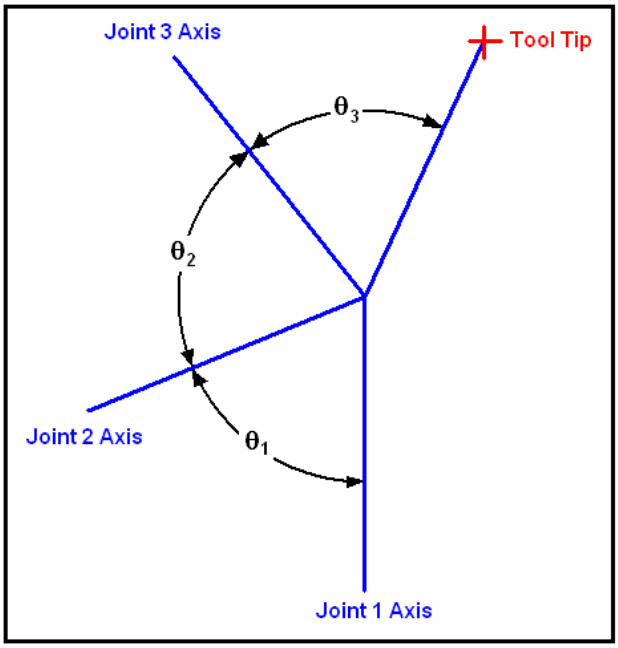

Figure 4: Relationship between joint axes in the shoulder

where all angles are positive numbers between zero and π. To explain the origin of these inequalities, first consider the joint 3 axis and the tool tip alone. Figure 5a shows the tool tip as a red cross, the joint 3 axis as a magenta line, and the point of intersecting joint axes as a blue cross. Revolving the tool tip about the joint 3 axis produces the green circle shown in Figure 5b. Now also consider the effect of the joint 2 axis. Revolving the green circle about this axis produces the orange surface shown in Figure 5c. The orange surface is a spherical region, bounded by two latitudes, and represents the workspace of the tool tip if only the joint 2 axis and joint 3 axis are considered. To guarantee that the workspace of the tool tip is maximized, rotating the orange surface about joint axis 1 will have to produce an entire sphere. In order for this to occur, the orange surface must contain a full great circle, and the joint 1 axis must intersect this circle. Equation 2 describes the conditions under which the orange surface will contain a full great circle,

while equation 3 describes the conditions under which the first joint axis will intersect this circle.

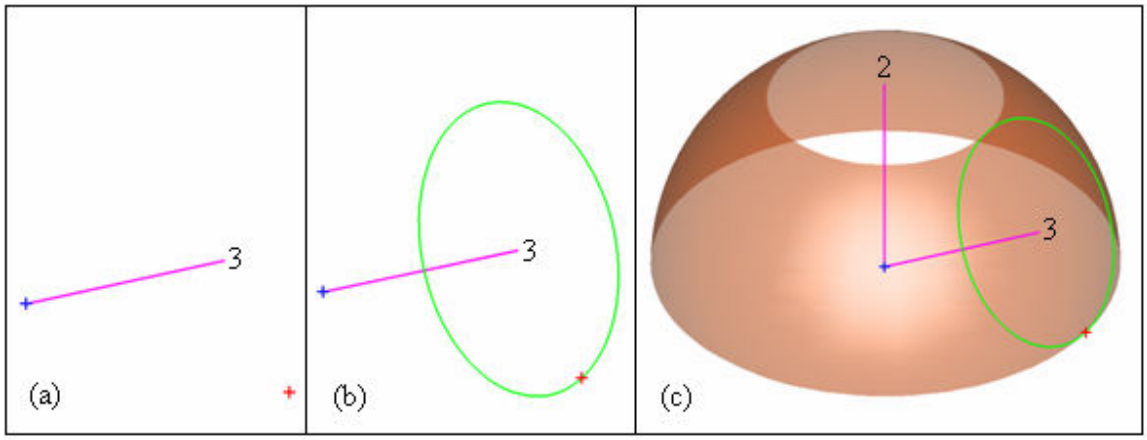

Figure 5: Steps in determining the workspace of three intersecting axes

The exact values chosen for the angles between adjacent joint axes affect the location of singularities in the workspace and the extent of joint limits, so these are the factors that helped to determine those angles. To aid in this decision, a series of prototypes were constructed to illustrate the properties of different kinematic configurations.

4.2.1 Prototype I

The first version of the shoulder geometry used a kinematic configuration corresponding to standard biomechanical terminology for the DOFs in the shoulder. As illustrated in Figure 6, the first DOF corresponded exactly to abduction/adduction, the second to flexion/extension, and the third to medial/lateral rotation.

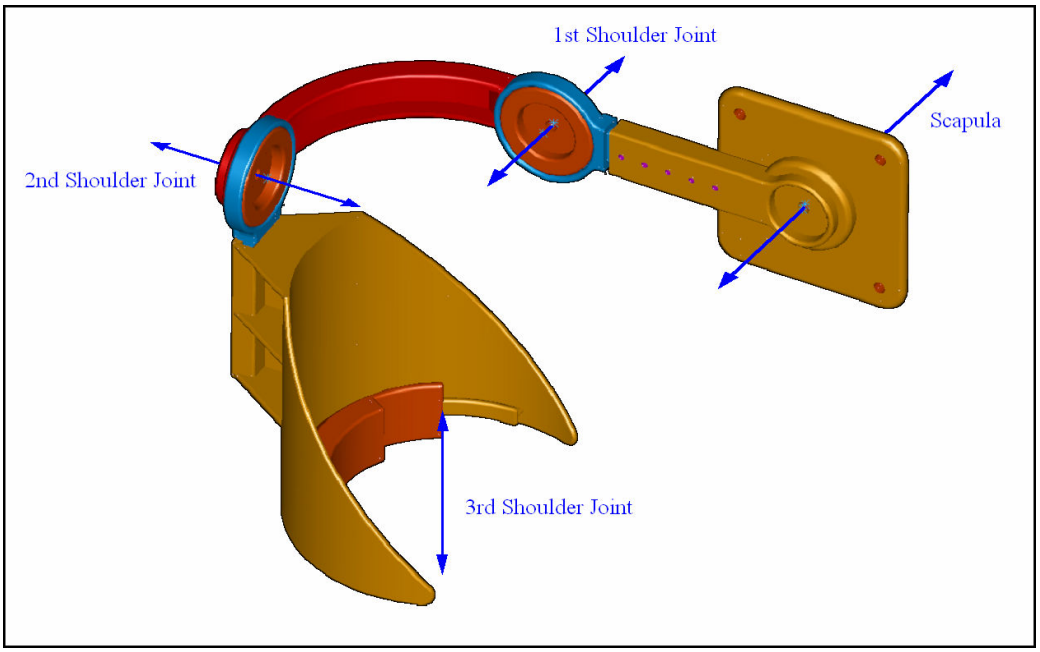

Figure 6: CAD model of prototype I

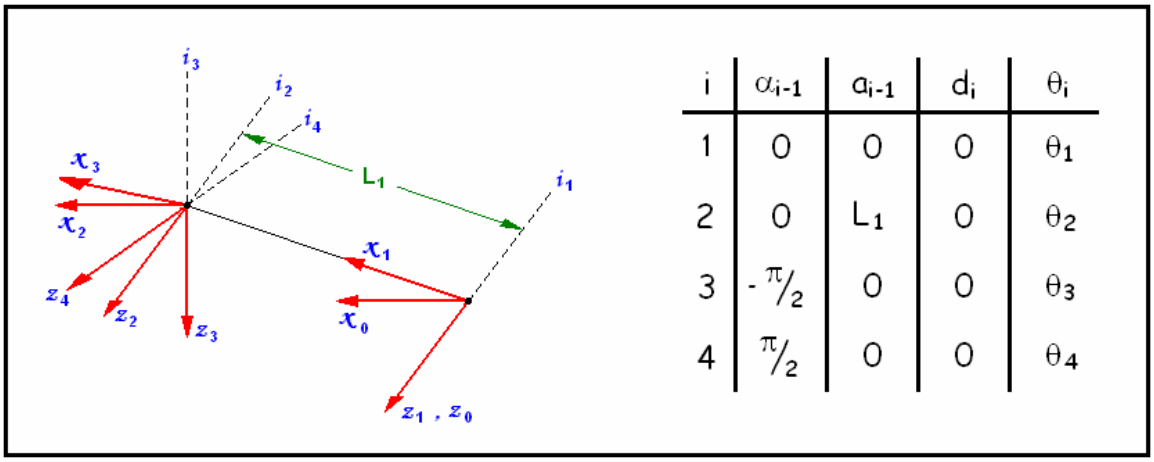

i	α_{i-1}	a_{i-1}	d_i	θ_i
1	0	0	0	θ_1
2	0	L_1	0	θ_2
3	$-\pi/2$	0	0	θ_3
4	$\pi/2$	0	0	θ_4

Figure 7: D-H parameters and link frame assignments for prototype I

Figure 7 shows the link frame assignments on the left and a table of the Denavit-Hartenberg (D-H) parameters on the right. The “home” configuration of the manipulator, shown in Figure 6, can be described by:

$$\underline{\theta} = \left[0, \frac{\pi}{2}, \frac{\pi}{2}, \theta_4\right] \tag{4}$$

Considering only the three shoulder joints (z_2, z_3, z_4), the rotational Jacobian and its determinant can be written as:

$${}^2J = \begin{bmatrix} 0 & 0 & \sin\theta_3 \\ 0 & 1 & 0 \\ 1 & 0 & \cos\theta_3 \end{bmatrix} \tag{5}$$

$$\det\left({}^2J\right) = -\sin\theta_3 \tag{6}$$

Since a singularity only occurs when the determinant of the Jacobian is equal to zero, this shows that the shoulder is singular when the second shoulder joint is at either zero or π radians. This corresponds to where the arm points straight forward or straight back (Figure 8), resulting in alignment of the abduction and rotation joints.

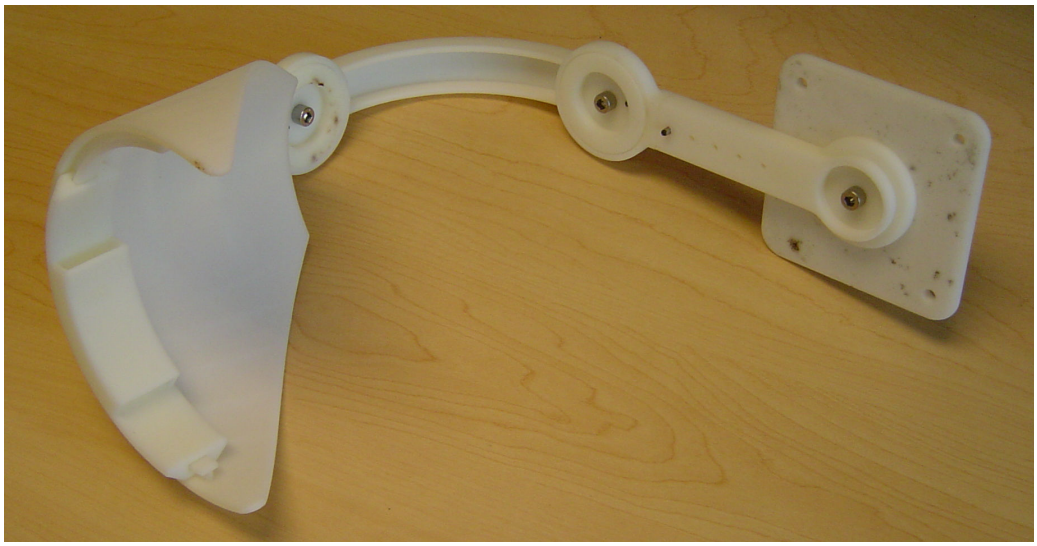

Figure 8: Singular configuration for prototype I

The latter was not a problem because its position was not within the workspace of the average human arm. On the other hand, the former was in the middle of the workspace of the average human arm, and would therefore interfere with normal operation.

4.2.2 Prototype II

To address the placement of the singularity, the kinematics of the arm was slightly adjusted by rotating the first shoulder joint 45 degrees from the frontal plane, as shown in Figure 9.

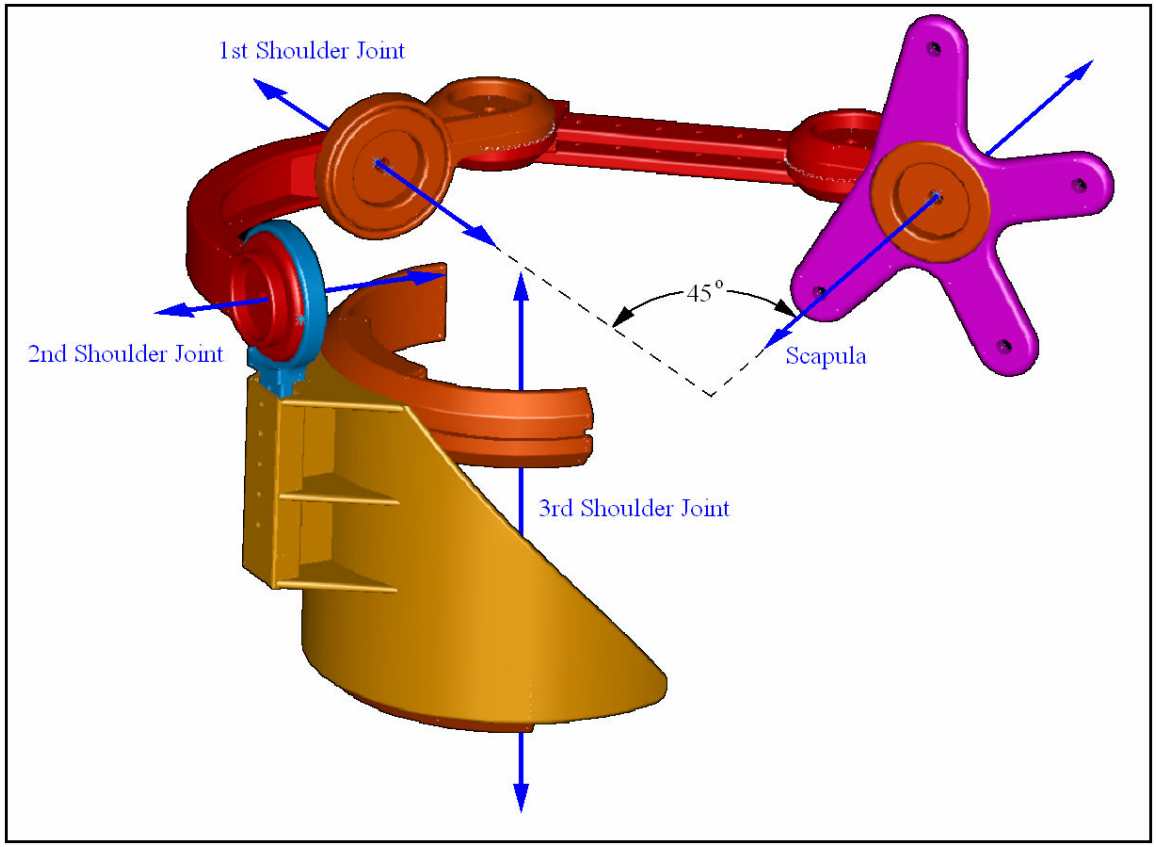

Figure 9: CAD model of prototype II

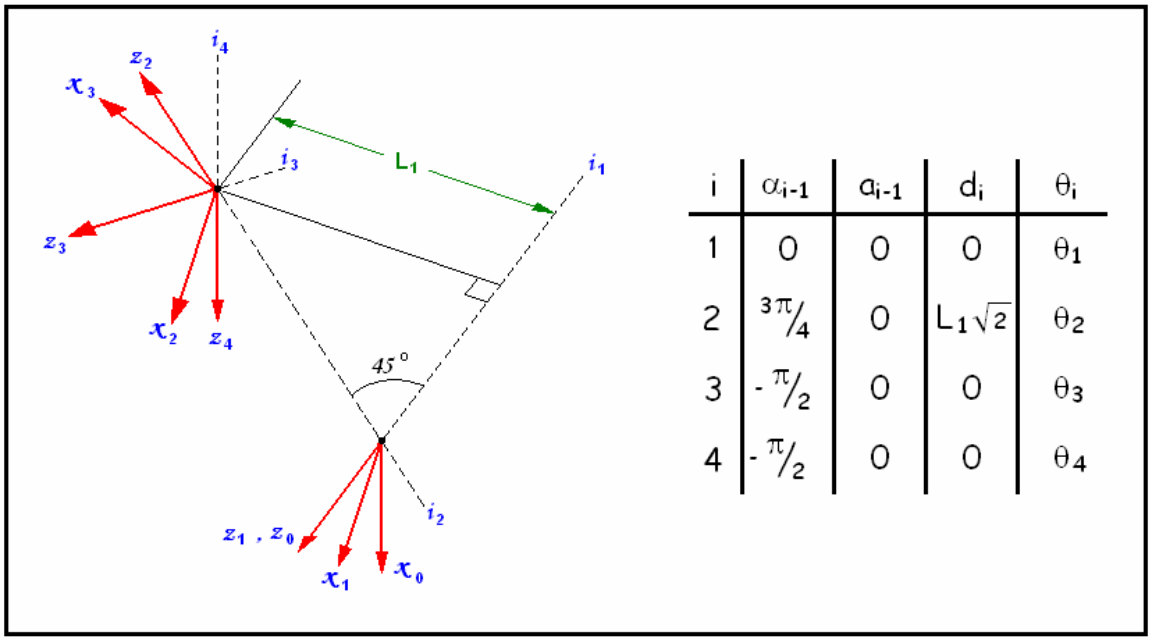

i	α_{i-1}	a_{i-1}	d_i	θ_i
1	0	0	0	θ_1
2	$3\pi/4$	0	$L_1\sqrt{2}$	θ_2
3	$-\pi/2$	0	0	θ_3
4	$-\pi/2$	0	0	θ_4

Figure 10: D-H parameters and link frame assignments for prototype II

Figure 10 shows the link frame assignments on the left and a table of the D-H parameters on the right. The configuration of the manipulator shown in Figure 9 can be described by:

$$\underline{\theta} = \left[0,0,-\frac{\pi}{2},\theta_4\right] \tag{7}$$

The kinematics in the three shoulder joints is exactly the same as it was in the first prototype, so the singularity again occurs when the second shoulder joint angle is zero or π radians. However, because of the 45 degree offset, the singularity was in a different location in the global reference frame (45° left from pointing straight forward), as illustrated in Figure 11.

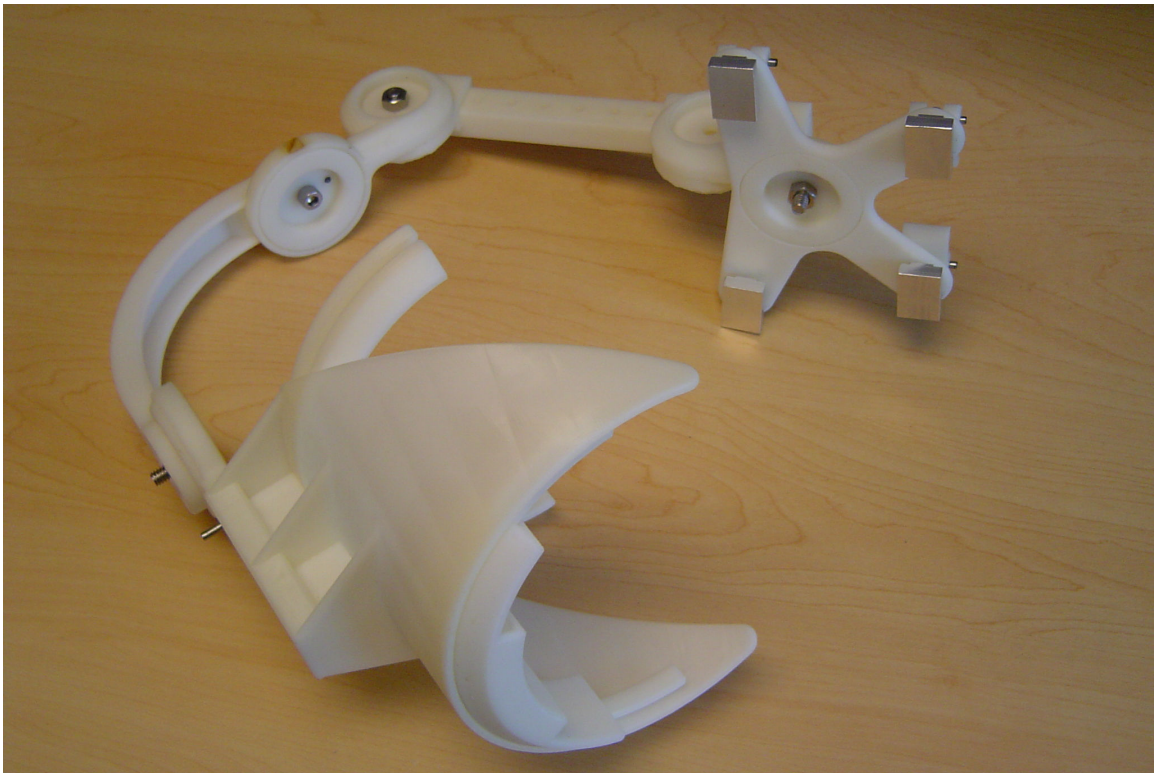

Figure 11: Singular configuration for prototype II

However, this location still intruded too far into the workspace. Another major problem with this design was the implicit requirements it put on the actuator for the third shoulder DOF. For all of the other DOFs, the joint axis extends outside of the region occupied by the human arm. For the third shoulder DOF, the joint axis is always inside the human arm. If the actuator is placed distal of the elbow, then it would collide with the forearm before the elbow could be fully extended. If the actuator is placed on the upper arm, then it would have to have a rather sizable pass-through in order to avoid interfering with the user's arm. Finally, if the actuator is placed above the shoulder, then it would collide with the user's head or torso during shoulder abduction. This fact greatly complicates the design of the actuator for that DOF. Sections 4.2.4 and 5.2 will go into further detail about the difficulties that would be imposed.

4.2.3 Prototype III

Another joint design was developed concurrently with the previous one. Unlike the first prototype, manipulator shoulder DOFs were not matched with the biomechanical definitions of shoulder DOFs. Instead of abduction/adduction and flexion/extension, azimuth and elevation were used. As with the previous two designs, the third shoulder DOF was medial/lateral rotation.

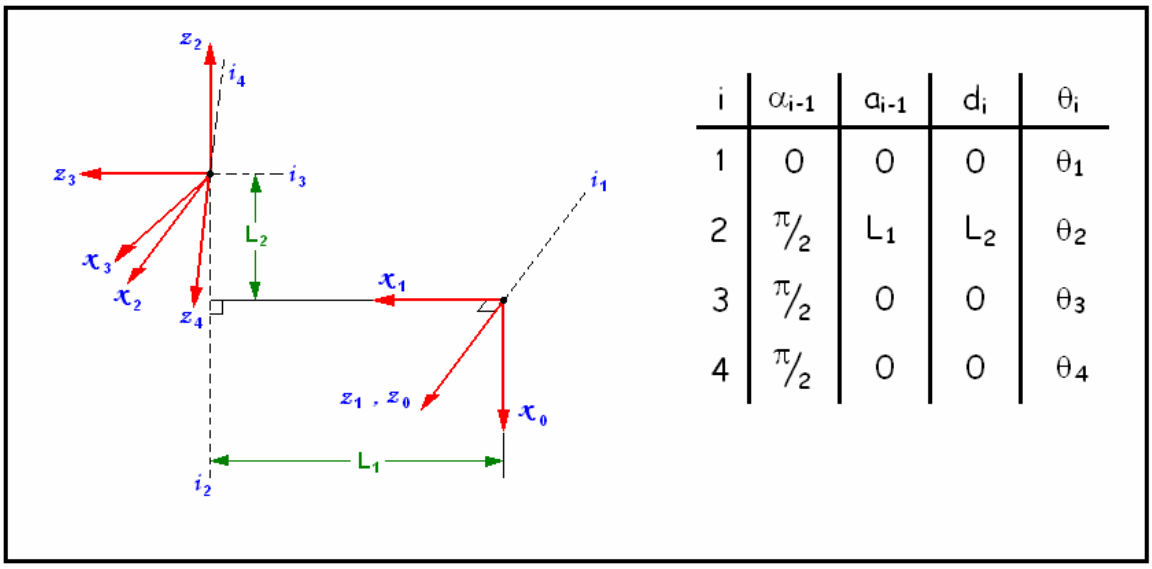

i	α_{i-1}	a_{i-1}	d_i	θ_i
1	0	0	0	θ_1
2	$\pi/2$	L_1	L_2	θ_2
3	$\pi/2$	0	0	θ_3
4	$\pi/2$	0	0	θ_4

Figure 12: D-H parameters and link frame assignments for prototype III

In the literature review a passive arm exoskeleton was discovered with the same kinematic configuration. Instead of making a prototype of this design, the MB Exoskeleton [27] was studied first-hand for its kinematic properties.

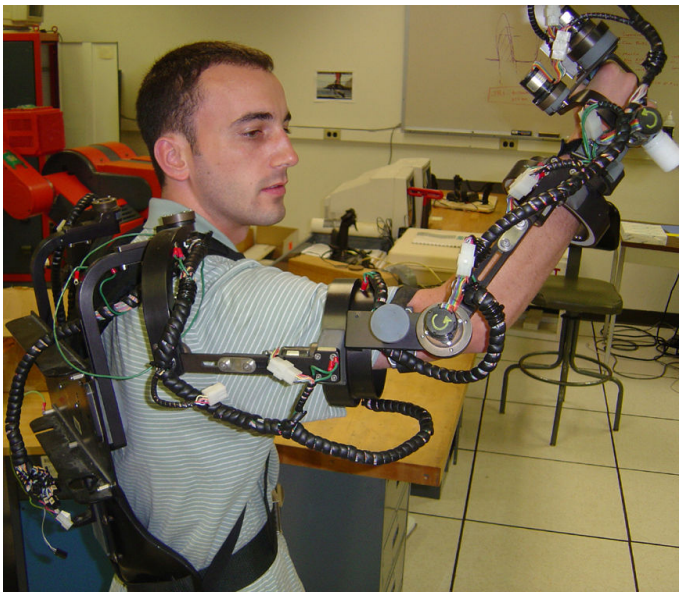

Figure 13: The author evaluating the workspace of the MB Exoskeleton

Although its range of motion was extensive, singularity location was again problematic. The relative kinematics of the shoulder DOFs are exactly the same as the first two prototypes, so again the singularity occurs when the second shoulder joint angle is zero or π radians. The difference lies in the orientation of the first shoulder joint with respect to the global frame; in this case, the singularity occurred when the arm hung straight down. This too was in an unwanted location. In addition to the singularity, this design had the same feature in the third shoulder DOF as the previous design, and therefore had the same problems.

4.2.4 Prototype IV

The final kinematic design made no attempt to align the third shoulder axis of the exoskeleton with the shoulder medial/lateral roll axis. Instead, the objectives were to:

avoid the problems with the third shoulder DOF in the previous two designs; avoid singularities in the middle of the usable workspace; and expand the manipulator's workspace to cover the majority of the human arm's workspace.

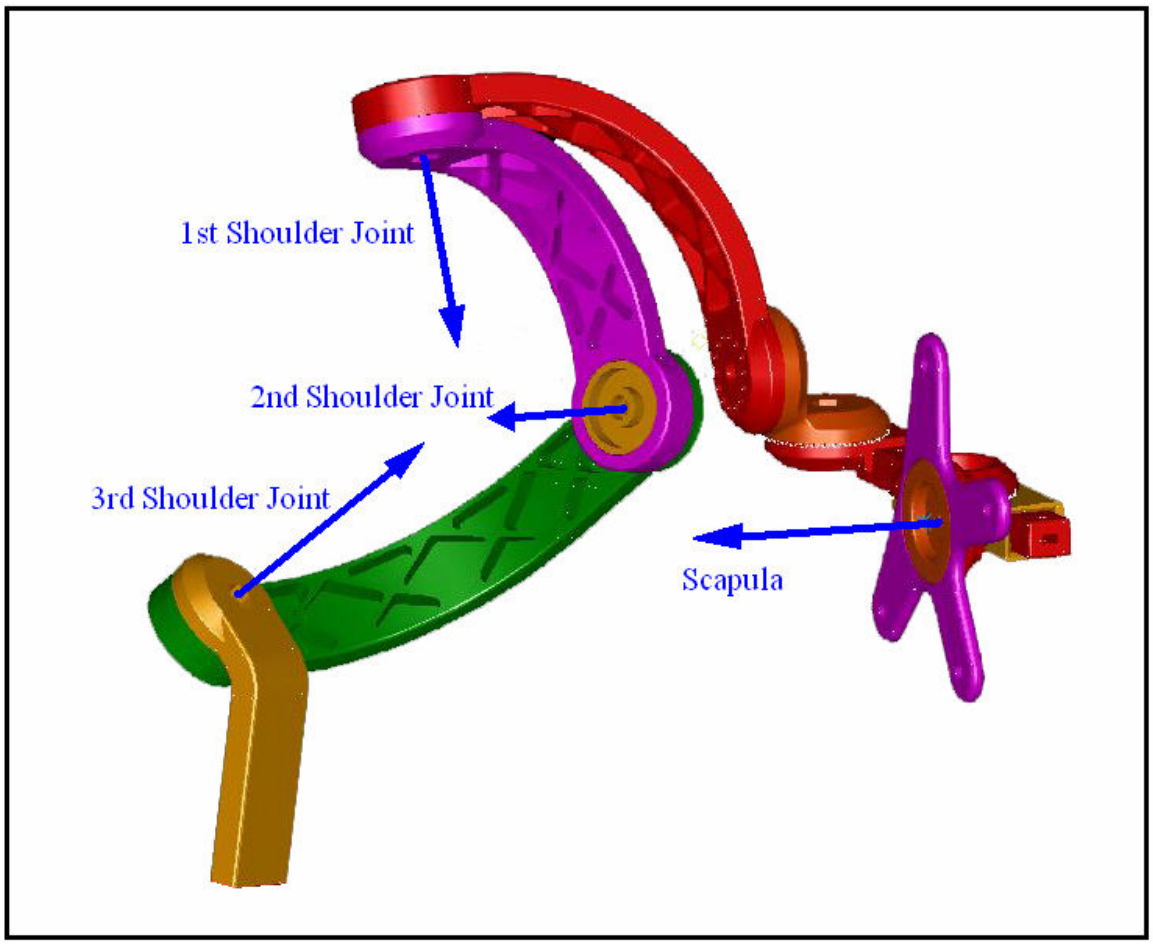

Figure 14: CAD model of prototype IV

Instead of the first shoulder DOF aligning with the vertical axis (azimuth), it is rotated 30 degrees from the vertical in the frontal plane. The third shoulder DOF axis makes a 45-degree angle with the imaginary line connecting the center of the GH joint with the center

of the elbow joint. The second shoulder joint is orthogonal to the first and third shoulder joints.

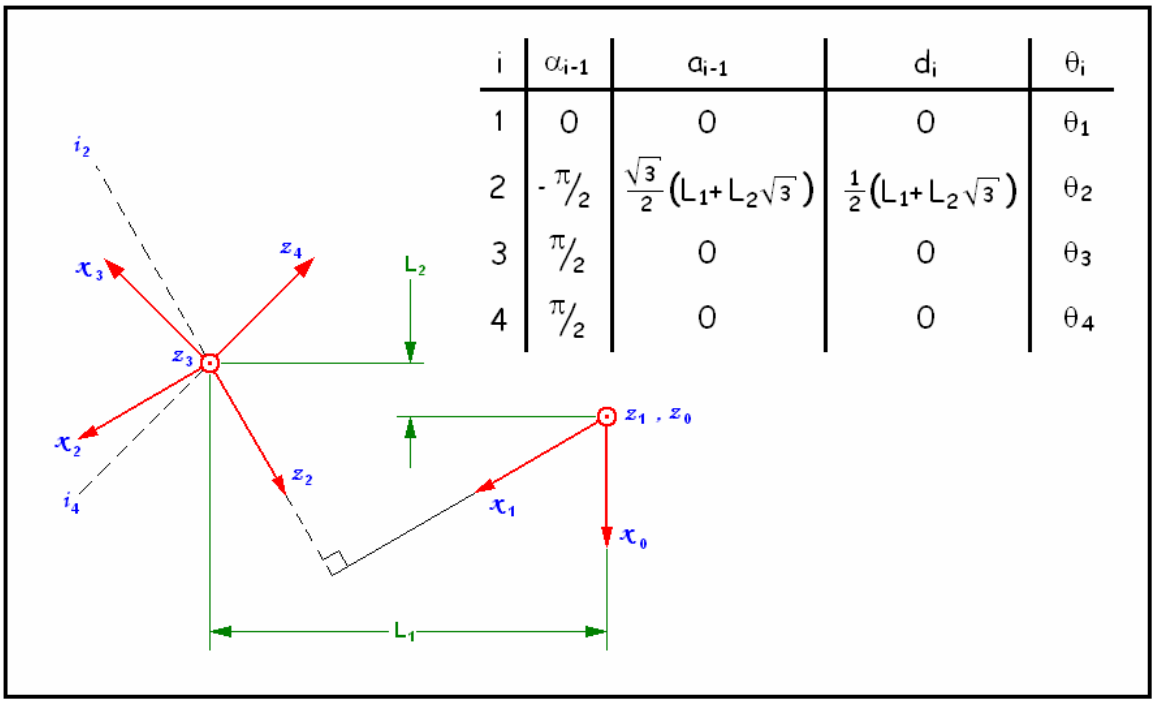

i	α_{i-1}	a_{i-1}	d_i	θ_i
1	0	0	0	θ_1
2	$-\pi/2$	$\frac{\sqrt{3}}{2}(L_1+L_2\sqrt{3})$	$\frac{1}{2}(L_1+L_2\sqrt{3})$	θ_2
3	$\pi/2$	0	0	θ_3
4	$\pi/2$	0	0	θ_4

Figure 15: D-H parameters and link frame assignments for the final joint design

Figure 15 shows the link frame assignments on the left and a table of the D-H parameters on the right. The configuration of the manipulator shown in the Figure 14 can be described by:

$$\underline{\theta} = \left[-\frac{\pi}{3}, 0, -\frac{5\pi}{12}, \theta_4 \right] \tag{8}$$

There are two trade-offs associated with the aforementioned angular offsets. The larger the angular offset between the first manipulator shoulder DOF and the vertical axis, the further the arm can adduct (move towards the body) before a singularity is reached. The

smaller this angle is, the further the arm can abduct (move away from the body) before shoulder joint 3 collides with shoulder joint 1. The larger the angular offset between the third shoulder DOF axis and the GH-elbow line (upper arm), the farther the arm can adduct before a singularity is encountered. At the same time, the larger this angle, the more shoulder abduction is limited. In addition, the smaller this angle gets, the further the third shoulder actuator must be from the GH center in order to avoid contact with the subject's arm. This would bring the third shoulder actuator closer to the elbow actuator, eventually creating interference problems.

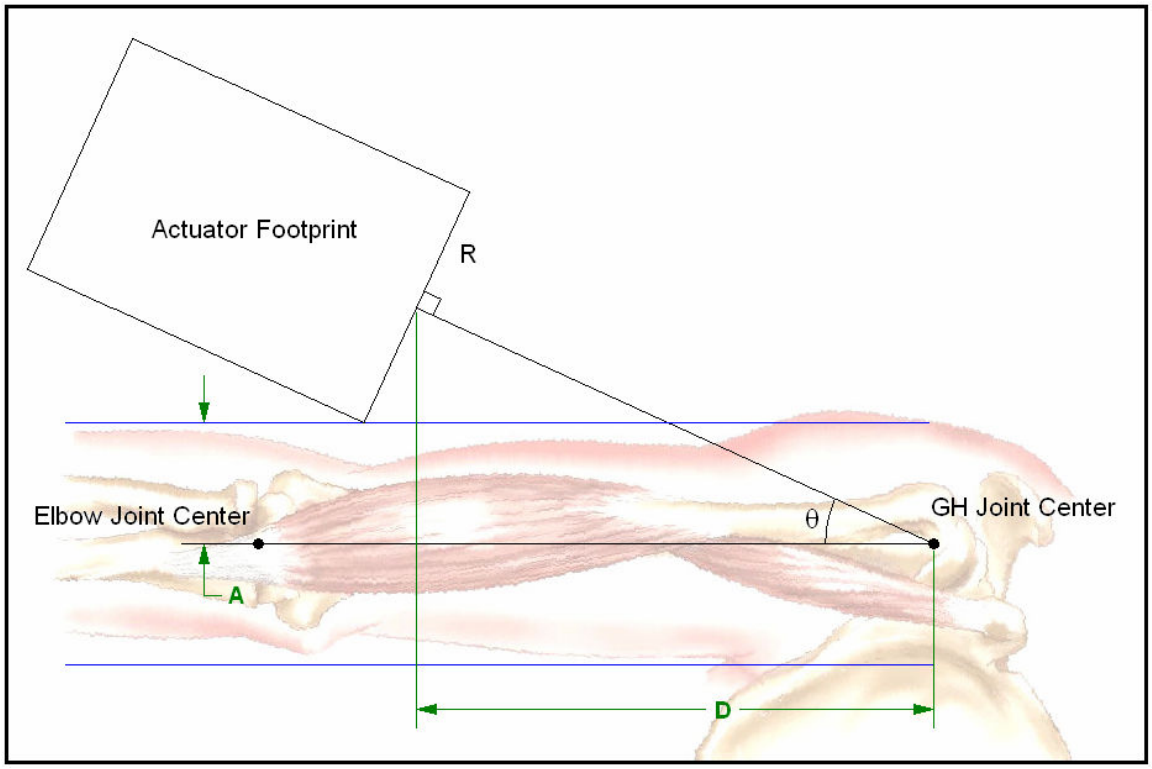

Figure 16: Geometric representation of the offset angle's (θ) effect on distance between the third actuator and the center of the GH joint (D)

In Figure 16, the blue lines represent the footprint of a person's arm. The distance, D, between the GH center and the third shoulder axis is given by

$$D = \frac{A + R\cos\theta}{\tan\theta} \tag{9}$$

where R is the radius of the actuator. As θ goes to zero, D approaches infinity. The aforementioned values for these angular offsets were chosen as a compromise between these restrictions. The singularity occurs when the arm is in the frontal plane and adducted 75 degrees from vertically down.

Figure 17: Singular configuration for prototype IV

The shoulder workspace has the following characteristics, estimated from the prototypes discussed in this section. For comparison, the human joint limits are shown.

Table 3: Angular joint limits for prototypes and human

	Joint Limit (degrees)				
Shoulder DOF	**Prototype I**	**Prototype II**	**Prototype III**	**Prototype IV**	**Human [11]**
Abduction	134*†	120†	130†	90†	134
Adduction	48*	48*	130	48*	48
Flexion	45	45	130	45	61
Extension	188*	120	130	165	188
Medial Rotation	unrestricted	unrestricted	130**	97*	97
Lateral Rotation	unrestricted	unrestricted	130**	34*	34

* = value restricted by average human joint limit, not manipulator joint limit
** = assuming joint range is centered
† = value does not include additional 30 degrees of abduction provided by the scapula joint

4.3 Elbow

The kinematics of the human elbow is close enough to that of a single rotary joint that it can be modeled as such. To that end, the exoskeleton has a single rotary actuator aligned with the human elbow axis. Although the kinematics of the elbow is simple, the geometry of the joint requires further explanation. When the elbow is fully extended, the forearm does not exactly align with the upper arm. The angle between the two segments of the arm in this configuration is called the carry angle, as illustrated in Figure 18.

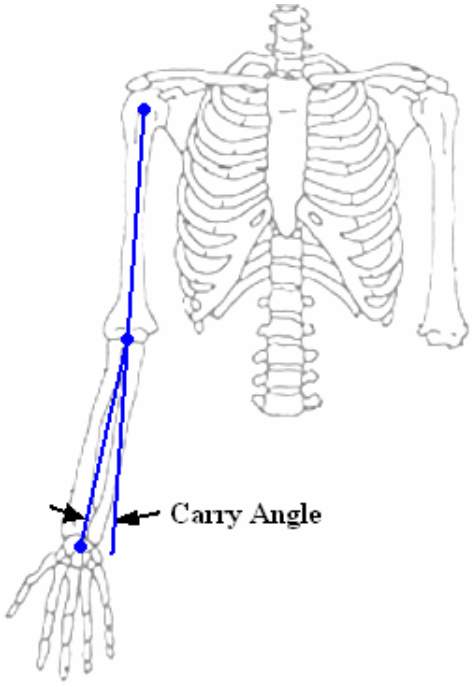

Figure 18: Carry angle

The exoskeleton has two features to accommodate this variation from collinearity. First, there is a bracket that keeps the user's elbow secured to the exoskeleton (Figure 19b). In addition, the passive forearm supination/pronation DOF in the exoskeleton allows the user to rotate his or her arm to a comfortable position in accordance with his or her specific carry angle (Figure 19a).

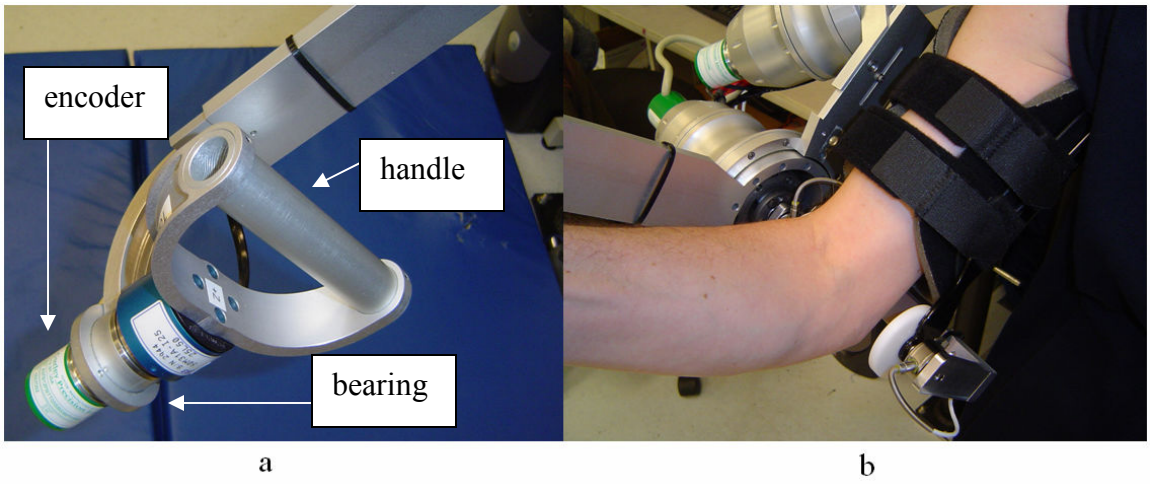

Figure 19: (a) detail of handle, (b) elbow bracket

4.4 Forearm

As with the elbow, the kinematics of forearm rotation (supination/pronation) can be modeled as a single degree of freedom. As mentioned earlier, this DOF is passive, and is therefore implemented with a simple bearing located distal of the hand and an angular encoder to measure rotation (Figure 19a).

4.5 Link Adjustments

The discussion of kinematics thus far has assumed that the manipulator joint axes can be aligned arbitrarily well to the human joint axes. In order to accomplish this, the exoskeleton's structural links must have length adjustments built in. For this manipulator, the important dimensions are the distances from the scapula to the GH joint, from the GH joint to the elbow, and from the elbow to the hand. Since these lengths vary significantly from person to person, adjustability was designed into the manipulator link lengths.

Table 4: Exoskeleton link adjustment range and human arm dimensions

Passive Link*	Exoskeleton Minimum Length	Exoskeleton Maximum Length	5th Percentile Human [2],[15]	95th Percentile Human [2], [15]
Scapula to GH center, L_1 (in)	7.31	10.07	-	-
GH center to elbow, L_2 (in)	10.76	12.33	11.9	14.1
Elbow to handle center, L_3 (in)	11.81	15.35	11.8	15.4

* = see Figure 15 for link definitions

Table 4 shows the range of limb lengths for the 5^{th} to 95^{th} percentile human along side the exoskeleton link adjustment range. Although the adjustment range of the scapula-GH

distance was somewhat arbitrary, its nominal value was based on the circular curve fit of the GH center movement found in section 4.1.

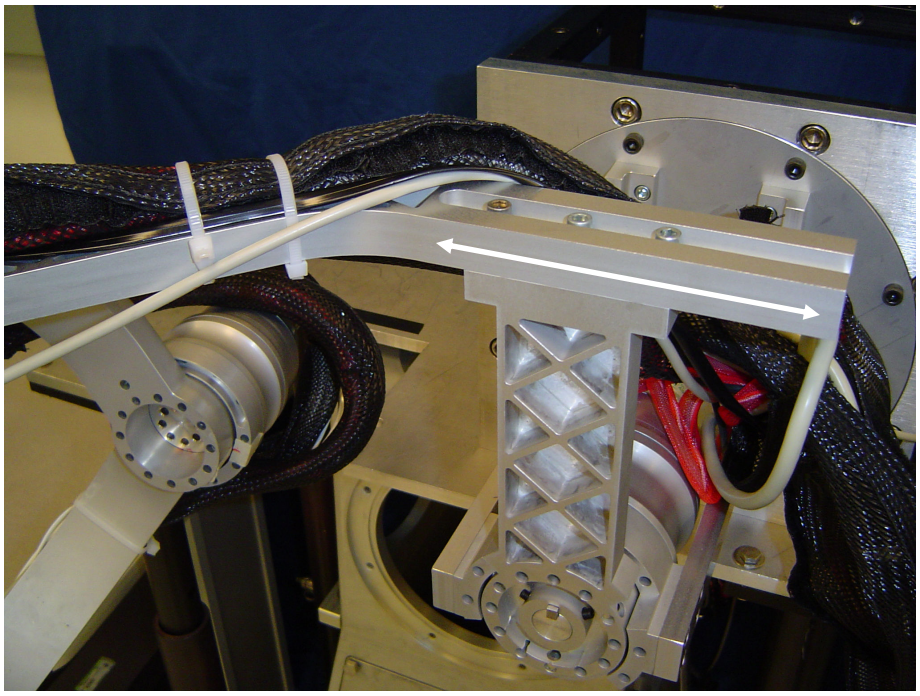

Figure 20: Photograph of the adjustment mechanism for scapula-to-GH distance

The 5th to 95th percentile range for the GH-elbow length was not achieved in the manipulator because the original anthropometric data on which this range was based was found to be inaccurate [15]. Only after the exoskeleton's design had been finalized was this mistake found.

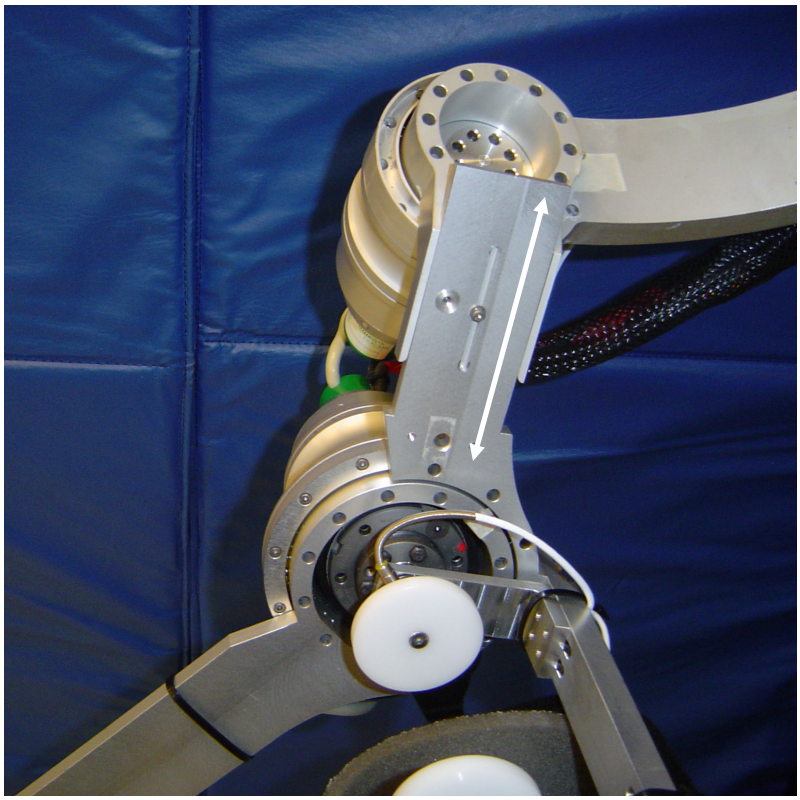

Figure 21: Photograph of the adjustment mechanism for GH-to-elbow distance

The range for the elbow-hand length was fully achievable in the manipulator.

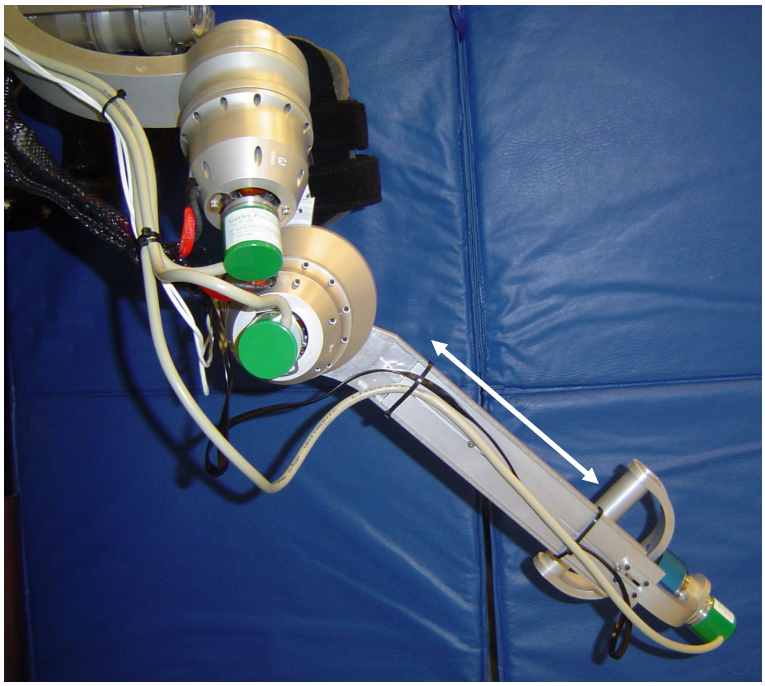

Figure 22: Photograph of the adjustment mechanism for elbow-to-handle distance

4.6 Full Kinematic Model

In summary, the kinematics of the entire manipulator can be described by the link frames and D-H parameters shown in Figure 23. The forward kinematics can be found in Appendix C.2. Axis 1 corresponds to the scapula joint, and the base frame (frame 0) shares the same origin. Axes 2, 3, and 4 comprise the shoulder joint, while axis 5 represents the elbow joint and axis 6 represents forearm roll. The "home" position of the manipulator, as shown in Figure 23, is described by the joint angles:

$$\bar{\theta} = \left[-\frac{\pi}{3}, 0, -\frac{5\pi}{12}, \frac{\pi}{2}, 0, 0 \right] \tag{10}$$

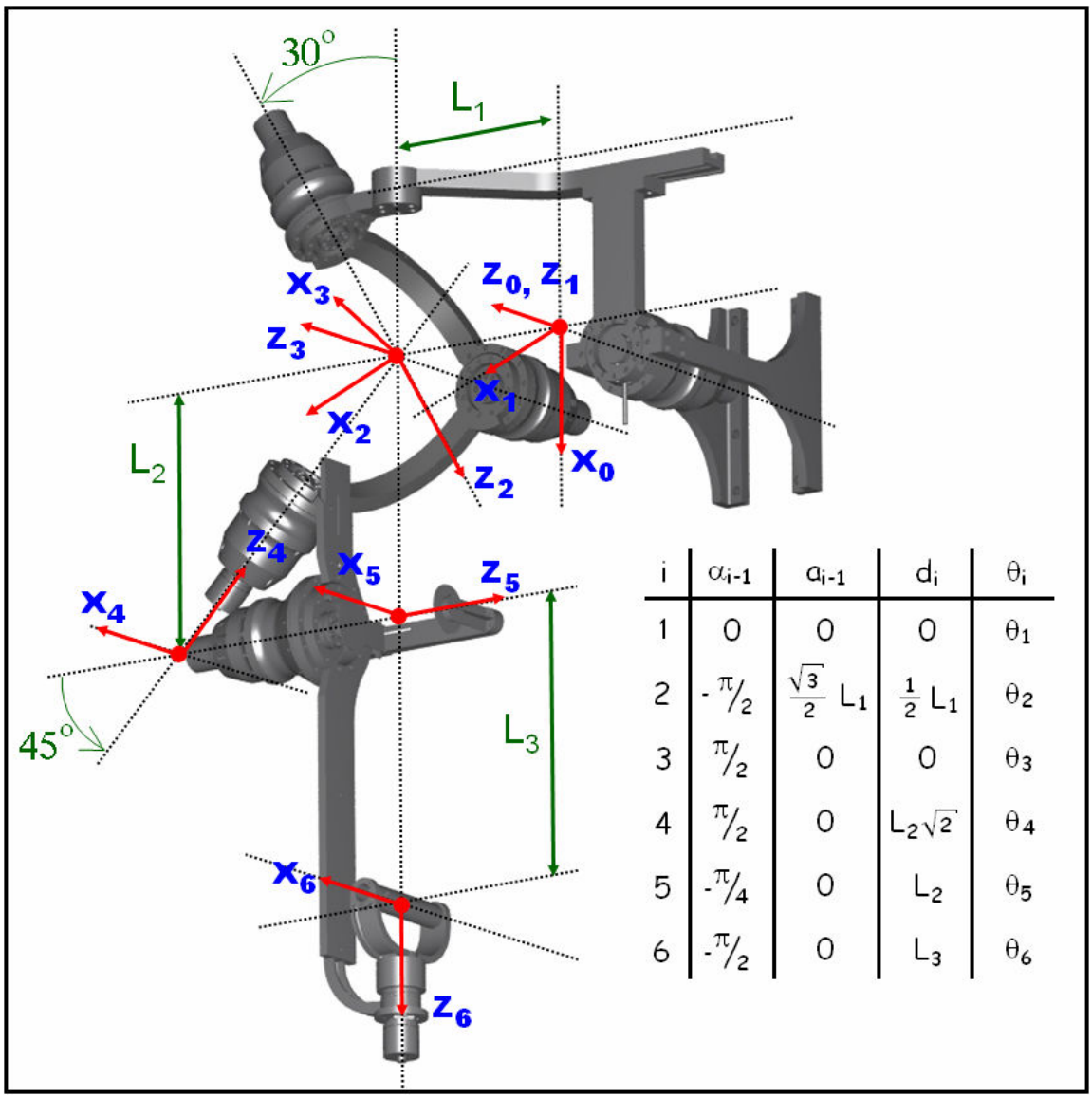

i	α_{i-1}	a_{i-1}	d_i	θ_i
1	0	0	0	θ_1
2	$-\pi/2$	$\frac{\sqrt{3}}{2} L_1$	$\frac{1}{2} L_1$	θ_2
3	$\pi/2$	0	0	θ_3
4	$\pi/2$	0	$L_2\sqrt{2}$	θ_4
5	$-\pi/4$	0	L_2	θ_5
6	$-\pi/2$	0	L_3	θ_6

Figure 23: D-H parameters and link frame assignments for the entire manipulator

Chapter 5 Actuator and Transmission Design

In actuator design, there are numerous methods of producing torque and motion. This chapter will focus on how the project requirements were used to select an actuation method, and how specific components were chosen to meet the needs of the exoskeleton.

5.1 Actuators

Since the target strength of the manipulator is 50% of average human capacity (Table 5), a target value of 55 Nm was set for shoulder flexion/extension, and 62.5 Nm was set for shoulder abduction/adduction.

Table 5: Human torque limits for the shoulder and elbow

DOF		Torque (Nm) [31]
Shoulder	Flexion/Extension	110
	Abduction/Adduction	125
	Medial/Lateral Rotation	-
Elbow	Flexion/Extension	72.5

No value was found for average human roll torque capability, so a value was assumed that was on the order of the other two shoulder DOFs. The exact value of this number turned out not to matter, for reasons that will be discussed later. Lastly, a target value of 36.25 Nm was set for elbow flexion/extension. It should be noted that these values are the target torques if the exoskeleton had no weight. When actual actuator torque capabilities are set, the exoskeleton's mass must be taken into account

In choosing an actuator type, only those involving DC brushless motors were considered because they are the only type of actuator with enough control bandwidth and stiffness to accommodate the exoskeleton's intended task. The ranges of bandwidth and power-to-weight ratio for several types of actuators are shown in Figure 24.

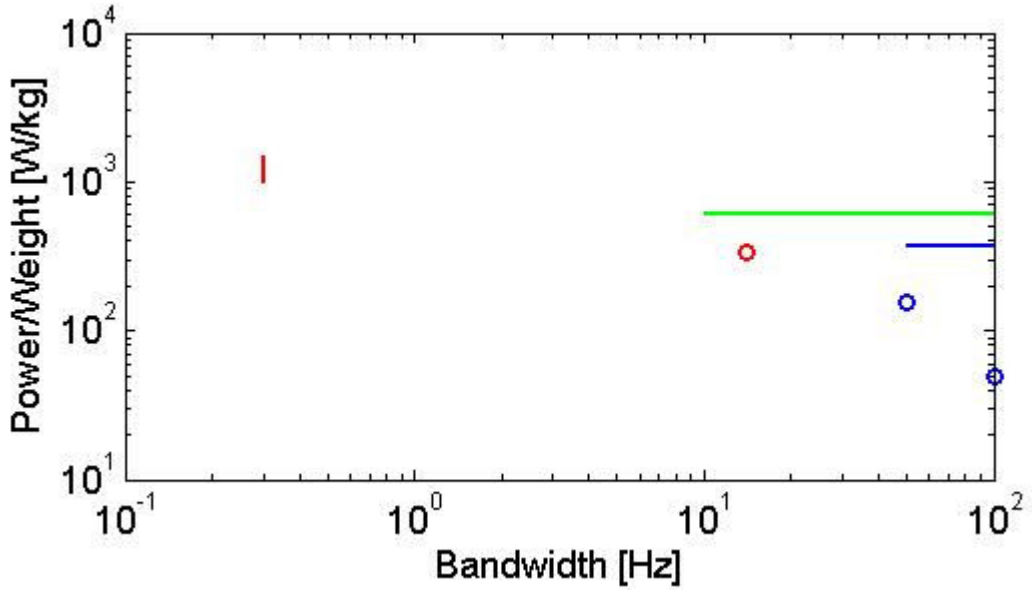

Figure 24: Bandwidth and power/weight ratio ranges for various electric (blue), hydraulic (green), and pneumatic (red) actuators

Although this graph shows hydraulic actuators as being a better candidate than electric actuators, the weight of the massive hydraulic pumps were not accounted for in the power to weight ratio calculation. This additional weight makes hydraulic actuators impractical for use in a portable exoskeleton. Modern pneumatic McKibben actuators can achieve bandwidth comparable to that of electric actuators, but the low static stiffness of these devices would significantly decrease the first natural frequency of the exoskeleton.

5.2 Transmission

In general, all electric motors excel at providing low torque at high speeds. Since the manipulator joints will need high torque at low speeds, some form of speed reduction must be implemented. Again, the control bandwidth imposes some restrictions on the type of transmission that can be used. It must be stiff, and it must provide minimal backlash. Harmonic drives seem ideally suited for this application, since they are relatively stiff and provide near-zero backlash. However, they are not well suited for the type of joint connection found in the most distal of the three shoulder joints in the first three manipulator prototypes. That type of connection requires a large through-hole in the center of the actuator to make room for the human arm. Such a connection could be accomplished with traditional gears, but spur gears do not provide a nearly large enough transmission ratio, nor do they provide zero backlash. Worm gears, on the other hand, can provide a large enough transmission ratio.

However, worm gears have some features that are in direct contrast to the requirements of this project. First of all, normal worm gears do not provide a zero backlash connection. There is a type of zero backlash worm gear drive, but it uses springs, making a flexible connection. Also, worm gears with high transmission ratios are not backdriveable. One of the safety requirements states that the manipulator should be easy to don and doff. If the exoskeleton shuts down in an awkward position and the joints are not backdriveable, then it will be difficult to doff the manipulator. For these reasons, worm gear drives and the first three manipulator prototypes were eliminated in favor of harmonic drives and the fourth prototype.

Since the exoskeleton was desired to be as light as possible, a consideration was given to mounting the motors remotely, since they comprise a significant portion of the total actuator weight. Offloading this weight from the arm portion of the exoskeleton decreases the strength requirement of the actuators, saving weight. In order for this configuration to work, a mechanism must exist that could transmit torque from a stationary motor to the gearing inside of a mobile actuator. To this end flexible drive shafts were investigated. Flexible drive shafts consist of a multi-layer braided metal cable inside of a braided metal sheath. The entire assembly is flexible, so the input is not required to be oriented in any particular way to the output.

However, this type of transmission has some characteristics that conflict with the exoskeleton's requirements. First of all, the shafts are not just flexible in bending, but also in torsion. Flexibility in and of itself is not a problem, but the torsional stiffness of these devices is low enough that it lowers the control bandwidth. Additionally, the torsional stiffness is different whether you turn the shaft clockwise or counterclockwise. This type of discontinuity is very difficult to accommodate in the controller. Lastly, the flexible shafts provide torsional friction. Friction can be modeled in a controller if its characteristics are well known. However, the frictional characteristics of the flexible shaft are dependant on the shape of the shaft. For example, if the shaft were bent into an "S," it would have different frictional characteristics than if it were bent into a "C." Since the actuator will always be changing its position and orientation with respect to the motor,

the shaft shape would also constantly be changing – and in an unknown way. Therefore, it was decided that flexible shafts would not be used.

Cable drives were also considered as a means of mounting some of the heavy components (i.e. motor and harmonic drive) remotely. Similar to flexible shafts, cable drives would allow the motor and harmonic drive to be located far from the joint they are controlling. Instead of transmitting rotational motion, cables would transmit linear motion much like a pulley system. The difficulty with this system is that cable tension must be maintained, or else the cable would slip on the pulleys and transmit no torque. In most robotic applications that use cable drives, this is accomplished by using a specific cable route accompanied by precisely placed idler pulleys. However, this type of solution does not easily accommodate any length adjustment in the links, which is needed to adjust to the geometry of different subjects. It is possible, but only with the use of tensioner pulleys, which add flexibility to the transmission. In an effort to reduce the complexity and increase the stiffness of the manipulator, cable drives were not used, and instead all actuator components were locally mounted at the joint.

5.3 Effect of Mass

As previously mentioned, the manipulator's mass must be taken into account when calculating actuator torque requirements. Now that the general configuration of the exoskeleton has been decided, a rough calculation can be made. First, the geometry of the arm must be estimated. These numbers can be taken from the third manipulator prototype. Additionally, estimates must be made of the manipulator's weight. Using

guesses of what components would be used in an actuator or link, this number can be found. Lastly, the worst-case pose of the arm must be found – that is, the manipulator configuration that puts the highest amount of gravity-generated torque on a particular actuator (Figure 25).

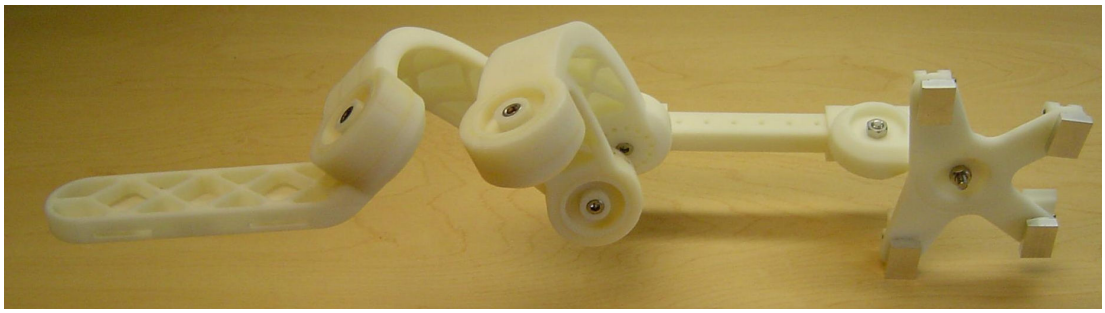

Figure 25: Worst-case pose for scapula joint

Table 6: Module contributions to gravity generated torque about the scapula in worst-case pose

Component	Mass (Kg)	Moment arm (in)	Moment Arm (m)	Moment (Nm)
Scapula	1.5	0	0	0
link	0.3	5	0.127	0.37
Shoulder 1	1.5	9	0.2286	3.36
link	0.3	8	0.2032	0.60
Shoulder 2	1.5	7	0.1778	2.62
link	0.3	9	0.2286	0.67
Shoulder 3	1.5	11	0.2794	4.11
link	0.3	15	0.381	1.12
Elbow	2.5	18	0.4572	11.21
link	0.6	29	0.7366	4.34
				28.41

Table 6 shows the amount each major component of the arm contributes to the torque about the scapula in the worst-case pose for the scapula. Since the base torque requirement for the scapula is 62.5 Nm, the total torque requirement for the scapula is 90.9 Nm, assuming that the strength of the exoskeleton scapula needs to be at least as strong as shoulder abduction/adduction.

Table 7: Module contributions to gravity generated torque about the second shoulder actuator in worst-case pose

Component	Mass (Kg)	Moment arm (in)	Moment Arm (m)	Moment (Nm)
Shoulder 2	1.5	7	0	0.00
link	0.3	9	0.0508	0.15
Shoulder 3	1.5	11	0.1016	1.50
link	0.3	15	0.2032	0.60
Elbow	2.5	18	0.2794	6.85
link	0.6	29	0.5588	3.29
				12.38

Table 7 shows the amount each major component of the arm contributes to the torque about the second shoulder actuator in the worst-case pose for that joint. For comparison, the amount of torque generated about the shoulder by the weight of the average (height: 1.75 m, mass: 83 kg) human's arm is about 43 Nm, as illustrated in Table 8 below.

Table 8: Torque generated about the shoulder by human arm mass (adapted from [26])

	Weight (N)	Moment Arm (m)	Moment (Nm)
Upper Arm	26.462	0.763	20.191
Forearm	15.226	1.054	16.041
Hand	5.292	1.328	7.030
			43.261

The loaded torque for the human arm under full abduction is therefore three times higher than for the exoskeleton. Thus, more than one-third of the human shoulder torque capability is consumed by gravity off-loading at full abduction.

In the exoskeleton, one would expect the gravity-generated torque on the first shoulder joint to be much less because its axis is nearly vertical. The gravity generated torque

about the third shoulder axis would be slightly less than that of the second shoulder axis because its moment arm is less. However, the three manipulator shoulder axes do not align with the three DOF definitions of the human shoulder. Therefore, the torque requirements cannot be directly applied to the actuators. For example, the shoulder flexion/extension torque requirement cannot be solely applied to any of the shoulder actuators, because none of them produce motion that is purely flexion/extension for every arm orientation. Since all of the shoulder axes have different torque requirements, the only way that one can guarantee that the torque requirement is being satisfied on the manipulator in every configuration that the arm can be in is to take the largest torque requirement of all the shoulder DOFs and apply it to each shoulder actuator. The largest gravity generated torque (12.4 Nm) is added to half of the largest shoulder joint torque requirement (62.5 Nm) to obtain 74.9 Nm as the final torque requirement for each of the three shoulder actuators.

The gravity-generated torque about the elbow actuator only has to take into account the last link. This produces a torque of 1.6 Nm, making the total torque requirement for the elbow 37.9 Nm.

5.4 Effect of Friction

Not only does the weight of the exoskeleton and of the human arm restrict the effective torque output of the actuators, but so does the frictional characteristics of the internal actuator components. The most significant contributors to the actuator friction are the motor and harmonic drive. For the motor, both the static and dynamic friction must be

considered. The static friction represents how much torque is required to start the motor spinning, while the dynamic friction describes the viscous damping felt by the motor. These values for the two motors used in the exoskeleton are shown in Table 9 below.

Table 9: Motor friction effects on actuator output torque

	Starting Torque (Nm)	Viscous Damping (Nm/RPM)
RBEH-01810	3.504	6.36E-06
RBEH-01811	5.12	1.29E-05

For the harmonic drive, static and dynamic friction must also be considered. Here, the static friction is represented by the starting torque, and dynamic friction is characterized by torque efficiency. Data for the two harmonic drives used in the exoskeleton is shown in Table 10 below.

Table 10: Harmonic drive friction effects on actuator output torque

	Efficiency at 3500 RPM, 25° C (%)	Starting Torque (Nm)
CSD-20-160	54	0.034
CSF-20-160	64	0.029

Together, the friction losses from the motor and transmission therefore represent less than 5% of the stall torque capacity, which is significantly less than the gravity loading.

5.5 Component Selection

The next task was to decide which motor and which harmonic drive to use. Most commonly, these devices are sold prepackaged. That is, the motor would come as a housing with the rotor and stator preassembled inside, and the harmonic drive would also come with its own housing with the circular spline, flex spline, wave generator, and Oldham coupling preassembled inside. This works well for some applications, but it can

lead to excessive bulkiness and weight when custom designing an actuator. For this reason, the "component set" version of these devices was used in the actuator design. This version comes with only the main components, so that a custom housing, drive shaft, supports, and etcetera can be designed to package both the motor and harmonic drive together. This design approach imposes an important requirement on the motor and harmonic drive selection. In order to make packaging the motor with the harmonic drive easier, both components should have roughly the same outer diameter.

For the elbow actuator, the harmonic drive selection was based on the required torque of 37.9 Nm. In addition, an effort was made to minimize the axial length of the transmission so that other components (such as the torque limiter) could be accommodated within the actuator without making the actuator excessively long. The CSD series of HD Systems harmonic drives is a shorter version of the traditional cup-type harmonic drive. Therefore, this was the only type of transmission considered for the elbow actuator. Also, only harmonic drives and motors with an outer diameter of 70 mm or less were considered. This restriction emerged from studying the third manipulator prototype. The larger the actuator diameter, the more the joint limits are restricted. In an effort to give as much latitude to the joint limits as possible without overly restricting the actuator design, the diameter limit of 70 mm was set for the harmonic drive and motor. The smallest harmonic drive of this series capable of transmitting 37.9 Nm of output torque is the CSD-20, which has an outside diameter of 70 mm and comes in three different models with varying gear ratios and repeat peak torques.

Table 11: Harmonic drive decision matrix for the elbow

Harmonic Drive Model	Gear Ratio	Outer Diameter (mm)	Mass (Kg)	Repeat Peak Torque (Nm)	Repeat Peak Torque/Gear Ratio (Nm)
CSD-20-50	50	70	0.13	39	0.78
CSD-20-100	100	70	0.13	57	0.57
CSD-20-160	160	70	0.13	64	0.4

The harmonic drive that most closely meets the torque requirement is the CSD-20-50 model. The last column in the chart represents the amount of input torque required to achieve the repeat peak torque. If the CSD-20-160 model is used instead of the CSD-20-50, then a weaker motor can be paired with the harmonic drive while achieving a higher maximum torque output.

In order to choose the accompanying motor, Kollmorgen's line of brushless DC motors was considered. To determine the desired motor stall torque, the harmonic drive's repeated peak torque was divided by its transmission ratio. Here, the desired torque is 0.40 Nm. However, the maximum momentary torque of the harmonic drive should also be considered. If this value is exceeded, the harmonic drive may be damaged. Therefore, a motor should be selected that cannot provide this amount of torque. For the CSD-20-50 model harmonic drive, the maximum momentary torque is 76 Nm. The input torque that would provide the maximum momentary torque is 0.475 Nm. Therefore, a motor should be selected that has a stall torque close to 0.40 Nm, but not exceeding 0.475 Nm.

Table 12: Motor decision matrix for the elbow

Motor Model	Stall Torque (Nm)	OD (mm)	Axial Length (mm)	Mass (Kg)
RBEH-1213	0.387	49.200	40.640	0.344
RBEH-1214	0.467	49.200	48.260	0.428
RBEH-1511	0.384	60.350	27.940	0.298
RBEH-1810	0.429	75.970	23.500	0.340

Listed above are the only motor models that met the aforementioned criterion. The RBEH-01511 model is lightest, its outer diameter is within the range of the target diameter (≤ 70 mm), and its axial length is the shortest of the four. However, this model motor is prohibitively expensive for this project. The next best choice, model RBEH-01810, is slightly heavier, slightly longer, but still has a diameter within the range of the target diameter. In addition, this model motor is affordable.

For the shoulder actuators, again the harmonic drive selection was based on the required torque of 74.9 Nm. For these actuators, axial length was not as much of a concern as it was for the elbow actuator. Therefore, the shorter but weaker CSD series harmonic drives were not considered. Instead, the traditional cup-type CSF series harmonic drives and the high-torque CSG series harmonic drives were considered. Again, only harmonic drives and motors with an outer diameter of 70 mm or less were considered.

Table 13: Harmonic drive decision matrix for the shoulder

Harmonic Drive Model	Gear Ratio	Outer Diameter (mm)	Mass (kg)	Repeat Peak Torque (Nm)	Repeat Peak Torque/Gear Ratio (Nm)
CSF-20-100	100	70	0.28	82	0.82
CSF-20-120	120	70	0.28	87	0.73
CSF-20-160	160	70	0.28	92	0.58
CSG-20-80	80	70	0.28	96	1.20
CSG-20-100	100	70	0.28	107	1.07
CSG-20-120	120	70	0.28	113	0.94
CSG-20-160	160	70	0.28	120	0.75

The harmonic drive that most closely meets the torque requirements is the CSF-20-100 model. However, if the CSF-20-160 model is used instead, then a weaker motor can be paired with the harmonic drive while achieving a higher maximum torque output. The same harmonic drive was chosen for each of the three shoulder actuators because it is the only way to ensure that the overall minimum requirements for the shoulder as a whole are met in every angular configuration of the shoulder.

For the motor selection, again Kollmorgen's line of DC brushless motors was considered. Using the same type of analysis used to determine the elbow motor, a motor was found that has a stall torque close to 0.575 Nm, but not exceeding 0.919 Nm (based on a momentary peak torque of 147 Nm).

Table 14: Motor decision matrix for the shoulder

Motor Model	Stall Torque (Nm)	OD (mm)	Axial Length (mm)	Mass (kg)
RBEH-01214	0.467	49.20	48.26	0.428
RBEH-01215	0.639	49.20	66.04	0.624
RBEH-01512	0.508	60.35	34.29	0.406
RBEH-01513	0.645	60.35	40.64	0.514
RBEH-01514	0.808	60.35	48.26	0.644
RBEH-01515	0.897	60.35	53.34	0.730
RBEH-01811	0.856	75.97	31.75	0.561

While some models in the RBEH-012xx and RBEH-015xx are better suited, they are either prohibitively expensive or unavailable in small quantities. Therefore, RBEH-01811 was chosen because it met all of the requirements and was also affordable.

For the scapula actuator, the harmonic drive selection was based on the required torque of 90.9 Nm. The same set of harmonic drives was considered for this application as was considered for the shoulder transmissions.

Table 15: Harmonic drive decision matrix for the scapula

Harmonic Drive Model	Gear Ratio	Outer Diameter (mm)	Mass (kg)	Repeat Peak Torque (Nm)	Repeat Peak Torque/Gear Ratio (Nm)
CSF-20-160	160	70	0.28	92	0.58
CSG-20-80	80	70	0.28	96	1.20
CSG-20-100	100	70	0.28	107	1.07
CSG-20-120	120	70	0.28	113	0.94
CSG-20-160	160	70	0.28	120	0.75

Once again, the CSF-20-160 model harmonic drive is the best choice, and therefore the RBEH-01811 must also be chosen as the best model motor for this application.

In summary, each actuator on the manipulator has the following characteristics:

Table 16: System characteristics for the exoskeleton manipulator

	Motor Characteristics				Transmission Characteristics				System Characteristics		
Actuator	Model	Stall Torque (Nm)	Mass (kg)	Outer Diameter (mm)	Model	Gear Ratio	Mass (kg)	Outer Diameter (mm)	Stall Torque (Nm)	Total Mass (kg)	Delta O.D. (mm)
Scapula	RBEH-01811	0.856	0.561	75.97	CSF-20-160	160	0.28	70	136.96	0.841	-5.97
Shoulder 1	RBEH-01811	0.856	0.561	75.97	CSF-20-160	160	0.28	70	136.96	0.841	-5.97
Shoulder 2	RBEH-01811	0.856	0.561	75.97	CSF-20-160	160	0.28	70	136.96	0.841	-5.97
Shoulder 3	RBEH-01811	0.856	0.561	75.97	CSF-20-160	160	0.28	70	136.96	0.841	-5.97
Elbow	RBEH-01810	0.429	0.340	75.97	CSD-20-160	160	0.40	70	68.64	0.740	-5.97

It should be noted that the maximum actuator torques are far greater than the target torques. The reason for this is that in the motor selection, the motors were chosen to match the capability of the harmonic drive instead of the output torque requirement. There are several reasons why this was done. While this decision did necessitate more powerful motors, these motors were not significantly more massive than the motor that would have been chosen if the motor was sized to fit the actuator torque requirement. Also, slightly oversizing the actuators prevents the hardware from being the limiting factor in actuator torque capability. Instead, the software can be coded to artificially limit the output torque if so desired. The torque margin created by oversizing the actuators can also accommodate any error in the manipulator model used to estimate the gravity-

generated torque in worst-case poses. Lastly, larger motors draw less current than smaller motors for the same torque. Less current means that less heat will be generated, which is important in a device that will be in such close proximity to people.

5.6 Torque Limiter

A safety feature mentioned in Section 3.4 is the ability of the manipulator to move freely during the event of a muscle spasm. The easiest way to accomplish this is to utilize a device that mechanically decouples the actuators from the main structure of the arm when a predetermined torque threshold is exceeded. Such a device is already commercially available and is known as a torque limiter. It is a passive mechanical device, meant to be installed in series with the drive train. If a predetermined torque is exceeded, then the torque limiter allows the output to twist freely with respect to the input. Because these devices are relatively large and massive, it was decided that only one actuator (the elbow) would be designed to accommodate a torque limiter. If it were found that the torque limiter proved to be indispensable, then one would be designed into all the actuators in a future generation of the design. This design of the exoskeleton, however, will only use the torque limiter experimentally. As a torque limiter's torque capacity increases, so does its mass. Therefore, the model that was selected was the lightest one available that had a torque range matching the torque range of the elbow actuator.

5.7 Wire Routing

In any electromechanical device, accommodations must be made for the physical integration between electrical and mechanical components. For example, mounting points for circuit boards may be required in the design, as may routes for various wires and cables. Although mounting points and wire routes were included in the actuator design with relative ease, due consideration was not given to wire routes external of the individual actuators. All wires coming out of the actuators needed to terminate in an electronics box located behind the scapula actuator. To accomplish this, the wires were bundled together in braided expandable sleeves and zip-tied to the links.

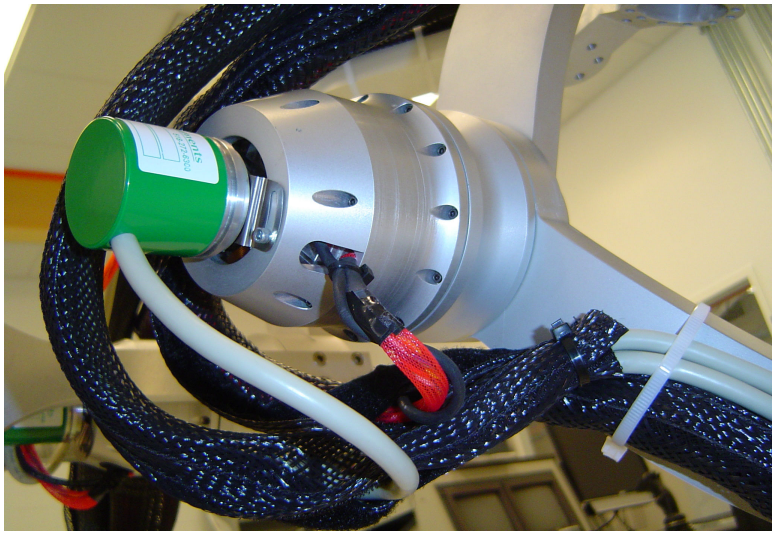

Figure 26: Typical wire routing scheme on exoskeleton manipulator

This type of wire routing left the wires vulnerable in several places to being pinched by the manipulator. In addition, it made for a less than ideal aesthetic. Given more time during the design process, wire routing could have been given more consideration, and the aforementioned problems, although minor, could have been avoided by reducing the total amount of wires or providing a better path for the wires.

Chapter 6 Sensor and Safety System

The control system that will govern the motion of this manipulator requires sensory inputs in order to function properly. In general, the two types of data the control system needs are the joint angles and the contact forces between the manipulator and the human arm. Also, the safety system requires additional sensor capability. Specifically, the safety system needs to be able to sense when the torque limiter has been engaged and when one of several "emergency stop" buttons has been activated.

6.1 Encoders

As discussed in the project requirements section, two different sensors are used to measure joint angles for each actuator. One reason for this redundancy is safety. If one sensor is reporting false values, then this situation can be detected because the readings from both sensors will not agree. Another reason for this redundancy is to allow both high accuracy and absolute positioning in the angular readings. The importance of absolute positioning is that it will allow the controller to know exactly how the manipulator is configured as soon as it is powered up. If only incremental positioning were used, then the manipulator would first have to go through a start-up sequence during which each joint would move to a known location and then "zero" itself.

To this end, both incremental and absolute angular encoders were used on each actuator. The incremental encoder was fixed to the input side of the actuator transmission so that its accuracy would be maximized. The absolute encoder was fixed to the output of the actuator transmission so that the limits on its angular sensing capabilities would not be exceeded. Because both types of encoders must be connected in series with the motor and harmonic drive, axial length was a criterion under which the encoders were chosen. As with the motors and harmonic drives, angular encoders are available as a stand-alone unit or as a "component set," with none of the support structure. The former is easier to use, but the latter gives the designer more flexibility in how it integrates into the actuator design. A component set was chosen for the incremental encoder, but a stand-alone absolute encoder had to be chosen because no reliable component set was available.

The incremental encoder that was chosen was a Numerik Jena optical encoder with 1800 lines per revolution and quadrature capability, giving it an effective output (post-transmission) resolution of 0.31 milli-degrees. Most of the sensor decision making was performed by the electronics team associated with this project. However, from a mechanical perspective, this encoder was chosen to have an appropriately sized outer diameter, a large enough through-hole, and a very small axial length. In addition, this encoder was chosen because it was available as a component set and could therefore be tightly packaged within the actuator. As with the incremental encoder, the absolute encoder was specified mostly by the electronics team. After all of the electronic requirements were specified, the small Gurley model A37 absolute encoder was chosen, which has 12 bits of resolution.

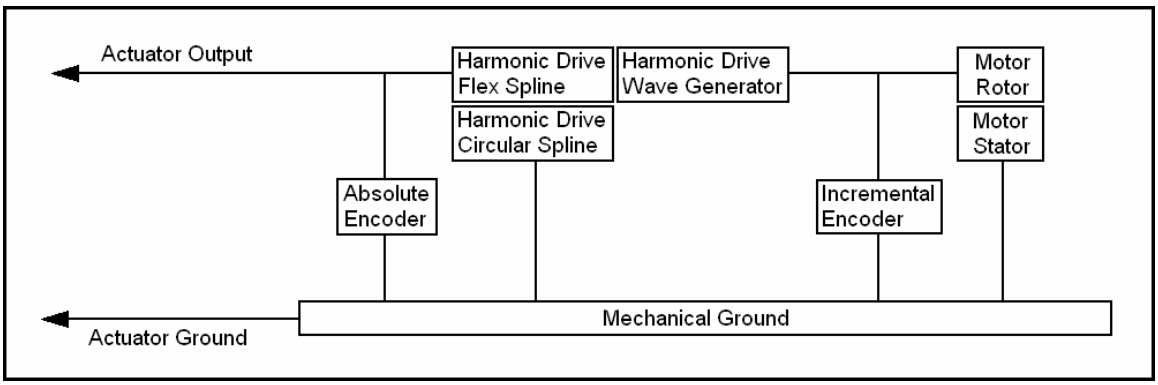

Figure 27: Block diagram of mechanical connections within the actuators

Figure 27 shows how the absolute and incremental encoders mechanically connect to other components within the actuator.

6.2 Force Sensors

In order for exoskeleton to react to interaction forces with the human arm, it must be able to sense these forces. To do this, the number of sensing DOFs must be greater than or equal to the number of kinematic DOFs of the manipulator, although this does not guarantee controllability of all kinematic DOFs. The 5 kinematic degrees of freedom can be described by the scapula angle, the 3-DOF position of the handle, and the SEW angle. The SEW angle is the angle that the plane defined by the shoulder center, elbow center, and wrist center makes with some stationary reference vector. In Figure 28, the SEW plane is defined by the points "S,"" E," and "W," while the reference vector is represented by $\hat{p}_l$. Thus, the SEW angle is given by ϕ.

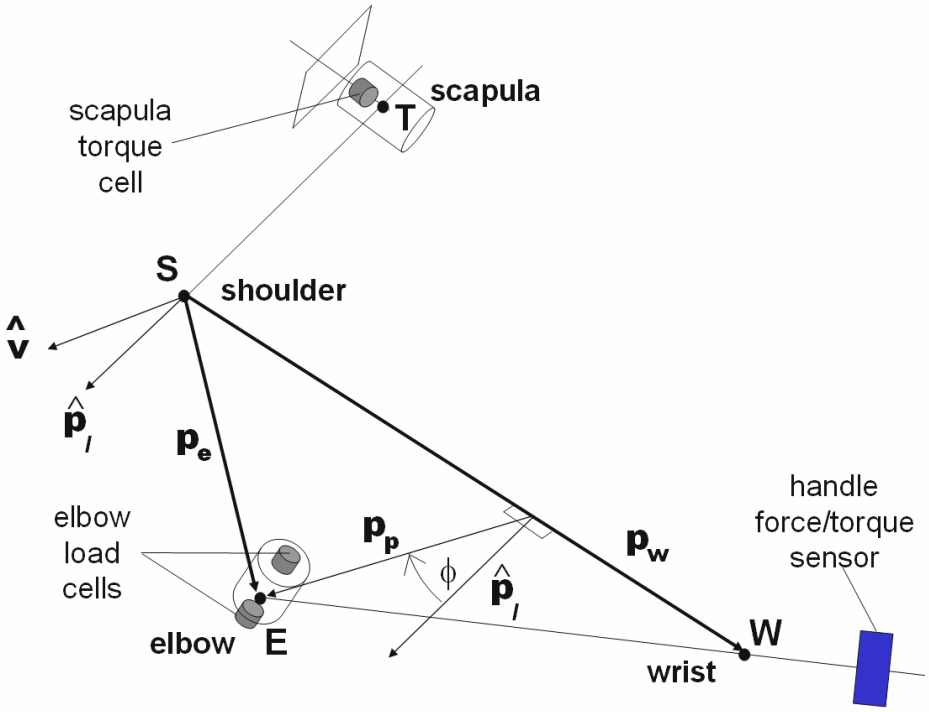

Figure 28: Illustration of SEW angle

Accordingly, force sensors were chosen to mirror this description of the manipulator kinematics. A 6-DOF force/torque sensor – only the three translational DOFs are used – was installed in the handle mount. Additionally, a torque cell was installed in the scapula actuator and two compression load cells were placed on either side of the elbow. The two compression load cells worked together to provide one full DOF, as each compression cell only describes half of a degree of freedom.

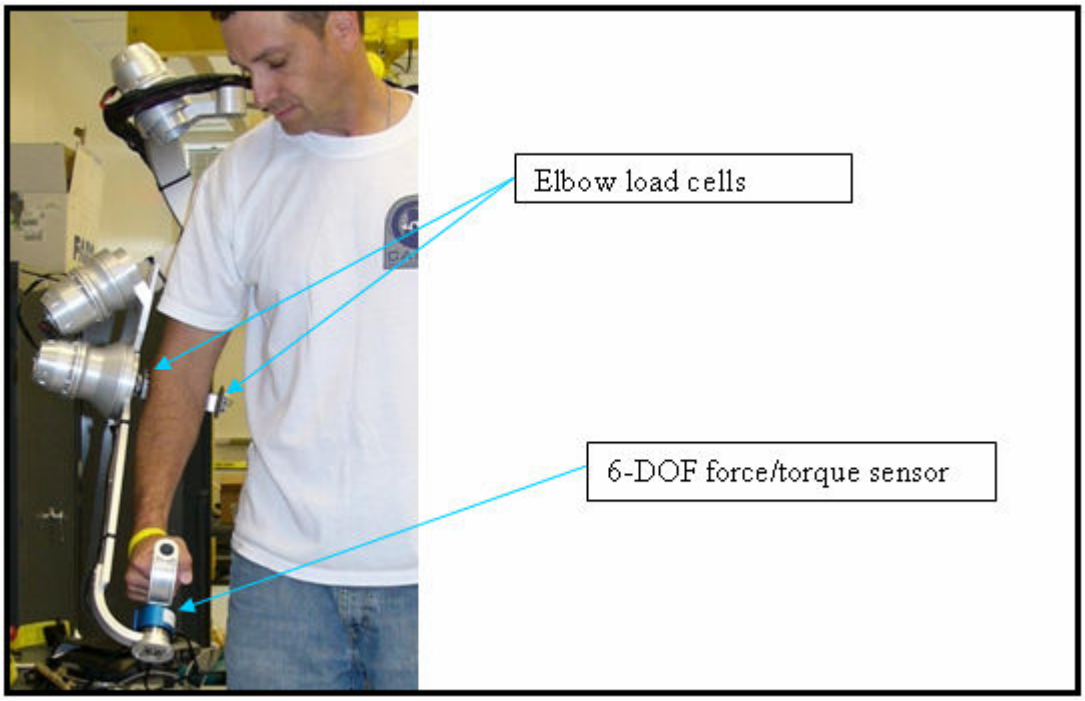

Figure 29: Contact force sensor layout

Lastly, there must be a force sensor for the scapula DOF. This sensor came in the form of a single DOF torque cell installed in series with the output of the scapula actuator. This will allow the scapula to be commanded independently from the other 4 active DOFs.

6.3 User Interface

In order for the exoskeleton to be able to impart forces onto the user, the two must physically interact. The previous section described how reaction forces are measured, but there must be an interface in between the sensor and the user. For the force sensor at the hand, there is a handle that the user can grasp and easily release, if necessary. For the load cell at the elbow, there is a metal bracket attached to a Townsend™ Low Profile Dual Hinge ROM elbow brace using Velcro ® straps. The brace and straps secure the

user's upper arm to the load cells while providing a quick release mechanism (Figure 19). The scapula torque cell does not need a user interface since it is measuring the reaction force indirectly.

6.4 Torque Limiter Activation

As previously discussed, the elbow actuator is torque limited by a purely mechanical device. However, the software system needs to be aware of when the torque limiter is tripped so that it can temporarily halt all manipulator motion. In order to do this, two push-button switches were installed near the torque limiter. When the torque limiter is tripped, a collar on the torque limiter moves axially, activating the push-button switches. The reason there are two push-button switches is for safety and sensor redundancy.

6.5 Emergency Stop

Another aspect important to safety is the inclusion of emergency stop buttons. Along with one next to the operator, there is one mounted in the manipulator handle. The latter must be activated in order for the arm to run, while activation of the former will cause the exoskeleton to deactivate.

Chapter 7 Mechanical Analysis

Although many of the project requirements were satisfied theoretically in the design process, it is important to verify that the final product actually meets the design goals. In this chapter, range of motion and joint torques will be discussed along with a modal analysis of the exoskeleton.

7.1 Range of Motion

As with any robotic device, the workspace is a very important characteristic. However, defining a workspace can be very complicated, especially with the exoskeleton. In this case, only parts of the workspace were defined in the original project requirements. Therefore, only those parts will be verified in the final design. In the project requirements, range of motion minimums were set for the shoulder and scapula combined, and the elbow separately. Verification of the elbow range of motion is trivial, since it only comprises one DOF. In order to verify the shoulder/scapula range of motion, the shoulder and scapula were analyzed separately. First the joint limits of the shoulder in abduction/adduction, flexion/extension, and medial/lateral rotation were calculated using a geometric approach to inverse kinematics. Because the exoskeleton shoulder is comprised of three intersecting axes that are serially perpendicular, this method of inverse kinematics is very straight-forward. The orientation of the first shoulder axis is always known because it does not change direction when the manipulator moves; it is

fixed with respect to the scapula. For a given orientation of the manipulator, the orientation of the third shoulder axis can be found easily because it has a constant angular offset from the manipulator's orientation. Since the second shoulder axis is perpendicular to both the first and third shoulder axes, it can be calculated as the vector cross product of the first and third axes. Considering just the three shoulder axes, the link frames can be described by Figure 30, where frame {0} is the base frame, frame {1} corresponds to the first shoulder joint, frame {2} corresponds to the second shoulder joint, frame {3} corresponds to the third shoulder joint, and frame {T} represents the orientation of the tool tip.

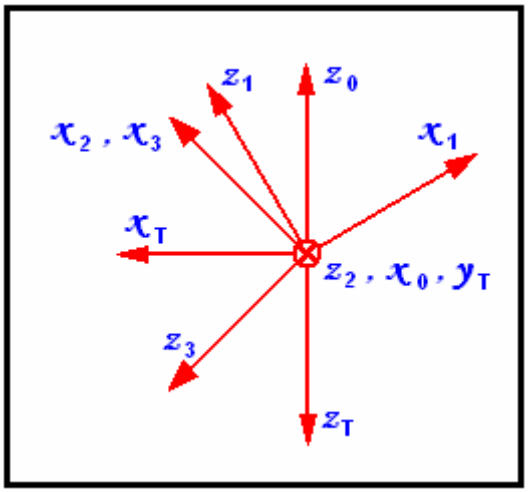

Figure 30: Link frames for shoulder analysis

Because z_1 is always 30° offset from z_0, z_1 can be written as:

$$ {}^{0}\underline{z}_1 = \frac{1}{2}\begin{bmatrix} 0 \\ 1 \\ \sqrt{3} \end{bmatrix} \tag{11} $$

Also, because z_3 is always 45° offset from z_T, z_3 can be written as:

$$ {}^{T}\underline{z}_3 = \frac{1}{2}\begin{bmatrix} \sqrt{2} \\ 0 \\ \sqrt{2} \end{bmatrix} \tag{12} $$

For the inverse kinematics problem, ${}^{0}R_T$, which describes the transformation between the {T} frame and the {0} frame, is always given. Thus, a description of z_3 in the {0} frame can be found:

$$ {}^{0}\underline{z}_3 = {}^{0}R_T \cdot {}^{T}\underline{z}_3 \tag{13} $$

Once both the third shoulder joint axis and the first shoulder joint axis are known in the same frame, the second shoulder joint axis direction can be calculated using the vector cross product:

$$ {}^{0}\underline{z}_2 = {}^{0}\underline{z}_3 \times {}^{0}\underline{z}_1 \tag{14} $$

Now that the directions of all three shoulder axes are known, the dot product can be used to determine the corresponding joint angles.

$$ \theta_1 = \cos^{-1}\left(\frac{\underline{x}_0 \cdot \underline{z}_2}{|\underline{x}_0||\underline{z}_2|}\right) \tag{15} $$

$$ \theta_2 = \cos^{-1}\left(\frac{\underline{z}_1 \cdot \underline{z}_3}{|\underline{z}_1||\underline{z}_3|}\right) \tag{16} $$

$$ \theta_3 = \cos^{-1}\left(\frac{\underline{y}_T \cdot \underline{z}_2}{|\underline{y}_T||\underline{z}_2|}\right) \tag{17} $$

While equations (15), (16), and (17) give the joint angles in the shoulder, some correction factor (e.g. ±180°) must be applied such that the values conform to the D-H definition of joint angles.

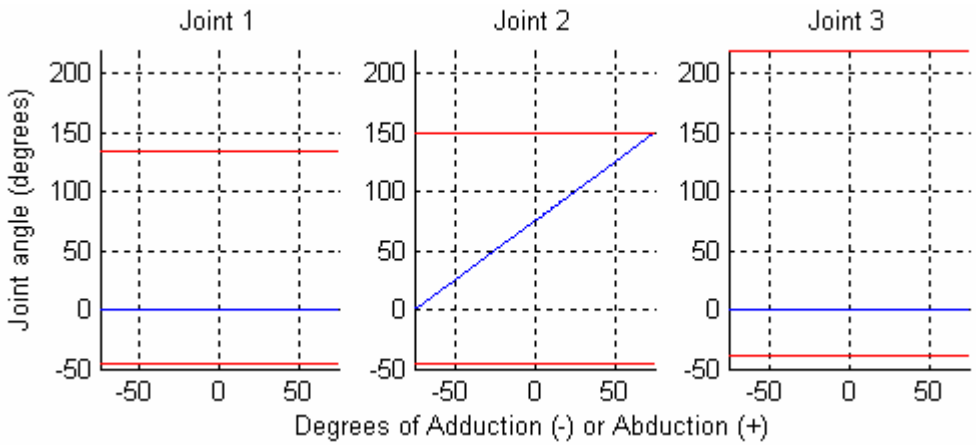

Figure 31: Shoulder joint angles as a function of abduction/adduction angle

Figure 31 shows the D-H joint angles in blue of the individual shoulder axes throughout the abduction (positive angle) and adduction (negative angle) motions, where zero abduction is achieved when the arm is pointing straight down ("home" position).

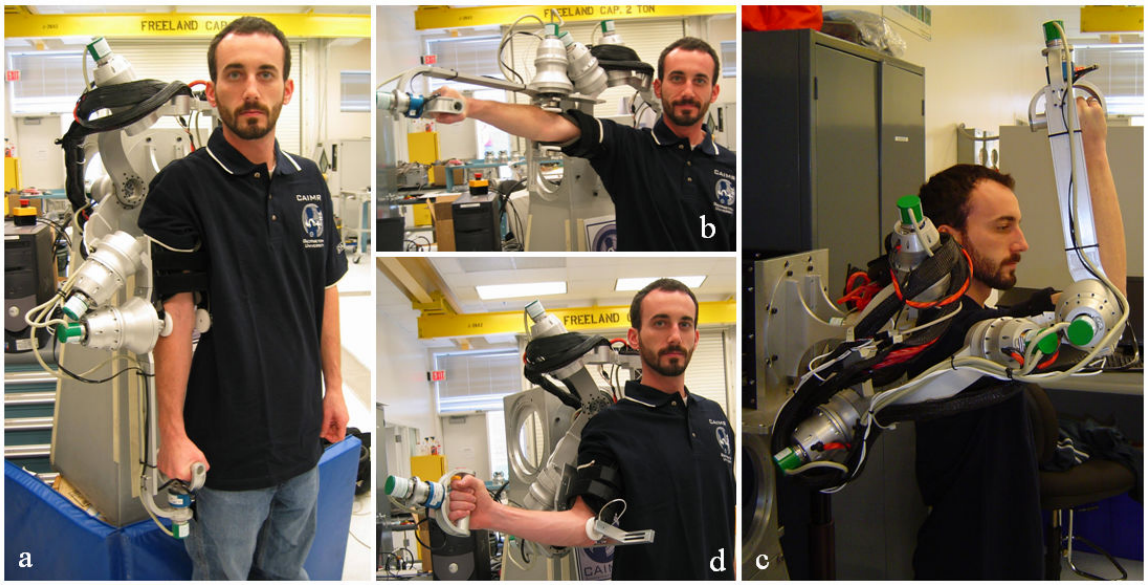

Figure 32: (a) "home" position of arm, (b) near maximum shoulder abduction, (c) near maximum shoulder flexion, (d) near maximum shoulder medial rotation

The red lines represent the physical joint limits of the individual actuators. Once 75 degrees of abduction has occurred, shoulder joint 2 hits its joint limit. Thus, the shoulder

cannot contribute any more motion towards pure abduction. However, the scapula joint axis is also parallel to the abductive rotational axis. It can contribute another 30 degrees towards pure abduction. Thus, the total amount of pure abduction able to be produced by the manipulator is 105 degrees.

In the opposite direction, proceeding from straight down, the adductive (motion towards the body) limit of the shoulder is also 75 degrees, but not because of any individual joint limit. In this case, the limit is the result of a singularity encounter. Once 75 degrees has been reached, the first shoulder joint axis aligns perfectly with the third shoulder joint axis. If the singularity could be ignored, then the manipulator would be able to adduct another 50 degrees before reaching a physical joint limit.

A similar analysis can be done for shoulder flexion/extension.

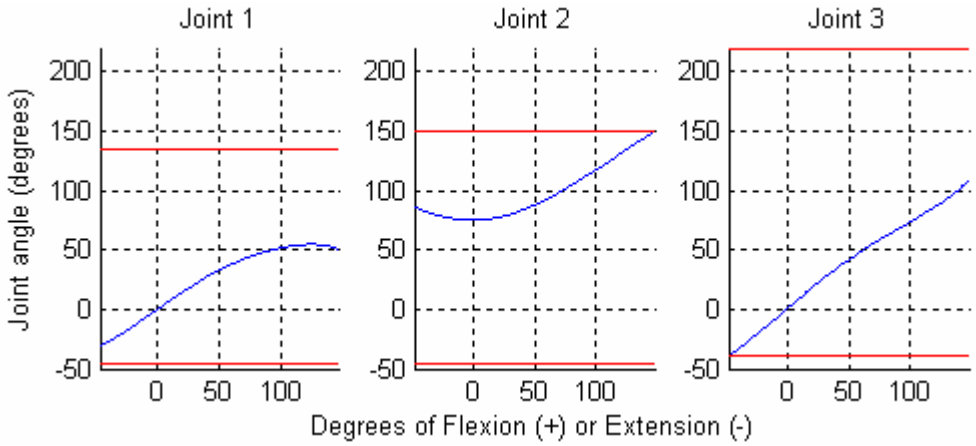

Figure 33: Shoulder joint angles as a function of flexion/extension angle

Here, extension movement is limited by the third shoulder actuator meeting its joint limit, and flexion movement is limited by the second shoulder actuator. The total amount of

pure extension possible with this manipulator is 46.5 degrees, and the amount of flexion is 146.8 degrees.

Lastly, the same study is completed for shoulder medial/lateral rotation.

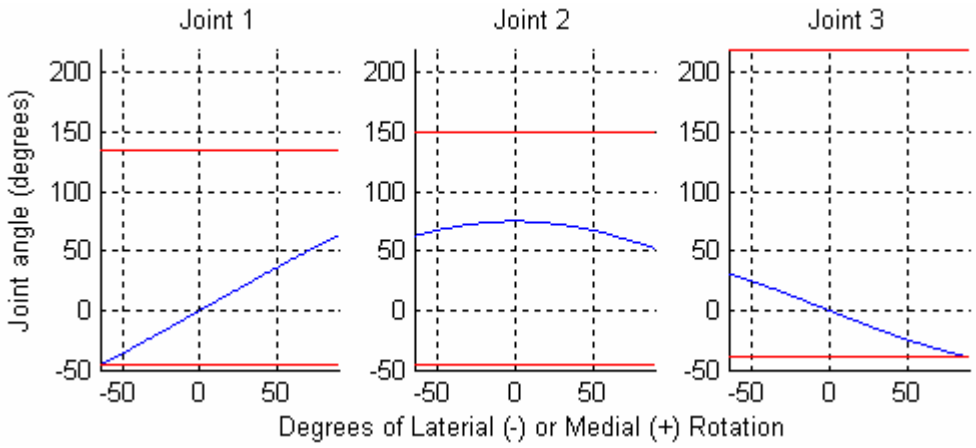

Figure 34: Shoulder joint angles as a function of medial/lateral rotation angle

Medial rotational movement is limited by the third actuator meeting its joint limit, while lateral rotational movement is limited by the first shoulder joint reaching its joint limit. The total amount of pure medial rotation possible with this manipulator is 89.2 degrees, and the amount of lateral rotation is 63.1 degrees. Table 17 shows a summary of the joint limits of the manipulator in comparison to that of the average human.

Table 17: Human joint limits and manipulator joint limits

	Joint Limit (degrees)	
Shoulder DOF	**Human [11]**	**MGA**
Abduction	134	105*
Adduction	48	75
Extension	61	46.5
Flexion	188	146.8
Medial Rotation	97	89.2
Lateral Rotation	34	63.1

* = includes 30 degrees from scapula

Although there were no requirements on the overall workspace of the exoskeleton shoulder, it might still be useful to observe its properties. The information of interest is what combinations of azimuth, elevation, and roll are possible based upon the exoskeleton kinematics and imposed joint limits. This data is not difficult to obtain, as it can be calculated brute-force using the forward kinematics of the shoulder. However, visualizing the data is a more complicated problem. The data is in the form of an enclosed 3-D surface, which is difficult to represent on paper. Instead, the data was reduced by removing information about roll angle. The result is shown below in Figure 35.

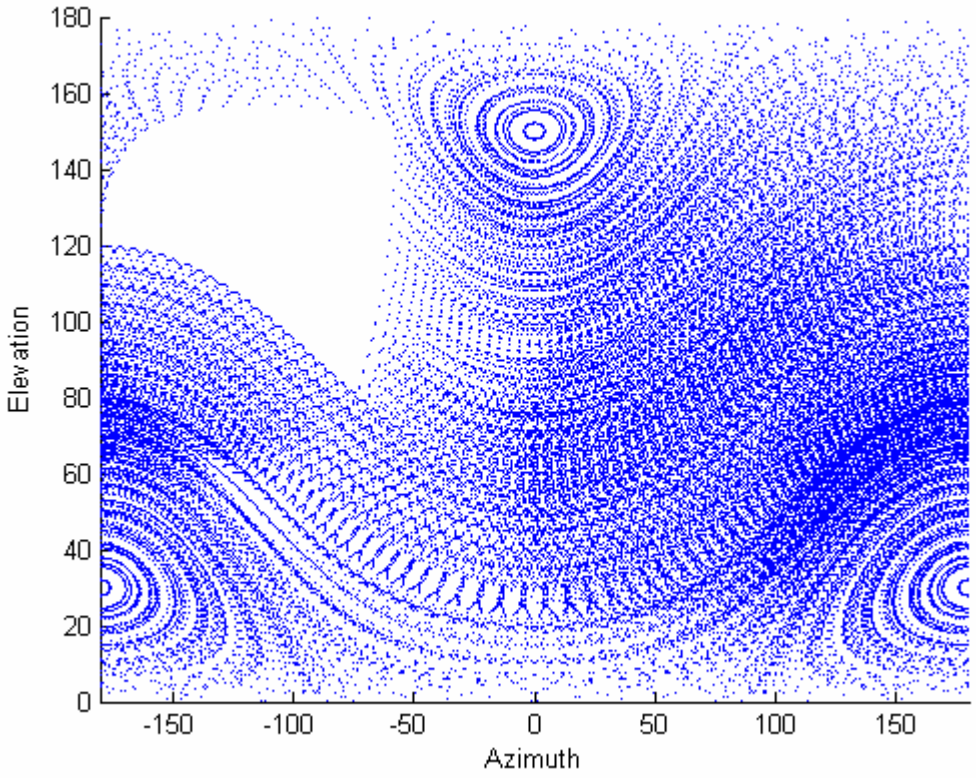

Figure 35: Azimuth and elevation components of the exoskeleton shoulder workspace

The plot was produced by taking a cubic grid of points in shoulder joint space, working them through the forward kinematics of the exoskeleton, then applying inverse kinematics to obtain the azimuth and elevation angles. Here, zero azimuth is defined by a vector in the frontal plane pointing laterally, with positive degrees defined by the right-hand-rule and the vertical vector, and elevation is defined by the angle between the upper arm and the negative vertical. The only region that appears unreachable to the exoskeleton can be seen in the upper-left quadrant of Figure 35. This region, where the arm is pointed straight back and elevated at least 90 degrees, is outside of the workspace of the human shoulder. However, the utility of this graph is limited since it does not account for the self-collision of the exoskeleton. In addition, the plot may show that a

given azimuth and elevation is reachable, but it does not show if the reachable roll angles are within the limits of human capability.

7.2 Torque Limits

In conjunction with calculating joint limits, torque limits were also analyzed. As with joint limits, only certain torque limits were considered. For example, only the abductive torque limit throughout pure abduction, the flexion torque limit throughout pure flexion, and the roll torque limit throughout pure roll were looked at. For any given set of joint angles, computing the torque limit is relatively simple, as the joint torques are defined by

$$\underline{\tau} = J^T \underline{F} \tag{18}$$

where $\underline{\tau}$ is a vector containing the joint torques, J is the Jacobian, and $\underline{F}$ is a vector containing the externally applied forces and torques. Using the link frames in Figure 30, the Jacobian for the shoulder can be written as:

$${}^0J_{Sh,ROT} = \begin{bmatrix} 0 & -\sin\theta_1 & \sin\theta_2\cos\theta_1 \\ \frac{1}{2} & \frac{1}{2}\cos\theta_1 & \frac{1}{2}\left(\cos\theta_2 + \sin\theta_2\sin\theta_1\right) \\ \frac{1}{2}\sqrt{3} & -\frac{1}{2}\sqrt{3}\cos\theta_1 & -\frac{1}{2}\sqrt{3}\left(\cos\theta_2 - \sin\theta_2\sin\theta_1\right) \end{bmatrix} \tag{19}$$

In the abductive case, the only non-zero value in $\underline{F}$ was the torque corresponding to abduction, which was arbitrarily set to f. For a given set of joint angles, the joint torques can be written as:

$$\underline{\tau} = \begin{bmatrix} \alpha_1 f \\ \alpha_2 f \\ \alpha_3 f \end{bmatrix} \tag{20}$$

Where the alphas are constants obtained by substituting in values for θ_1 and θ_2 in equation (19) and then solving equation (18). Taking the infinity-norm of $\underline{\tau}$ gives the largest value of $\underline{\tau}$. The joint corresponding to this value will reach its maximum before the other joints as f is increased. By scaling for f and accounting for the maximum joint torque, the maximum shoulder abductive torque can be written as

$$\tau_{\max} = \frac{T \cdot f}{\left|\underline{\tau}\right|_{\infty}} \tag{21}$$

where T is the maximum torque output of a shoulder actuator. Since f also appears in $\underline{\tau}$, it cancels out of the above equation, and τ_{max} gives the maximum torque in a given direction for a given set of joint angles. The same analysis can be applied to flexion, roll, or any other arbitrary torque axis. A more useful quantity is the maximum shoulder torque minus the torque due to weight of the exoskeleton. The shoulder torque due to the weight of the manipulator is

$$\tau_g = T_w \left|\sin\theta\right| \tag{22}$$

where T_w is the worst-case pose shoulder torque calculated in section 5.3, and θ is the amount of abduction in degrees. The difference between these two torques is shown in Figure 36.

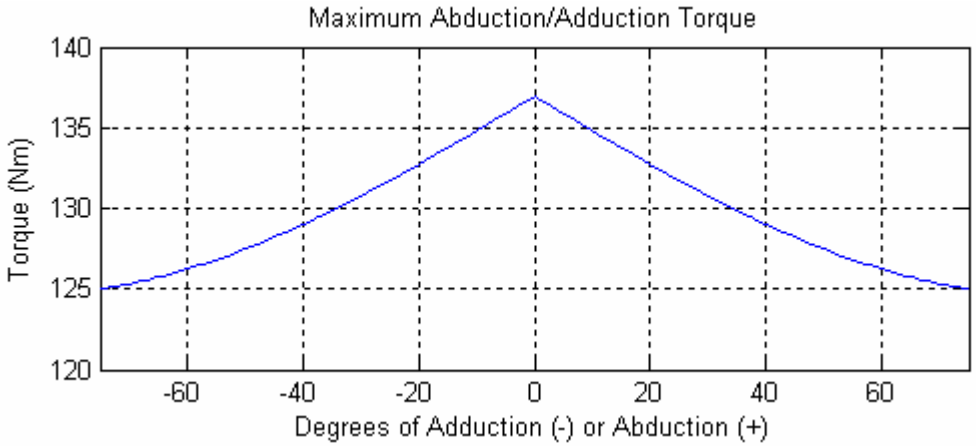

Figure 36: Maximum abduction/adduction torque capacity as a function of abduction/adduction angle

As expected, τ_{max} is constant, but τ_g causes the maximum abduction/adduction torque to vary between 137 Nm and 125 Nm. A similar analysis can be performed for shoulder flexion/extension.

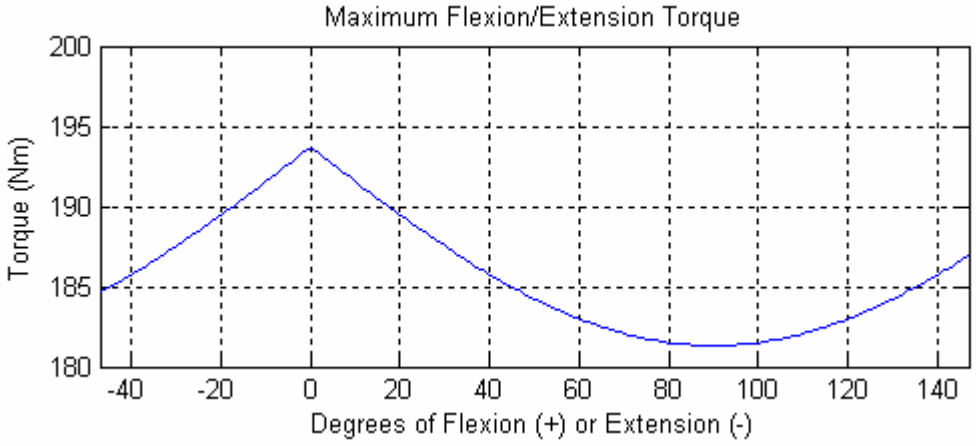

Figure 37: Maximum flexion/extension torque capacity as a function of flexion/extension angle

Again, τ_{max} for flexion/extension is constant, but τ_g causes the maximum flexion/extension torque to vary between 194 Nm and 181 Nm. Throughout the

movement, the third shoulder actuator is the limiting factor, and since its axis always makes the same angle with the flexion torque vector, τ_{max} remains constant.

Again, τ_{max} for medial/lateral rotation is constant. However, τ_g is zero, since the local gravity vector is parallel to the rotation vector. Throughout the movement, the first shoulder actuator is the limiting factor, and since its axis always makes the same angle with the rotation torque vector, τ_{max} remains constant at 158 Nm. Table 18 shows a summary of the torque capacity of the exoskeleton in comparison to the average human torque capacity.

Table 18: Torque capacity for humans and the exoskeleton

DOF		Human Torque (Nm) [31]	Exoskeleton Torque (Nm)
Shoulder	Flexion/Extension	110	125
	Abduction/Adduction	125	181
	Medial/Lateral Rotation	-	158
Elbow	Flexion/Extension	72.5	66

7.3 Flexible Modes

As mentioned in Chapter 0, achieving high stiffness of the manipulator was a driving factor in the design. Since the intended control frequency was 10 Hz, the lowest natural frequency of the manipulator would have to be greater than 20 Hz, according to the Nyquist-Shannon sampling theorem [24]. Initially, this requirement was only used to design the actuator components and not the links. Instead, the links were designed to be strong enough to withstand the expected loads without buckling. Once the exoskeleton was assembled, it was determined that its natural frequency was too low. The natural

frequency was experimentally determined by exciting the exoskeleton with an impulse function and recording the second shoulder joint encoder values.

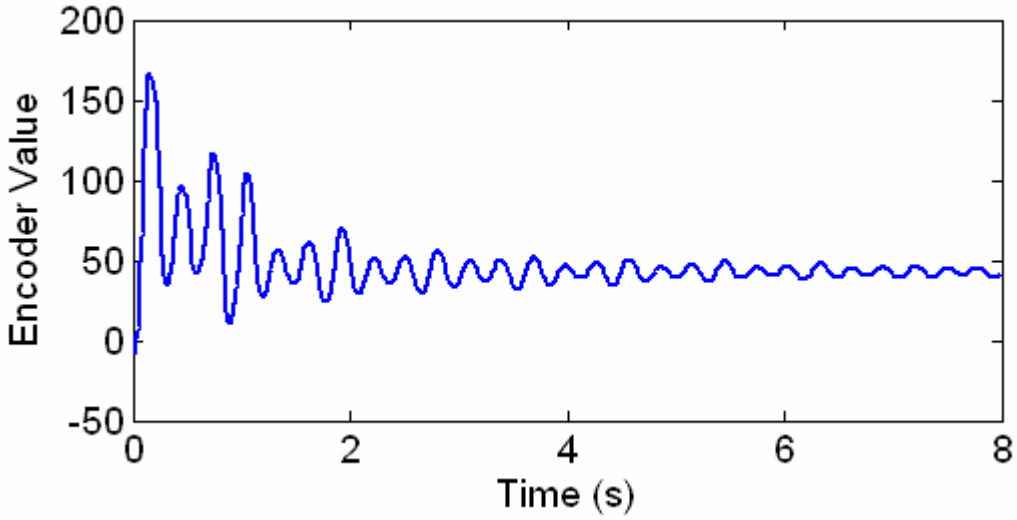

Figure 38: Response of manipulator (with original links) to impulse

An FFT performed on these data revealed the natural frequency to be about 3.3 hertz (in the configuration shown in Figure 23, but with the elbow flexed 90 degrees), whereas the desired natural frequency was 20 Hz.

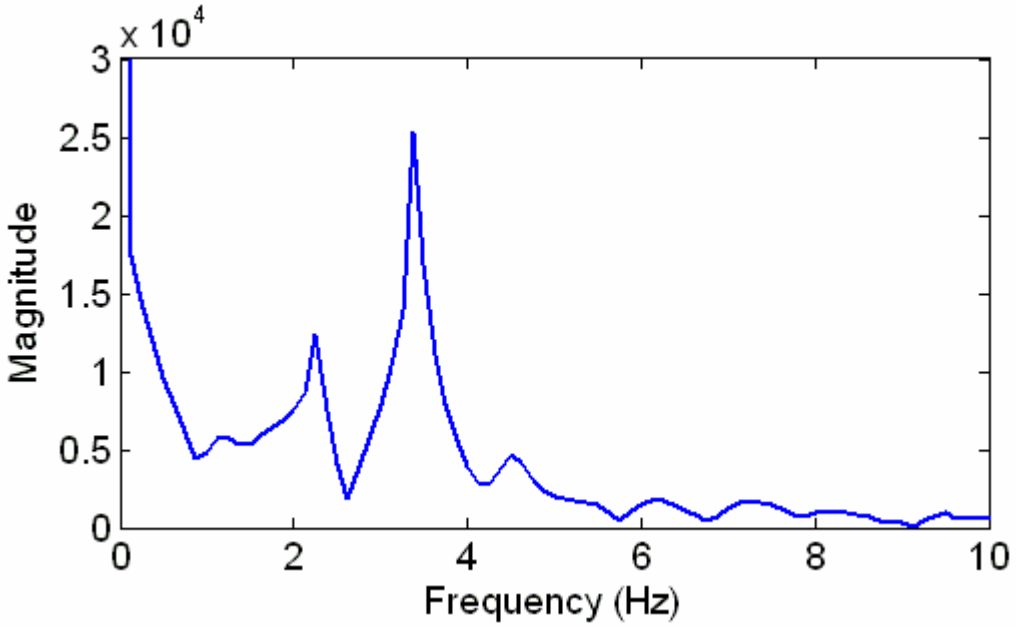

Figure 39: FFT of data in Figure 38

An attempt was made to model the vibration response of the exoskeleton, but time constraints prevented this from being completed.

Since most of the manipulator's flexibility was suspected to originate from the large, curved shoulder links, these components were analyzed individually for their stiffness properties. As a rough estimate, the natural frequency of the arm could be multiplied by a factor of six if the individual link stiffnesses could be multiplied by a factor of 36, since $f_n = \sqrt{k/m}$ for a simple spring-mass system. To determine how the link design should be modified, a modal analysis was performed on the links and the mode shapes and areas of greatest strain were noted. Additional material was added to the links in key locations to stiffen the portions of the link that were most strained at its lowest natural frequency. The link design was then iterated several times in a CAD environment (I-DEAS) in a further attempt to improve the stiffness. Due to cost constraints, the new link design was to affect

the least number of additional components as possible, and it was also to be relatively cheap to manufacture. A solution could not be found that satisfied the time, money, and stiffness requirements. Instead, a design was settled upon that did not exceed the cost or time constraints, but added as much stiffness as possible to the link design.

Figure 40: Original shoulder link design (left) and modified shoulder link design (right), which connects the first shoulder joint with the second shoulder joint

New shoulder links (Figure 40) were designed, fabricated, and fitted to the manipulator. Although the overall stiffness of the manipulator was greatly improved, it still did not provide the minimum desired natural frequency. To measure the natural frequency, the manipulator was excited with an impulse function, and the second shoulder joint encoder output was recorded (Figure 41).

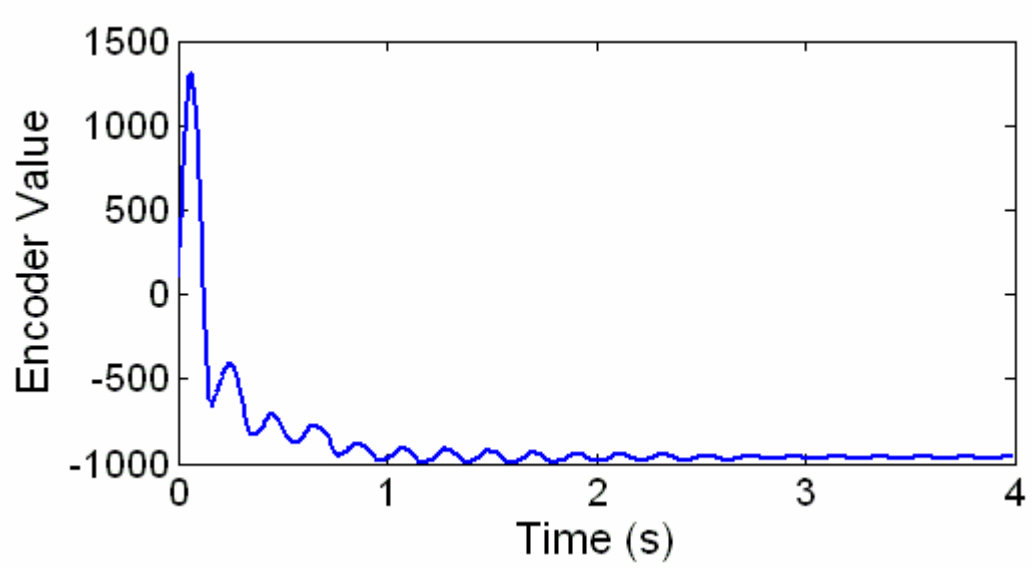

Figure 41: Response of manipulator (with new links) to impulse

A discrete Fourier transform was used to show that the most strongly expressed frequency in the response was about 4.75 Hz.

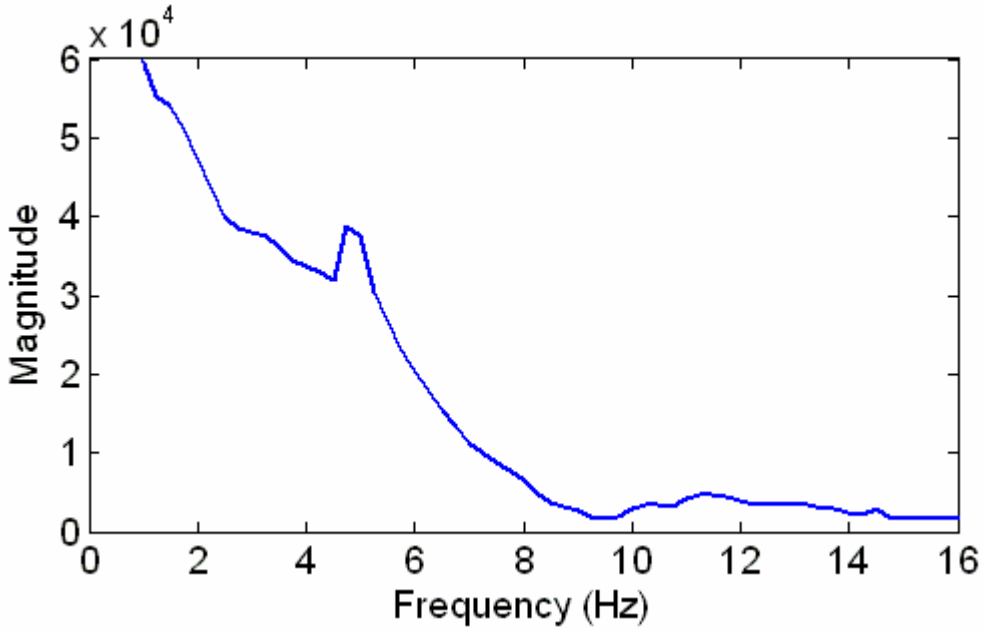

Figure 42: FFT of data in Figure 41

It is important to note that the control bandwidth requirement stems from the desire to use the exoskeleton for VR applications. With its current modal properties, the exoskeleton

can still be used for shoulder rehabilitation, but might not be applicable to high stiffness VR simulations.

7.4 Torque Cell Connection

The scapula actuator is the only actuator that incorporates a 1-DOF torque cell. It is serially connected between the output of the harmonic drive and the output of the actuator. Once the manipulator was assembled, it was discovered that the torque cell's coupling to the harmonic drive introduced some backlash into the actuator. The connection consists of a hub on one side that fits over a shaft on the other side. The shaft has three flats machined into it, equally spaced around the circumference. The hub features three threaded holes, oriented radially from the axis of the hub and also spaced equally about the hub's circumference. When the shaft is inserted into the hub, the threaded holes of the hub align with the flats on the shaft. Set screws are inserted into the threaded holes and tightened against the flats.

This setup is supposed to keep the shaft from spinning relative to the hub. It was assumed that the torque capacity of this connection was at least as much as the torque sensing capability of the torque cell. Since the torque cell was chosen to match the torque capability of the motor and harmonic drive, the torque cell should never be over-torqued, and thus the torque cell connection should not fail. Originally, the only thing considered a failure was complete decoupling of one side of the connection from the other. However, another occurrence that should have also been considered a failure was a loosening of the connection, which produces backlash. Once the connection was torque-cycled a number

of times, the set screws began to locally deform and shear the shaft flats, introducing a significant amount of backlash.

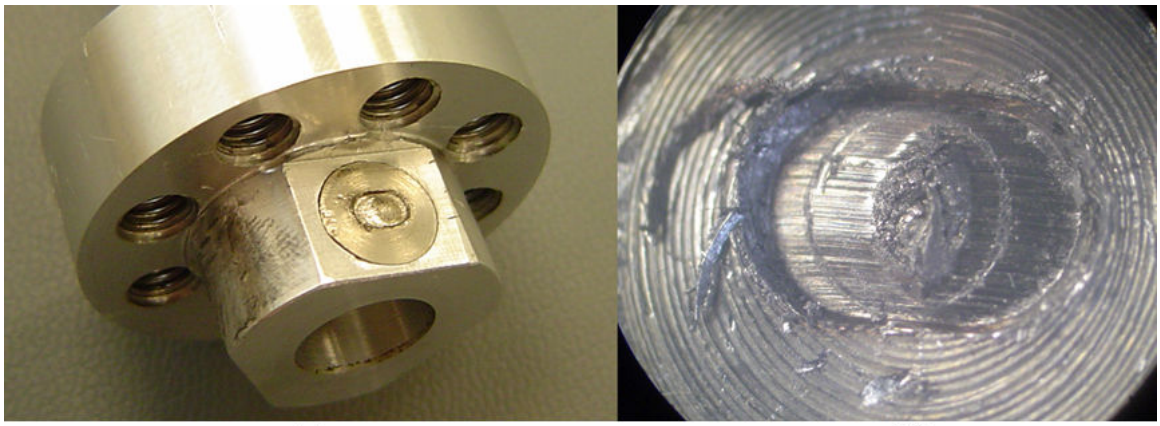

Figure 43: Picture of shaft flats (a) and close-up view of damage (b)

Initially, the cause for this was seen to be the material strength of the flats, since they were machined from aluminum. To remedy this, the flats were drilled out and replaced with steel inserts. This reduced the problem, but did not eliminate it. There was nothing else that could be done to the set-screw connections that would make them any more resistant to backlash. Since the torque cell was designed for a set screw connection, two options existed: 1) remove the torque cell completely and install a new type of connection, or 2) replace the torque cell with a different torque cell that has a more appropriate type of connection. Although the functional requirements necessitate the inclusion of a torque cell in the scapula, the beginning phases of the exoskeleton testing do not require it. Therefore, as a temporary solution, option 1 was considered. Option 2 was decided against because it would require the redesign of many components, which the project cost constraints could not support. Option 1 necessitated the design of a new

component and the modification of another component, and a keyway was chosen to serve as the connection. Standard keyway dimensions were chosen for the shaft and hub based upon the recommendations found in Machinery's Handbook [23]. Rough calculations showed that the key and keyway could withstand the bearing stress induced by the torque applied to the connection. Upon installation of the new component and modification of the old components, it was obvious that the keyway was not strong enough to provide zero backlash. A possible reason for this is that the keyway in the hub was not machined properly, or that the new aluminum shaft is not strong enough. This issue was not pursued any further due to cost constraints.

Chapter 8 Conclusions and Future Work

8.1 Conclusion

Throughout the design and evaluation process many lessons were learned. Although the workspace of a manipulator can be calculated using kinematics, making rough prototypes of the manipulator geometry was very helpful in understanding how the arm self collides. In addition, the prototypes gave some clue as to what reasonable joint limits would be so that workspace could be evaluated. Also, the prototypes could be fitted to people to quickly determine if the human arm's workspace is being limited. While the singular configurations of a manipulator can be calculated, having a prototype or CAD model makes it much easier to visualize the locations of singularities and how these locations change as the manipulator kinematics change. Since the locations of singularities turned out to be a major design consideration, these prototypes became invaluable tools.

The selection of actuator components also provided some valuable lessons. In finding a motor and harmonic drive combination that satisfied the strength requirements, item availability was much more of a factor than expected. Several motors could not be considered because of their long lead time and high cost associated with low volume production runs. Transmission selection was not trivial either, since many of the ideas for how to reduce the arm mass (flexible shafts, cable drives) turned out to be infeasible for

this project. For a robotic manipulator, the drive train should be as stiff as possible. Pursuing flexible transmissions was an unneeded tangent.

Flexibility of the exoskeleton was also a significant issue. Originally, manipulator stiffness was not that high of a priority. Instead, mass and material strength were more of a concern. When it became apparent that the stiffness of the exoskeleton was too low, addressing this problem became a higher priority. Although the exoskeleton's lowest natural frequency is lower than the project requires, this does not mean that the device is unusable until the problem is fixed. The bandwidth requirement was set by the desire to use this device for virtual reality applications. The bandwidth requirement for using the exoskeleton as a rehabilitation device is much lower. Since preliminary evaluation of the device will not include virtual reality applications, the low natural frequency of the exoskeleton is not an immediate problem.

Safety was a significant factor in the design of the exoskeleton. Because this device is intended to be in close proximity with people, it has the potential to cause harm. While many features of the software architecture are intended to mitigate this risk, there are several mechanical components that also contribute. Redundant sensors provide an added level of safety, but they also add weight and bulkiness to the exoskeleton. The slip clutch protects the user from injuring himself during elbow spasms, but it also adds to the size and mass (~0.7 kg) of the elbow actuator.

When assembling the exoskeleton for the first time, several small problems were encountered that necessitated the disassembly of the exoskeleton. During the components design process, special attention was paid to ensuring that the entire device was simple to both assemble and disassemble. This was fortunate foresight, since disassembly was often required. If due attention was not paid, it would have been easy to design an assembly that was impossible to disassemble without destroying some components. If this had been the case, much more time and money would have been spent trying to fix these small problems that were found during initial assembly.

8.2 Future Work

As alluded to in the previous few chapters, there are some features of the exoskeleton that are less than desirable. Although wire routing is adequate for the manipulator's current stage of testing, a cleaner solution should be sought. The likely solution would not be accomplished by a simple design modification. Rather, it would need to be a higher priority functional requirement in the next revision of the manipulator design. Wire management is a much more significant factor in manipulator design than originally thought, and thus it should be considered more carefully in the next design iteration.

In addition, the stiffness of the manipulator needs more attention. The new link design did improve the overall stiffness, but not to a level suitable for virtual reality applications. In the next revision of the design, different link shapes and materials should be analyzed for their contribution to overall stiffness. Also, other factors should be investigated for their effect on stiffness, such as the link-actuator connection and the transmission

stiffness. Lastly, other kinematic configurations could be researched. The ESA exoskeleton [30] uses a combination of parallel and serial manipulators. The parallel mechanism in its shoulder increases the overall stiffness.

The issue of backlash in the torque cell connection should also be addressed in a new exoskeleton revision. Some of the constraints affecting the design of the temporary keyway solution, such as cost, would not be as much of a factor in a completely new design. Lessons learned from this problem could be used in choosing a torque cell and connection type that would accomplish the project requirements more affectively. Instead of a torque cell, a load cell could be placed between the exoskeleton and the top of the user's shoulder. The force measured here could be multiplied by a known moment arm to determine the scapula torque.

Although not a problem in the manipulator design described in this paper, weight is an ever-present issue. The intention for this device is that it be portable, eventually to the point that the entire mass of the manipulator could be comfortably born by the user. A weighing of the entire exoskeleton revealed the mass to be about 13.6 kg, which meets the project requirement of a 15 kg maximum. This figure includes the weight of any electrical wires connecting the actuators to the control computers, but it does not include the structure that connects the scapula to a stable platform. Also included is the new link design, which was discussed in section 7.3. Since this mass figure is meant to be a metric for evaluating the manipulator's usefulness as a wearable device, components of the design that would not appear in the wearable version of the manipulator were not

included in the mass figure. Although 13.6 kg is not an extraordinarily large amount of mass to carry, it may be too much for the weaker subjects likely to need such a device. Thus, in the next design revision, effort must be made to reduce the weight of the manipulator without sacrificing any functionality. This would most likely be accomplished by choosing materials with higher stiffness to density ratios for key components in the manipulator.

There are also some more significant issues that warrant attention. Much of the dynamic properties of the exoskeleton are not known. The only way in which they are discussed in this thesis is through theoretical numbers. Although the frictional properties of the motor and harmonic drive are given by the manufacturer's specification sheets, it would be valuable to take experimental data on the relationship between torque and speed for each actuator and fit a model to the data. Although this has been done for a similarly designed actuator [1], it would be helpful from a controls perspective to have a good model for the exoskeleton.

This thesis included an analysis of the flexible modes of the exoskeleton through experimental data. To better understand how the exoskeleton responds to vibration, the transfer function for the entire mechanism could be found. Once this is understood, the human factor must also be accounted for. Once the exoskeleton is brought in contact with the user's arm, the dynamic properties of the entire system could change dramatically. Essentially, one complete control system is being combined with another complete control system. The effect of this combination should be further researched.

Appendix A: MATLAB Code for Calculating Range of Motion, Torque Capacity, Workspace, and FFT

A.1 abduction2.m

```
%Program: abduction2.m
%Calculates range of motion and torque capacity of shoulder abduction

clear all

z10=[-.5; 0; sqrt(3)/2];              %z1 vector in {0}
z3T=[sqrt(2)/2; 0; sqrt(2)/2];        %z3 vector in {T}
y0=[0;1;0];                           %y0 vector in {0}
RT0i=[-1 0 0; 0 1 0; 0 0 -1];         %rotation matrix between {T} and {0}, initial
theta1=[];
theta2=[];
theta3=[];
n1=75;
n2=75;
T=[];

for theta=-n1:n2;
   thetar=theta*pi/180;
   RT0=RT0i*[cos(thetar) 0 sin(thetar); 0 1 0; -sin(thetar) 0 cos(thetar)];
   z30=RT0*z3T;
   z20=cross(z30, z10)/norm(cross(z30, z10));
   yT0=RT0*[0;1;0];
   theta1=[theta1, acos(dot(y0, z20)/(norm(y0)*norm(z20)))*sign(dot(cross(y0, z20),
z10))];
   theta2=[theta2, acos(dot(z10, z30)/(norm(z10)*norm(z30)))*sign(dot(cross(z10, z30),
z20))];
   theta3=[theta3, acos(dot(yT0, z20)/(norm(yT0)*norm(z20)))*sign(dot(cross(z20, yT0),
z30))];
   J0=[z10, z20, z30];
   F=[0; 1; 0];
   T_ratio=J0'*F;
   T=[T, 136.96/norm(T_ratio, inf)-12.38*abs(sin(theta*pi/180))];
end

figure(1)
subplot(1,3,1)
hold on
plot([-n1:n2], theta1*180/pi)
plot([-n1:n2], -45*ones(1,n1+n2+1), 'r')
plot([-n1:n2], 135*ones(1,n1+n2+1), 'r')
```

```
title('Joint 1')
ylabel('Joint angle (degrees)')
grid on
axis([-n1 n2 -50 220])

subplot(1,3,2)
hold on
plot([-n1:n2], theta2*180/pi+180)
plot([-n1:n2], 150*ones(1,n1+n2+1), 'r')
plot([-n1:n2], -45*ones(1,n1+n2+1), 'r')
title('Joint 2')
xlabel('Degrees of Adduction (-) or Abduction (+)')
grid on
axis([-n1 n2 -50 220])

subplot(1,3,3)
hold on
plot([-n1:n2], theta3*180/pi)
plot([-n1:n2], -39*ones(1,n1+n2+1), 'r')
plot([-n1:n2], 219*ones(1,n1+n2+1), 'r')
title('Joint 3')
grid on
axis([-n1 n2 -50 220])

figure(2)
plot([-n1:n2], T)
title('Maximum Abduction/Adduction Torque')
xlabel('Degrees of Adduction (-) or Abduction (+)')
ylabel('Torque (Nm)')
grid on
axis([-n1 n2 0 200])
```

A.2 extension2.m

```
%Program: extension2.m
%Calculates range of motion and torque capacity of shoulder extension

clear all

z10=[-.5; 0; sqrt(3)/2];          %z1 vector in {0}
z3T=[sqrt(2)/2; 0; sqrt(2)/2];    %z3 vector in {T}
y0=[0;1;0];                       %y0 vector in {0}
RT0i=[-1 0 0; 0 1 0; 0 0 -1];     %rotation matrix between {T} and {0}, initial
theta1=[];
theta2=[];
theta3=[];
n1=47;
n2=147;
T=[];

for theta=-n1:n2;
   thetar=theta*pi/180;
   RT0=RT0i*[1 0 0; 0 cos(thetar) -sin(thetar); 0 sin(thetar) cos(thetar)];
   z30=RT0*z3T;
   z20=cross(z30, z10);
   yT0=RT0*[0;1;0];
   theta2=[theta2, acos(dot(z10, z30)/(norm(z10)*norm(z30)))*sign(dot(cross(z10, z30),
z20))];
   theta1=[theta1, acos(dot(y0, z20)/(norm(y0)*norm(z20)))*sign(dot(cross(y0, z20),
z10))];
   theta3=[theta3, acos(dot(yT0, z20)/(norm(yT0)*norm(z20)))*sign(dot(cross(z20, yT0),
z30))];
   J0=[z10, z20, z30];
   F=[1; 0; 0];
   T_ratio=J0'*F;
   T=[T, 136.96/norm(T_ratio, inf)-12.38*abs(sin(theta*pi/180))];
end

figure(1)
subplot(1,3,1)
hold on
plot([-n1:n2], theta1*180/pi)
plot([-n1:n2], -45*ones(1,n1+n2+1), 'r')
plot([-n1:n2], 135*ones(1,n1+n2+1), 'r')
title('Joint 1')
ylabel('Joint angle (degrees)')
grid on
```

```
axis([-n1 n2 -50 220])

subplot(1,3,2)
hold on
plot([-n1:n2], theta2*180/pi+180)
plot([-n1:n2], 150*ones(1,n1+n2+1), 'r')
plot([-n1:n2], -45*ones(1,n1+n2+1), 'r')
title('Joint 2')
xlabel('Degrees of Flexion (-) or Extension (+)')
grid on
axis([-n1 n2 -50 220])

subplot(1,3,3)
hold on
plot([-n1:n2], theta3*180/pi)
plot([-n1:n2], -39*ones(1,n1+n2+1), 'r')
plot([-n1:n2], 219*ones(1,n1+n2+1), 'r')
title('Joint 3')
grid on
axis([-n1 n2 -50 220])

figure(2)
plot([-n1:n2], T)
title('Maximum Flexion/Extension Torque')
xlabel('Degrees of Flexion (-) or Extension (+)')
ylabel('Torque (Nm)')
grid on
axis([-n1 n2 0 200])
```

A.3 rotation.m

```
%Program: rotation.m
%Calculates range of motion and torque capacity of shoulder rotation

clear all

z10=[-.5; 0; sqrt(3)/2];          %z1 vector in {0}
z3T=[sqrt(2)/2; 0; sqrt(2)/2];    %z3 vector in {T}
y0=[0;1;0];                       %y0 vector in {0}
RT0i=[-1 0 0; 0 1 0; 0 0 -1];     %rotation matrix between {T} and {0}, initial
theta1=[];
theta2=[];
theta3=[];
n1=65;
n2=90;
T=[];

for theta=-n1:n2;
   thetar=theta*pi/180;
   RT0=RT0i*[cos(thetar) -sin(thetar) 0; sin(thetar) cos(thetar) 0; 0 0 1];
   z30=RT0*z3T;
   z20=cross(z30, z10);
   yT0=RT0*[0;1;0];
   theta1=[theta1, acos(dot(y0, z20)/(norm(y0)*norm(z20)))*sign(dot(cross(y0, z20),
z10))];
   theta2=[theta2, acos(dot(z10, z30)/(norm(z10)*norm(z30)))*sign(dot(cross(z10, z30),
z20))];
   theta3=[theta3, acos(dot(yT0, z20)/(norm(yT0)*norm(z20)))*sign(dot(cross(z20, yT0),
z30))];
   J0=[z10, z20, z30];
   F=[0; 0; 1];
   T_ratio=J0'*F;
   T=[T, 136.96/norm(T_ratio, inf)];
end

figure(1)
subplot(1,3,1)
hold on
plot([-n1:n2], -theta1*180/pi)
plot([-n1:n2], -45*ones(1,n1+n2+1), 'r')
plot([-n1:n2], 135*ones(1,n1+n2+1), 'r')
title('Joint 1')
ylabel('Joint angle (degrees)')
grid on
```

```
axis([-n1 n2 -50 220])

subplot(1,3,2)
hold on
plot([-n1:n2], theta2*180/pi+180)
plot([-n1:n2], 150*ones(1,n1+n2+1), 'r')
plot([-n1:n2], -45*ones(1,n1+n2+1), 'r')
title('Joint 2')
xlabel('Degrees of Laterial (-) or Medial (+) Rotation')
grid on
axis([-n1 n2 -50 220])

subplot(1,3,3)
hold on
plot([-n1:n2], -theta3*180/pi)
plot([-n1:n2], -39*ones(1,n1+n2+1), 'r')
plot([-n1:n2], 219*ones(1,n1+n2+1), 'r')
title('Joint 3')
grid on
axis([-n1 n2 -50 220])

figure(2)
plot([-n1:n2], T)
title('Maximum Medial/Lateral Rotation Torque')
xlabel('Degrees of Lateral (-) or Medial (+) Rotation')
ylabel('Torque (Nm)')
grid on
axis([-n1 n2 0 200])
```

A.4 freqdata2.m

```
%Program: freqdata2.m
%Plots time response and frequency response of exoskeleton
%equipped with original links

clear all
load -ascii RESONANCE.txt
x=RESONANCE';
t=[0:.002:8-.002];

figure(1)
plot(t, x)
xlabel('Time (s)')
ylabel('Encoder Value')

X=fft(x);
f=(0:length(X)-1)'/length(X)/.002;
figure(2)
plot(f, abs(X))
xlabel('Frequency (Hz)')
ylabel('Magnitude')
```

A.5 freqdata.m

```
%Program: freqdata.m
%Plots time response and frequency response of exoskeleton
%equipped with modified links

clear all
load -ascii JOINT2_IMPULSE.txt
x=JOINT2_IMPULSE;
t=[0:.004:4-.004];

figure(1)
plot(t, x)
xlabel('Time (s)')
ylabel('Encoder Value')

X=fft(x);
f= (0:length(X)-1)'/length(X)/.004;
figure(2)
plot(f, abs(X))
xlabel('Frequency (Hz)')
ylabel('Magnitude')
```

A.6 R2PsiN

```
function PsiN=R2PsiN(R)
%Converts rotation matrix into angle-axis vector

Psi=acos((R(1,1)+R(2,2)+R(3,3)-1)/2);
N=(1/(2*sin(Psi)))*[R(3,2)-R(2,3); R(1,3)-R(3,1); R(2,1)-R(1,2)];
PsiN=Psi*N;
```

A.7 nonlincircreg.m

```
%Program: nonlincircreg.m
%Calculates least-squares circle fit to data

clear all

x=[-47 -47 -40 -35 -30 -15 -4 -2 -4 0 7 10 10 17 22 21 25 30 34]';  %vert displacement
y=[22 21 23 21 14 8 6 1 -4 0 11 14 9 13 17 13 9 6 5]';              %horizontal displacement
n=length(x);

amin=-50;
amax=50;
bmin=-100;
bmax=200;

F=zeros(amax-amin+1, bmax-bmin+1);

for a=amin:amax
   for b=bmin:bmax
      r=sqrt((x-a).^2+(y-b).^2);
      R=(1/n)*sum(r);
      F(a-amin+1,b-bmin+1)=sum((r-R).^2);
   end
end

[A,B]=meshgrid([amin:amax],[bmin:bmax]);
%surf(A, B, F')

Fmin=min(min(F));
Amin=A(find(F'==Fmin));
Bmin=B(find(F'==Fmin));
Rmin=(1/n)*sum(sqrt((x-Amin).^2+(y-Bmin).^2));

figure(2)
plot(x,y,'o:')
hold on
X=[Amin-Rmin:.1:Amin+Rmin];
Y=-sqrt(Rmin^2-(X-Amin).^2)+Bmin;
plot(X, Y, 'r')
grid on
xlabel('Vertical Displacement [mm]')
ylabel('Horizontal Displacement [mm]')
axis equal
axis([-50 40 -5 25])
```

A.8 workspace2.m

```
%Program: workspace2.m
%Plots the shoulder workspace in terms of azimuth and elevation

clear all

syms t1 t2 t3
%t1=-45:135 (degrees)
%t2=-45:150 (degrees)
%t3=-39:219 (degrees)

R0B=[-sqrt(3)/2 0 -0.5; 0 -1 0; -0.5 0 sqrt(3)/2];          %Rotation matrix from {0} to
{B}
R10=[cos(t1) -sin(t1) 0; sin(t1) cos(t1) 0; 0 0 1];        %Rotation matrix from {1} to {0}
R21=[cos(t2) -sin(t2) 0; 0 0 -1; sin(t2) cos(t2) 0];       %Rotation matrix from {2} to {1}
R32=[cos(t3) -sin(t3) 0; 0 0 -1; sin(t3) cos(t3) 0];       %Rotation matrix from {3} to {2}
RT3=[sqrt(2)/2 0 -sqrt(2)/2; 0 1 0; sqrt(2)/2 0 sqrt(2)/2]; %Rotation matrix from {T} to
{3}
RTB=R0B*R10*R21*R32*RT3;                                   %Rotation matrix from {T} to
{B}

hold on
for theta1=-45:5:135
   for theta2=-45:5:150
      for theta3=-39:6:219
         R=subs(RTB, {t1, t2, t3}, {theta1*pi/180, theta2*pi/180, theta3*pi/180});
         Phi=R2AZEL(R);
         plot(Phi(1)*180/pi, Phi(2)*180/pi)
      end
   end
end
xlabel('Azimuth')
ylabel('Elevation')
```

A.9 R2AZEL.m

```
function phi=R2AZEL(R)
%Converts a rotation matrix into azimuth and elevation angles

zT=R*[0;0;1];
AZ=atan2(-zT(2), -zT(1));
EL=acos(dot(zT, [0;0;-1]));
phi=[AZ, EL];
```

Appendix B: Mechanical Drawings

Drawing Number	Description
FD22-0005	actuator, carrier disk
FD22-0006	actuator, clamp, bearing
FD22-0007	actuator, bearing nut
FD22-0008	actuator, bearing spacer
FD22-0009	elbow, actuator, case
FD22-0010	elbow, actuator, clamp, motor
FD22-0011	elbow, actuator, slip clutch, coupling, output
FD22-0012	shoulder/scapula, actuator, shaft, motor
FD22-0013	actuator, oldham coupling, mount
FD22-0014	elbow, actuator, shaft, motor
FD22-0015	actuator, oldham coupling, torque plate
FD22-0016	scapula, actuator, case
FD22-0017	shoulder, actuator, case
FD22-0018	shoulder/scapula, actuator, clamp, motor
FD22-0019	elbow, actuator, slip clutch, coupling, input
FD22-0020	segment 1
FD22-0021	segment 2
FD22-0022	actuator, clamp, card
FD22-0023	actuator, mount, electronics
FD22-0024	actuator, cover, electronics
FD22-0025	actuator, clamp, wire
FD22-0026	elbow, actuator, shaft encoder
FD22-0027	scapula, actuator, clamp, bearing
FD22-0028	scapula, actuator, shaft, encoder
FD22-0029	scapula, actuator, coupling, HD
FD22-0030	shoulder, actuator, shaft, encoder
FD22-0031	shoulder, actuator, coupling, HD
FD22-0032	elbow, load cell, bracket, inner
FD22-0033	elbow, load cell, bracket, outer
FD22-0034	elbow, load cell, slider, inner
FD22-0035	elbow, load cell, slide, outer
FD22-0036	scapula, bracket, mounting
FD22-0037	segment 0
FD22-0038	segment 3
FD22-0038A	revised segment 3
FD22-0039	segment 4
FD22-0039A	revised segment 4
FD22-0040	segment 5
FD22-0040A	revised segment 5
FD22-0041	segment 6
FD22-0041A	revised segment 6
FD22-0042	segment 7
FD22-0043	segment 8
FD22-0044	segment 9
FD22-0045	actuator, absolute encoder, hub
FD22-0046	elbow, load cell, pad
FD22-0047	wrist, support, bearing
FD22-0048	wrist, encoder, support

FD22-0049	wrist, handle
FD22-0050	wrist, bracket, handle
FD22-0051	wrist, shaft
AY22-0052	wrist assembly
AY22-0053	elbow assembly
AY22-0054	elbow load cell assembly
AY22-0055	shoulder assembly
AY22-0056	scapula assembly
AY22-0057	exoskeleton assembly

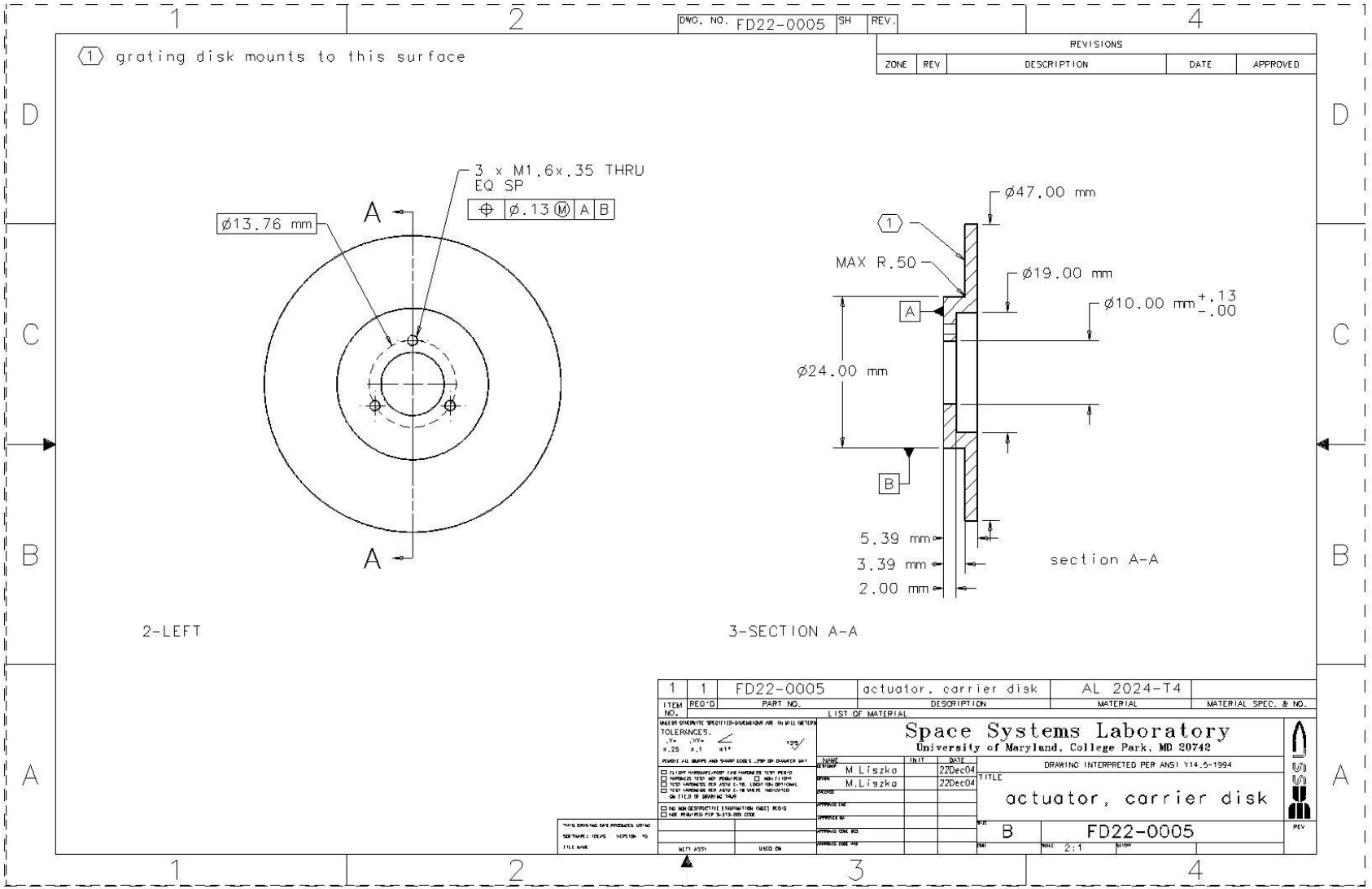
DWG. NO. FD22-0005
SH
REV.
1 grating disk mounts to this surface
REVISIONS
ZONE
REV
DESCRIPTION
DATE
APPROVED
3 x M1.6x.35 THRU
EQ SP
⌖ ø.13 Ⓜ A B
ø13.76 mm
A
A
2-LEFT
ø47.00 mm
1
MAX R.50
ø19.00 mm
ø10.00 mm +.13 -.00
A
ø24.00 mm
B
5.39 mm
3.39 mm
2.00 mm
section A-A
3-SECTION A-A
1
1
FD22-0005
actuator, carrier disk
AL 2024-T4
ITEM NO.
REQ'D
PART NO.
DESCRIPTION
MATERIAL
MATERIAL SPEC. & NO.
LIST OF MATERIAL
TOLERANCES.
Space Systems Laboratory
University of Maryland, College Park, MD 20742
NAME
INIT
DATE
M Liszka
22Dec04
M.Liszka
22Dec04
DRAWING INTERPRETED PER ANSI Y14.5-1994
TITLE
actuator, carrier disk
SIZE
B
FD22-0005
REV
SCALE 2:1
WEIGHT
SHEET
USED ON

DWG NO. FD22-0006 | SH | REV.

(1) UNLESS OTHERWISE NOTED, RADIUS ALL INSIDE CORNERS AT .020 MAX

REVISIONS				
ZONE	REV	DESCRIPTION	DATE	APPROVED

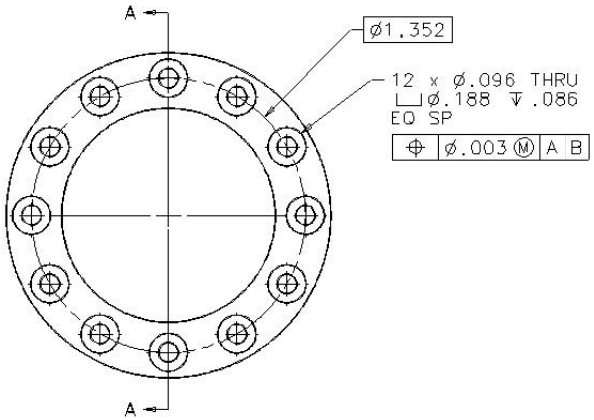

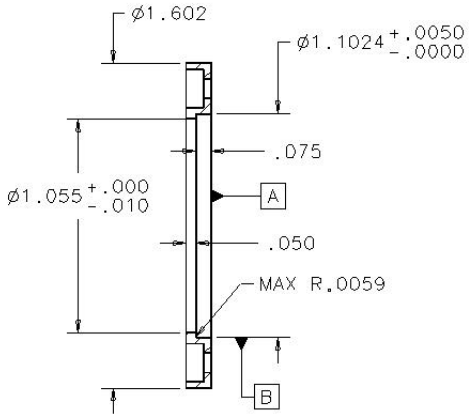

SECTION A-ITEM NO. | REQ'D | PART NO. | DESCRIPTION | MATERIAL | MATERIAL SPEC. & NO.

LIST OF MATERIAL

ITEM NO.	REQ'D	PART NO.	DESCRIPTION	MATERIAL	MATERIAL SPEC. & NO.
1	1	FD22-0006	actuator, clamp, bearing	AISI 304 S.S.	

UNLESS OTHERWISE SPECIFIED DIMENSIONS ARE IN INCHES
TOLERANCES.
XX. ± .01 XXX. ± .005 FRACTIONS ± 1/16 125
REMOVE ALL BURRS AND SHARP EDGES 0.010 OR 1/64 MAX

☐ FLIGHT HARDWARE (ADD FOR HARDNESS TEST REQ'D)
☐ HARDNESS TEST NOT REQUIRED ☐ NON FLIGHT
☐ TEST HARDNESS PER ASTM E-18, LOCATION OPTIONAL
☐ TEST HARDNESS PER ASTM E-18 WHERE INDICATED ON FACE OF DRAWING THIS
☐ NO NON-DESTRUCTIVE EXAMINATION (NDE) REQ'D
☐ NDE REQUIRED PER S-313-100 XXXX

THIS DRAWING WAS PRODUCED USING
SOFTWARE: IDEAS VERSION 8
FILE NAME:

NEXT ASSY | USED ON

Space Systems Laboratory
University of Maryland, College Park, MD 20742

	NAME	INIT	DATE
DRAWN	M.Liszka		14Jan05
TRACED	M.Liszka		14Jan05
DESIGNED			
APPROVED ENG			
APPROVED QA			
APPROVED CONF MGR			
APPROVED CONF MGR			

DRAWING INTERPRETED PER ANSI Y14.5-1994

TITLE
actuator, clamp, bearing

SIZE B | FD22-0006 | REV

SCALE 2:1 | SHEET

DWG NO. FD22-0007 | SH | REV.

1 UNLESS OTHERWISE NOTED, RADIUS ALL INSIDE CORNERS AT .020 MAX

REVISIONS				
ZONE	REV	DESCRIPTION	DATE	APPROVED

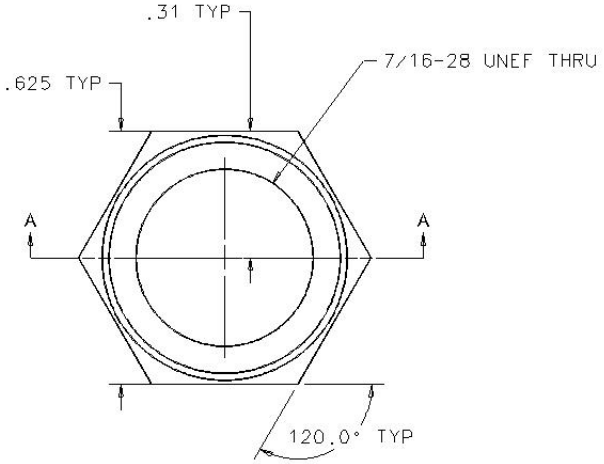

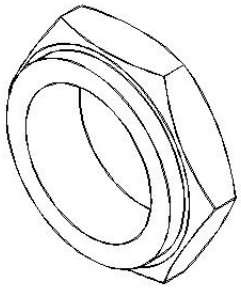

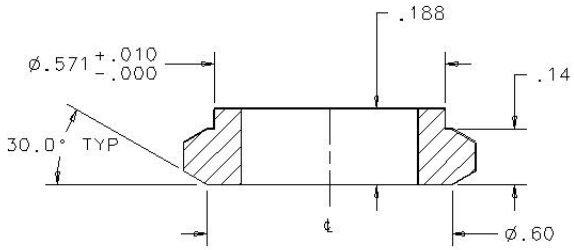

SECTION A-A

ITEM NO.	REQ'D	PART NO.	DESCRIPTION	MATERIAL	MATERIAL SPEC. & NO.
1	1	FD22-0007	actuator, bearing nut	AISI 304 S.S.	

LIST OF MATERIAL

UNLESS OTHERWISE SPECIFIED DIMENSIONS ARE IN INCHES
TOLERANCES:
FRACTIONS ±1/16 125
.XX ±.01 .XXX ±.005 ANGLES ±1°
REMOVE ALL BURRS AND SHARP EDGES 0.010 OR GREATER MAX

☐ FLIGHT HARDWARE/MOST FAIR HARDNESS TEST REQ'D
☐ WORKMAN TEST NOT REQUIRED ☐ NON FLIGHT
☐ TEST HARDNESS PER ASTM E-18, LOCATION OPTIONAL
☐ TEST HARDNESS PER ASTM E-18 WHERE INDICATED ON FACES OF DRAWING THIS
☐ NO NON-DESTRUCTIVE EXAMINATION (NDE) REQ'D
☐ NDE REQUIRED PER S-313-100 CODE

	NAME	INIT	DATE
DRAWN	M.Liszka		14Jan05
ENGR	M.Liszka		14Jan05
CHECKED			
APPROVED (QA)			
APPROVED (PM)			
APPROVED (SSAC AM)			

THIS DRAWING WAS PRODUCED USING SOFTWARE: NX 2.0 VERSION 0 FILE NAME:

NEXT ASSY | USED ON

Space Systems Laboratory
University of Maryland, College Park, MD 20742

DRAWING INTERPRETED PER ANSI Y14.5-1994

TITLE: actuator, bearing nut

SIZE B | FD22-0007 | REV

SCALE 4:1 | SHEET

1 2 3 4

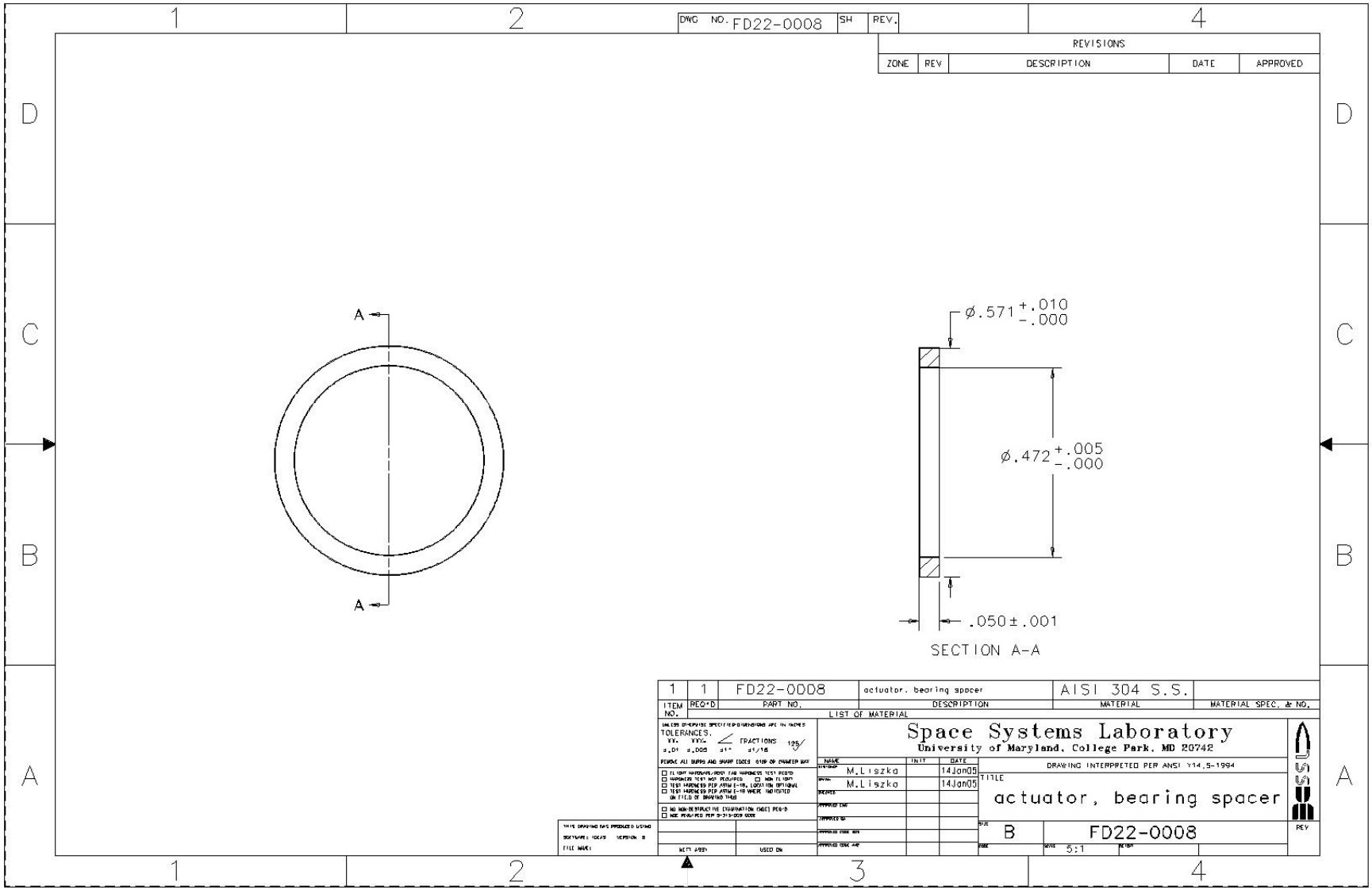
DWG NO. FD22-0008
SH
REV.
REVISIONS
ZONE
REV
DESCRIPTION
DATE
APPROVED
A
A
ø.571 +.010 -.000
ø.472 +.005 -.000
.050±.001
SECTION A-A
ITEM NO.
REQ'D
PART NO.
DESCRIPTION
MATERIAL
MATERIAL SPEC. & NO.
1
1
FD22-0008
actuator, bearing spacer
AISI 304 S.S.
LIST OF MATERIAL
TOLERANCES.
FRACTIONS
Space Systems Laboratory
University of Maryland, College Park, MD 20742
NAME
INIT
DATE
M.Liszka
14Jan05
M.Liszka
14Jan05
DRAWING INTERPRETED PER ANSI Y14.5-1994
TITLE
actuator, bearing spacer
B
FD22-0008
REV
SIZE
DWG
SCALE 5:1
SHEET
1
2
3
4

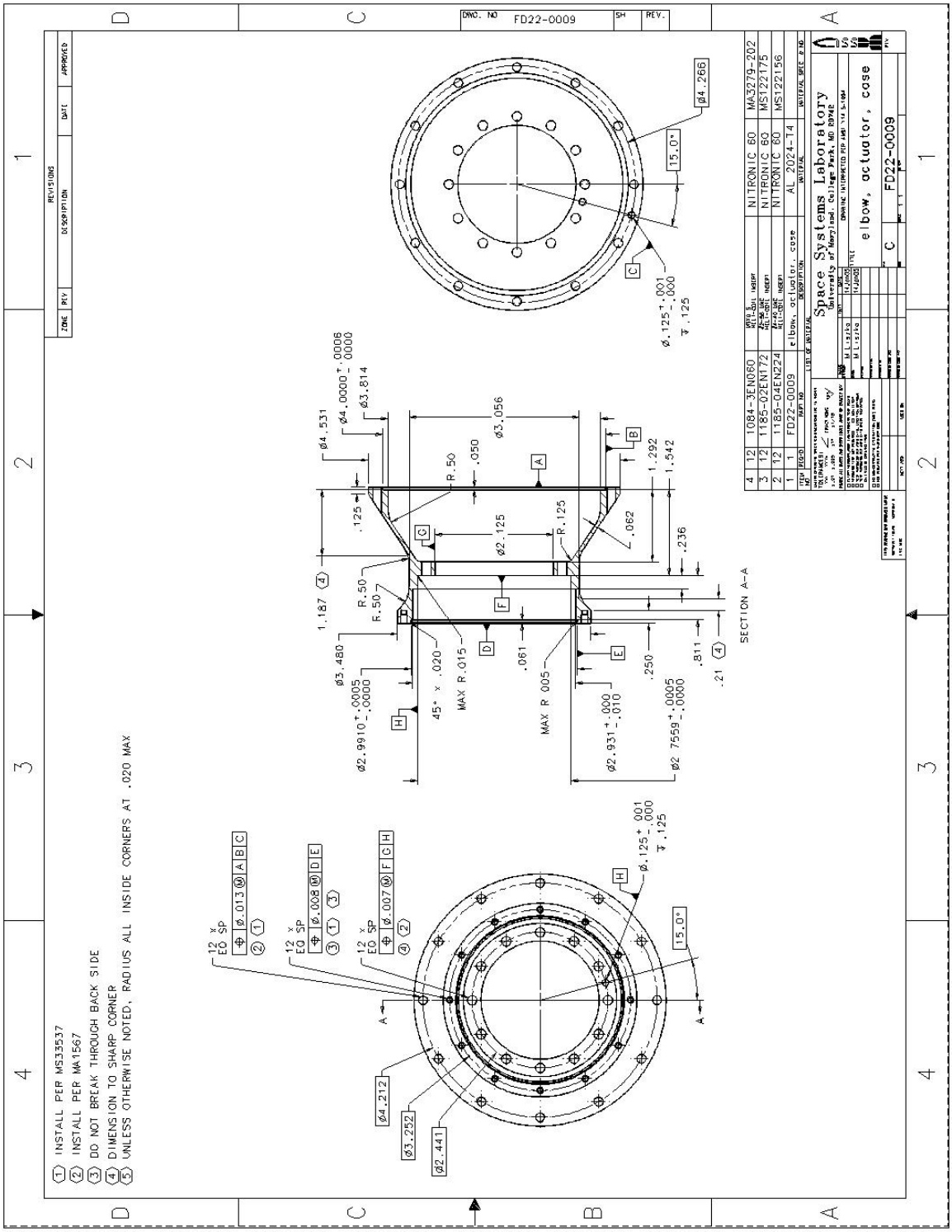
DWG. NO FD22-0009
SH
REV.
REVISIONS
ZONE
REV
DESCRIPTION
DATE
APPROVED
1 INSTALL PER MS33537
2 INSTALL PER MA1567
3 DO NOT BREAK THROUGH BACK SIDE
4 DIMENSION TO SHARP CORNER
5 UNLESS OTHERWISE NOTED, RADIUS ALL INSIDE CORNERS AT .020 MAX
SECTION A-A
Space Systems Laboratory
University of Maryland, College Park, MD 20742
elbow, actuator, case
FD22-0009
NITRONIC 60
AL 2024-T4
MA3279-202
MS122175
MS122156
1084-3EN060
1185-02EN172
1185-04EN224
FD22-0009

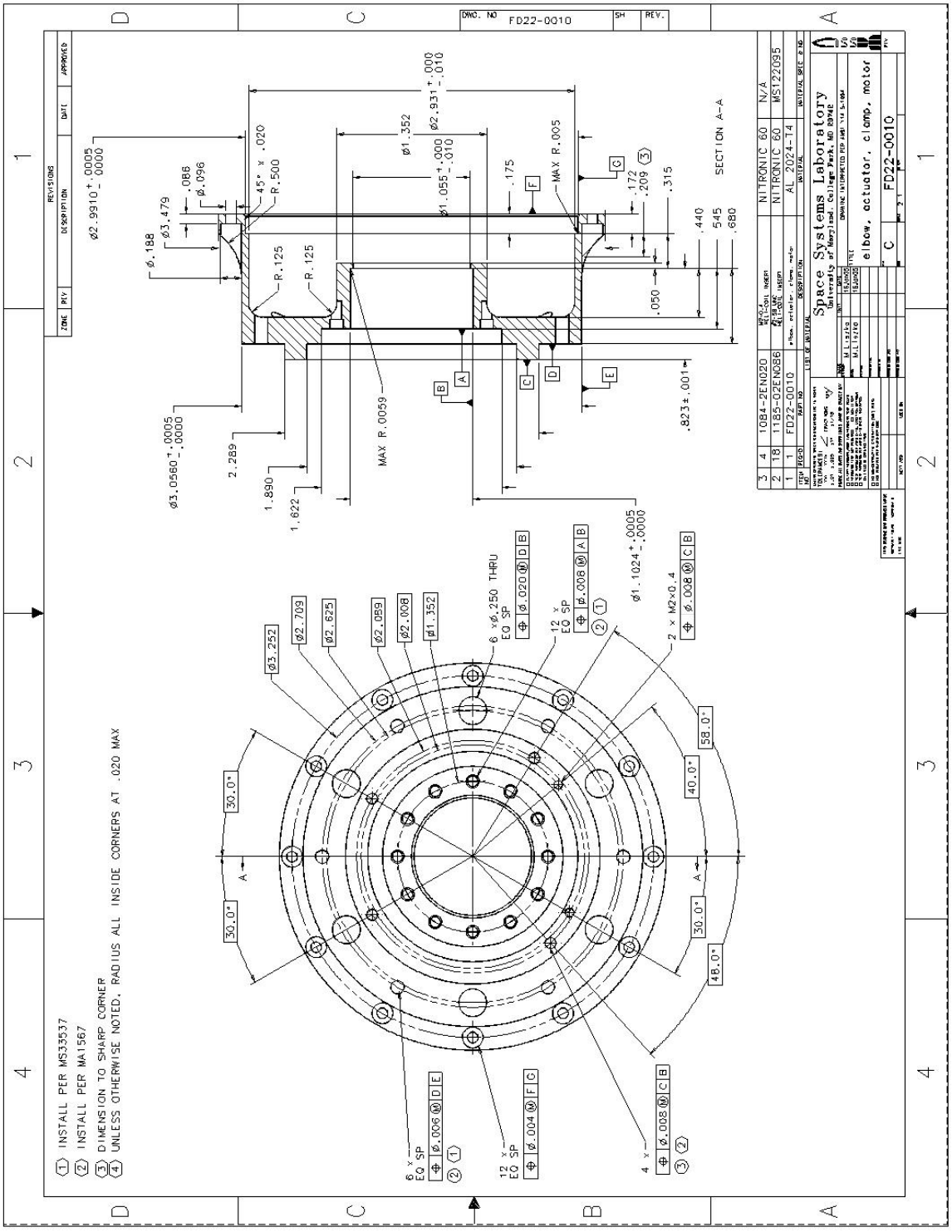
DWG. NO FD22-0010
SH
REV.
REVISIONS
ZONE
REV
DESCRIPTION
DATE
APPROVED
SECTION A-A
MAX R.0059
MAX R.005
45° x .020
R.500
R.125
R.125
.086
ø.096
ø.188
ø3.479
.175
.172
.209
.315
.050
.440
.545
.680
.823±.001
2.289
1.890
1.622
6 x ø.250 THRU EQ SP
12 x EQ SP
2 x M2x0.4
4 x
6 x EQ SP
12 x EQ SP
30.0°
30.0°
40.0°
58.0°
30.0°
48.0°
1. INSTALL PER MS33537
2. INSTALL PER MA1567
3. DIMENSION TO SHARP CORNER
4. UNLESS OTHERWISE NOTED, RADIUS ALL INSIDE CORNERS AT .020 MAX
Space Systems Laboratory
University of Maryland, College Park, MD 20742
elbow, actuator, clamp, motor
FD22-0010
C

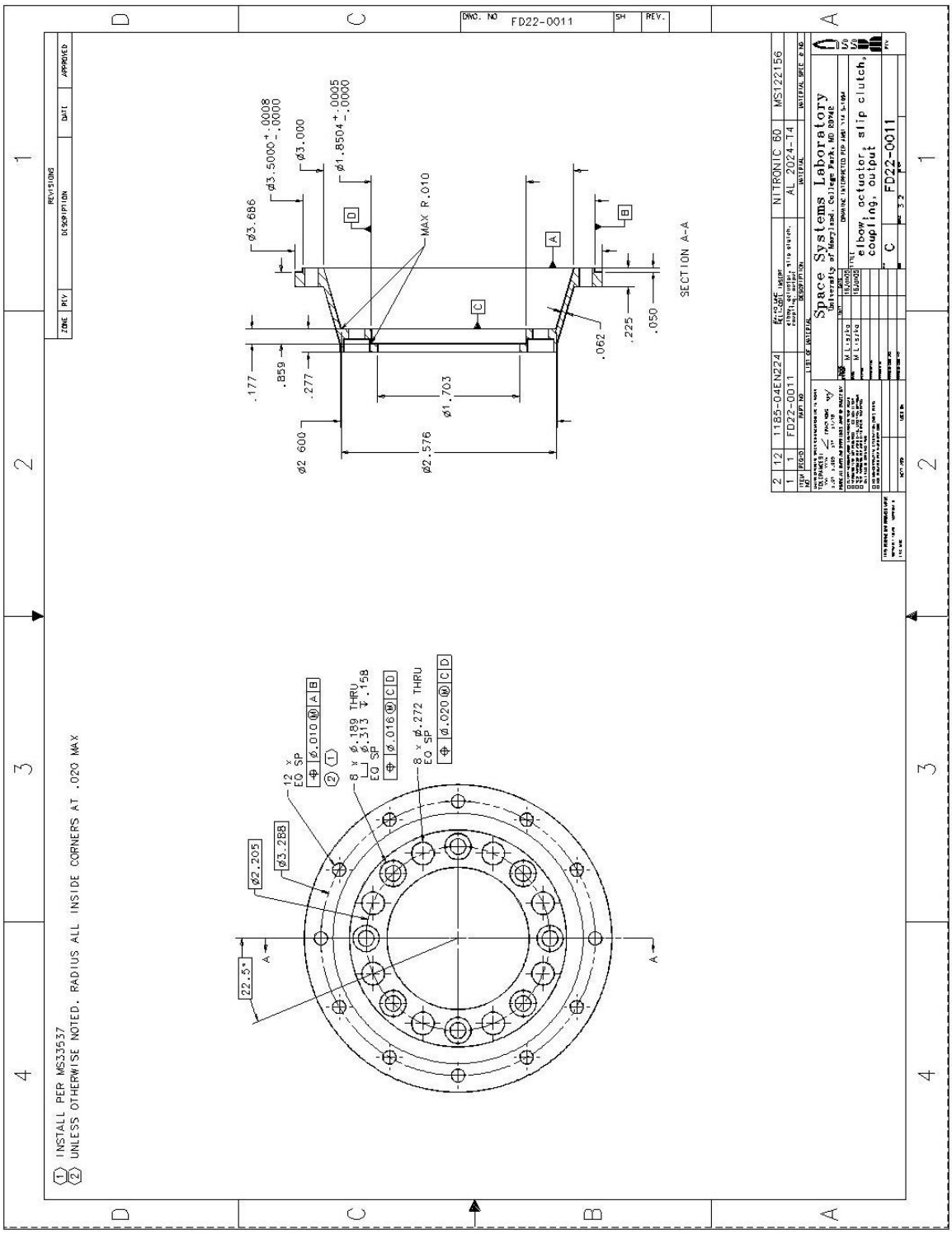
DWG. NO FD22-0011
SH
REV.
REVISIONS
ZONE
REV
DESCRIPTION
DATE
APPROVED
SECTION A-A
MAX R.010
ø3.686
ø3.5000+.0008 -.0000
ø3.000
ø1.8504+.0005 -.0000
.177
.859
.277
ø2.600
ø1.703
ø2.576
.062
.225
.050
12 X EO SP ⌖ ø.010 Ⓜ A B ② ①
8 X ø.189 THRU EO SP ⌖ ø.016 Ⓜ C D ↧ .158 ↧ .313
8 X ø.272 THRU EO SP ⌖ ø.020 Ⓜ C D
ø2.205
ø3.288
22.5°
1 INSTALL PER MS33537
2 UNLESS OTHERWISE NOTED, RADIUS ALL INSIDE CORNERS AT .020 MAX
NITRONIC 60
MS122156
AL 2024-T4
Space Systems Laboratory
University of Maryland, College Park, MD 20742
elbow, actuator, slip clutch, coupling, output
C
FD22-0011
1185-04EN224
FD22-0011

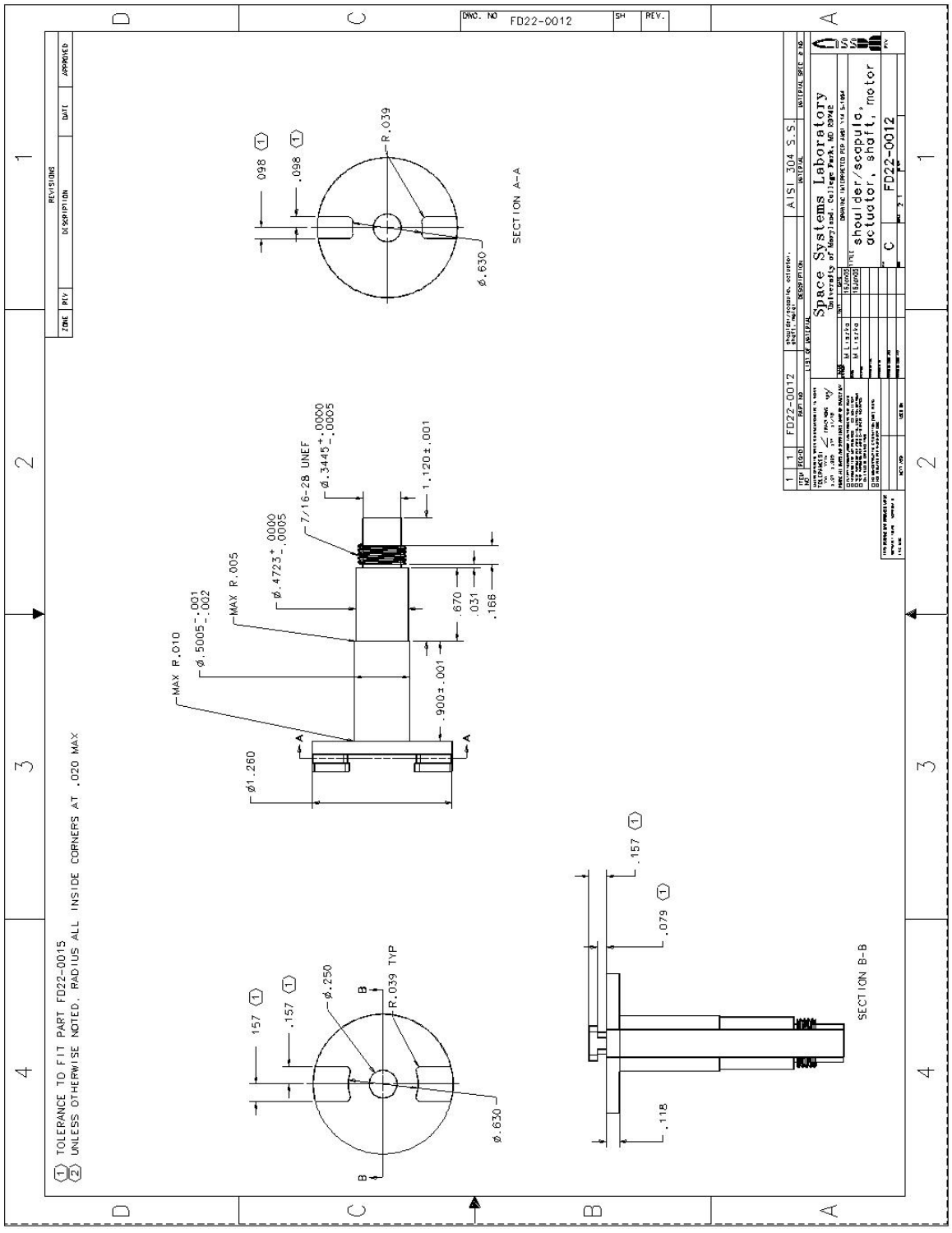
DWG. NO FD22-0012
SH
REV.
REVISIONS
ZONE
REV
DESCRIPTION
DATE
APPROVED
SECTION A-A
SECTION B-B
R.039
ø.630
.098
.098
MAX R.005
MAX R.010
ø.4723+.0000 -.0005
7/16-28 UNEF
ø.3445+.0000 -.0005
1.120±.001
.900±.001
.670
.031
.166
ø.5005-.001 -.002
ø1.260
.157
.157
.079
.118
ø.250
R.039 TYP
AISI 304 S.S.
Space Systems Laboratory
University of Maryland, College Park, MD 20742
shoulder/scapula, actuator, shaft, motor
FD22-0012
C
1 1 FD22-0012
ITEM NO
PART NO
DESCRIPTION
MATERIAL
1. TOLERANCE TO FIT PART FD22-0015
2. UNLESS OTHERWISE NOTED, RADIUS ALL INSIDE CORNERS AT .020 MAX

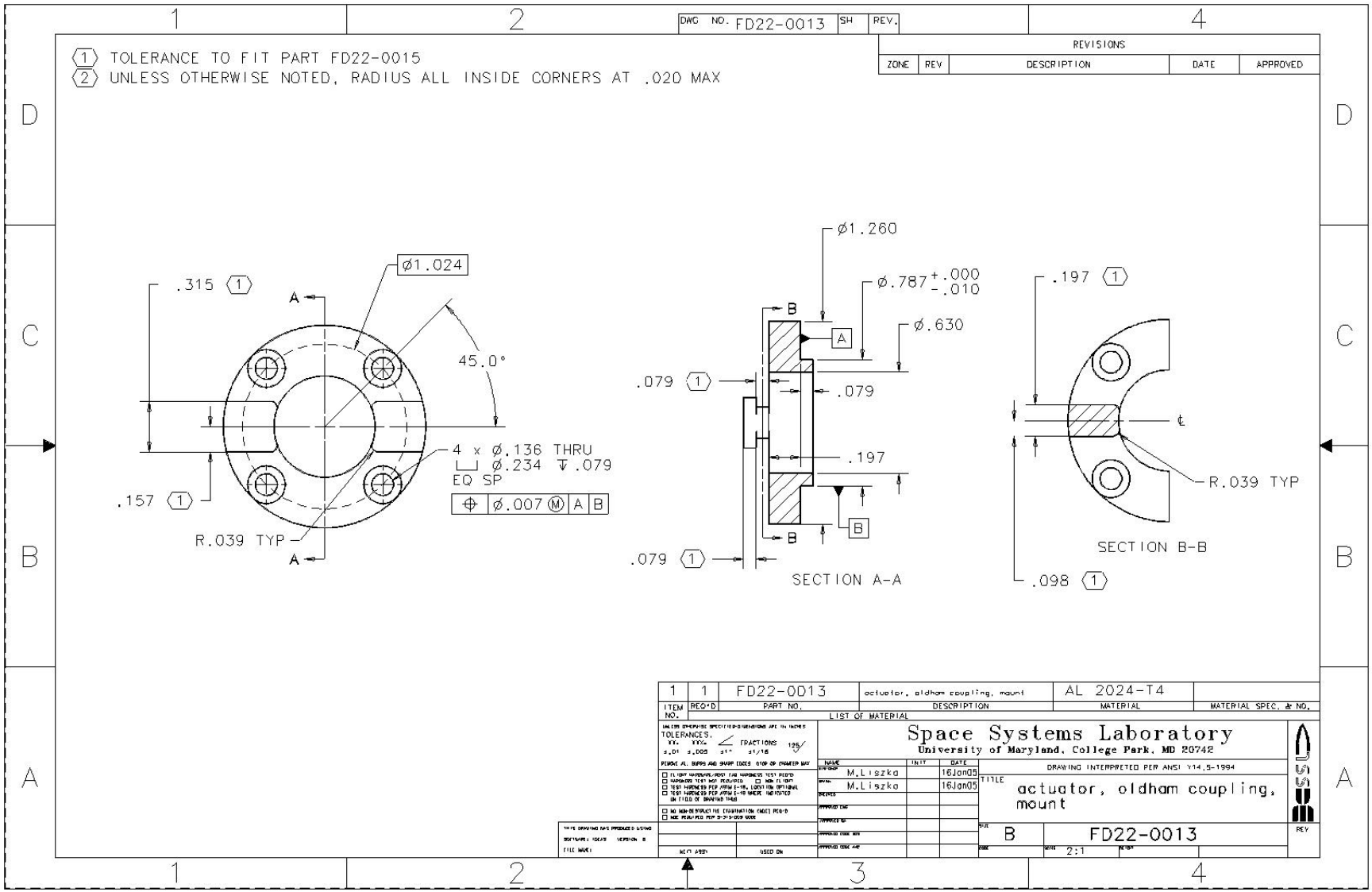
DWG NO. FD22-0013
SH
REV.
REVISIONS
ZONE
REV
DESCRIPTION
DATE
APPROVED
1 TOLERANCE TO FIT PART FD22-0015
2 UNLESS OTHERWISE NOTED, RADIUS ALL INSIDE CORNERS AT .020 MAX
.315 1
Ø1.024
45.0°
4 x Ø.136 THRU
⌴ Ø.234 ↧.079
EQ SP
Ø.007 M A B
.157 1
R.039 TYP
SECTION A-A
Ø1.260
Ø.787 +.000 -.010
Ø.630
.079 1
.079
.197
.079 1
.197 1
R.039 TYP
SECTION B-B
.098 1
ITEM NO.
QTY
PART NO.
DESCRIPTION
MATERIAL
MATERIAL SPEC. & NO.
1
1
FD22-0013
actuator, oldham coupling, mount
AL 2024-T4
LIST OF MATERIAL
TOLERANCES.
Space Systems Laboratory
University of Maryland, College Park, MD 20742
DRAWING INTERPRETED PER ANSI Y14.5-1994
M.Liszka
16Jan05
TITLE
actuator, oldham coupling, mount
SIZE
B
FD22-0013
REV
SCALE 2:1
SHEET

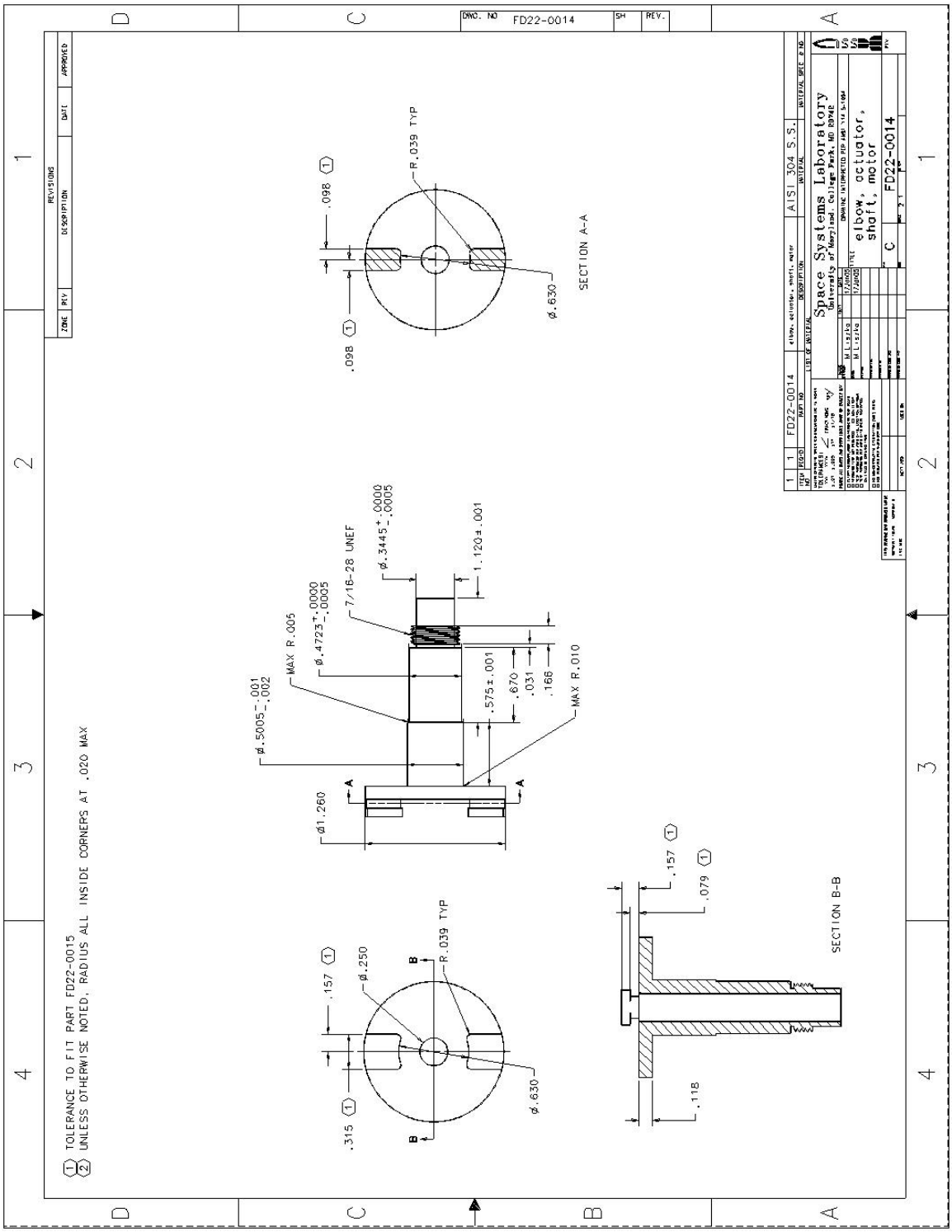
DWG. NO FD22-0014
SH
REV.
REVISIONS
ZONE
REV.
DESCRIPTION
DATE
APPROVED
Space Systems Laboratory
University of Maryland, College Park, MD 20742
elbow, actuator, shaft, motor
FD22-0014
AISI 304 S.S.
SECTION A-A
SECTION B-B
R.039 TYP
.098
ø.630
MAX R.005
ø.4723+.0000 -.0005
7/16-28 UNEF
ø.3445+.0000 -.0005
1.120±.001
ø.5005-.001 -.002
.575±.001
.670
.031
.166
MAX R.010
ø1.260
.157
ø.250
.315
.079
.118
TOLERANCE TO FIT PART FD22-0015
UNLESS OTHERWISE NOTED, RADIUS ALL INSIDE CORNERS AT .020 MAX

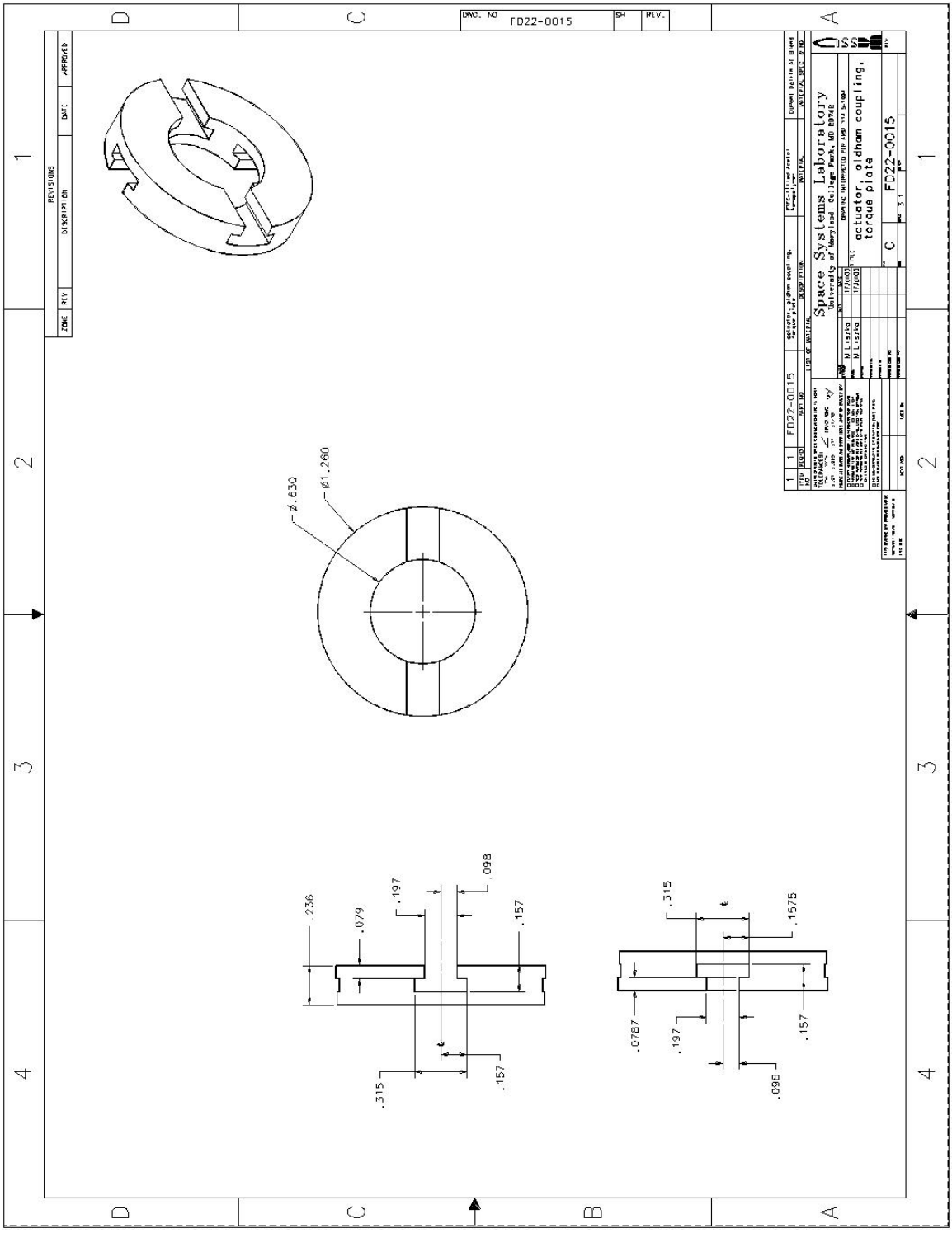
DWG. NO FD22-0015
SH
REV.
Space Systems Laboratory
University of Maryland, College Park, MD 20742
actuator, oldham coupling, torque plate
FD22-0015
ø.630
ø1.260
.236
.079
.197
.098
.157
.315
.157
.315
.1575
.0787
.197
.157
.098

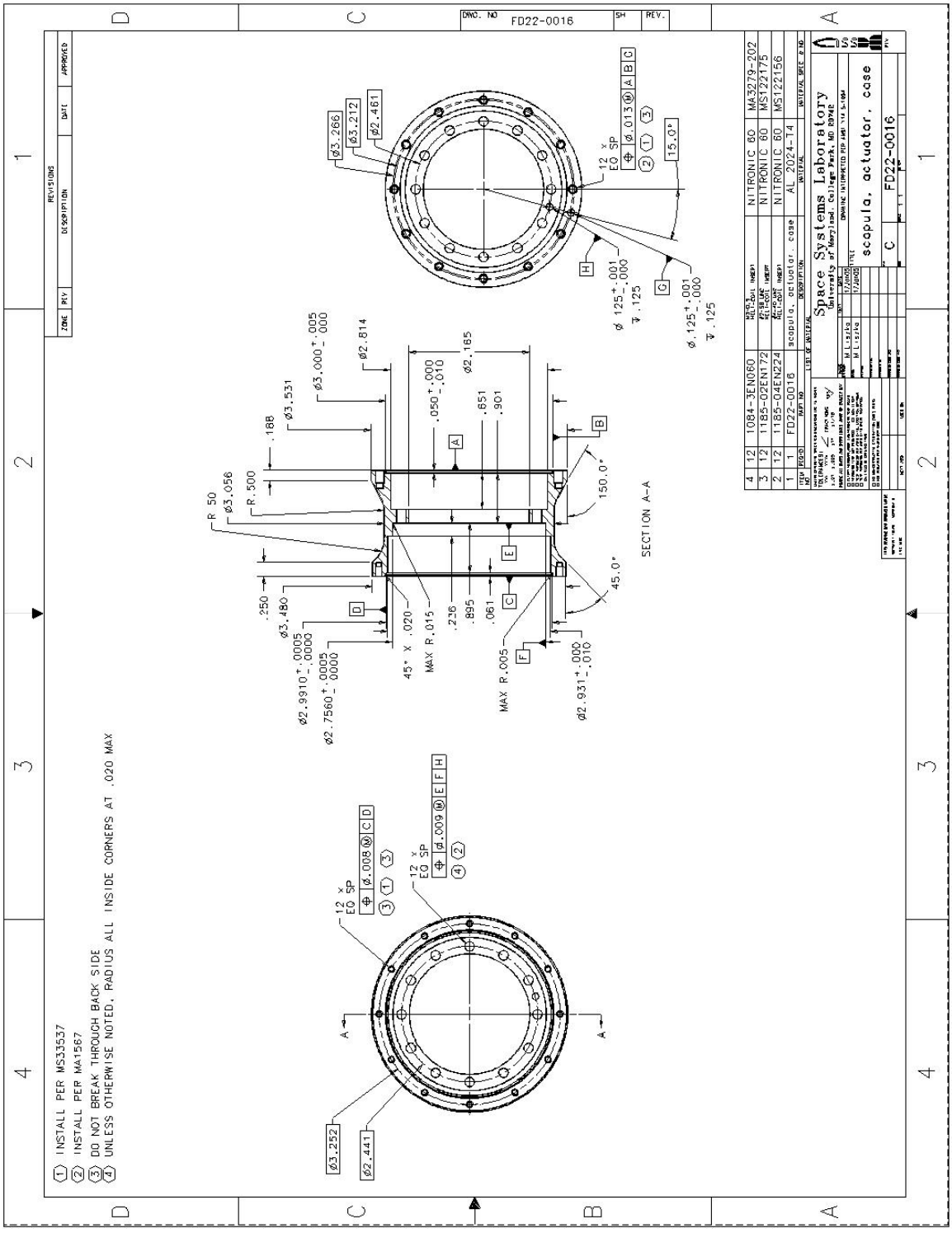
DWG. NO FD22-0016
SH
REV.
REVISIONS
ZONE
REV
DESCRIPTION
DATE
APPROVED
1 INSTALL PER MS33537
2 INSTALL PER MA1567
3 DO NOT BREAK THROUGH BACK SIDE
4 UNLESS OTHERWISE NOTED, RADIUS ALL INSIDE CORNERS AT .020 MAX
SECTION A-A
12 X EQ SP
Ø.008 M C D
Ø.009 M E F H
Ø.013 M A B C
Ø3.252
Ø2.441
Ø3.266
Ø3.212
Ø2.461
15.0°
150.0°
45.0°
R.50
Ø3.056
R.500
.188
Ø3.531
Ø3.000+.005 -.000
Ø2.814
.050+.000 -.010
Ø2.165
.851
.901
.250
Ø3.480
Ø2.9910+.0005 -.0000
Ø2.7560+.0005 -.0000
45° X .020
MAX R.015
.236
.895
.061
MAX R.005
Ø2.931+.000 -.010
Ø.125+.001 -.000
⌖.125
Space Systems Laboratory
University of Maryland, College Park, MD 20742
scapula, actuator, case
FD22-0016
C
4 12 1084-3EN060 NITRONIC 60 MA3279-202
3 12 1185-02EN172 NITRONIC 60 MS122175
2 12 1185-04EN224 NITRONIC 60 MS122156
1 1 FD22-0016 scapula, actuator, case AL 2024-T4

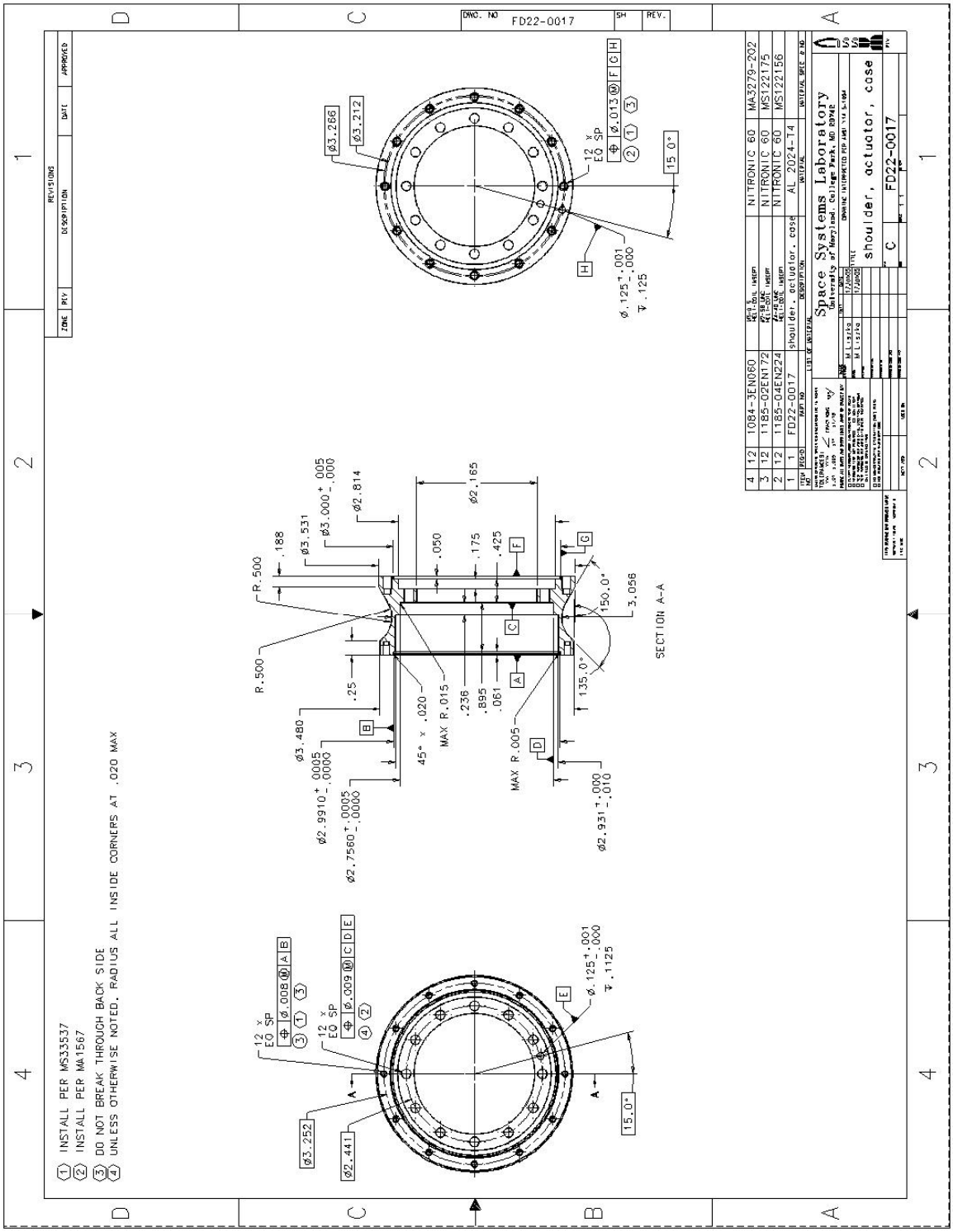
DWG. NO FD22-0017
SH
REV.
REVISIONS
ZONE
REV
DESCRIPTION
DATE
APPROVED
1 INSTALL PER MS33537
2 INSTALL PER MA1567
3 DO NOT BREAK THROUGH BACK SIDE
4 UNLESS OTHERWISE NOTED, RADIUS ALL INSIDE CORNERS AT .020 MAX
SECTION A-A
Space Systems Laboratory
University of Maryland, College Park, MD 20742
shoulder, actuator, case
FD22-0017
NITRONIC 60
MA3279-202
MS122175
MS122156
AL 2024-T4
1084-3EN060
1185-02EN172
1185-04EN224
FD22-0017

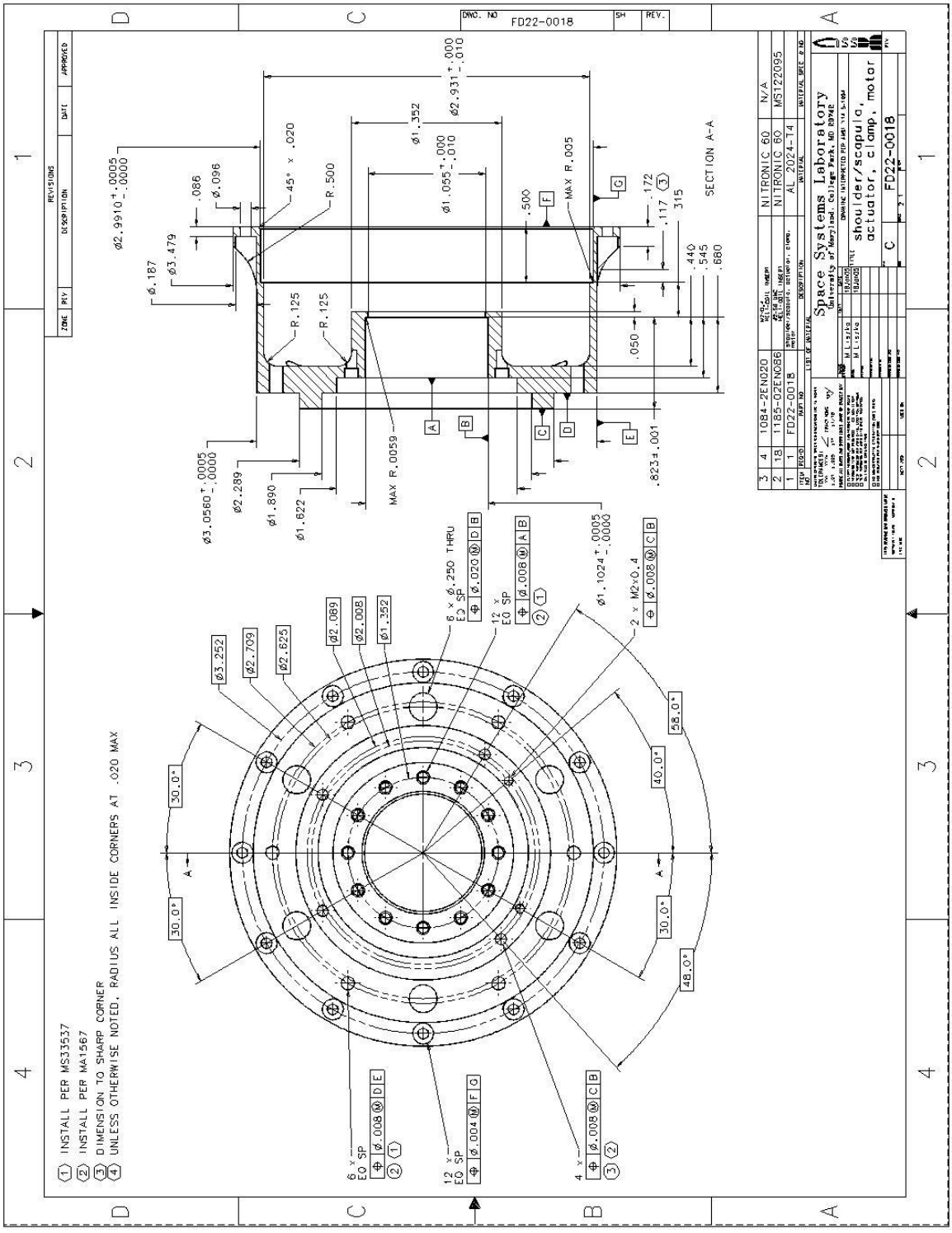
DWG. NO FD22-0018
SH
REV.
SECTION A-A
Space Systems Laboratory
University of Maryland, College Park, MD 20742
shoulder/scapula, actuator, clamp, motor
FD22-0018
NITRONIC 60
NITRONIC 60
AL 2024-T4
1084-2EN020
1185-02EN086
FD22-0018
INSTALL PER MS33537
INSTALL PER MA1567
DIMENSION TO SHARP CORNER
UNLESS OTHERWISE NOTED, RADIUS ALL INSIDE CORNERS AT .020 MAX

DWG NO. FD22-0019 | SH | REV.

1. INSTALL PER MA1567
2. CREATE LOCATIONAL INTERFERENCE FIT WITH FD22-0026. SEE DRAWING AY22-0053
3. UNLESS OTHERWISE NOTED, RADIUS ALL INSIDE CORNERS AT .020 MAX

REVISIONS				
ZONE	REV	DESCRIPTION	DATE	APPROVED

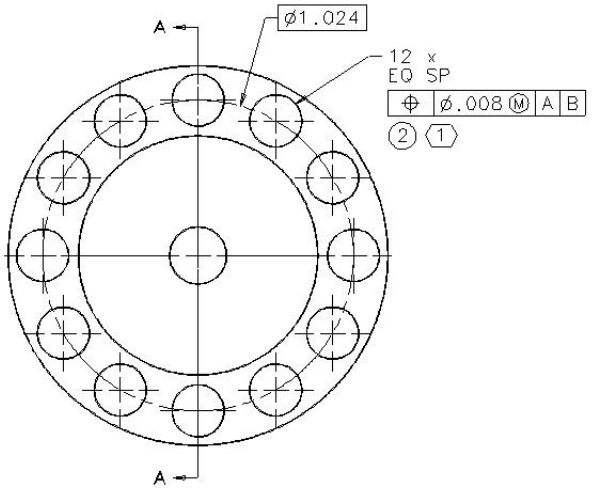

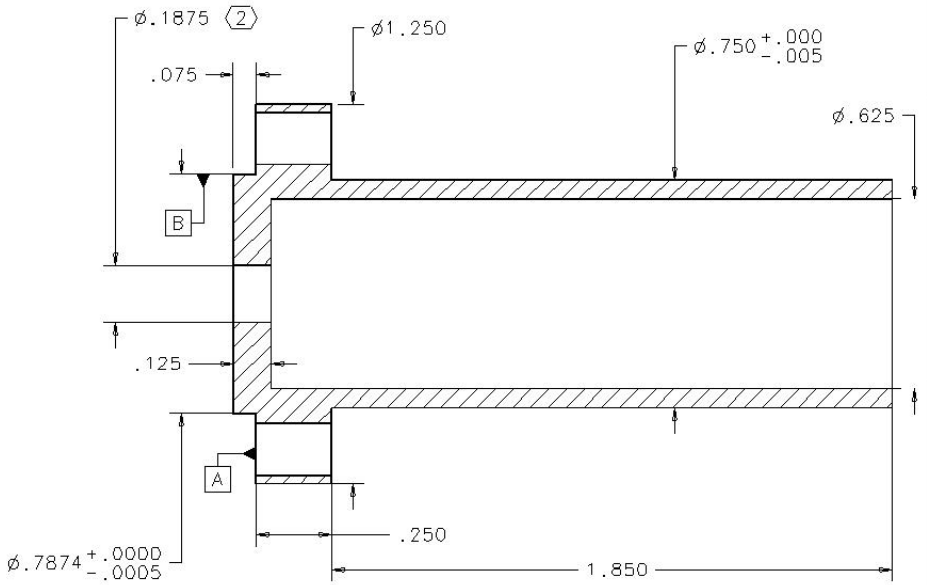

SECTION A-A

ITEM NO.	REQ'D	PART NO.	DESCRIPTION	MATERIAL	MATERIAL SPEC. & NO.
LIST OF MATERIAL					
2	12	1084-3EN045	M3x0.5 HELI-COIL INSERT	NITRONIC 60	MA3279-152
1	1	FD22-0019	elbow, actuator, slip clutch, coupling, input	AL 2024-T4	

TOLERANCES. XX- ±.01 XXX- ±.005 FRACTIONS ±1/16 125/

REMOVE ALL BURRS AND SHARP EDGES 0.010 OR GREATER MAX

☐ FLIGHT HARDWARE/BODY FAB HARDNESS TEST REQ'D
☐ WORKMANSHIP TEST NOT REQUIRED ☐ NON FLIGHT
☐ TEST HARDNESS PER ASTM E-18, LOCATION OPTIONAL
☐ TEST HARDNESS PER ASTM E-18 WHERE INDICATED ON FIELD OF DRAWING THIS

☐ NO NON-DESTRUCTIVE EXAMINATION (NDE) REQ'D
☐ NDE REQUIRED PER S-313-100 SSXX

THIS DRAWING WAS PRODUCED USING SOFTWARE: IDEAS VERSION 8 FILE NAME:

NEXT ASSY | USED ON

Space Systems Laboratory
University of Maryland, College Park, MD 20742

NAME	INIT	DATE
DRAWN M.Liszka		18Jan05
DESIGN M.Liszka		18Jan05
ENGR		
APPROVED (QA)		
APPROVED		
APPROVED (CSSC Rep)		
APPROVED (CSSC Adv)		

DRAWING INTERPRETED PER ANSI Y14.5-1994

TITLE: elbow, actuator, slip clutch, coupling, input

SIZE B | FD22-0019 | REV

DWG | SCALE | SHEET

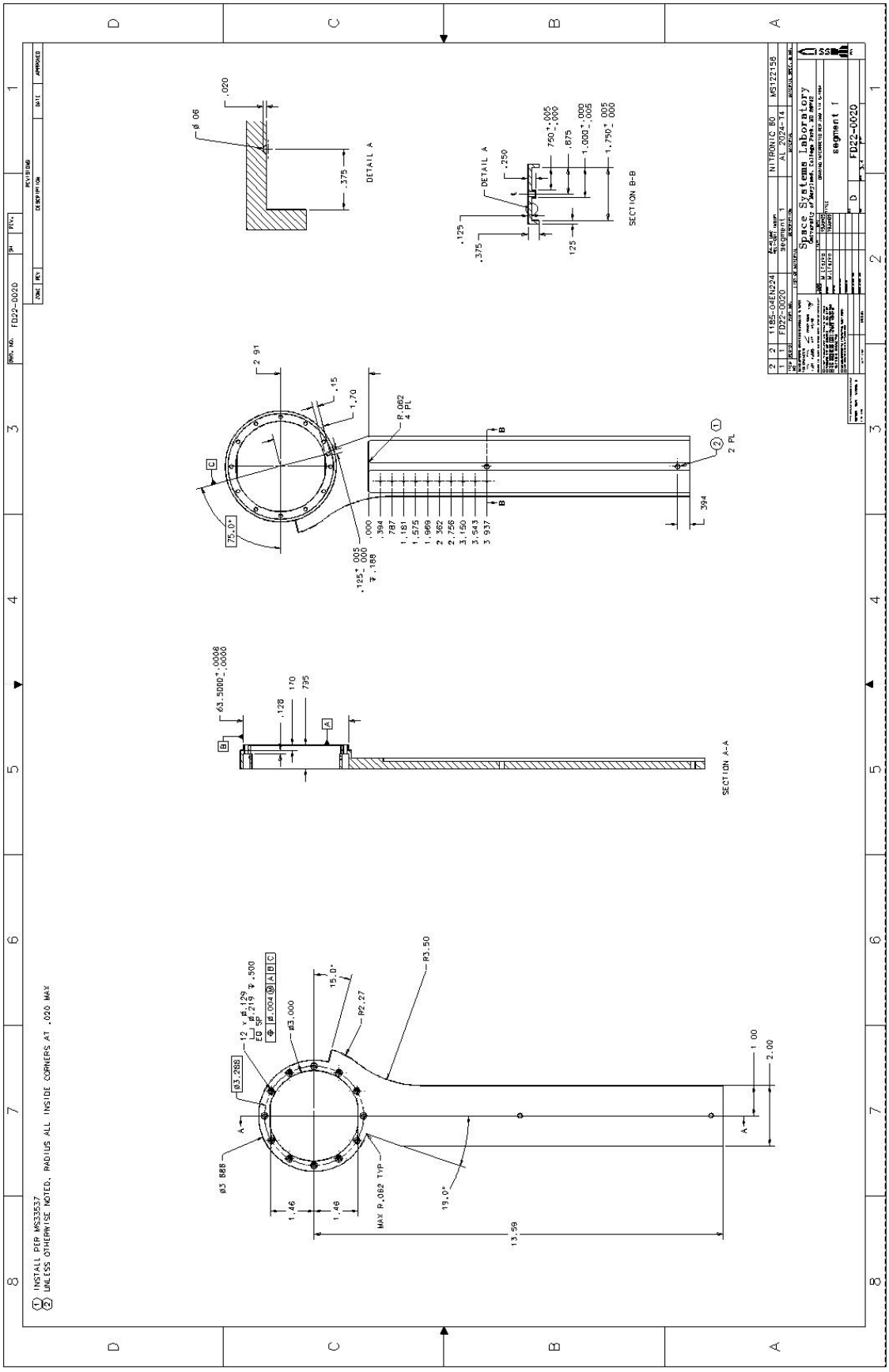
DETAIL A
SECTION B-B
SECTION A-A
INSTALL PER MS33537
UNLESS OTHERWISE NOTED, RADIUS ALL INSIDE CORNERS AT .020 MAX
Space Systems Laboratory
segment 1
FD22-0020
NITRONIC 60
MS122158

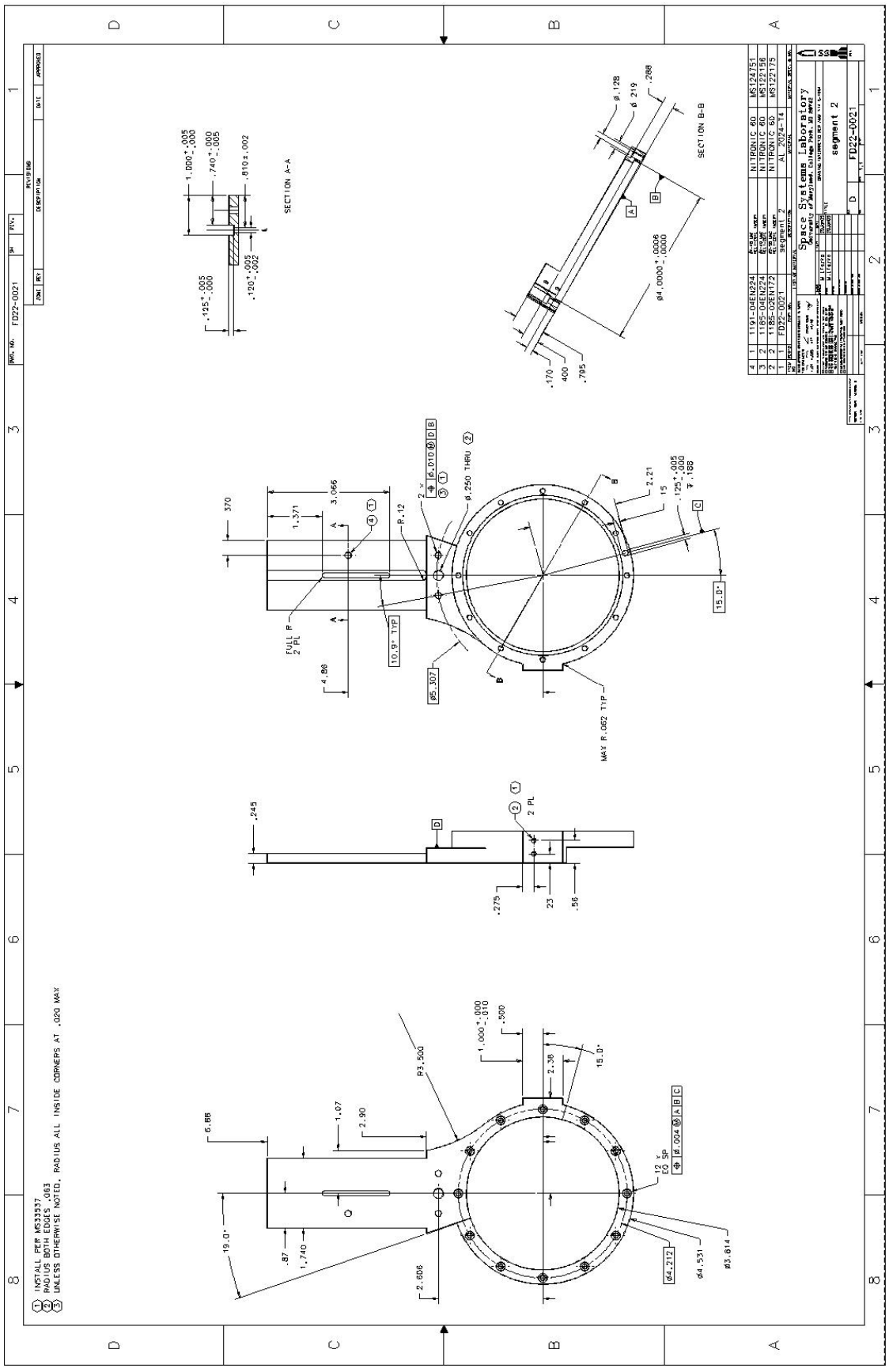
SECTION A-A
SECTION B-B
Space Systems Laboratory
segment 2
FD22-0021
NITRONIC 60
AL 2024-T4
INSTALL PER MS33537
RADIUS BOTH EDGES .063
UNLESS OTHERWISE NOTED, RADIUS ALL INSIDE CORNERS AT .020 MAX
MAX R.062 TYP
FULL R 2 PL
10.9° TYP
2 PL

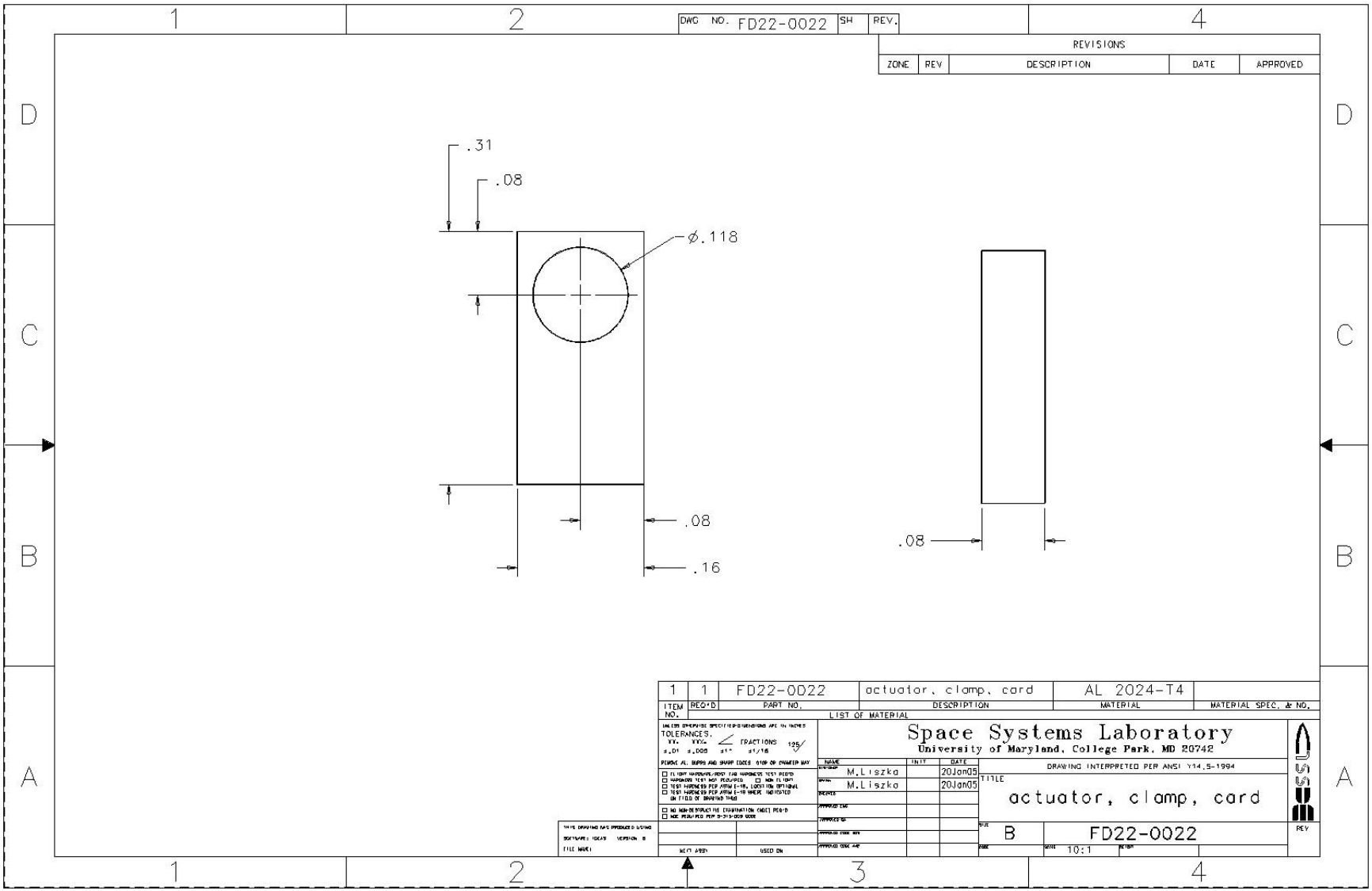
DWG NO. FD22-0022
SH
REV.
REVISIONS
ZONE
REV
DESCRIPTION
DATE
APPROVED
.31
.08
ø.118
.08
.16
.08
1
1
FD22-0022
actuator, clamp, card
AL 2024-T4
ITEM NO.
REQ'D
PART NO.
DESCRIPTION
MATERIAL
MATERIAL SPEC. & NO.
LIST OF MATERIAL
TOLERANCES.
FRACTIONS
Space Systems Laboratory
University of Maryland, College Park, MD 20742
NAME
INIT
DATE
M.Liszka
20Jan05
M.Liszka
20Jan05
DRAWING INTERPRETED PER ANSI Y14.5-1994
TITLE
actuator, clamp, card
B
FD22-0022
REV
SCALE 10:1
SHEET
1
2
3
4
A
B
C
D

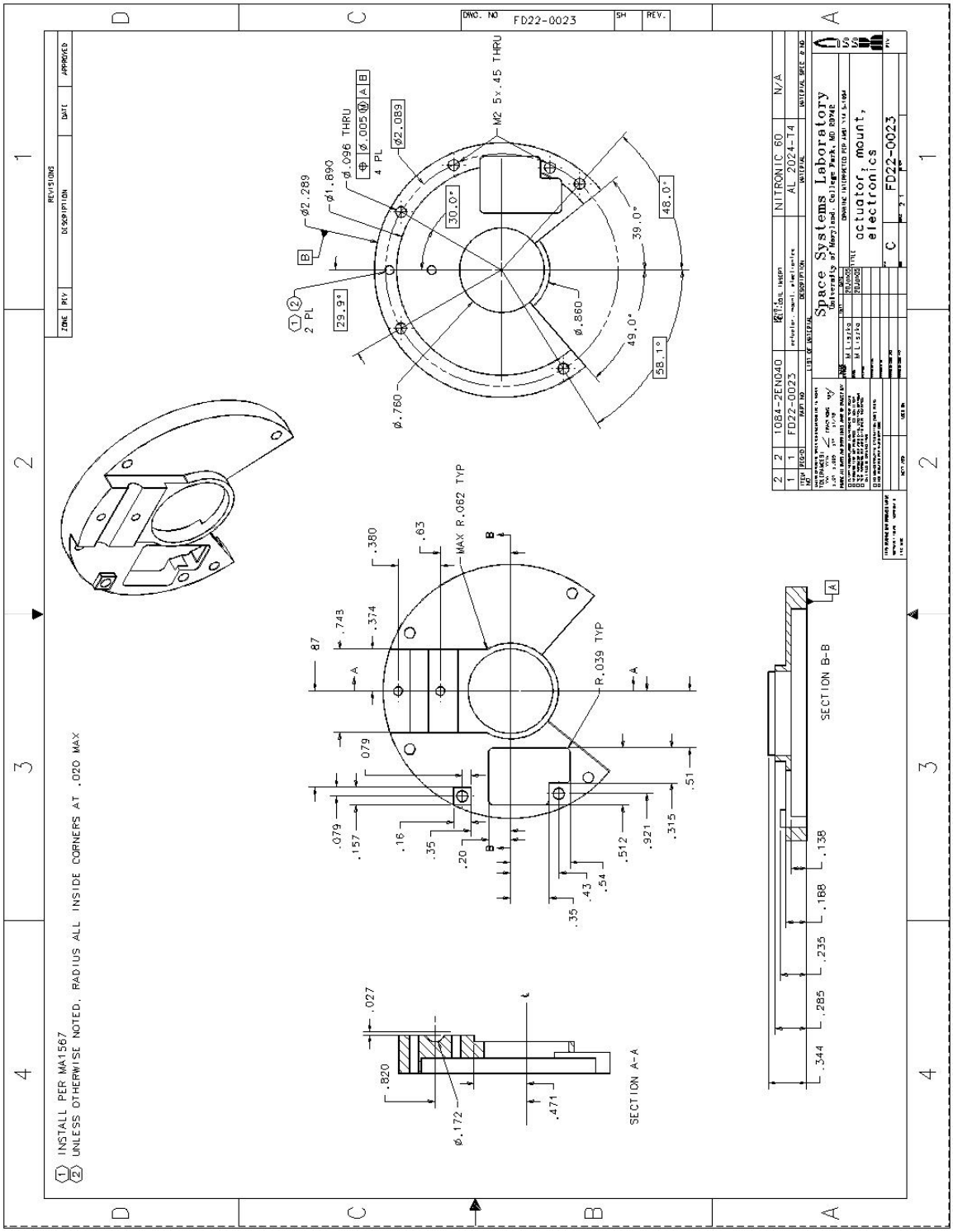
DWG. NO FD22-0023
SH
REV.
Space Systems Laboratory
University of Maryland, College Park, MD 20742
actuator, mount, electronics
FD22-0023
NITRONIC 60
AL 2024-T4
1084-2EN040
INSTALL PER MA1567
UNLESS OTHERWISE NOTED, RADIUS ALL INSIDE CORNERS AT .020 MAX
M2 5x.45 THRU
4 PL
2 PL
29.9°
30.0°
39.0°
48.0°
49.0°
58.1°
MAX R.062 TYP
R.039 TYP
SECTION A-A
SECTION B-B

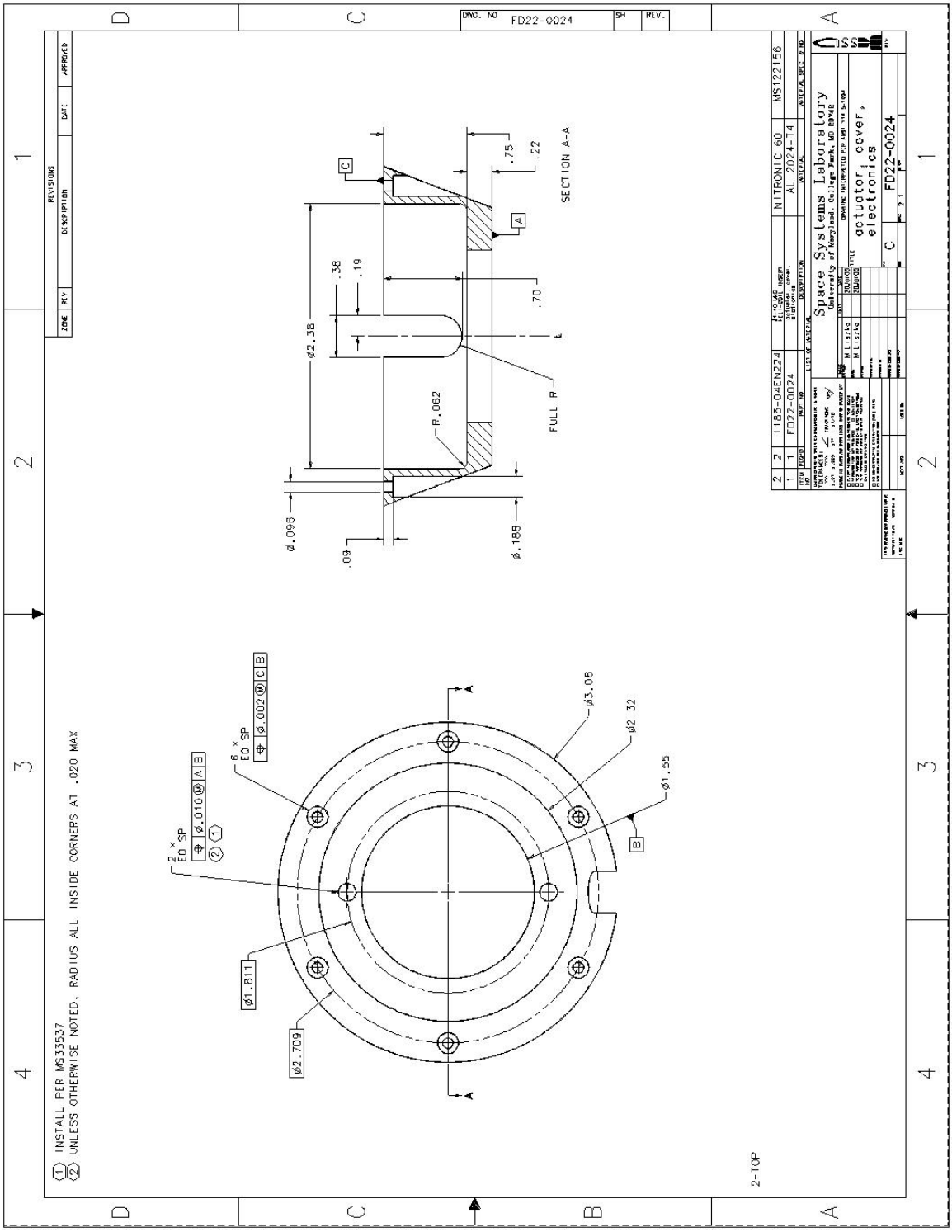
DWG. NO FD22-0024
SH
REV.
SECTION A-A
FULL R
R.062
ø2.38
.38
.19
.70
.75
.22
ø.098
.09
ø.188
ø3.06
ø2.32
ø1.55
ø1.811
ø2.709
6 X EQ SP ø.002 M C B
7 X EQ SP ø.010 M A B
1 INSTALL PER MS33537
2 UNLESS OTHERWISE NOTED, RADIUS ALL INSIDE CORNERS AT .020 MAX
2-TOP
NITRONIC 60
AL 2024-T4
MS122156
1185-04EN224
FD22-0024
Space Systems Laboratory
University of Maryland, College Park, MD 20742
actuator, cover, electronics
C
FD22-0024

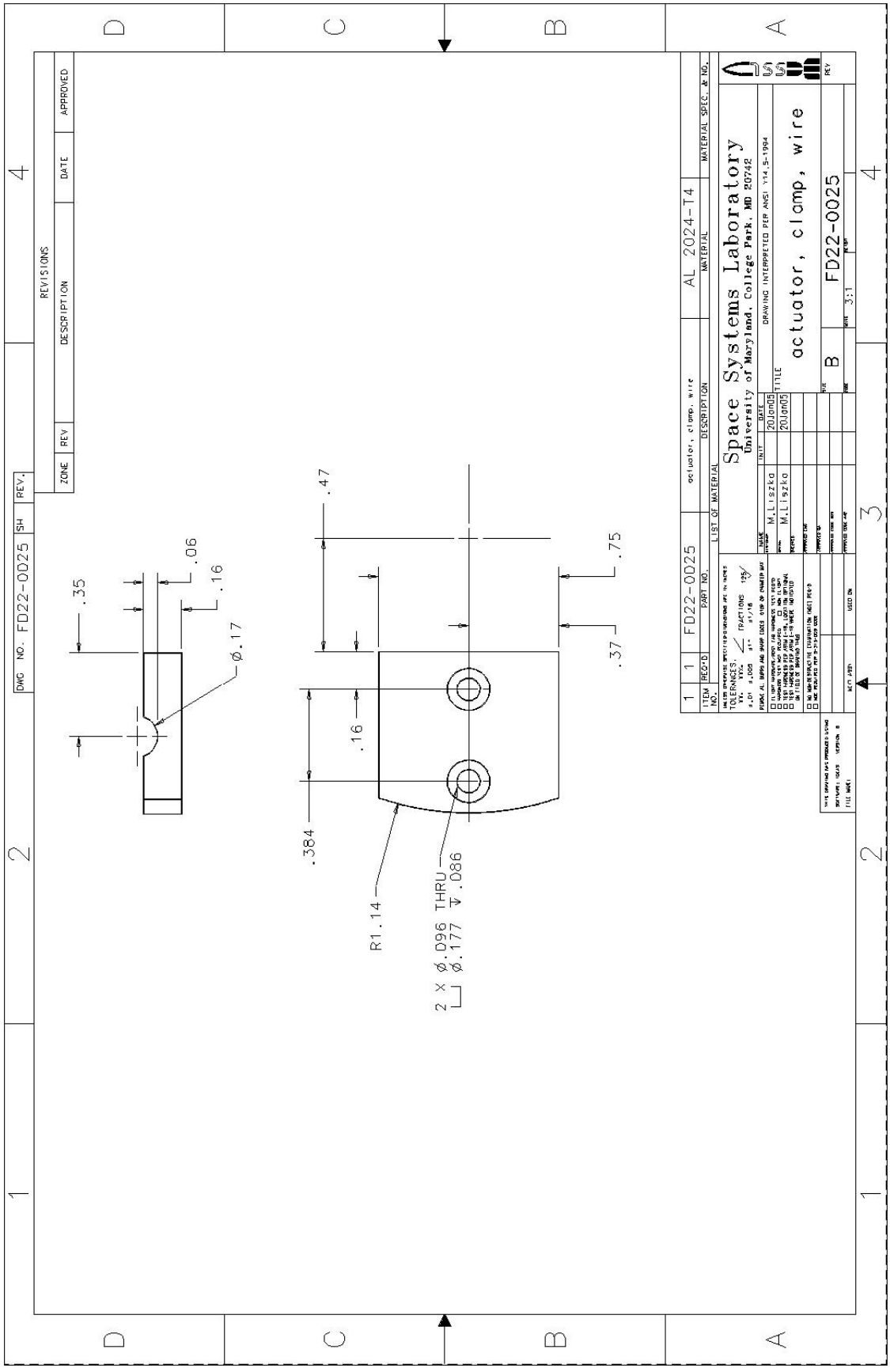
REVISIONS
ZONE
REV
DESCRIPTION
DATE
APPROVED
DWG NO. FD22-0025
SH
REV.
.35
.06
.16
ø.17
.47
.16
.384
.75
.37
R1.14
2 X ø.096 THRU
ø.177 ↧ .086
actuator, clamp, wire
AL 2024-T4
FD22-0025
Space Systems Laboratory
University of Maryland, College Park, MD 20742
M.Liszko
20Jun05
actuator, clamp, wire
FD22-0025
B
3:1

DWG NO. FD22-0026 | SH | REV.

1 CREATE LOCATIONAL INTERFERENCE FIT WITH FD22-0019. SEE DRAWING AY22-0053
2 UNLESS OTHERWISE NOTED, RADIUS ALL INSIDE CORNERS AT .020 MAX

REVISIONS				
ZONE	REV	DESCRIPTION	DATE	APPROVED

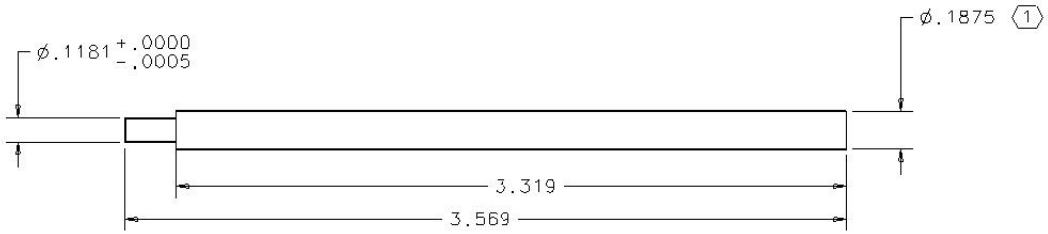

ITEM NO.	REQ'D	PART NO.	DESCRIPTION	MATERIAL	MATERIAL SPEC. & NO.
1	1	FD22-0026	elbow, actuator, shaft, encoder	AL 2024-T4	

LIST OF MATERIAL

UNLESS OTHERWISE SPECIFIED DIMENSIONS ARE IN INCHES
TOLERANCES: XX. ±.01 XXX. ±.005 ∠ ±1° FRACTIONS ±1/16 125
REMOVE ALL BURRS AND SHARP EDGES .010 OR CHAMFER MAX

☐ FLIGHT HARDWARE/ROOT CAD HARDNESS TEST REQ'D
☐ HARDNESS TEST NOT REQUIRED ☐ NON FLIGHT
☐ TEST HARDNESS PER ASTM E-18, LOCATION OPTIONAL
☐ TEST HARDNESS PER ASTM E-18 WHERE INDICATED ON FIELD OF DRAWING TREE
☐ NO NON-DESTRUCTIVE EXAMINATION (NDE) REQ'D
☐ NDE REQUIRED PER S-313-100 CODE

THIS DRAWING WAS PRODUCED USING SOFTWARE: IDEAS VERSION 8 FILE NAME:

NEXT ASSY | USED ON

	NAME	INIT	DATE
DRAWN	M.Liszka		20Jan05
CHK'D	M.Liszka		20Jan05
ENGR APPROVED			
MFG APPROVED			
Q.A. APPROVED			
COMM'L APPROVED			

Space Systems Laboratory
University of Maryland, College Park, MD 20742

DRAWING INTERPRETED PER ANSI Y14.5-1994

TITLE: elbow, actuator, shaft, encoder

SIZE: B | FD22-0026 | REV

SCALE: 2:1 | SHEET

1 2 3 4

DWG NO. FD22-0027 | SH | REV.

1 INSTALL PER MS33537
2 UNLESS OTHERWISE NOTED, RADIUS ALL INSIDE CORNERS AT .020 MAX

REVISIONS				
ZONE	REV	DESCRIPTION	DATE	APPROVED

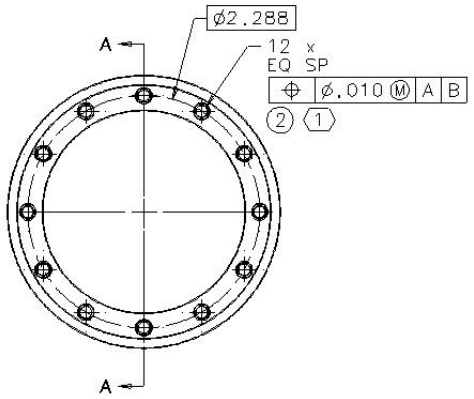

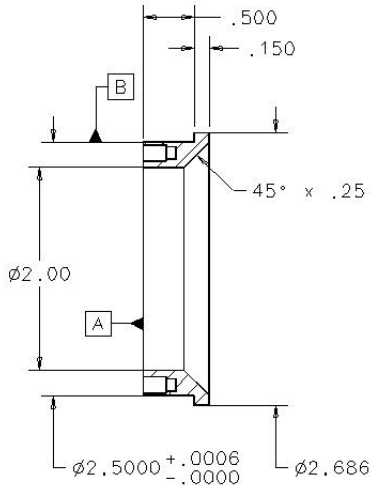

SECTION A-A

ITEM NO.	REQ'D	PART NO.	DESCRIPTION	MATERIAL	MATERIAL SPEC. & NO.
			LIST OF MATERIAL		
2	12	1185-04EN224	#4-40 UNC HELI-COIL INSERT	NITRONIC 60	MS122156
1	1	FD22-0027	scapula, actuator, clamp, bearing	AL 2024-T4	

UNLESS OTHERWISE SPECIFIED DIMENSIONS ARE IN INCHES
TOLERANCES: FRACTIONS 125
.XX ±.01 .XXX ±.005 ANGLES ±1°
REMOVE ALL BURRS AND SHARP EDGES 0.010 OR GREATER MAX

☐ FLIGHT HARDWARE/FIRST FLIGHT HARDWARE TEST REQ'D
☐ WORKMANSHIP TEST NOT REQUIRED ☐ NON FLIGHT
☐ TEST HARDNESS PER ASTM E-18, LOCATION OPTIONAL
☐ TEST HARDNESS PER ASTM E-18 WHERE INDICATED ON FIELD OF DRAWING TABS
☐ NO NON-DESTRUCTIVE EXAMINATION (NDE) REQ'D
☐ NDE REQUIRED PER S-313-100 CODE

	NAME	INIT	DATE
DRAWN	M.Liszka		20Jan05
CHECKED	M.Liszka		20Jan05
ENGR APPR			
MFG APPR			
APPROVED			
APPROVED			
APPROVED			

THIS DRAWING WAS PRODUCED USING SOFTWARE: IDEAS VERSION 8 FILE NAME:
NEXT ASSY | USED ON

Space Systems Laboratory
University of Maryland, College Park, MD 20742

DRAWING INTERPRETED PER ANSI Y14.5-1994

TITLE: scapula, actuator, clamp, bearing

SIZE B | FD22-0027 | REV
SCALE 1:1 | WEIGHT

DWG. NO. FD22-0028 | SH | REV.

1. CREATE LOACTIONAL INTERFERENCE FIT WITH FD22-0029. SEE DRAWING AY22-0056
2. UNLESS OTHERWISE NOTED, RADIUS ALL INSIDE CORNERS AT .020 MAX

REVISIONS				
ZONE	REV	DESCRIPTION	DATE	APPROVED

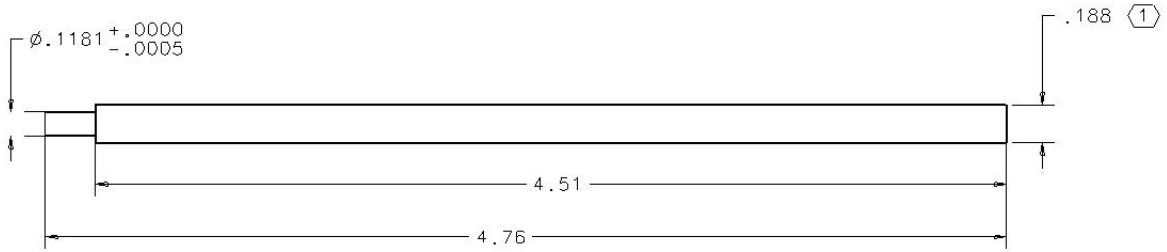

2-FRONT

ITEM NO.	REQ'D	PART NO.	DESCRIPTION	MATERIAL	MATERIAL SPEC. & NO.
1	1	FD22-0028	scapula, actuator, shaft, encoder	AL 2024-T4	

LIST OF MATERIAL

UNLESS OTHERWISE SPECIFIED DIMENSIONS ARE IN INCHES
TOLERANCES: XX- ±.01 XXX- ±.005 ∠ ±1° FRACTIONS ±1/16 125

REMOVE ALL BURRS AND SHARP EDGES BREAK UP CHAMFER MAX

☐ FLUSH HARDWARE/HEAD AND HARDNESS TEST REQ'D
☐ HARDNESS TEST NOT REQUIRED ☐ NON FLUSH
☐ TEST HARDNESS PER ASTM E-18, LOCATION OPTIONAL
☐ TEST HARDNESS PER ASTM E-18 WHERE INDICATED ON FACE OF DRAWING VIEW

☐ NO NON-DESTRUCTIVE EXAMINATION (NDE) REQ'D
☐ NDE REQUIRED PER S-315-006 CODE

THIS DRAWING WAS PRODUCED USING SOFTWARE: NEVS VERSION: 4 FILE NAME:

NEXT ASSY: USED ON:

	NAME	INIT	DATE
DESIGNED	M.Liszka		20Jan05
DRAWN	M.Liszka		20Jan05
CHECKED			
APPROVED ENG			
APPROVED QA			
APPROVED DOD REP			
APPROVED DOD REP			

Space Systems Laboratory
University of Maryland, College Park, MD 20742

DRAWING INTERPRETED PER ANSI Y14.5-1994

TITLE: scapula, actuator, shaft, encoder

SIZE: B | FD22-0028 | REV

SCALE: 2:1 | WEIGHT

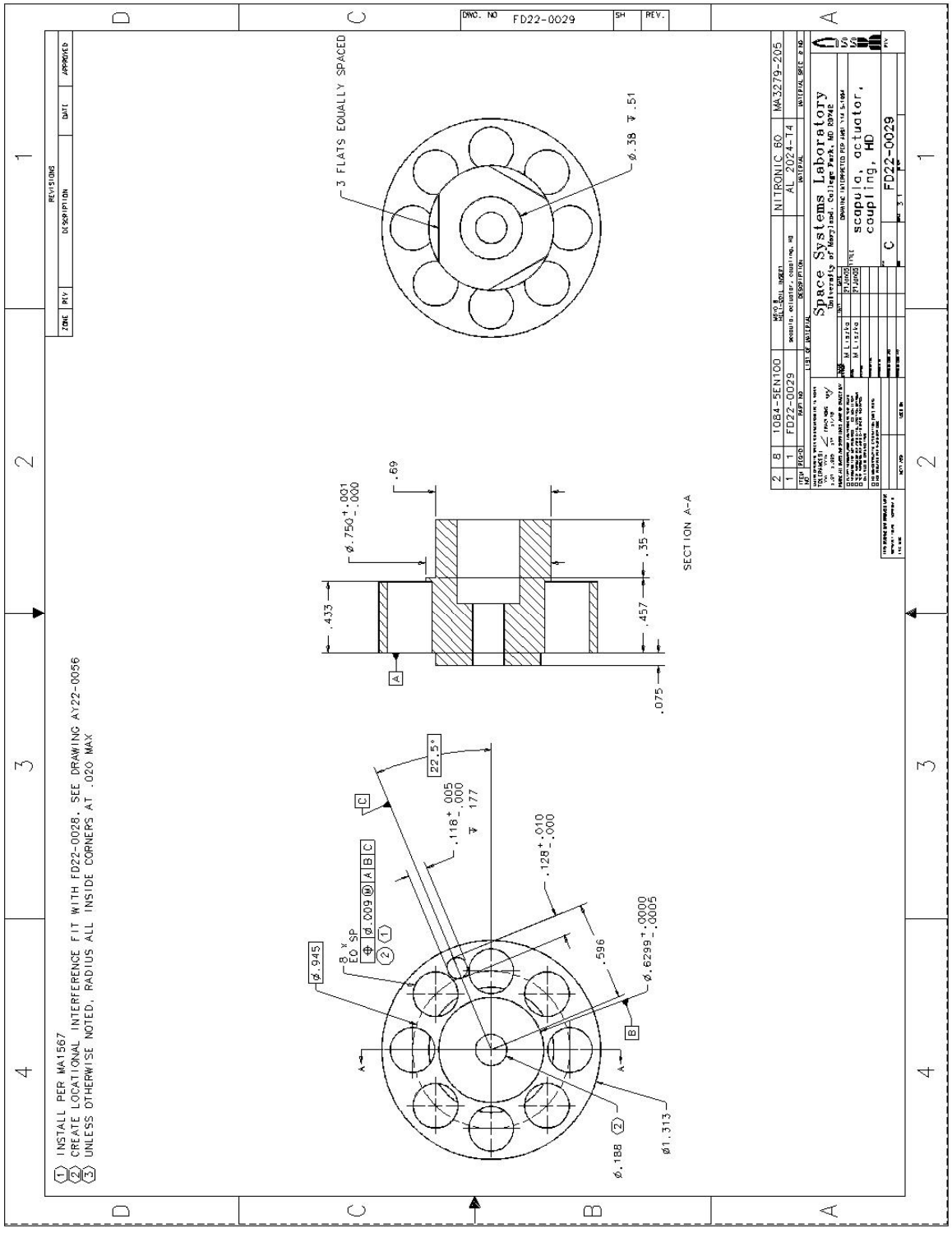
DWG. NO FD22-0029
REV.
3 FLATS EQUALLY SPACED
Ø.38 ↧ .51
SECTION A-A
.69
Ø.750 +.001 -.000
.35
.433
.457
.075
22.5°
.118 +.005 -.000
↧ .177
.128 +.010 -.000
.596
Ø.6299 +.0000 -.0005
Ø.945
8 X EQ SP
Ø.009 Ⓜ A B C
Ø.188
Ø1.313
1. INSTALL PER MA1567
2. CREATE LOCATIONAL INTERFERENCE FIT WITH FD22-0028, SEE DRAWING AY22-0056
3. UNLESS OTHERWISE NOTED, RADIUS ALL INSIDE CORNERS AT .020 MAX
Space Systems Laboratory
University of Maryland, College Park, MD 20742
scapula, actuator, coupling, HD
FD22-0029
NITRONIC 60
AL 2024-T4
MA3279-205
1084-5EN100
FD22-0029

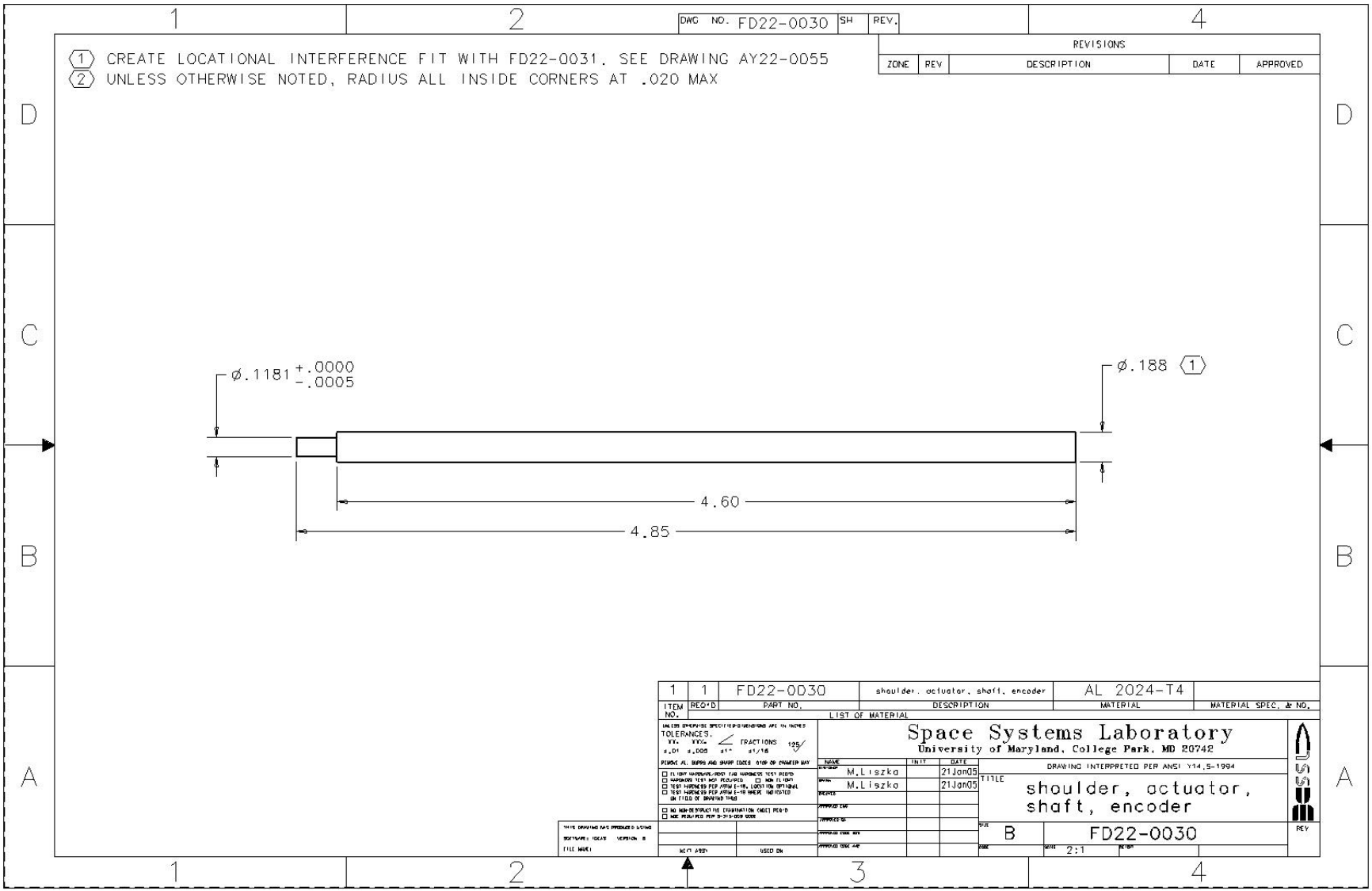
DWG NO. FD22-0030
SH
REV.
REVISIONS
ZONE
REV
DESCRIPTION
DATE
APPROVED
1 CREATE LOCATIONAL INTERFERENCE FIT WITH FD22-0031. SEE DRAWING AY22-0055
2 UNLESS OTHERWISE NOTED, RADIUS ALL INSIDE CORNERS AT .020 MAX
ø.1181 +.0000 -.0005
ø.188 1
4.60
4.85
1 1 FD22-0030 shoulder, actuator, shaft, encoder AL 2024-T4
ITEM NO. REQ'D PART NO. DESCRIPTION MATERIAL MATERIAL SPEC. & NO.
LIST OF MATERIAL
TOLERANCES.
FRACTIONS
Space Systems Laboratory
University of Maryland, College Park, MD 20742
DRAWING INTERPRETED PER ANSI Y14.5-1994
M.Liszka 21Jan05
M.Liszka 21Jan05
TITLE
shoulder, actuator, shaft, encoder
SIZE B
FD22-0030
REV
SCALE 2:1
SHEET
1
2
3
4
A
B
C
D

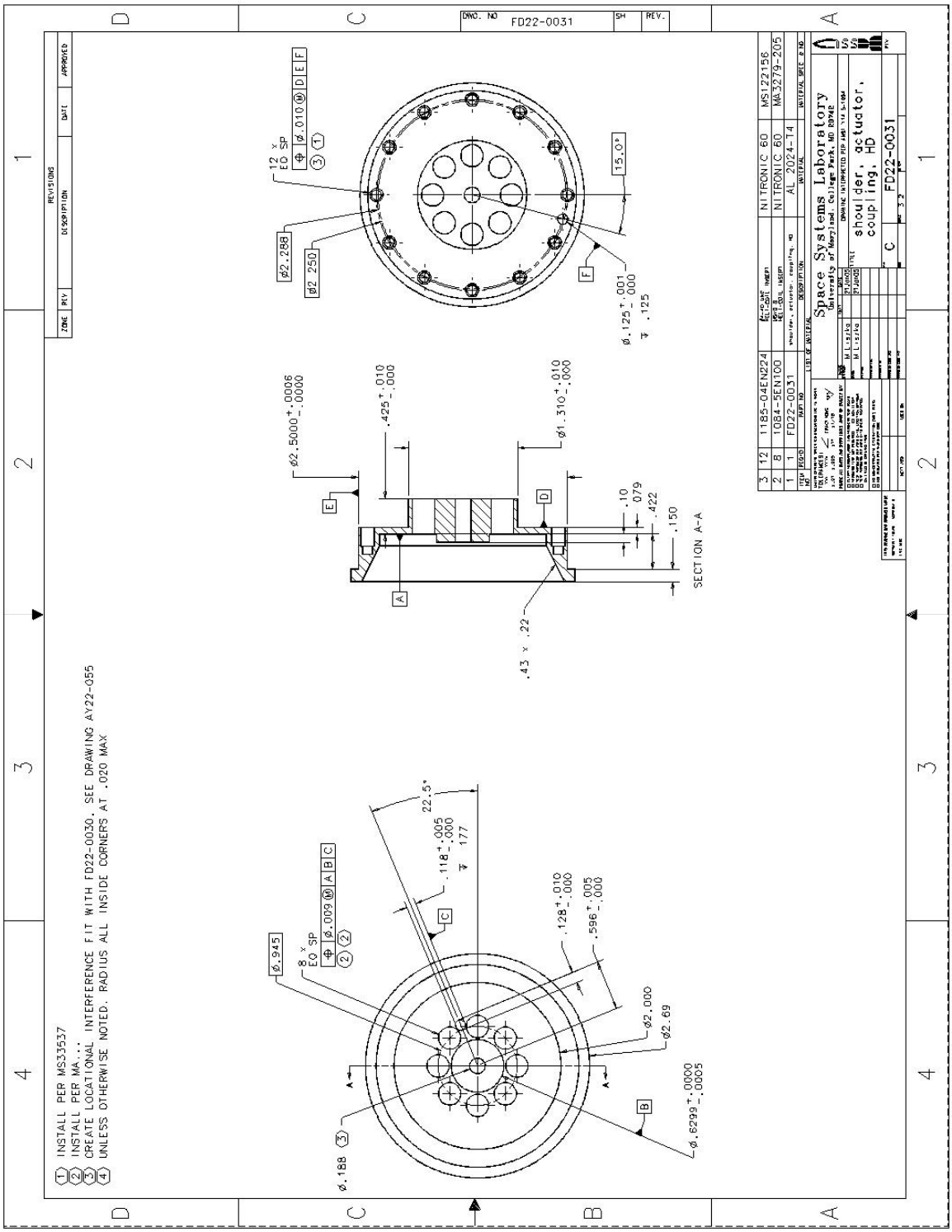
DWG. NO FD22-0031
SH
REV.
REVISIONS
ZONE
REV
DESCRIPTION
DATE
APPROVED
12 X EQ SP
ø.010 M A B C D E F
ø2.288
ø2.250
15.0°
F
ø.125 +.001 -.000
T .125
ø2.5000 +.0008 -.0000
.425 +.010 -.000
ø1.310 +.010 -.000
E
D
A
.10
.079
.422
.150
SECTION A-A
.43 x .22
ø.945
8 X EQ SP
ø.009 M A B C
2
22.5°
.118 +.005 -.000
T .177
C
.128 +.010 -.000
.596 +.005 -.000
ø2.000
ø2.69
ø.188
3
ø.6299 +.0000 -.0005
B
1 INSTALL PER MS33537
2 INSTALL PER MA...
3 CREATE LOCATIONAL INTERFERENCE FIT WITH FD22-0030, SEE DRAWING AY22-055
4 UNLESS OTHERWISE NOTED, RADIUS ALL INSIDE CORNERS AT .020 MAX
3 12 11185-04EN224 NITRONIC 60 MS122156
2 8 1084-5EN100 NITRONIC 60 MA3279-205
1 1 FD22-0031 AL 2024-T4
ITEM QTY PART NO DESCRIPTION MATERIAL
Space Systems Laboratory
University of Maryland, College Park, MD 20742
shoulder, actuator, coupling, HD
FD22-0031
C

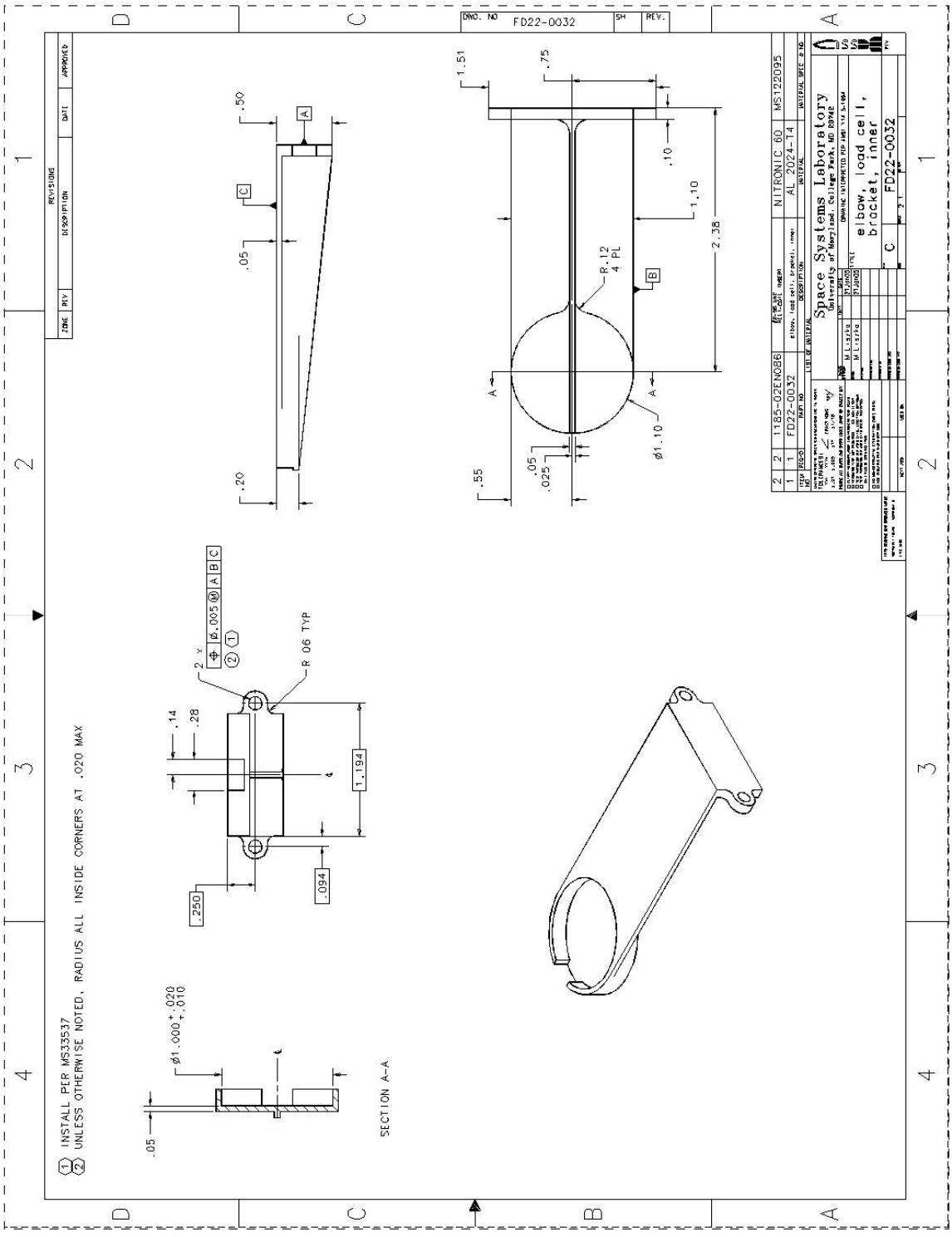
DWG. NO FD22-0032
REV.
REVISIONS
ZONE REV DESCRIPTION DATE APPROVED
Space Systems Laboratory
University of Maryland, College Park, MD 20742
elbow, load cell, bracket, inner
FD22-0032
NITRONIC 60
AL 2024-T4
MS122095
1185-02EN086
FD22-0032
R.12 4 PL
R 06 TYP
2 X Ø.005 M A B C
Ø1.10
1.51
.75
1.10
2.38
.10
.55
.05
.025
.50
.20
.14
.28
1.194
.250
.094
Ø1.000 +.020 +.010
SECTION A-A
.05
1 INSTALL PER MS33537
2 UNLESS OTHERWISE NOTED, RADIUS ALL INSIDE CORNERS AT .020 MAX

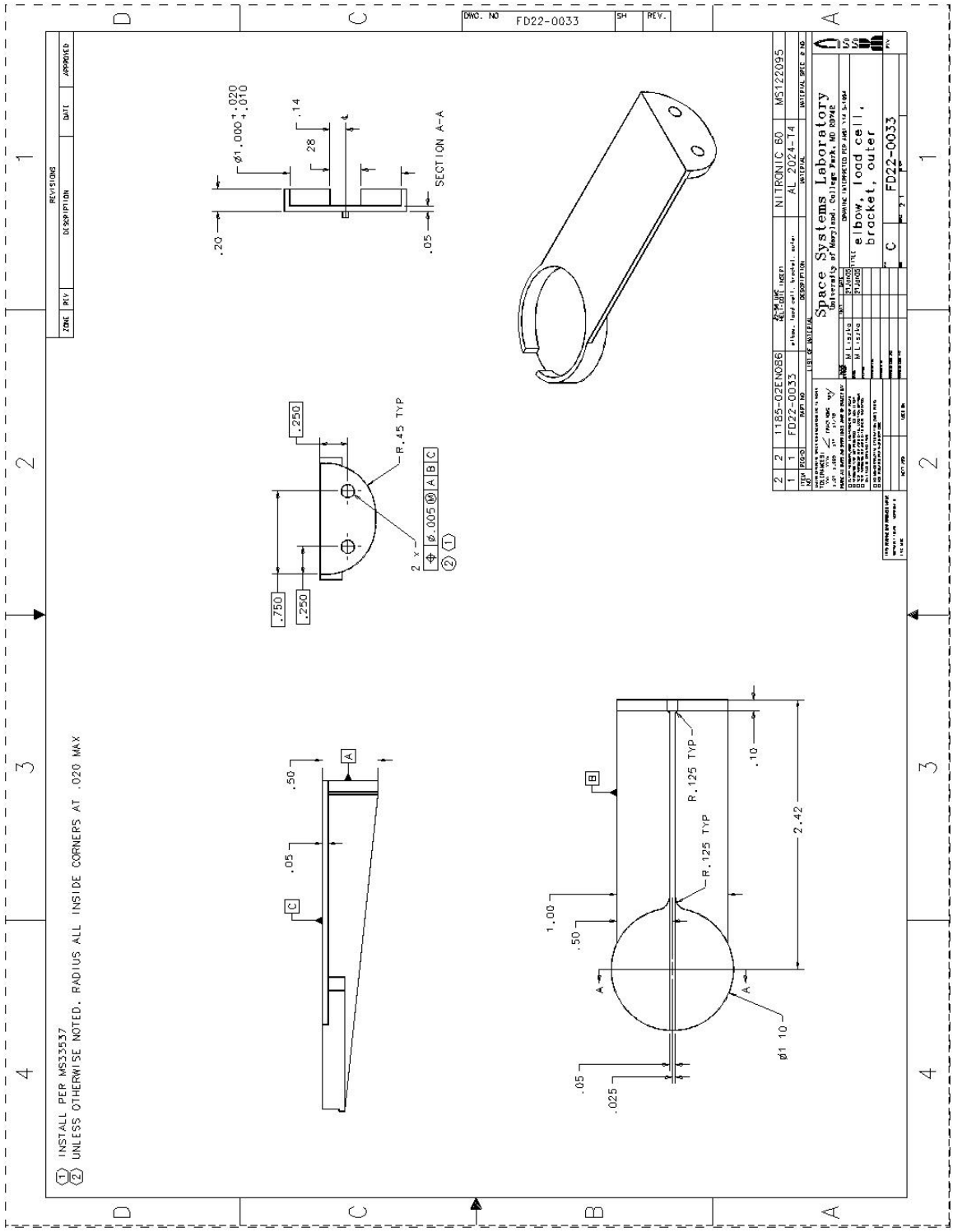
DWG. NO FD22-0033
SH
REV.
REVISIONS
ZONE
REV
DESCRIPTION
DATE
APPROVED
SECTION A-A
.20
.05
.14
.28
Ø1.000 +.020 +.010
R.45 TYP
.250
.750
.250
2 X Ø.005 M A B C
2 X 2
1 X 1
1185-02EN086
FD22-0033
NITRONIC 60
AL 2024-T4
MS122095
Space Systems Laboratory
University of Maryland, College Park, MD 20742
elbow, load cell, bracket, outer
C
FD22-0033
R.125 TYP
R.125 TYP
.10
2.42
1.00
.50
.05
.025
Ø1 10
.50
.05
1 INSTALL PER MS33537
2 UNLESS OTHERWISE NOTED, RADIUS ALL INSIDE CORNERS AT .020 MAX

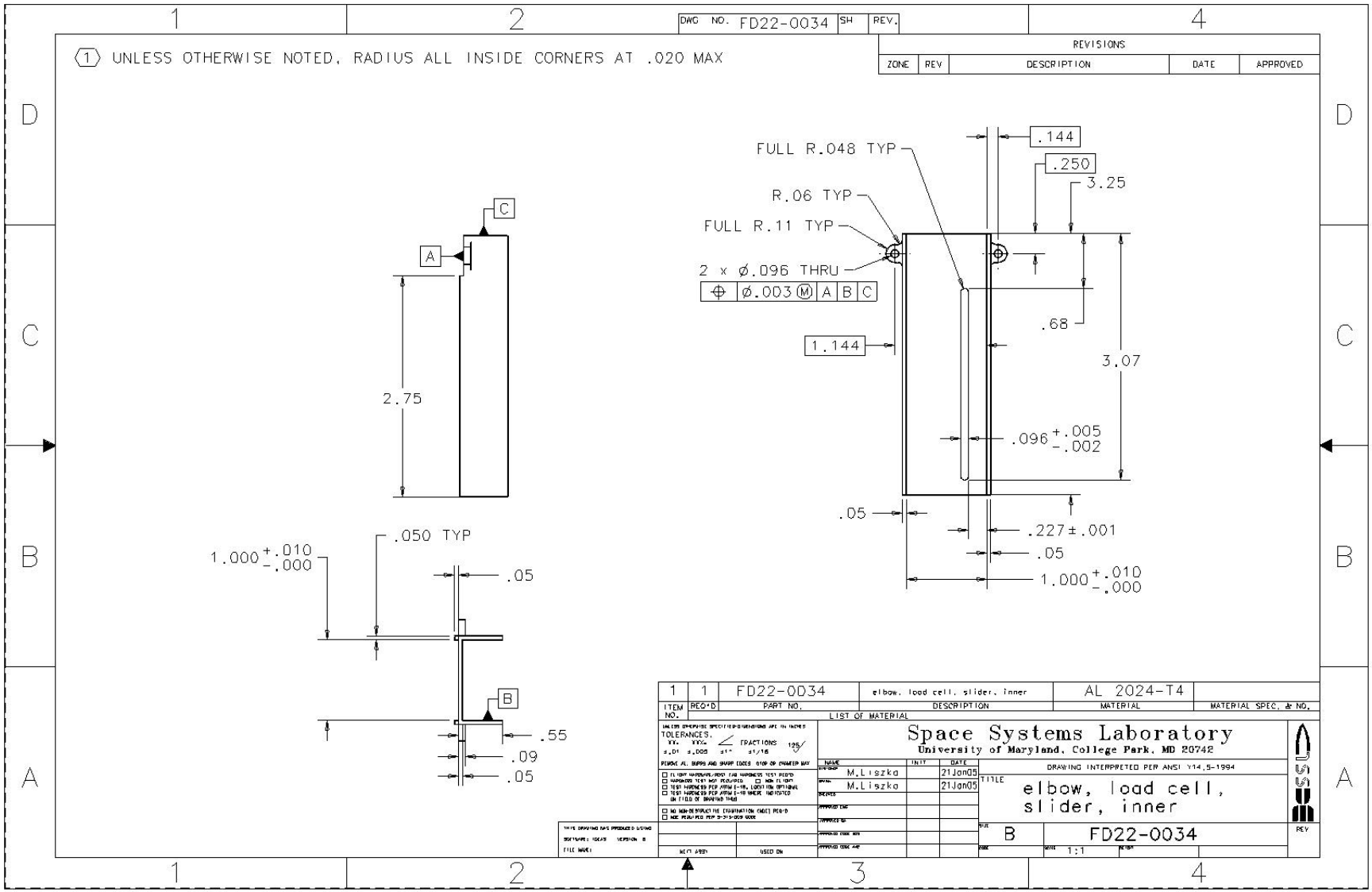
DWG NO. FD22-0034
SH
REV.
1 UNLESS OTHERWISE NOTED, RADIUS ALL INSIDE CORNERS AT .020 MAX
REVISIONS
ZONE
REV
DESCRIPTION
DATE
APPROVED
FULL R.048 TYP
R.06 TYP
FULL R.11 TYP
2 x Ø.096 THRU
Ø.003 M A B C
.144
.250
3.25
.68
1.144
3.07
.096 +.005 -.002
.05
.227±.001
.05
1.000 +.010 -.000
C
A
2.75
B
.050 TYP
1.000 +.010 -.000
.05
.55
.09
.05
1 1 FD22-0034 elbow, load cell, slider, inner AL 2024-T4
ITEM NO.
REQ'D
PART NO.
DESCRIPTION
MATERIAL
MATERIAL SPEC. & NO.
LIST OF MATERIAL
TOLERANCES.
FRACTIONS
DRAWING INTERPRETED PER ANSI Y14.5-1994
Space Systems Laboratory
University of Maryland, College Park, MD 20742
NAME
INIT
DATE
M.Liszka
21Jan05
M.Liszka
21Jan05
TITLE
elbow, load cell, slider, inner
SIZE
B
FD22-0034
REV
SCALE 1:1
WEIGHT
SHEET 1 OF 1

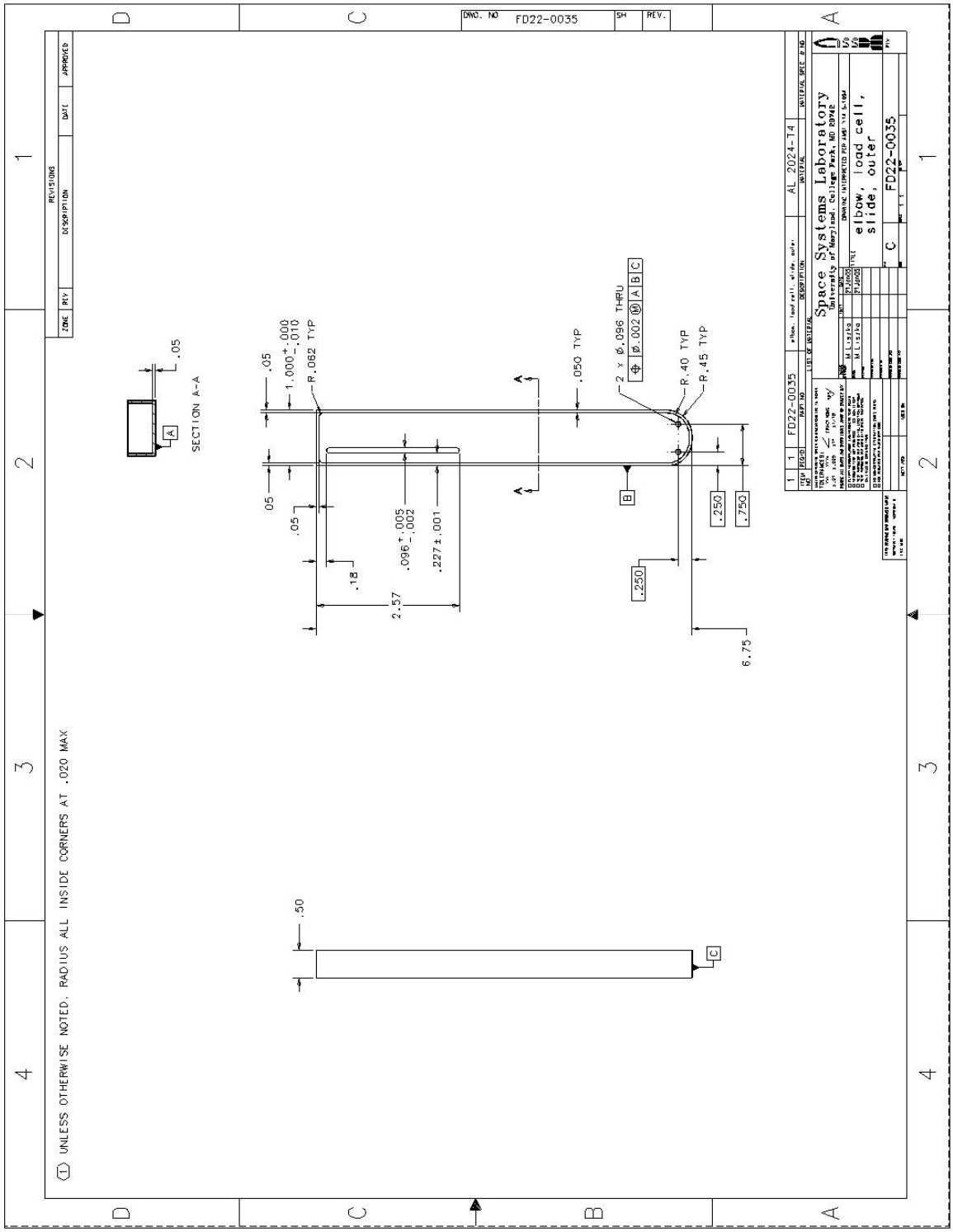
DWG. NO FD22-0035
SH
REV.
SECTION A-A
.05
R.082 TYP
1.000 +.000 -.010
.050 TYP
2 x Ø.096 THRU
Ø.002 M A B C
R.40 TYP
R.45 TYP
.096 +.005 -.002
.227 ±.001
2.57
.18
.250
.750
6.75
.50
UNLESS OTHERWISE NOTED, RADIUS ALL INSIDE CORNERS AT .020 MAX
Space Systems Laboratory
University of Maryland, College Park, MD 20742
elbow, load cell, slide, outer
FD22-0035
AL 2024-T4

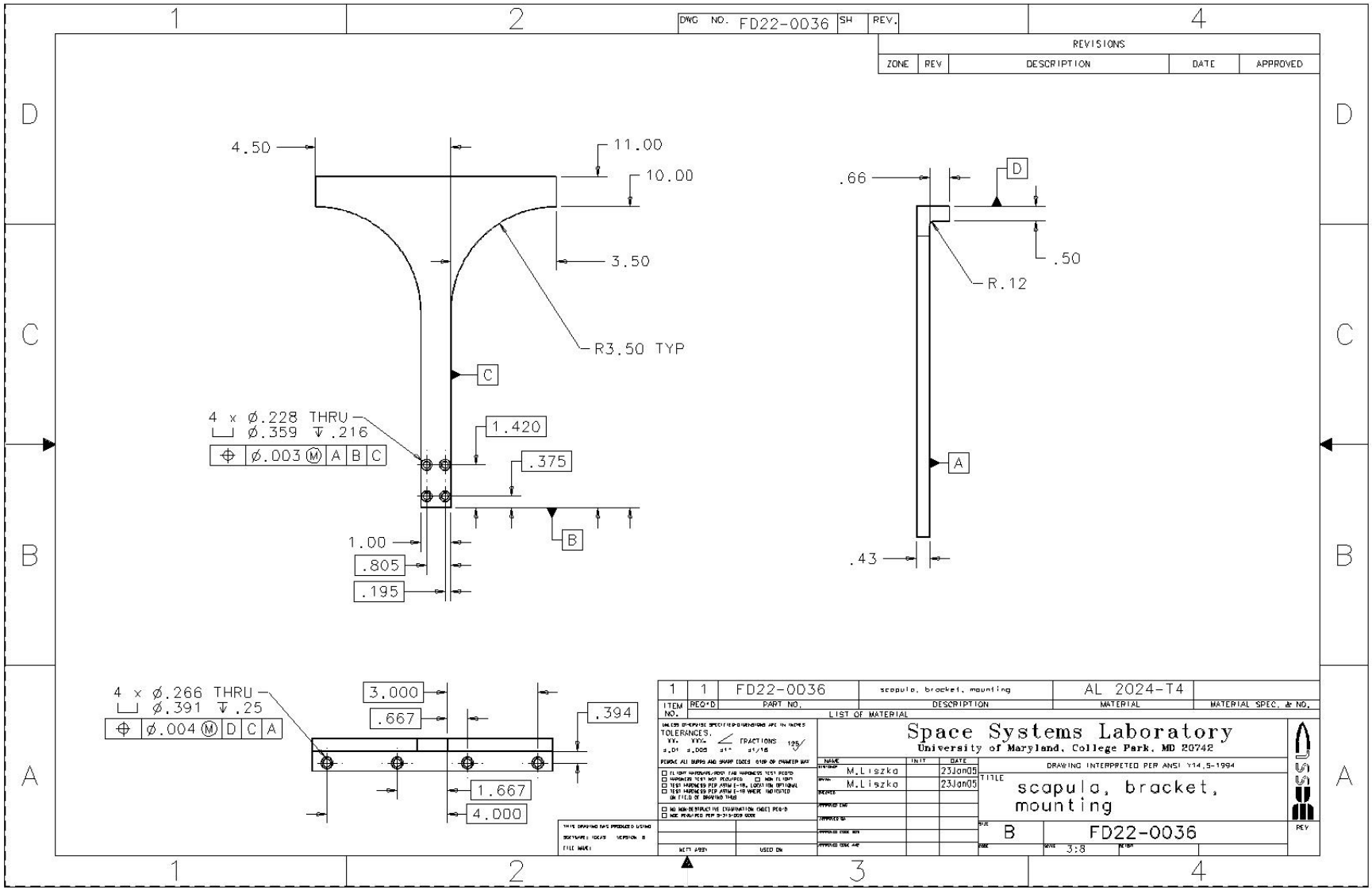
DWG NO. FD22-0036
SH
REV.
REVISIONS
ZONE
REV
DESCRIPTION
DATE
APPROVED
4.50
11.00
10.00
3.50
R3.50 TYP
C
4 x Ø.228 THRU
Ø.359 ↧ .216
Ø.003 M A B C
1.420
.375
B
1.00
.805
.195
.66
D
.50
R.12
A
.43
4 x Ø.266 THRU
Ø.391 ↧ .25
Ø.004 M D C A
3.000
.667
.394
1.667
4.000
1 1 FD22-0036 scapula, bracket, mounting AL 2024-T4
ITEM NO. REQ'D PART NO. DESCRIPTION MATERIAL MATERIAL SPEC. & NO.
LIST OF MATERIAL
TOLERANCES:
Space Systems Laboratory
University of Maryland, College Park, MD 20742
DRAWING INTERPRETED PER ANSI Y14.5-1994
NAME INIT DATE
M.Liszka 23Jan05
M.Liszka 23Jan05
TITLE
scapula, bracket, mounting
B
FD22-0036
REV
SCALE 3:8

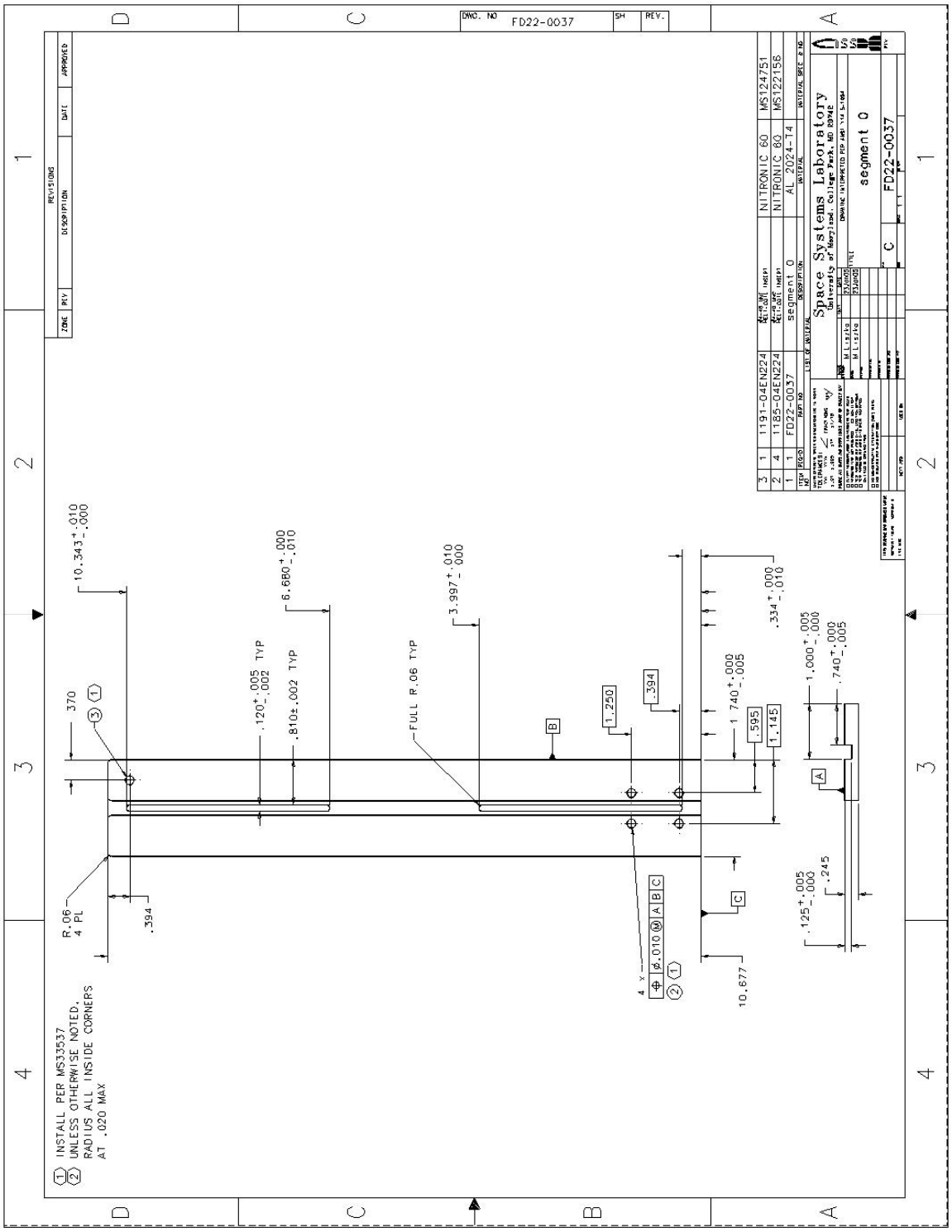
DWG. NO FD22-0037
REV.
segment 0
FD22-0037
Space Systems Laboratory
University of Maryland, College Park, MD 20742
10.343+.010 -.000
6.680+.000 -.010
3.997+.010 -.000
.334+.000 -.010
.120+.005 -.002 TYP
.810±.002 TYP
FULL R.06 TYP
1.740+.000 -.005
1.000+.005 -.000
.740+.000 -.005
.125+.005 -.000
.245
10.677
R.06 4 PL
.394
.370
1.250
.394
.595
1.145
4 X ⌀.010 Ⓜ A B C
INSTALL PER MS33537
UNLESS OTHERWISE NOTED,
RADIUS ALL INSIDE CORNERS
AT .020 MAX

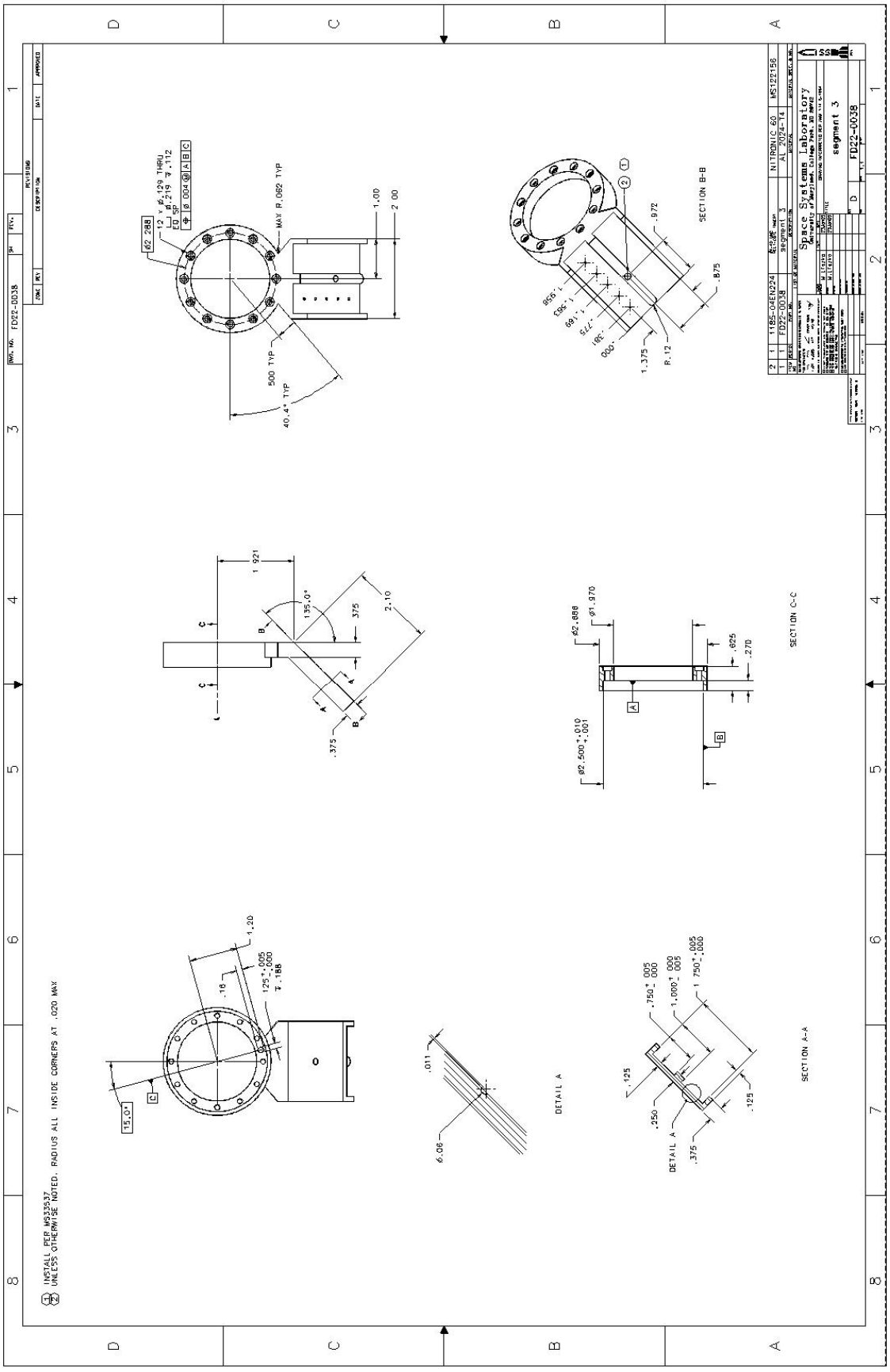
INSTALL PER MS33537
UNLESS OTHERWISE NOTED, RADIUS ALL INSIDE CORNERS AT .020 MAX
SECTION B-B
SECTION C-C
SECTION A-A
DETAIL A
segment 3
FD22-0038

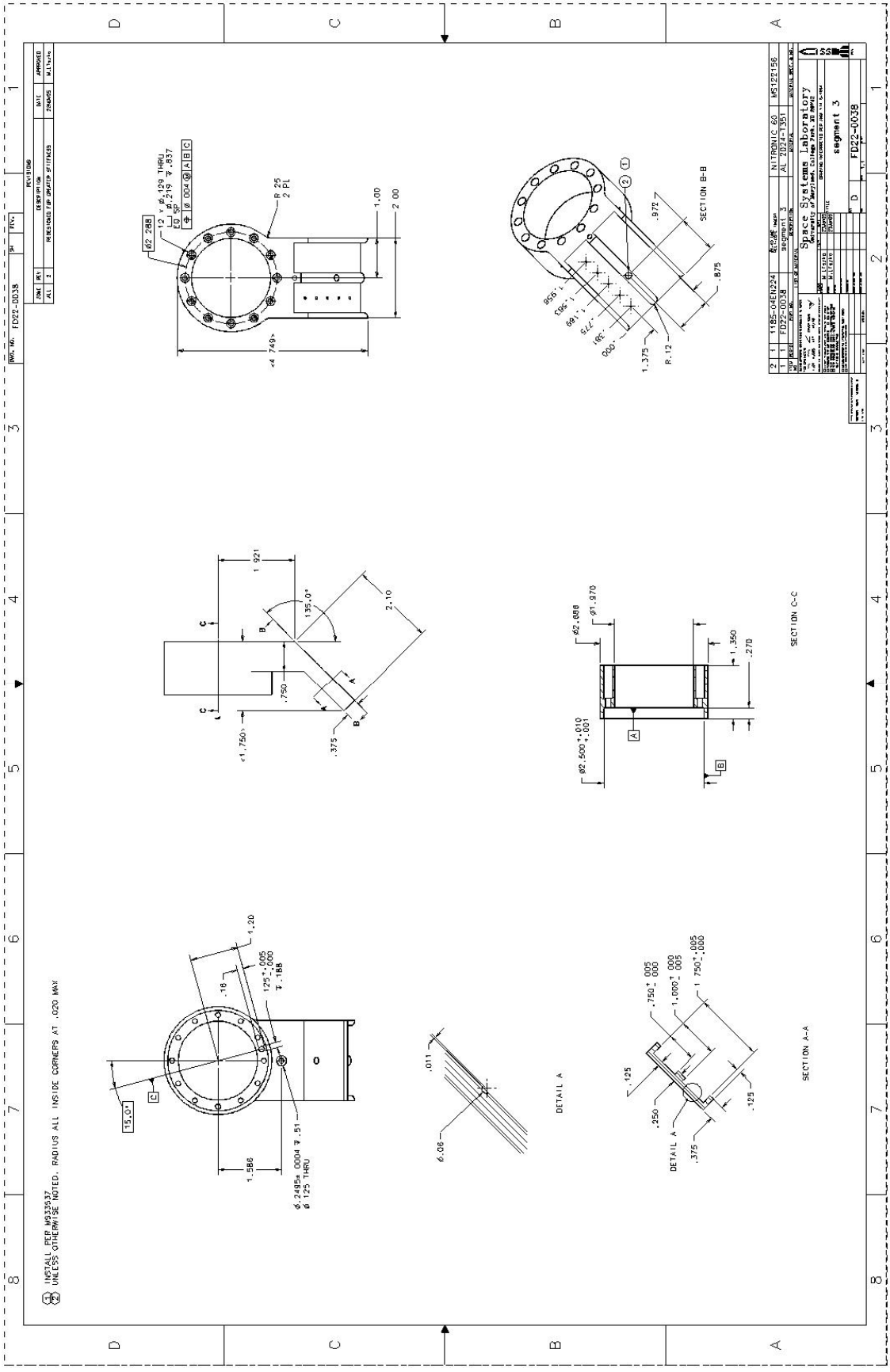

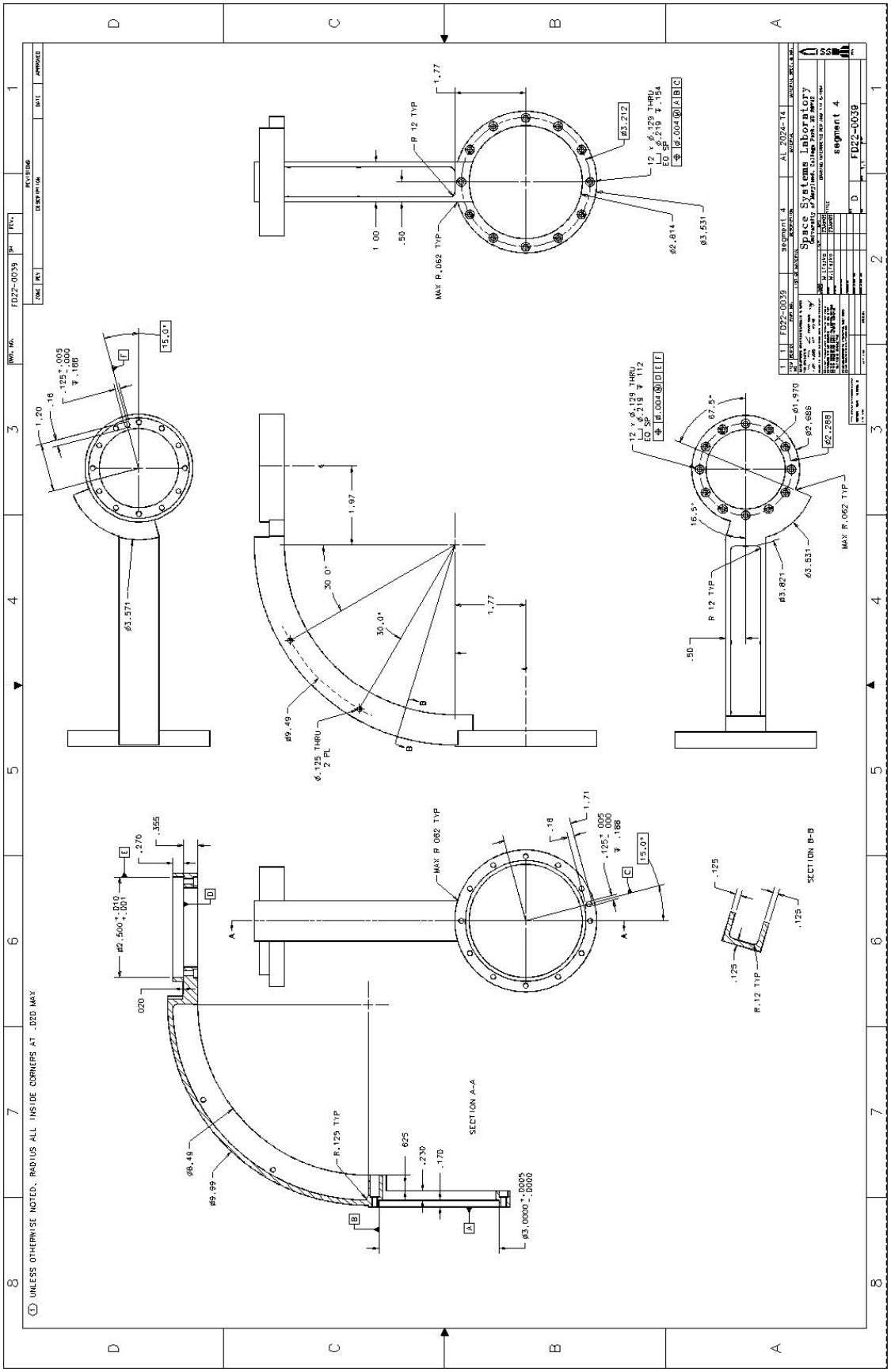
Space Systems Laboratory
segment 4
FD22-0039
UNLESS OTHERWISE NOTED, RADIUS ALL INSIDE CORNERS AT .020 MAX
SECTION A-A
SECTION B-B

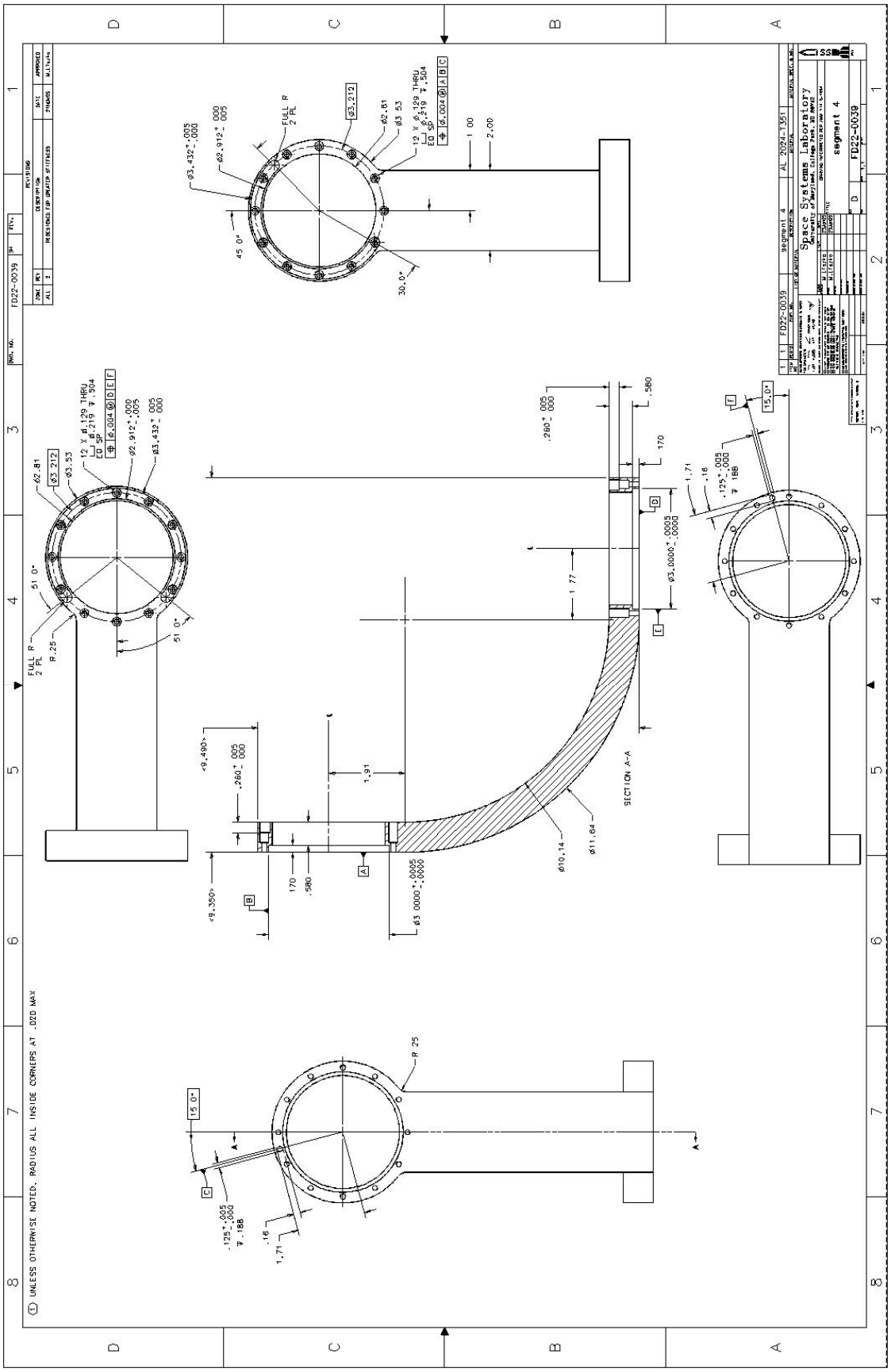
Space Systems Laboratory
segment 4
FD22-0039
SECTION A-A
UNLESS OTHERWISE NOTED, RADIUS ALL INSIDE CORNERS AT .020 MAX

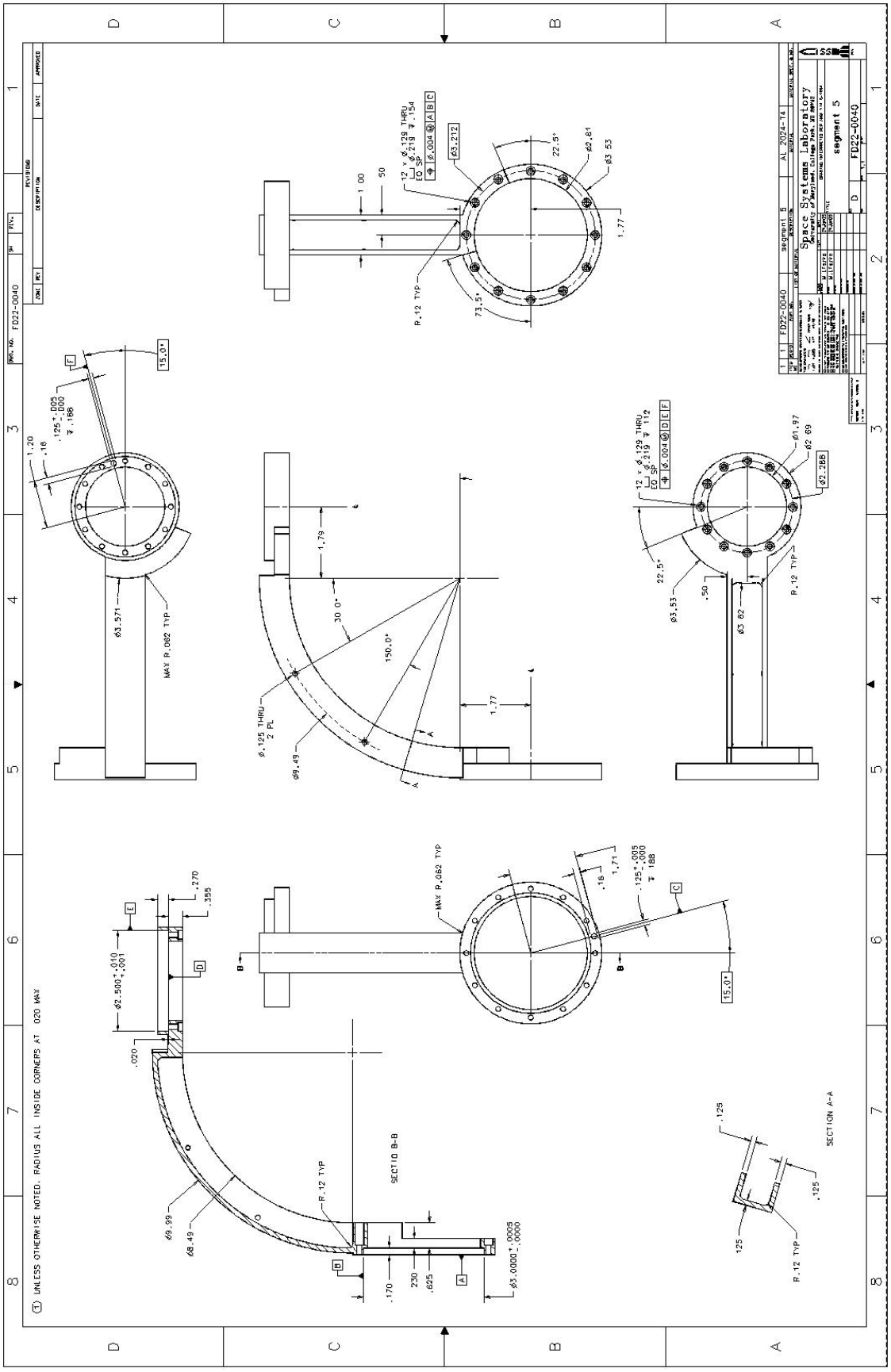
Space Systems Laboratory
segment 5
FD22-0040
SECTION A-A
SECTION B-B
UNLESS OTHERWISE NOTED, RADIUS ALL INSIDE CORNERS AT .020 MAX

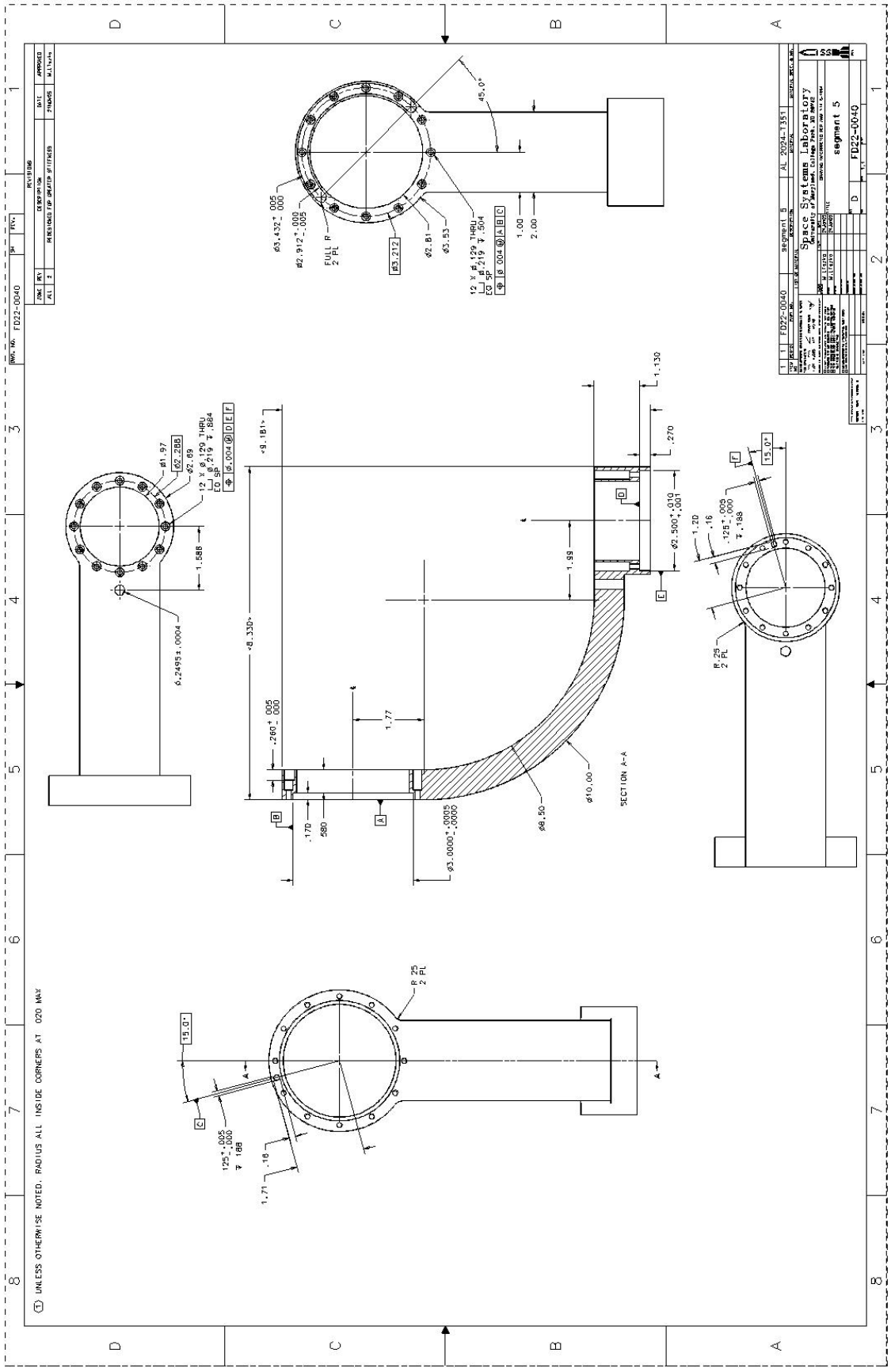
DWG. NO. FD22-0040
REV.
REVISIONS
DESCRIPTION
DATE
APPROVED
REVISED FOR GREATER OFFSETS
2/16/05
M.Hicks
segment 5
FD22-0040
Space Systems Laboratory
University of Maryland, College Park, MD 20742
SCALE: 1/2
SHEET 1 OF 1
SIZE B
AL 2024-T351
UNLESS OTHERWISE NOTED, RADIUS ALL INSIDE CORNERS AT .020 MAX
SECTION A-A
45.0°
15.0°
R.25
2 PL
FULL R
2 PL
12 X ø.129 THRU
ø.219 ↧.504
CB
ø.004 M A B C
ø3.432 +.005 -.000
ø2.912 +.000 -.005
ø3.212
ø2.81
ø3.53
1.00
2.00
ø1.97
ø2.285
ø2.69
ø.004 M D E F
1.588
6.24951.0004
<9.181>
<8.330>
1.130
.270
1.99
ø2.500 +.010 -.001
.260 +.005 -.000
1.77
.170
.580
ø3.0000 +.0005 -.0000
ø8.50
ø10.00
1.20
.16
.125 +.005 -.000
↧.188
.18
1.71

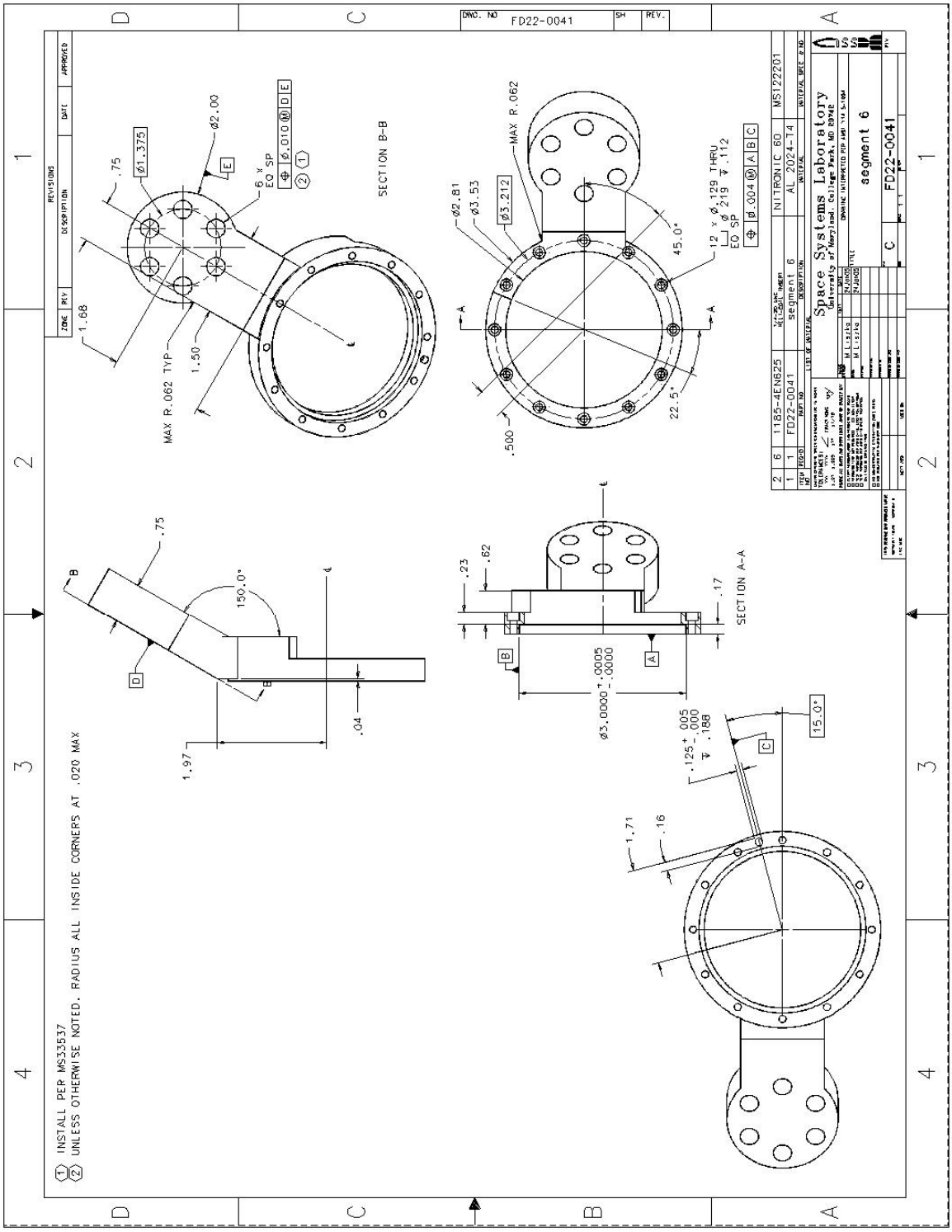
DWG. NO FD22-0041
SH
REV.
Space Systems Laboratory
University of Maryland, College Park, MD 20742
segment 6
FD22-0041
NITRONIC 60
AL 2024-T4
MS122201
1185-4EN625
SECTION B-B
SECTION A-A
MAX R.062 TYP
MAX R.062
12 x Ø.129 THRU EQ SP
6 x EQ SP
Ø2.00
Ø1.375
Ø2.81
Ø3.53
Ø3.212
45.0°
22.5°
150.0°
15.0°
1.68
1.50
1.97
1.71
.75
.62
.23
.17
.16
.04
.500
Ø3.0000 +.0005 -.0000
.125 +.005 -.000 ▼ .188
INSTALL PER MS33537
UNLESS OTHERWISE NOTED, RADIUS ALL INSIDE CORNERS AT .020 MAX

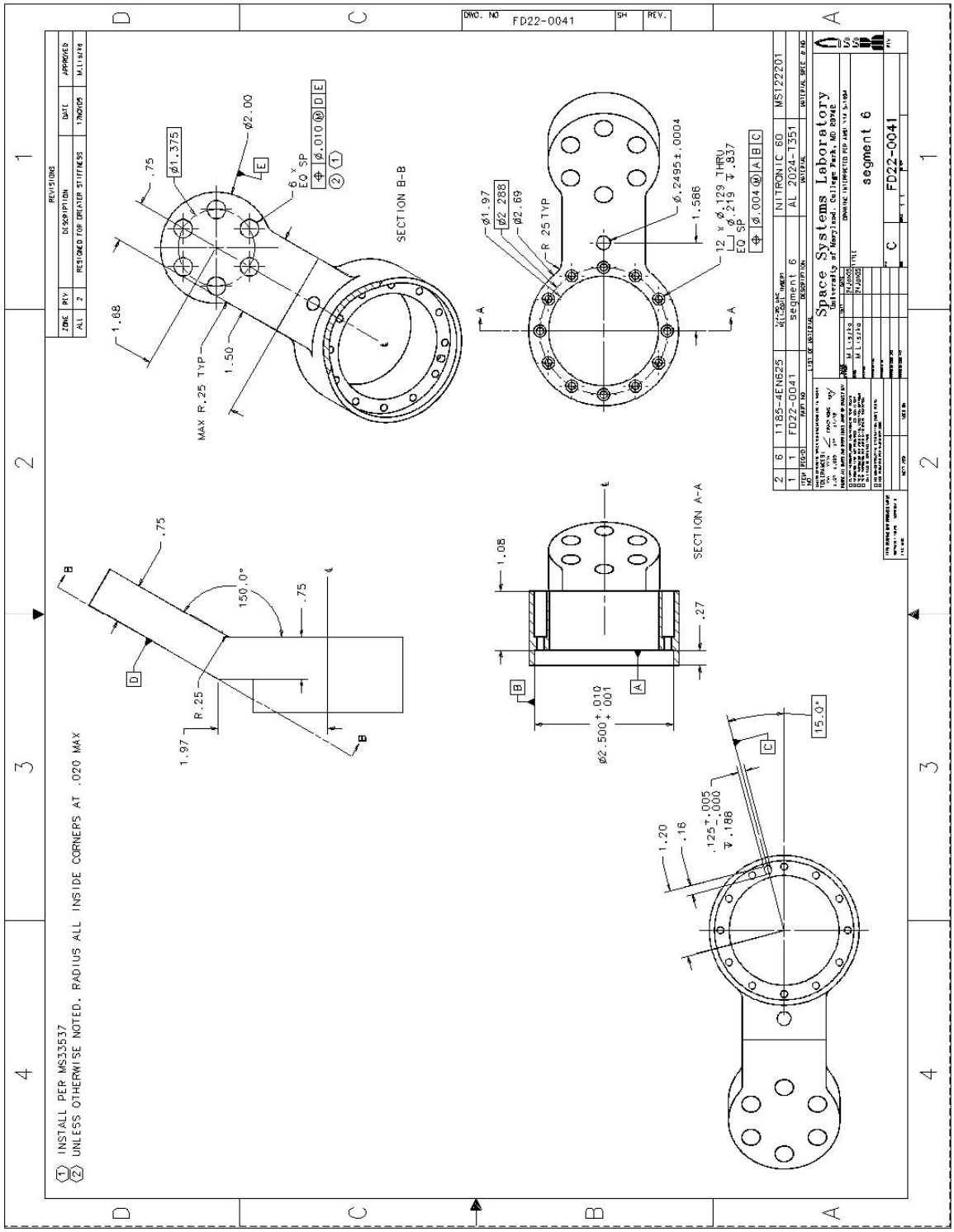
DWG. NO FD22-0041
SH
REV.
Space Systems Laboratory
University of Maryland, College Park, MD 20742
segment 6
FD22-0041
NITRONIC 60
MS122201
AL 2024-T351
SECTION B-B
SECTION A-A
INSTALL PER MS33537
UNLESS OTHERWISE NOTED, RADIUS ALL INSIDE CORNERS AT .020 MAX

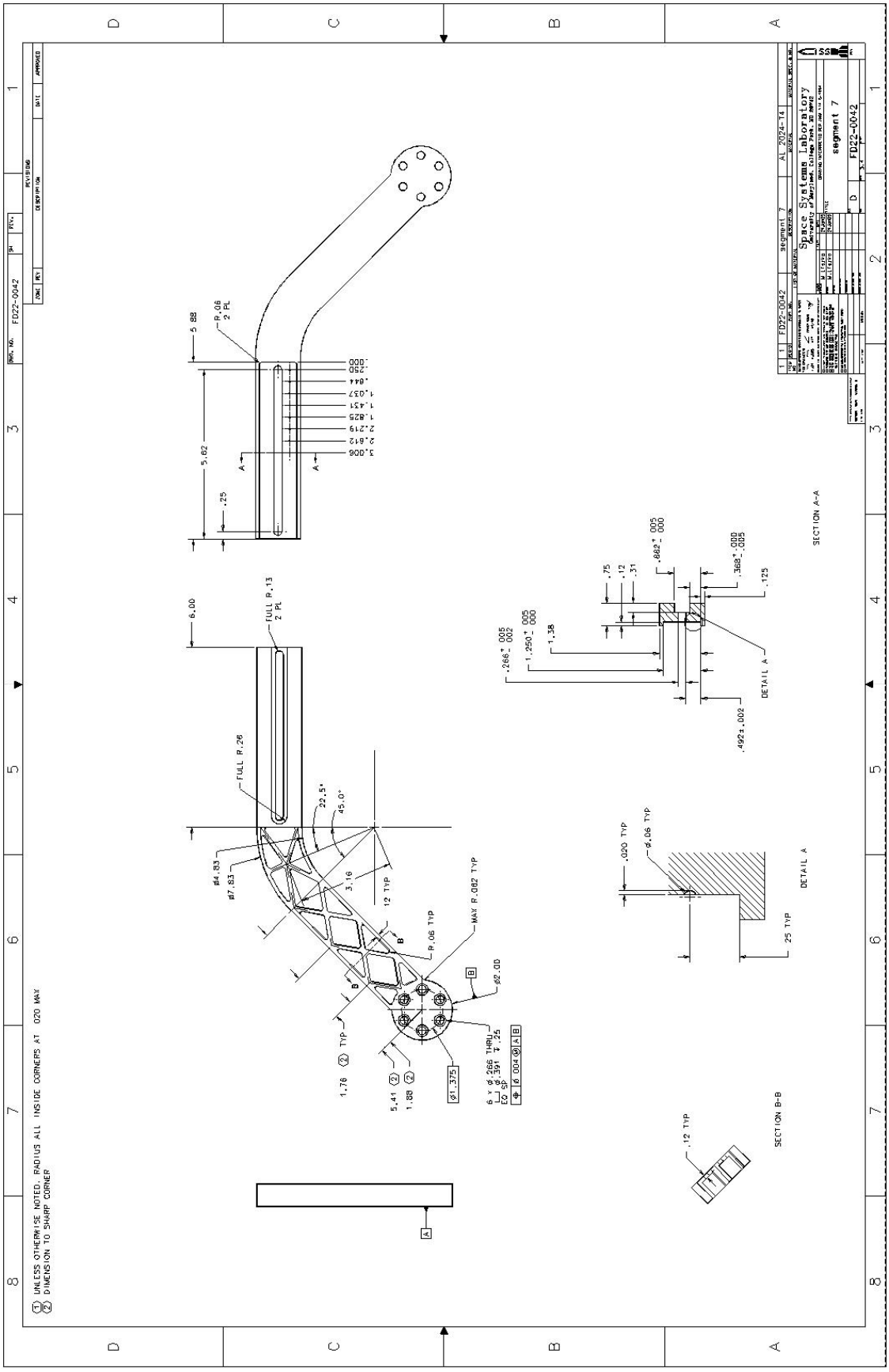
segment 7
FD22-0042
Space Systems Laboratory
UNLESS OTHERWISE NOTED, RADIUS ALL INSIDE CORNERS AT .020 MAX
DIMENSION TO SHARP CORNER
SECTION A-A
SECTION B-B
DETAIL A
DETAIL A

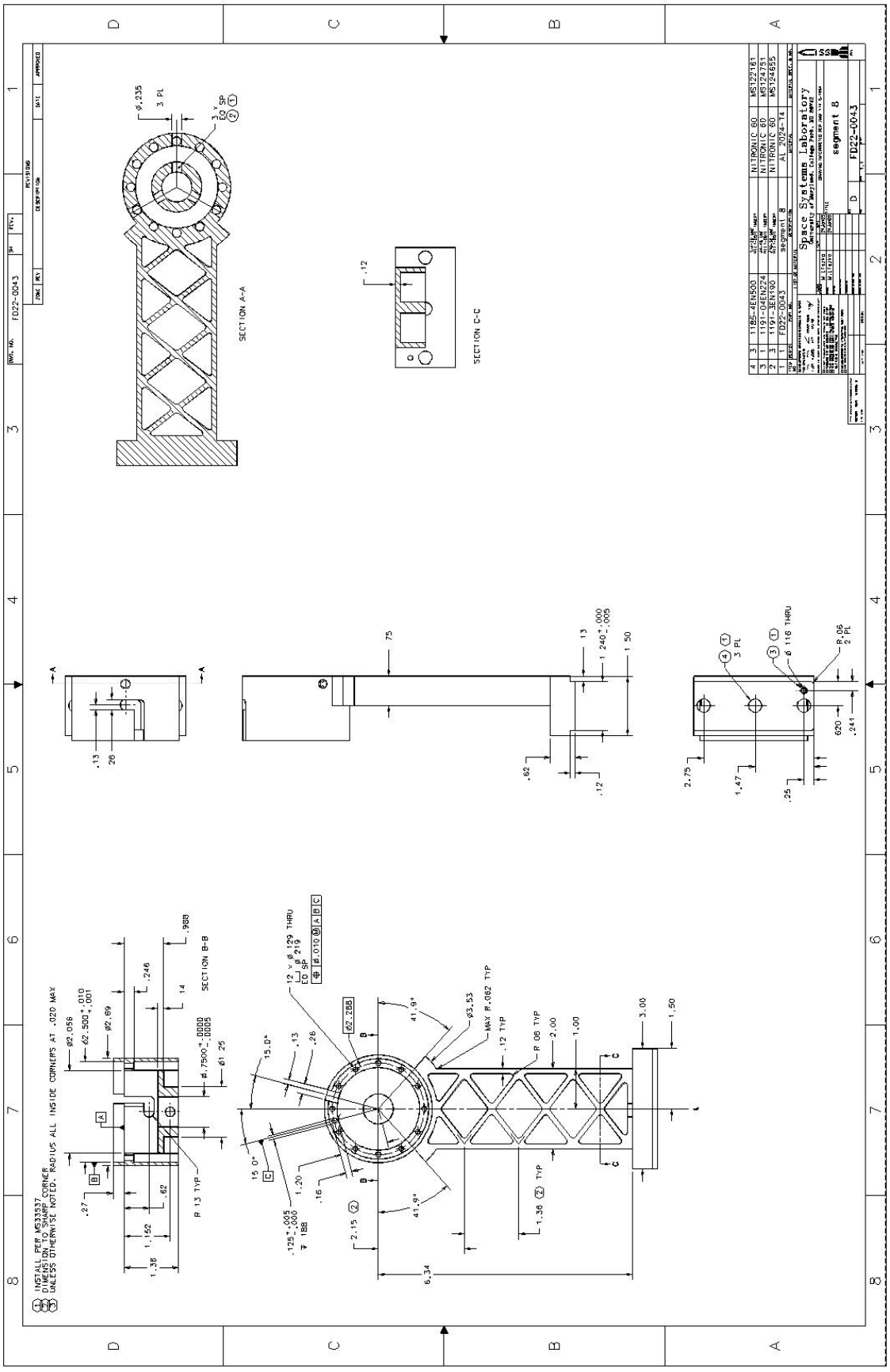
Space Systems Laboratory
segment 8
FD22-0043
SECTION A-A
SECTION B-B
SECTION C-C
INSTALL PER MS33537
DIMENSION TO SHARP CORNER
UNLESS OTHERWISE NOTED, RADIUS ALL INSIDE CORNERS AT .020 MAX

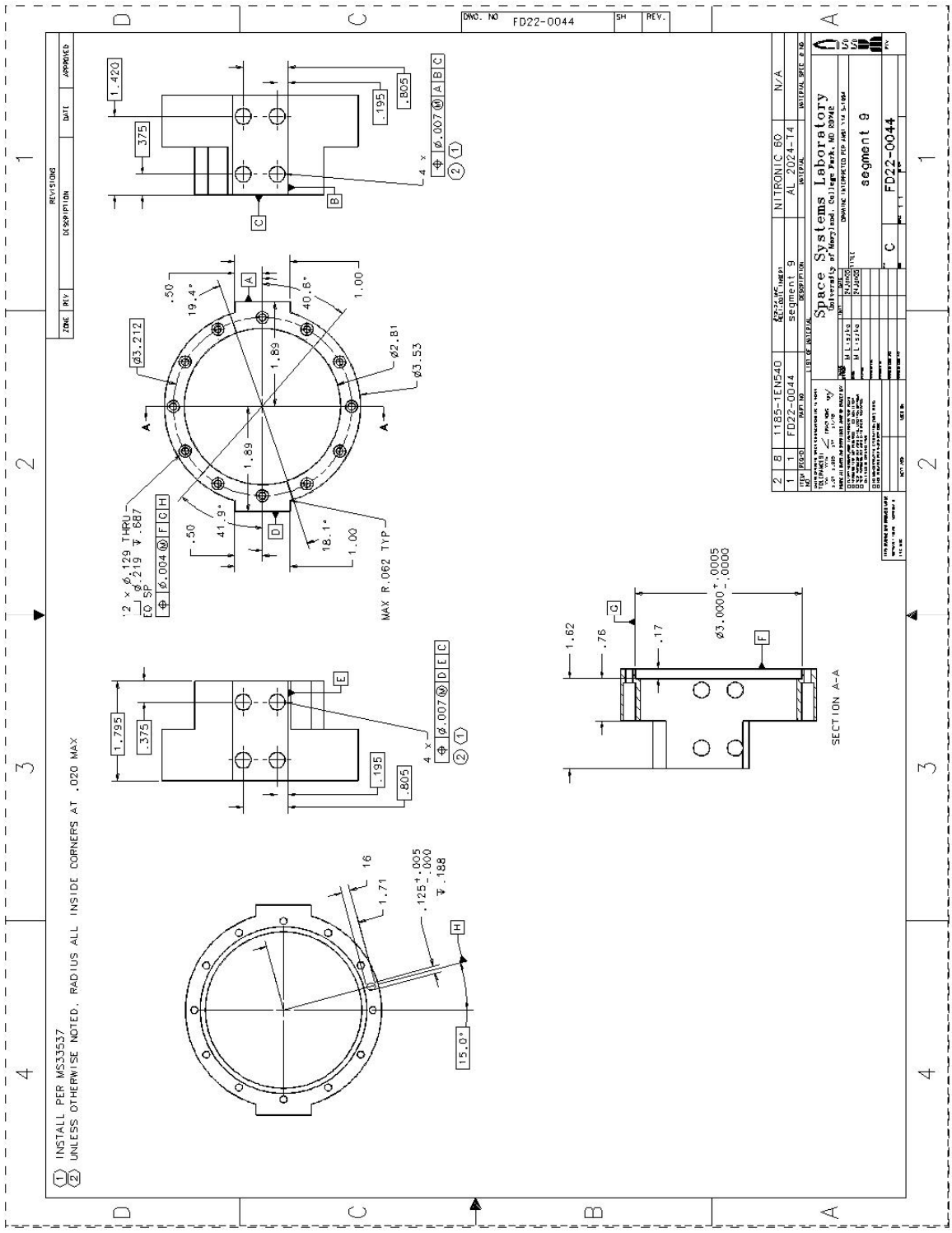
DWG. NO FD22-0044
REV.
Space Systems Laboratory
University of Maryland, College Park, MD 20742
segment 9
FD22-0044
NITRONIC 60
AL 2024-T4
N/A
SECTION A-A
MAX R.062 TYP
1. INSTALL PER MS33537
2. UNLESS OTHERWISE NOTED, RADIUS ALL INSIDE CORNERS AT .020 MAX

DWG NO. FD22-0045 | SH | REV.

(1) UNLESS OTHERWISE NOTED, RADIUS ALL INSIDE CORNERS AT .020 MAX

REVISIONS				
ZONE	REV	DESCRIPTION	DATE	APPROVED

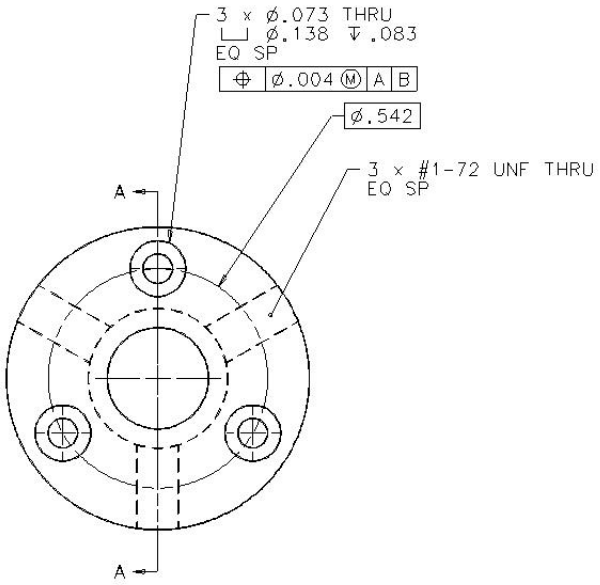

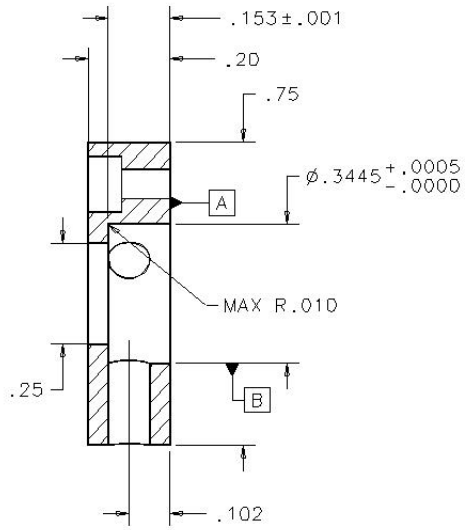

SECTION A-A

ITEM NO.	REQ'D	PART NO.	DESCRIPTION	MATERIAL	MATERIAL SPEC. & NO.
1	1	FD22-0045	actuator, absolute encoder, hub	AISI 304 S.S.	

LIST OF MATERIAL

UNLESS OTHERWISE SPECIFIED DIMENSIONS ARE IN INCHES
TOLERANCES.
XX. ±.01 XXX. ±.005 ANGLES ±1° FRACTIONS ±1/16 125

REMOVE ALL BURRS AND SHARP EDGES 0.05 OR CHAMFER MAX

- ☐ FLIGHT HARDWARE/ANY EAR HARDNESS TEST REQ'D
- ☐ WORKMANSHIP TEST NOT REQUIRED ☐ NON FLIGHT
- ☐ TEST HARDNESS PER ASTM E-18, LOCATION OPTIONAL
- ☐ TEST HARDNESS PER ASTM E-18 WHERE INDICATED ON FIELD OF DRAWING THIS
- ☐ NO NON-DESTRUCTIVE EXAMINATION (NDE) REQ'D
- ☐ NDE REQUIRED PER S-313-100 CODE

THIS DRAWING WAS PRODUCED USING SOFTWARE: IDEAS VERSION 8 FILE NAME:

NEXT ASSY	USED ON

	NAME	INIT	DATE
DRAWN	M.Liszka		24Jan05
CHK'D	M.Liszka		24Jan05
ENGR APPR.			
MFG APPR.			
APPROVED QUAL			
APPROVED QUAL MGR			
APPROVED QUAL AUTH			

Space Systems Laboratory
University of Maryland, College Park, MD 20742

DRAWING INTERPRETED PER ANSI Y14.5-1994

TITLE: actuator, absolute encoder, hub

SIZE	DWG NO.	REV
B	FD22-0045	

SCALE 3:1 SHEET

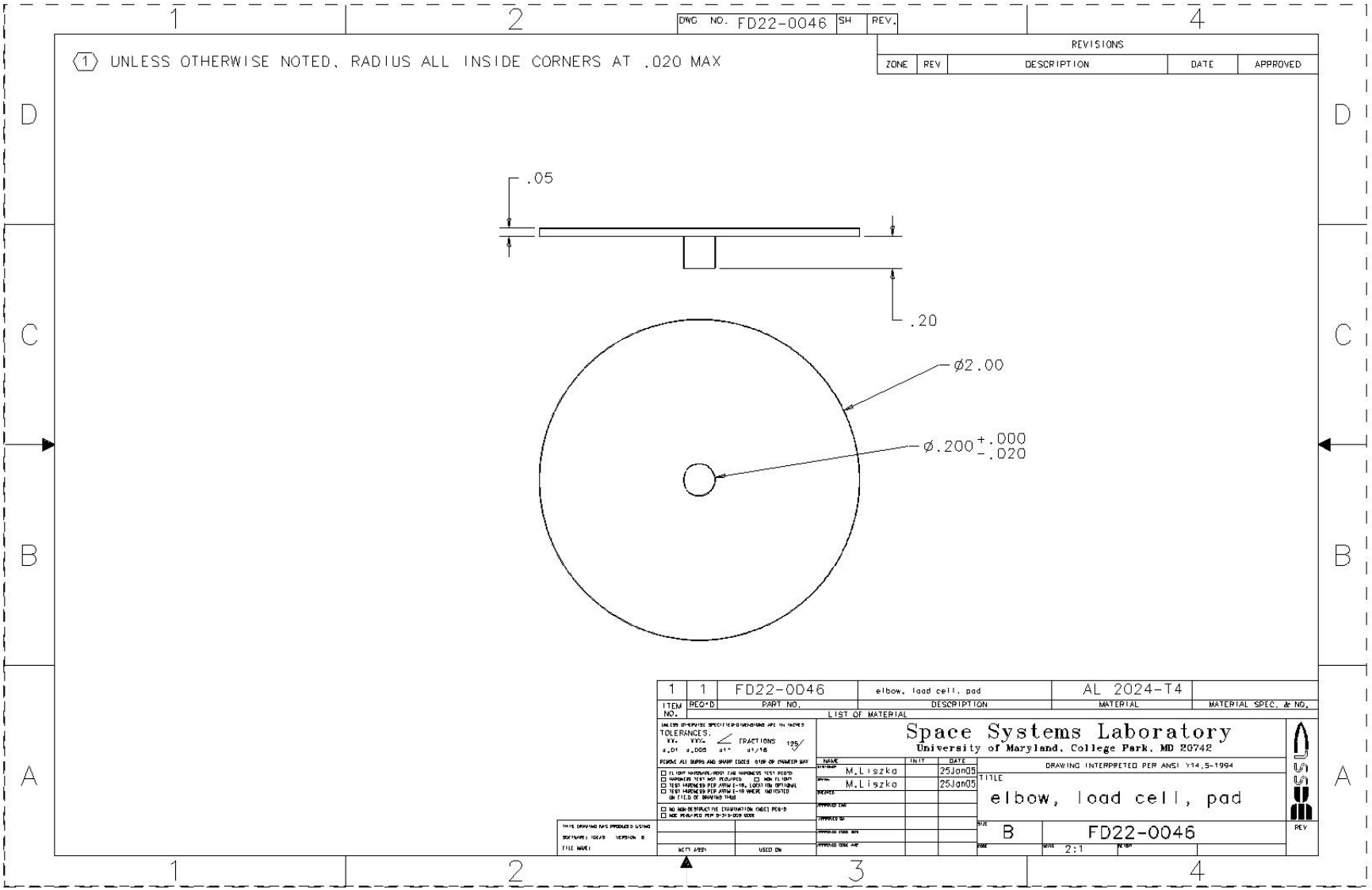
DWG NO. FD22-0046
SH
REV.
REVISIONS
ZONE
REV
DESCRIPTION
DATE
APPROVED
1 UNLESS OTHERWISE NOTED, RADIUS ALL INSIDE CORNERS AT .020 MAX
.05
.20
ø2.00
ø.200 +.000 -.020
ITEM NO.
REQ'D
PART NO.
DESCRIPTION
MATERIAL
MATERIAL SPEC. & NO.
1
1
FD22-0046
elbow, load cell, pad
AL 2024-T4
LIST OF MATERIAL
TOLERANCES.
FRACTIONS
Space Systems Laboratory
University of Maryland, College Park, MD 20742
NAME
INIT
DATE
M.Liszka
25Jan05
M.Liszka
25Jan05
DRAWING INTERPRETED PER ANSI Y14.5-1994
TITLE
elbow, load cell, pad
SIZE
B
FD22-0046
REV
SCALE
2:1
WEIGHT
SHEET
1
2
3
4
A
B
C
D

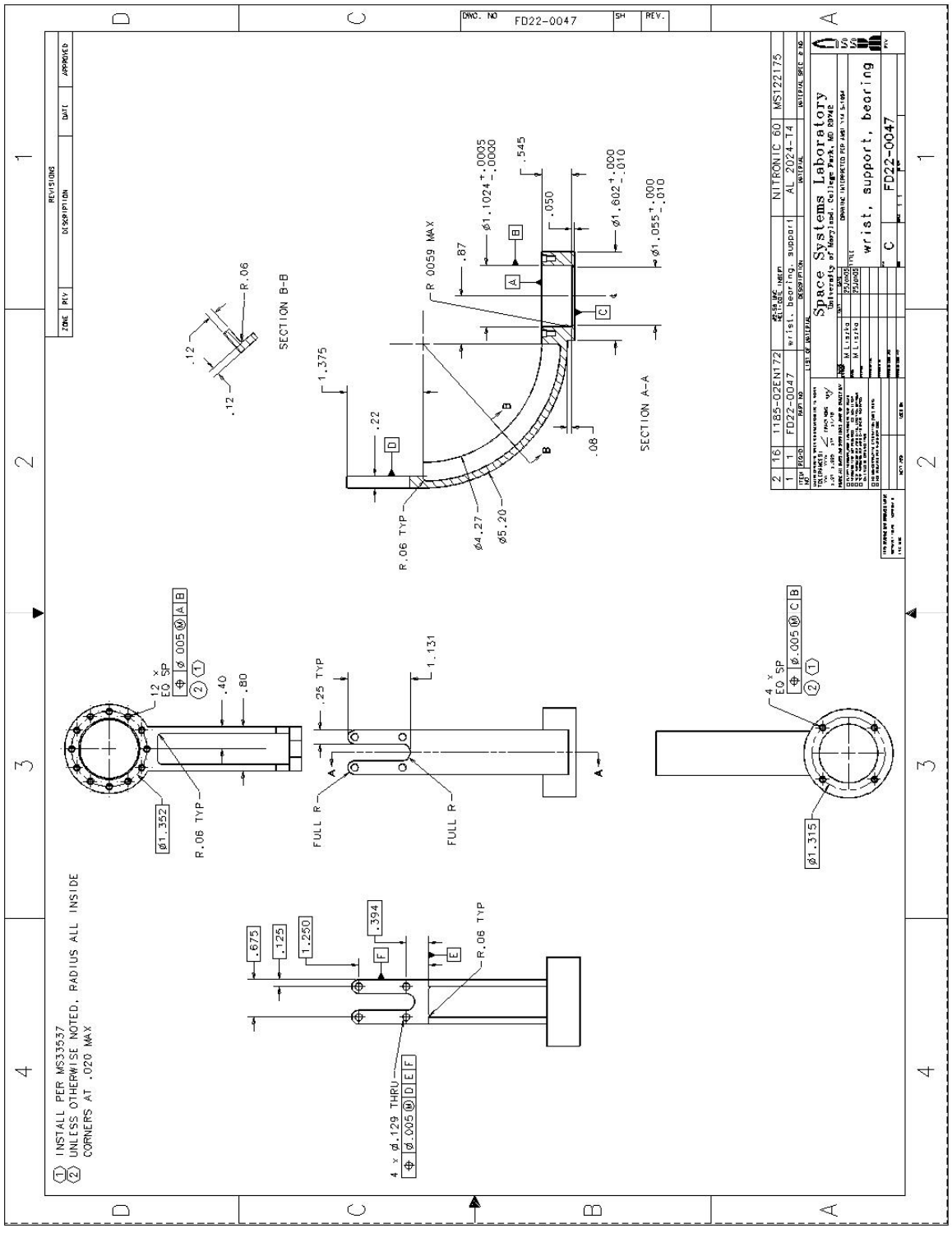
DWG. NO FD22-0047
SH
REV.
REVISIONS
ZONE
REV
DESCRIPTION
DATE
APPROVED
SECTION B-B
SECTION A-A
R.06
.12
.12
1.375
.22
R.06 TYP
R .0059 MAX
.87
.545
.050
.08
ø1.1024 +.0005 -.0000
ø1.602 +.000 -.010
ø1.055 +.000 -.010
ø4.27
ø5.20
12 X EQ SP
ø .005 M A B
2 1
.40
.80
ø1.352
R.06 TYP
.25 TYP
1.131
FULL R
FULL R
4 X EQ SP
ø.005 M C B
ø1.315
4 X ø.129 THRU
ø.005 M D E F
.675
.125
1.250
.394
R.06 TYP
1 INSTALL PER MS33537
2 UNLESS OTHERWISE NOTED, RADIUS ALL INSIDE CORNERS AT .020 MAX
2 16 1185-02EN172
1 1 FD22-0047
ITEM NO PART NO DESCRIPTION MATERIAL
NITRONIC 60 MS122175
AL 2024-T4
Space Systems Laboratory
University of Maryland, College Park, MD 20742
wrist, support, bearing
C FD22-0047

DWG NO. FD22-0048 | SH | REV.

(1) INSTALL PER MS33537
(2) UNLESS OTHERWISE NOTED, RADIUS ALL INSIDE CORNERS AT .020 MAX

REVISIONS				
ZONE	REV	DESCRIPTION	DATE	APPROVED

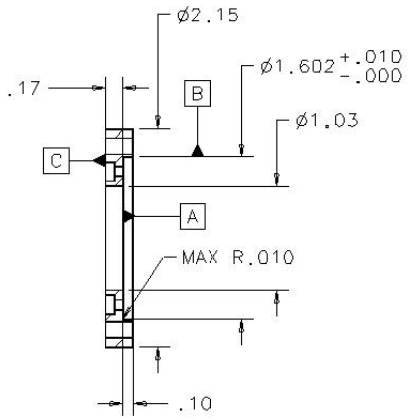

SECTION A-A

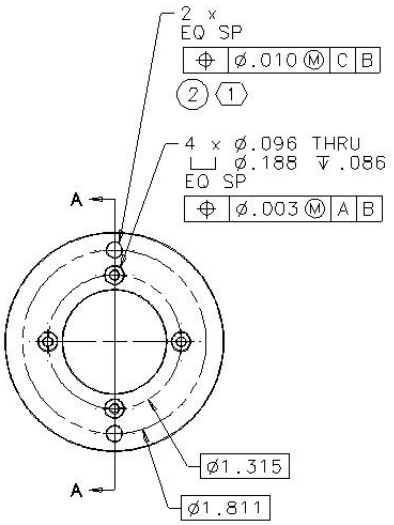

ITEM NO.	REQ'D	PART NO.	DESCRIPTION	MATERIAL	MATERIAL SPEC. & NO.
2	2	1185-04EN224	#4-40 UNC HELI-COIL INSERT	NITRONIC 60	MS122156
1	1	FD22-0048	wrist, encoder, support	AL 2024-T4	

LIST OF MATERIAL

UNLESS OTHERWISE SPECIFIED DIMENSIONS ARE IN INCHES
TOLERANCES.
XX- ±.01 XXX- ±.005 ∠ ±1° FRACTIONS ±1/16 125

REMOVE ALL BURRS AND SHARP EDGES 0.010 OR GREATER MAX

☐ FLIGHT HARDWARE/ROOT FAB HARDNESS TEST REQ'D
☐ HARDNESS TEST NOT REQUIRED ☐ NON FLIGHT
☐ TEST HARDNESS PER ASTM E-18, LOCATION OPTIONAL
☐ TEST HARDNESS PER ASTM E-18 WHERE INDICATED ON FIELD OF DRAWING TREE

☐ NO NON-DESTRUCTIVE EXAMINATION (NDE) REQ'D
☐ NDE PERFORMED PER S-313-009 CODE

THIS DRAWING WAS PRODUCED USING
SOFTWARE: IDEAS VERSION 8
TITLE MARK1

NEXT ASSY	USED ON

	NAME	INIT	DATE
DRAWN	M.Liszka		25Jan05
CHK'D	M.Liszka		25Jan05
ENGR'G			
APPROVED			
APPROVED			
APPROVED			
APPROVED			

Space Systems Laboratory
University of Maryland, College Park, MD 20742

DRAWING INTERPRETED PER ANSI Y14.5-1994

TITLE
wrist, encoder, support

SIZE B | FD22-0048 | REV

SCALE 1:1 | SHEET

USED ON

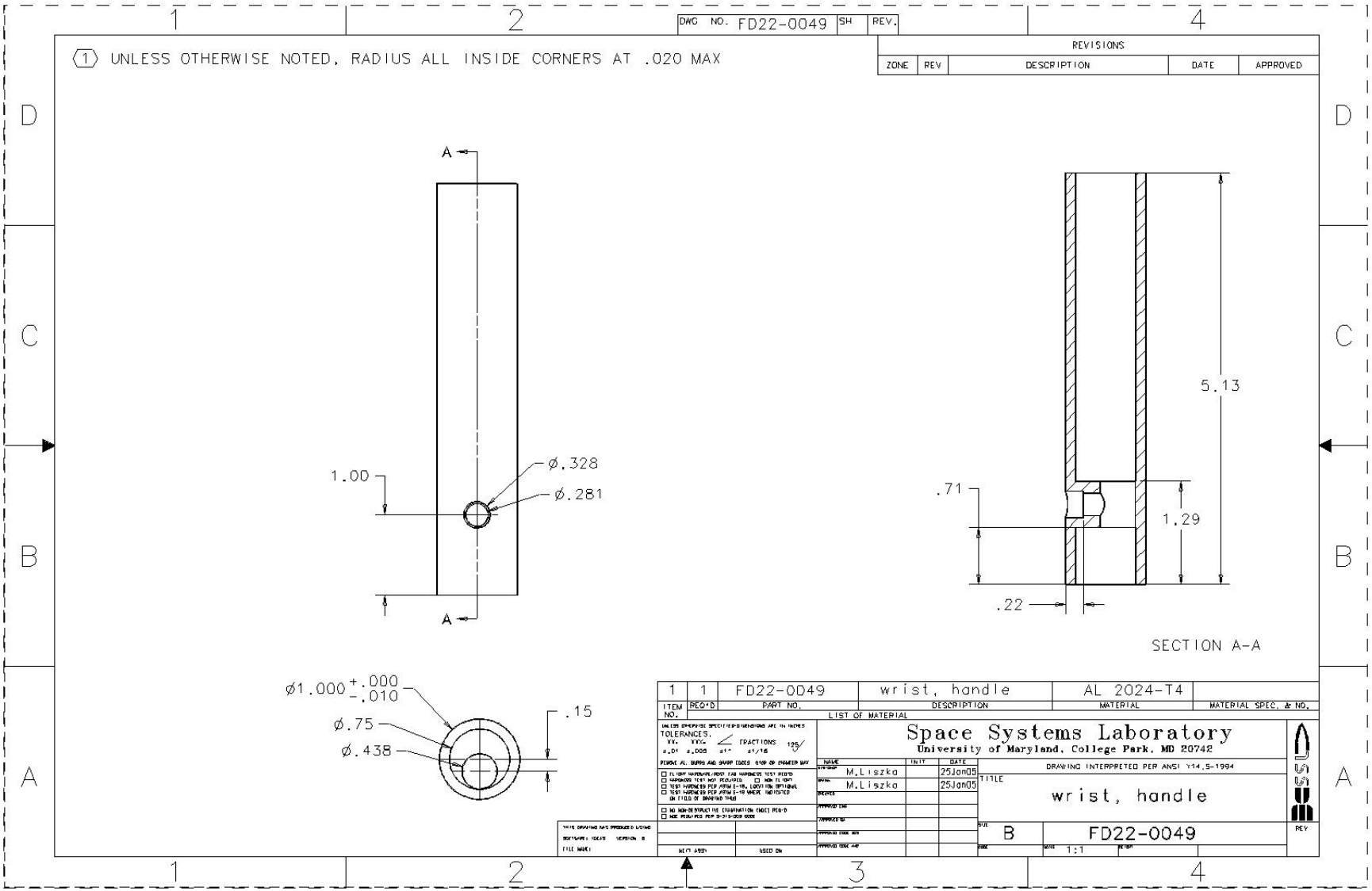
DWG NO. FD22-0049
SH
REV.
1 UNLESS OTHERWISE NOTED, RADIUS ALL INSIDE CORNERS AT .020 MAX
REVISIONS
ZONE
REV
DESCRIPTION
DATE
APPROVED
A
1.00
Ø.328
Ø.281
A
5.13
.71
1.29
.22
SECTION A-A
Ø1.000 +.000 -.010
Ø.75
Ø.438
.15
1 1 FD22-0049 wrist, handle AL 2024-T4
ITEM NO. REQ'D PART NO. DESCRIPTION MATERIAL MATERIAL SPEC. & NO.
LIST OF MATERIAL
TOLERANCES.
FRACTIONS
Space Systems Laboratory
University of Maryland, College Park, MD 20742
M.Liszka 25Jan05
M.Liszka 25Jan05
DRAWING INTERPRETED PER ANSI Y14.5-1994
TITLE
wrist, handle
B
FD22-0049
REV
SCALE 1:1
1
2
3
4
D
C
B
A

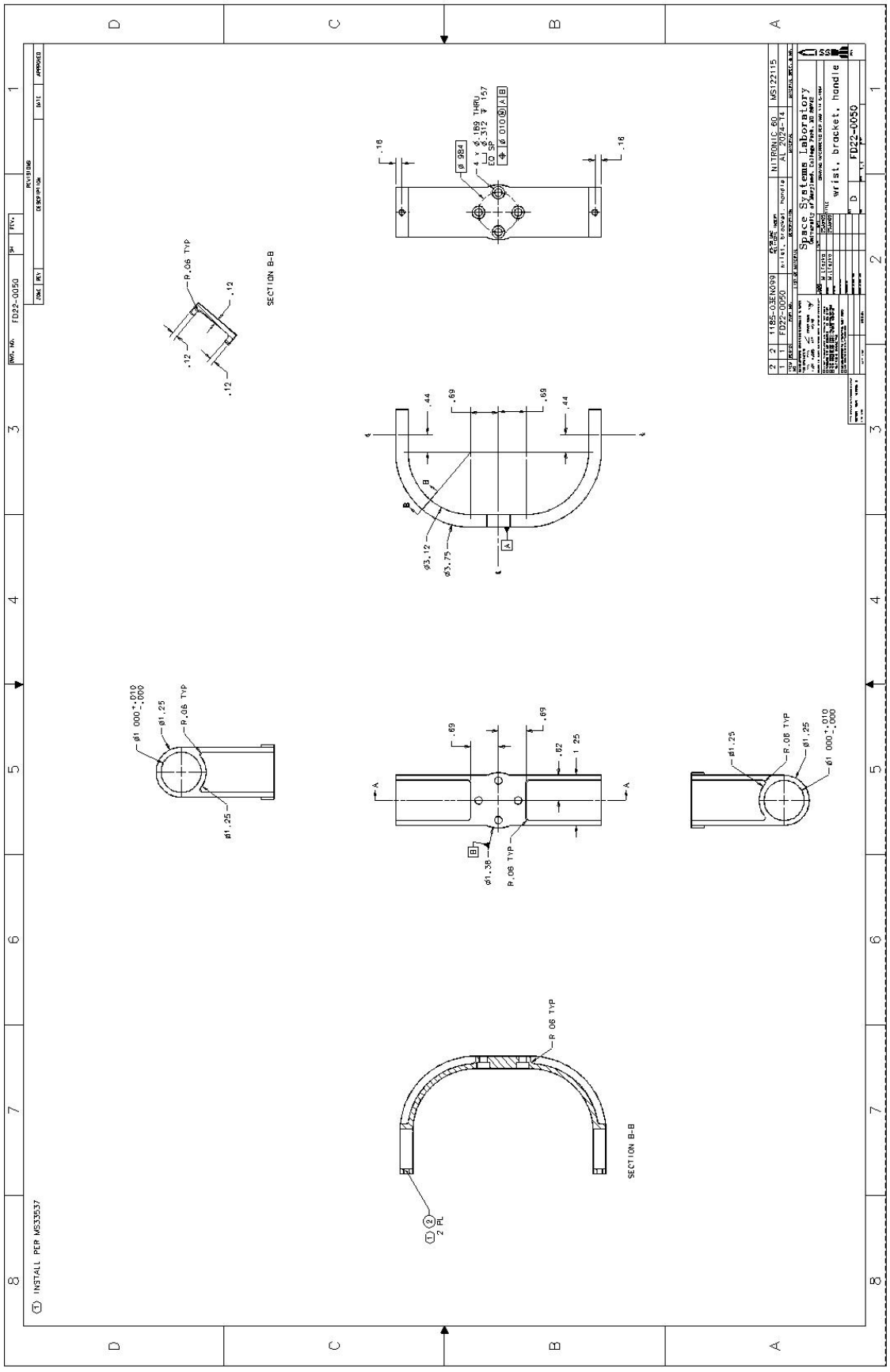
Space Systems Laboratory
wrist, bracket, handle
FD22-0050
SECTION B-B
SECTION B-B
INSTALL PER MS33537

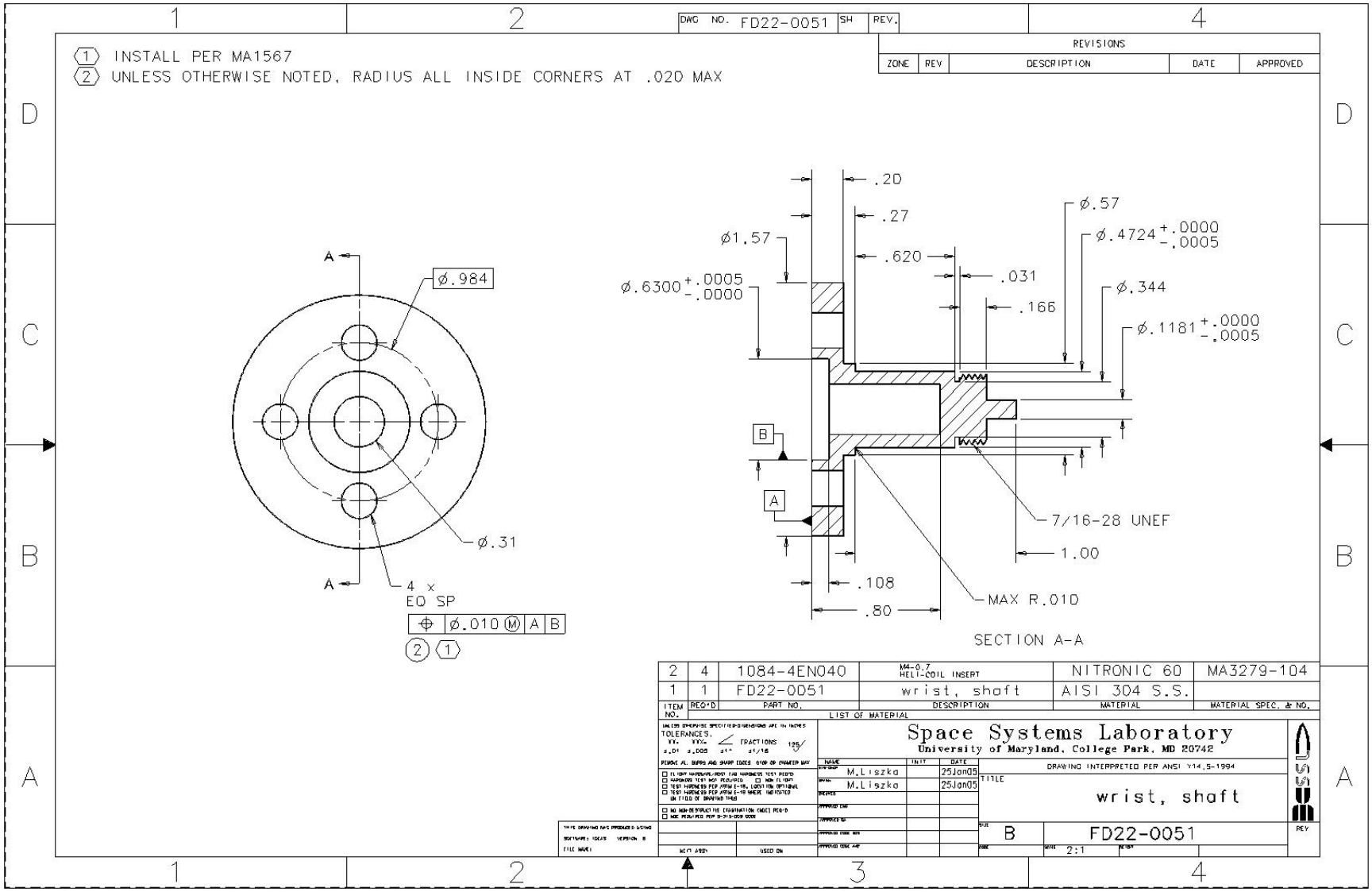
DWG NO. FD22-0051
SH
REV.
REVISIONS
ZONE
REV
DESCRIPTION
DATE
APPROVED
1 INSTALL PER MA1567
2 UNLESS OTHERWISE NOTED, RADIUS ALL INSIDE CORNERS AT .020 MAX
Ø.984
Ø.31
4 x EQ SP
Ø.010 M A B
.20
.27
Ø1.57
.620
.031
Ø.57
Ø.4724 +.0000 -.0005
Ø.6300 +.0005 -.0000
.166
Ø.344
Ø.1181 +.0000 -.0005
7/16-28 UNEF
1.00
.108
.80
MAX R.010
SECTION A-A
2 4 1084-4EN040 M4-0.7 HELI-COIL INSERT NITRONIC 60 MA3279-104
1 1 FD22-0051 wrist, shaft AISI 304 S.S.
ITEM NO. REQ'D PART NO. DESCRIPTION MATERIAL MATERIAL SPEC. & NO.
LIST OF MATERIAL
TOLERANCES.
FRACTIONS
Space Systems Laboratory
University of Maryland, College Park, MD 20742
DRAWING INTERPRETED PER ANSI Y14.5-1994
M.Liszka 25Jan05
M.Liszka 25Jan05
TITLE
wrist, shaft
B
FD22-0051
REV
2:1

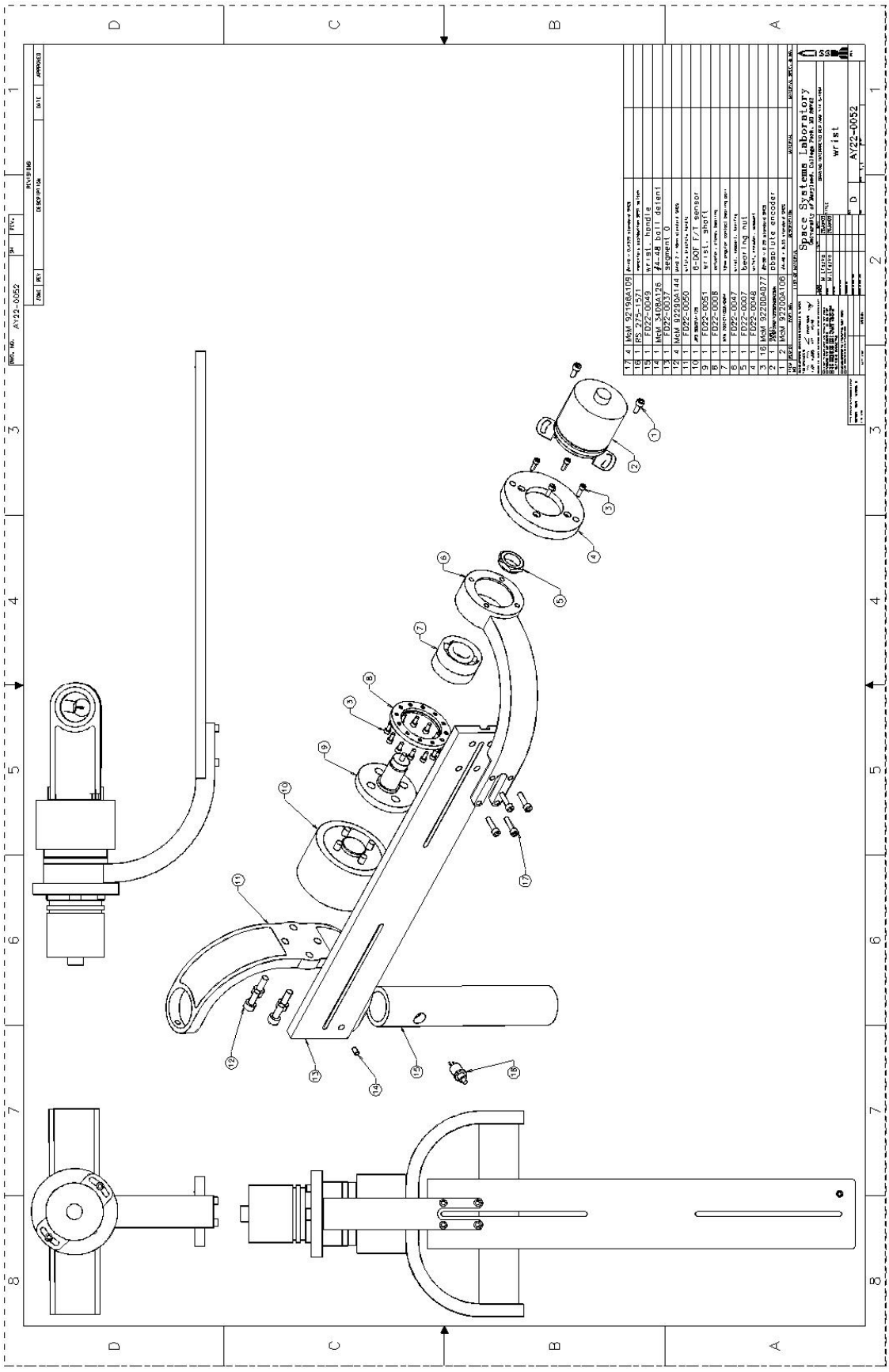
Space Systems Laboratory
wrist
AY22-0052

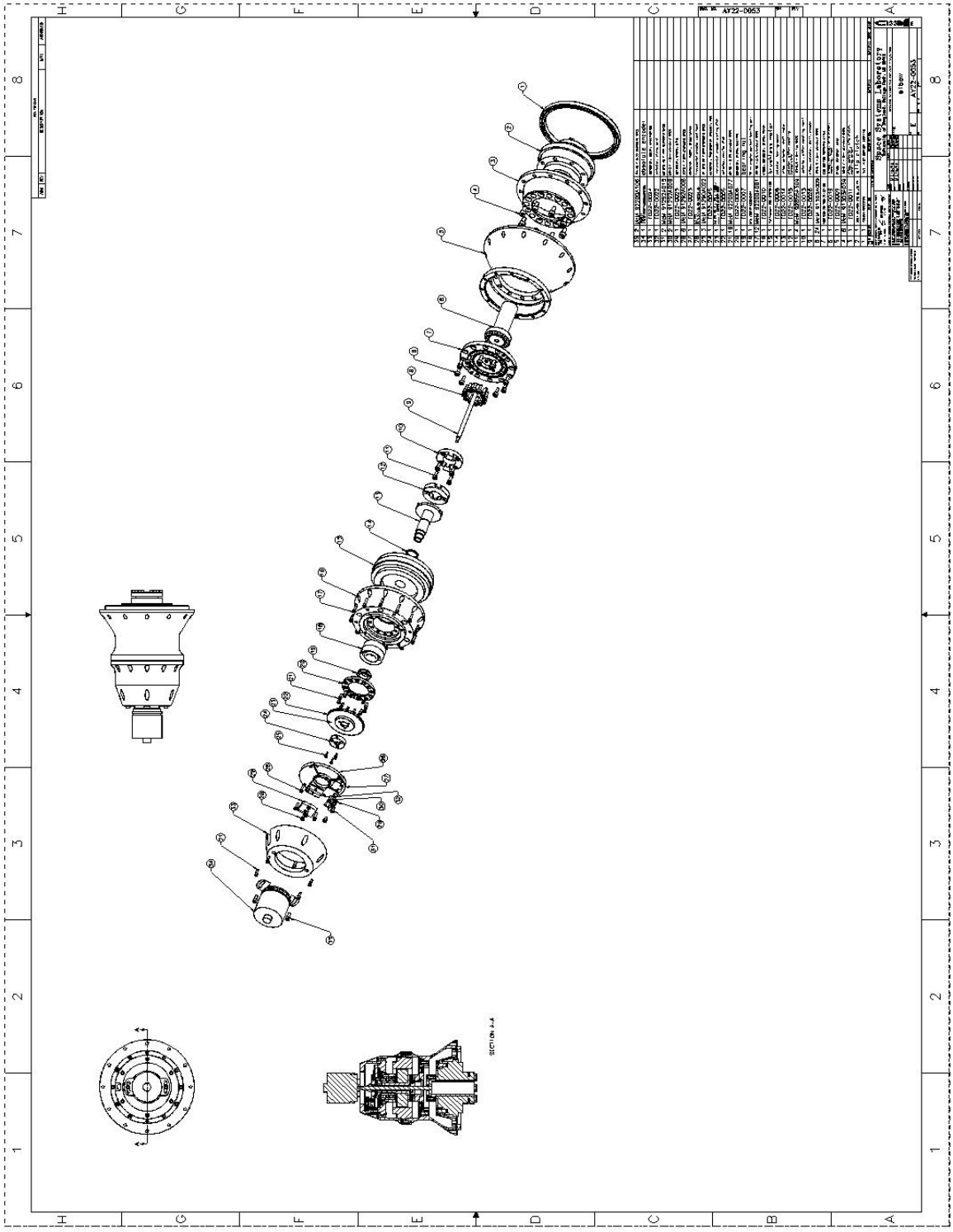

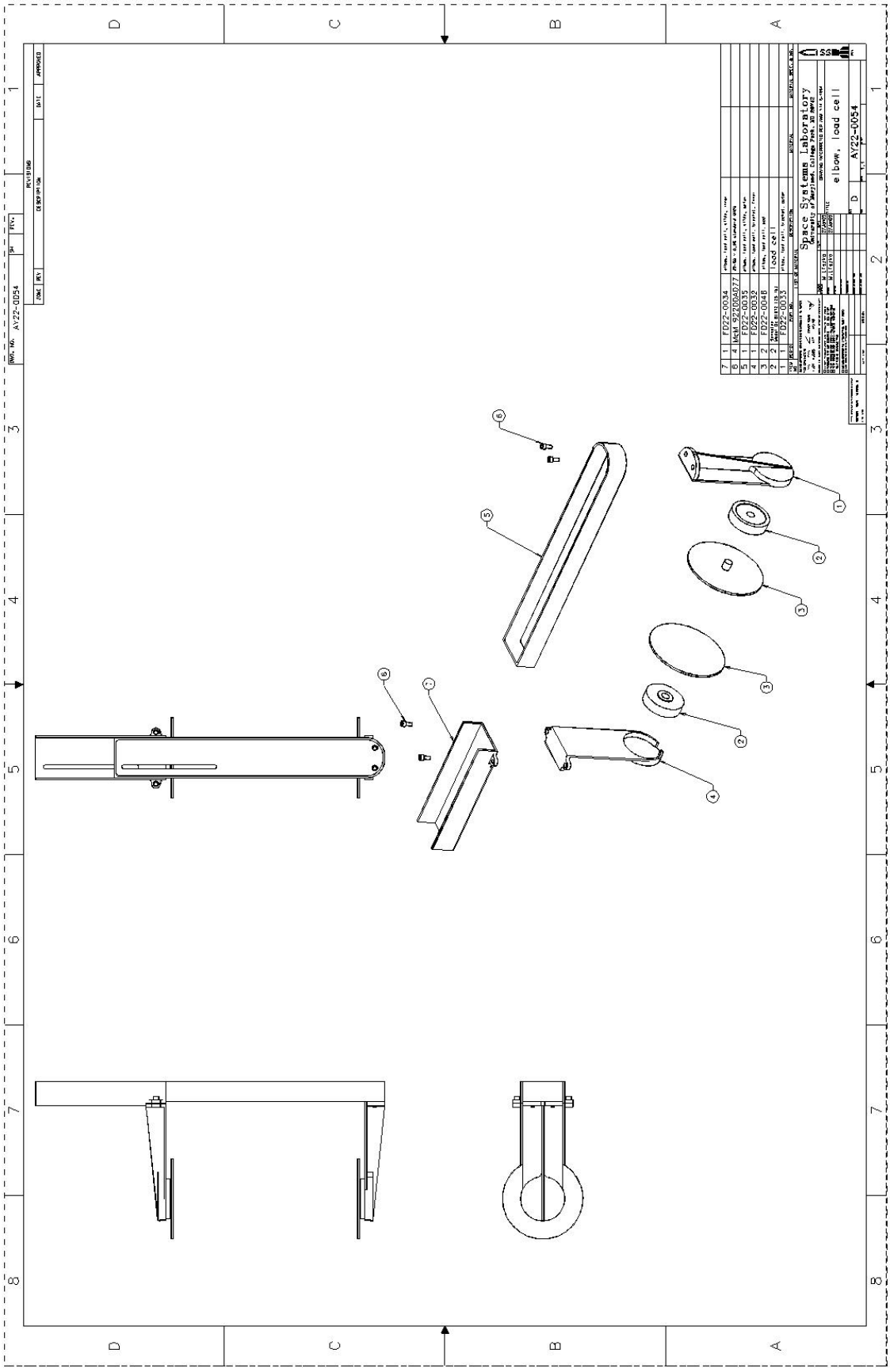
elbow, load cell
AY22-0054
Space Systems Laboratory

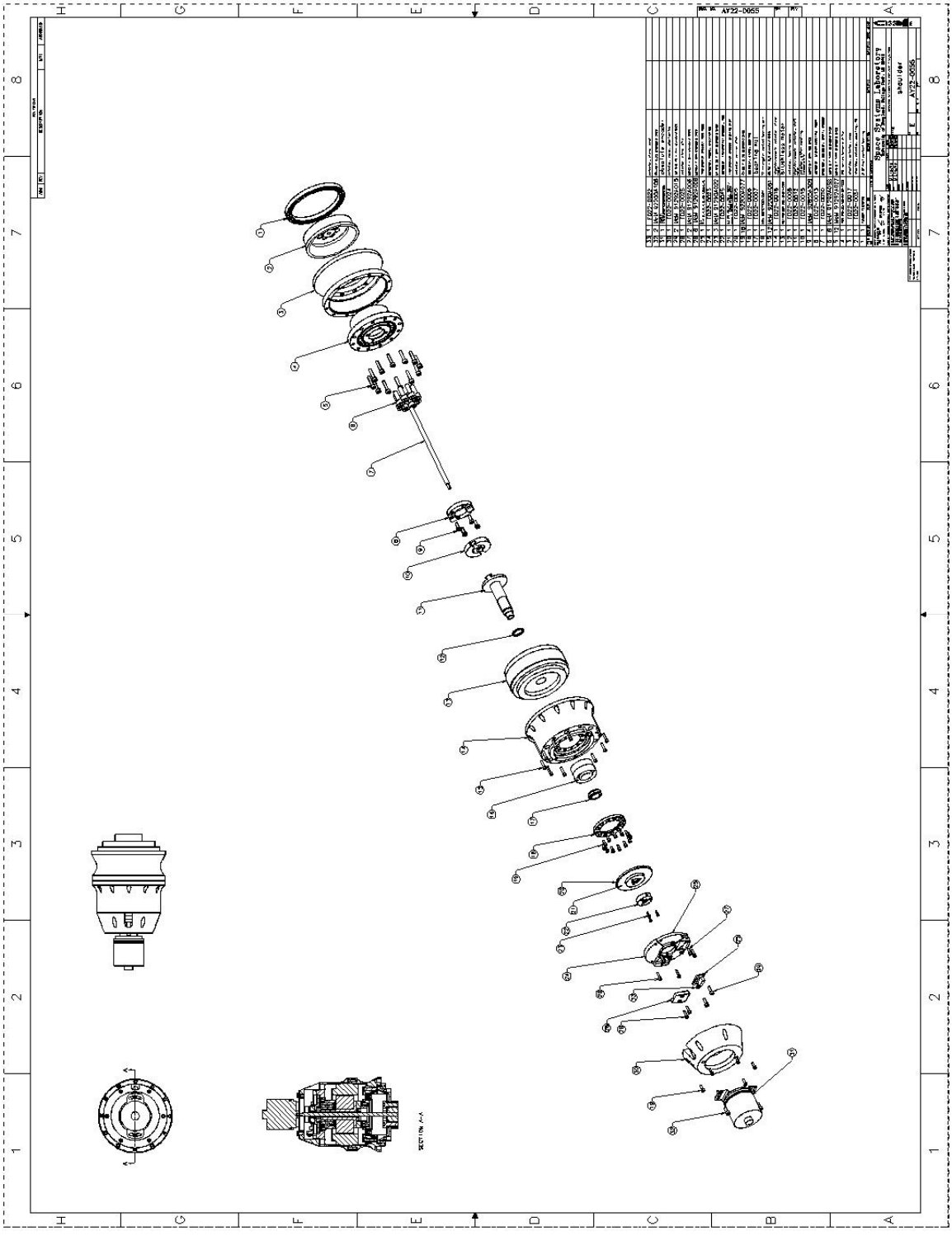

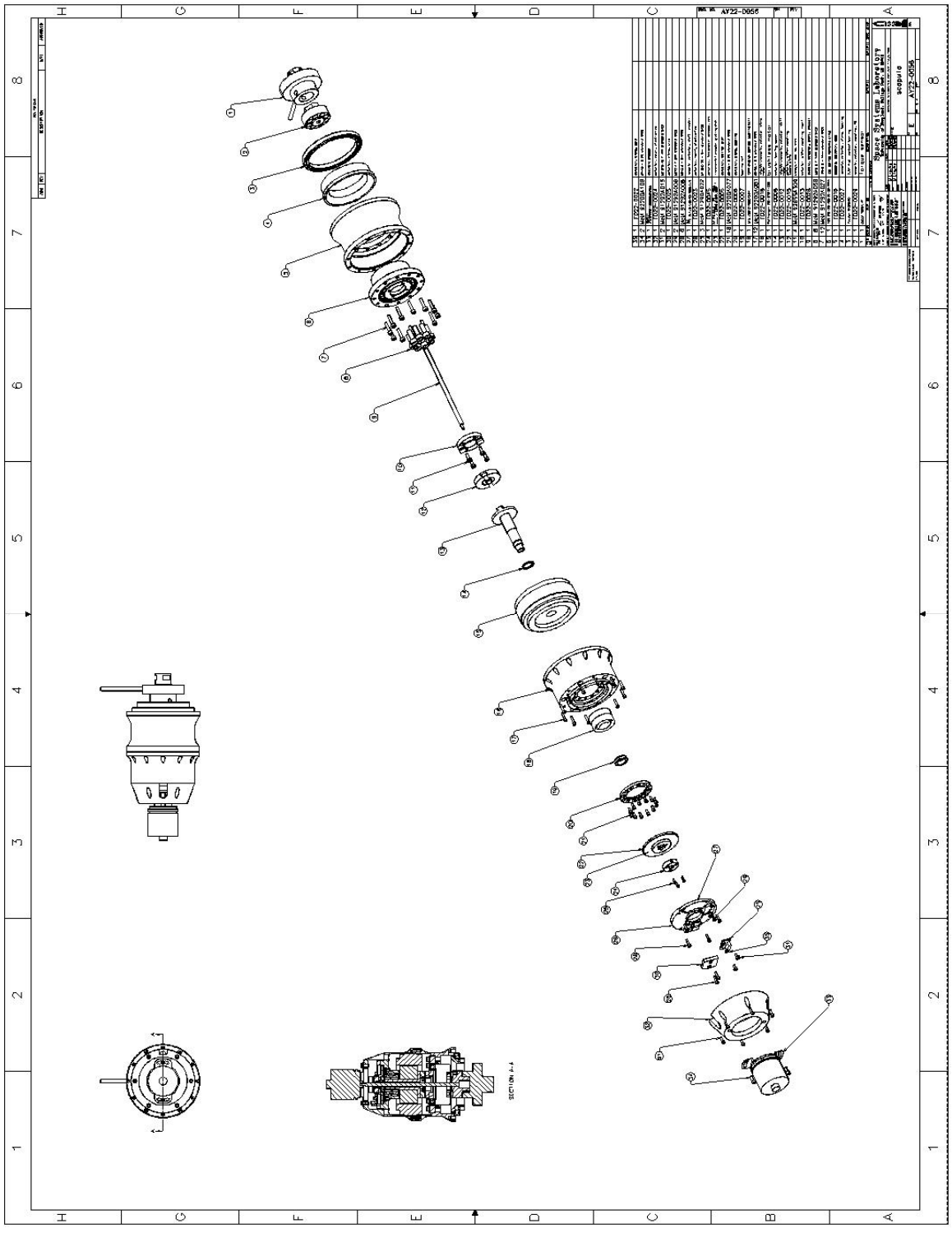

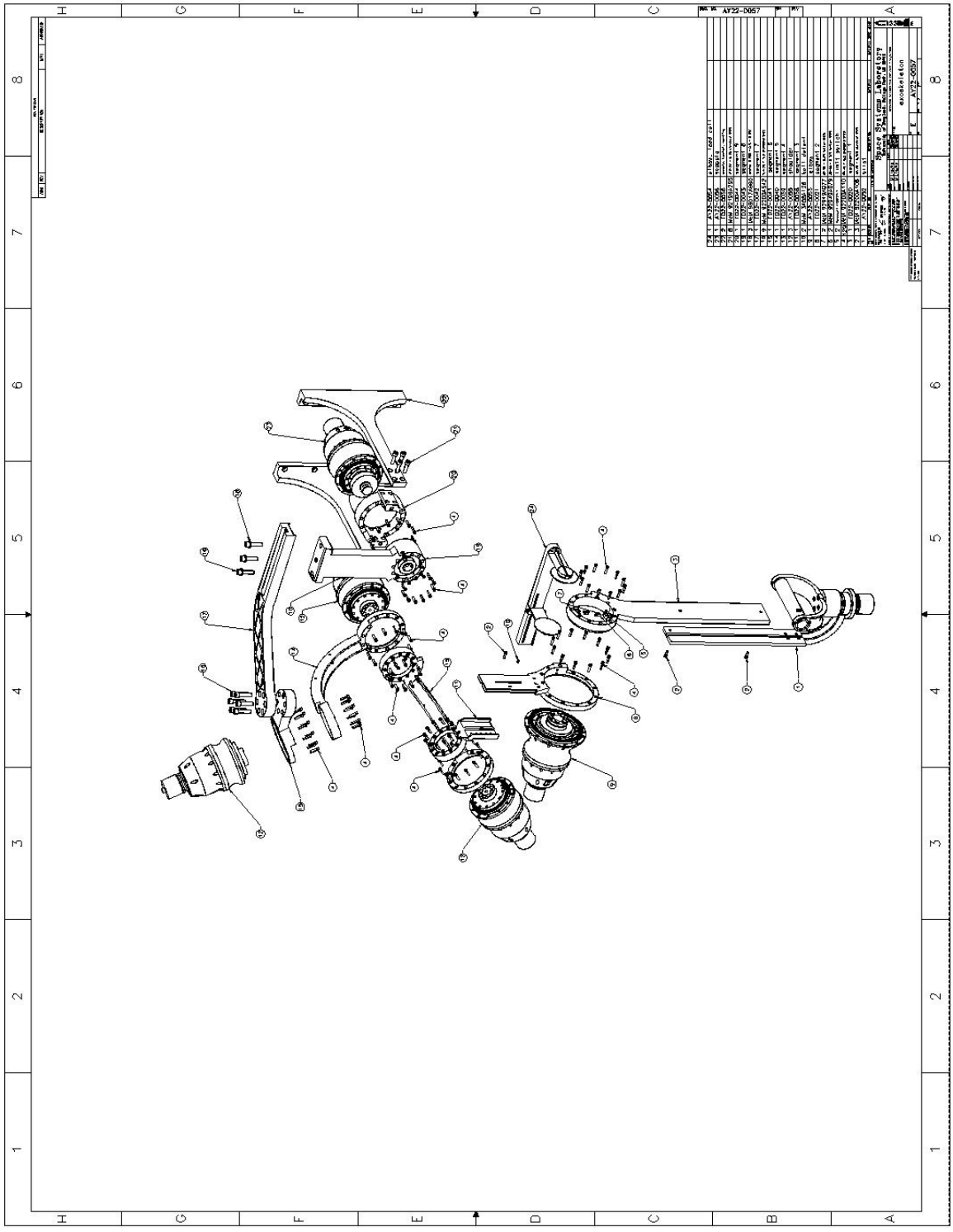

Appendix C: Forward Kinematics

C.1 Shoulder

Forward kinematics of the shoulder based on the frame assignments shown in Figure 30:

$$ {}^{0}_{1}R = \begin{bmatrix} \cos\theta_1 & -\sin\theta_1 & 0 \\ \frac{1}{2}\sin\theta_1 & \frac{1}{2}\cos\theta_1 & \frac{1}{2} \\ -\frac{1}{2}\sqrt{3}\sin\theta_1 & -\frac{1}{2}\sqrt{3}\cos\theta_1 & \frac{1}{2}\sqrt{3} \end{bmatrix} $$

$$ {}^{1}_{2}R = \begin{bmatrix} \cos\theta_2 & -\sin\theta_2 & 0 \\ 0 & 0 & 1 \\ -\sin\theta_2 & -\cos\theta_2 & 0 \end{bmatrix} $$

$$ {}^{2}_{3}R = \begin{bmatrix} \cos\theta_3 & -\sin\theta_3 & 0 \\ 0 & 0 & -1 \\ \sin\theta_3 & \cos\theta_3 & 0 \end{bmatrix} $$

$$ {}^{0}_{3}R = {}^{0}_{1}R \cdot {}^{1}_{2}R \cdot {}^{2}_{3}R $$

Shoulder Jacobian (equation 19):

$$ {}^{0}J_{ROT} = \Lambda\begin{bmatrix} {}^{0}\hat{z}_1 & {}^{0}\hat{z}_2 & {}^{0}\hat{z}_3 \end{bmatrix} = \begin{bmatrix} 1 & 0 & 0 \\ 0 & 1 & 0 \\ 0 & 0 & 1 \end{bmatrix}\begin{bmatrix} {}^{0}_{1}R \cdot {}^{1}\hat{z}_1 & {}^{0}_{1}R \cdot {}^{1}_{2}R \cdot {}^{2}\hat{z}_2 & {}^{1}_{0}R \cdot {}^{1}_{2}R \cdot {}^{2}_{3}R \cdot {}^{3}\hat{z}_3 \end{bmatrix} $$

$$ {}^{0}J_{ROT} = \begin{bmatrix} 0 & -\sin\theta_1 & \sin\theta_2\cos\theta_1 \\ \frac{1}{2} & \frac{1}{2}\cos\theta_1 & \frac{1}{2}\left(\cos\theta_2 + \sin\theta_2\sin\theta_1\right) \\ \frac{1}{2}\sqrt{3} & -\frac{1}{2}\sqrt{3}\cos\theta_1 & -\frac{1}{2}\sqrt{3}\left(\cos\theta_2 - \sin\theta_2\sin\theta_1\right) \end{bmatrix} $$

C.2 Full Exoskeleton

Forward kinematics of the exoskeleton based on the frame assignments in Figure 23:

$$ {}^{0}_{1}T = \begin{bmatrix} \cos\theta_1 & -\sin\theta_1 & 0 & 0 \\ \sin\theta_1 & \cos\theta_1 & 0 & 0 \\ 0 & 0 & 1 & 0 \\ 0 & 0 & 0 & 1 \end{bmatrix} $$

$$ {}^{1}_{2}T = \begin{bmatrix} \cos\theta_2 & -\sin\theta_2 & 0 & \frac{1}{2}\sqrt{3}L_1 \\ 0 & 0 & 1 & \frac{1}{2}L_1 \\ -\sin\theta_2 & -\cos\theta_2 & 0 & 0 \\ 0 & 0 & 0 & 1 \end{bmatrix} $$

$$ {}^{2}_{3}T = \begin{bmatrix} \cos\theta_3 & -\sin\theta_3 & 0 & 0 \\ 0 & 0 & -1 & 0 \\ \sin\theta_3 & \cos\theta_3 & 0 & 0 \\ 0 & 0 & 0 & 1 \end{bmatrix} $$

$$ {}^{3}_{4}T = \begin{bmatrix} \cos\theta_4 & -\sin\theta_4 & 0 & 0 \\ 0 & 0 & -1 & -\sqrt{2}L_2 \\ \sin\theta_4 & \cos\theta_4 & 0 & 0 \\ 0 & 0 & 0 & 1 \end{bmatrix} $$

$$ {}^{4}_{5}T = \begin{bmatrix} \cos\theta_5 & -\sin\theta_5 & 0 & 0 \\ \frac{1}{2}\sqrt{2}\sin\theta_5 & \frac{1}{2}\sqrt{2}\cos\theta_5 & \frac{1}{2}\sqrt{2} & \frac{1}{2}\sqrt{2}L_2 \\ -\frac{1}{2}\sqrt{2}\sin\theta_5 & -\frac{1}{2}\sqrt{2}\cos\theta_5 & \frac{1}{2}\sqrt{2} & \frac{1}{2}\sqrt{2}L_2 \\ 0 & 0 & 0 & 1 \end{bmatrix} $$

$$ {}^{5}_{6}T = \begin{bmatrix} \cos\theta_6 & -\sin\theta_6 & 0 & 0 \\ 0 & 0 & 1 & L_3 \\ -\sin\theta_6 & -\cos\theta_6 & 0 & 0 \\ 0 & 0 & 0 & 1 \end{bmatrix} $$

$$ {}^{0}_{6}T = {}^{0}_{1}T \cdot {}^{1}_{2}T \cdot {}^{2}_{3}T \cdot {}^{3}_{4}T \cdot {}^{4}_{5}T \cdot {}^{5}_{6}T $$

Appendix D: Component Specification Sheets

D.1 Motor

RBE(H) Motor Series

RBE(H) 01810 MOTOR SERIES PERFORMANCE DATA

Motor Parameters	Symbols	Units	01810	01811	01812	01813	01814	01815
Max Cont. Output Power	HP Rated	HP	0.280	0.402	0.488	0.572	0.611	0.646
at 25°C amb.	P Rated	Watts	209	300	364	427	456	482
Speed at Rated Power	N Rated	RPM	7040	5250	4350	3850	3520	3230
Max Mechanical Speed	N Max	RPM	14000	14000	14000	14000	14000	14000
Continuous Stall Torque	Tc	oz-in	60.8	121	173	218	262	305
at 25°C amb.		N-m	0.429	0.856	1.22	1.54	1.85	2.16
Peak Torque	Tp	oz-in	216	430	654	871	1069	1297
		N-m	1.53	3.04	4.62	6.15	7.55	9.16
Max Torque	Tsl	oz-in	136	273	413	554	679	825
for Linear KT		N-m	0.96	1.93	2.92	3.91	4.80	5.83
Motor Constant	Km	oz-in/$\sqrt{W}$	11.0	19.6	26.5	32.8	37.8	43.1
		N-m/$\sqrt{W}$	0.077	0.139	0.187	0.231	0.267	0.304
Thermal Resistance*	Rth	°C/Watt	2.55	2.11	1.91	1.83	1.70	1.62
Viscous Damping	Fi	oz-in/RPM	9.00E-04	1.83E-03	2.71E-03	3.56E-03	4.39E-03	5.30E-03
		N-m/RPM	6.36E-06	1.29E-05	1.91E-05	2.52E-05	3.10E-05	3.74E-05
Max Static Friction	Tf	oz-in	3.10	4.49	5.81	7.09	8.33	9.70
		N-m	0.0219	0.032	0.041	0.050	0.059	0.069
Max Cogging Torque	Tcog	oz-in	1.50	1.79	2.08	2.35	2.61	2.90
Peak to Peak		N-m	0.0106	0.0127	0.0147	0.0166	0.0184	0.020
Inertia	Jmf	oz-in-sec^2	5.10E-03	8.70E-03	1.22E-02	1.55E-02	1.88E-02	2.23E-02
Frameless		Kg-m^2	3.60E-05	6.14E-05	8.62E-05	1.09E-04	1.33E-04	1.57E-04
Motor Weight	Wtf	oz	12.0	19.8	27.2	34.5	41.4	49.1
		Kg	3.40E-01	5.61E-01	7.72E-01	9.77E-01	1.17E+00	1.39E+00
Inertia	Jmh	oz-in-sec^2	5.30E-03	8.80E-03	1.24E-02	1.58E-02	1.91E-02	2.27E-02
Housed		Kg-m^2	3.74E-05	6.21E-05	8.76E-05	1.12E-04	1.35E-04	1.60E-04
Motor Weight	Wth	oz	30.0	38.2	46.0	53.6	60.9	69.0
		Kg	8.50E-01	1.08E+00	1.30E+00	1.52E+00	1.73E+00	1.96E+00
No. of poles	P		12	12	12	12	12	12

Winding Constants	Symbols	Units	A	B	C	A	B	C	A	B	C	A	B	C	A	B	C	A	B	C
Current at Cont. Torque	Ic	Amps	5.28	2.85	7.39	5.24	2.82	7.34	4.91	2.64	6.87	5.87	3.49	10.2	5.73	3.41	9.93	5.51	3.28	9.54
Current at Peak Torque	Ip	Amps	21.3	10.0	30.2	21.3	10.0	30.2	21.3	10.0	30.2	26.9	14.2	40.3	26.9	14.2	40.3	26.9	14.2	40.3
Torque Sensitivity	Kt	oz-in/Amp	12.1	22.5	8.64	24.0	44.5	17.1	36.4	67.5	26.0	38.4	64.5	22.2	47.1	79.2	27.2	57.2	96.1	33.0
		N-m/Amp	0.0855	0.159	0.0610	0.170	0.315	0.121	0.257	0.477	0.184	0.271	0.456	0.157	0.333	0.559	0.192	0.404	0.679	0.233
Back EMF constant	Kb	V/KRPM	8.95	16.6	6.39	17.8	32.9	12.7	26.9	50.0	19.2	28.4	47.7	16.4	34.9	58.6	20.1	42.3	71.1	24.4
Motor Resistance	Rm	Ohms	1.22	4.16	0.615	1.49	5.10	0.753	1.88	6.42	0.949	1.38	3.79	0.458	1.55	4.28	0.518	1.76	4.85	0.588
Motor Inductance	Lm	mH	0.90	3.1	0.46	1.8	6.2	0.92	2.5	8.5	1.3	1.9	5.5	0.65	2.2	6.2	0.73	2.7	7.6	0.90

*Rth assumes a housed motor mounted to a 7" x 7.5" x 0.75" aluminum heatsink or equivalent

Continuous Duty Capability for 130°C Rise — RBE - 01810 Series

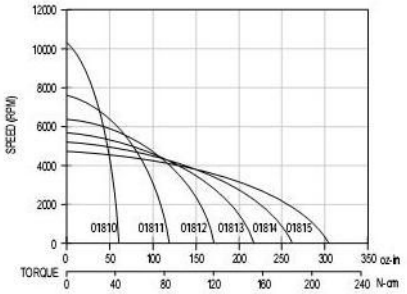

RBE-0181X-X00

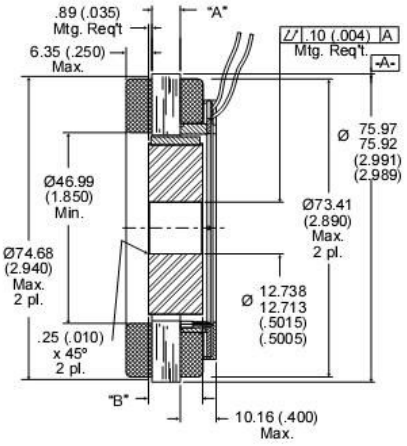

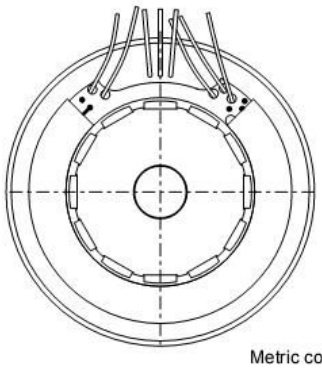

Dimensions in mm (inches).
Product designed in inches.
Metric conversions provided for reference only.

Notes:
1) For a C.W. rotation, as viewed from lead end, energize per excitation sequence table.
2) V-AB, V-BC and V-CA is back EMF of motor phases AB, BC and CA respectively, aligned with sensor output as shown for C.W. rotation only.
3) Mounting surface is between Ø 74.68 (2.940) and Ø 75.95 (2.990) on both sides.

MODEL NUMBER	RBE-01810	RBE-01811	RBE-01812	RBE-01813	RBE-01814	RBE-01815
"A" Dimension	6.99 (0.275)	15.24 (0.600)	23.11 (0.910)	30.73 (1.210)	38.10 (1.500)	46.23 (1.820)
"B" Dimension	13.34 (0.525)	21.59 (0.850)	29.46 (1.160)	37.08 (1.460)	44.45 (1.750)	52.58 (2.070)
Tolerance ± .010 on "A" Dimension.						

RBEH-0181X-X00

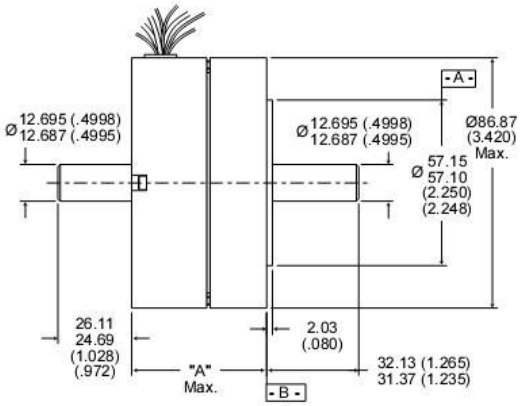

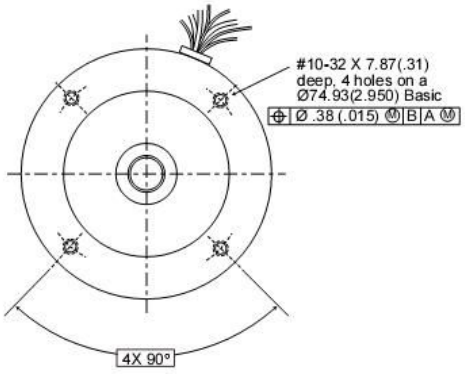

Dimensions in mm (inches).
Product designed in inches.
Metric conversions provided for reference only.

Notes:
1) Shaft end play: with a 9 lb reversing load, the axial displacement shall be .013-.15 (.0005-.006).
2) For a C.C.W. rotation, as viewed from pilot end, energize per excitation sequence table.
3) V-AB, V-BC and V-CA is back EMF of motor phases AB, BC and CA respectively, aligned with sensor output as shown for C.C.W. rotation only.

MODEL NUMBER	RBEH-01810	RBEH-01811	RBEH-01812	RBEH-01813	RBEH-01814	RBEH-01815
"A" Dimension	47.17 (1.857)	55.42 (2.182)	63.30 (2.492)	70.92 (2.792)	78.28 (3.082)	86.41 (3.402)

RBE/RBEH LEADWIRE

Motor Leads: #20 AWG Teflon coated per MIL-W-22759/11, 3 leads, 152 (6.00) min lg. ea. 1-black, 1-red, 1-white.

Sensor Leads: #26 AWG type "ET" Teflon coated per MIL-W-16878, 5 leads, 152 (6.00) min lg. ea. 1-blue, 1-brown, 1-green, 1-orange, 1-yellow.

PERFORMANCE CURVES

RBE-01810-B

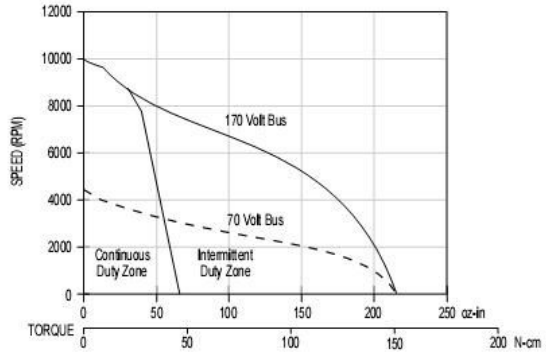

RBE-01810-C

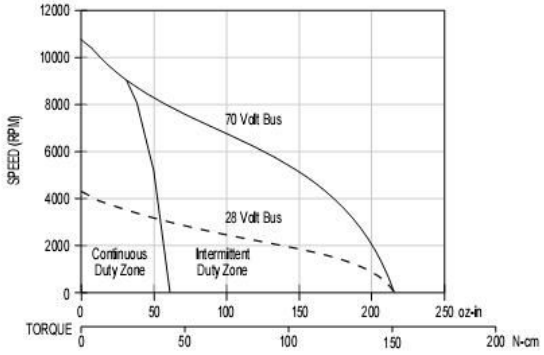

RBE-01815-B

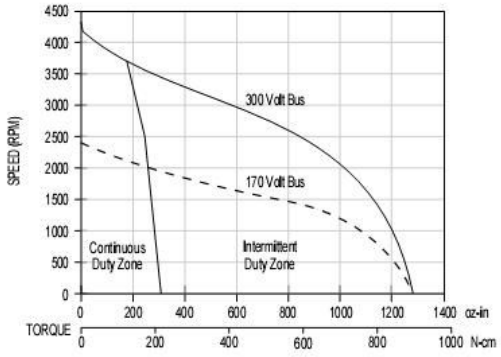

RBE-01815-C

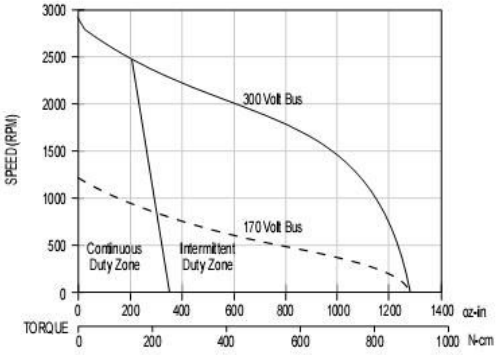

D.2 Force/Torque Sensor

Sensor Specific Information

Sensors with Internal Electronics			Sensors for use with External Electronics		
Model	Dimensions	Available Load Ratings (lbs.)*	Model	Dimensions	Available Load Ratings (lbs.)*
50M31A	50 mm dia. 31 mm thick	25	20E12A	2.0 in. dia. 1.25 in. thick	15, 25
67M25A	67 mm dia. 25 mm thick	15, 25, 50	30E12A	3.0 in. dia. 1.25 in. thick	15, 25, 50
			30E15A	3.0 in. dia. 1.5 in. thick	75, 100
90M31A	90 mm dia. 31 mm thick	25,50	35E12A	3.5 in. dia. 1.25 in. thick	15, 25, 50
			35E15A	3.5 in. dia. 1.5 in. thick	75, 100
100M40A	100 mm dia. 40 mm thick	25, 50, 100	40E12A	4.0 in. dia. 1.25 in. thick	15, 25, 50
			40E15A	4.0 in. dia. 1.5 in. thick	75, 100, 150
45E15A	4.5 in. dia. 1.5 in. thick	25, 50, 75, 100, 150, 250	45E12A	4.5 in. dia. 1.25 in. thick	15, 25, 50
			45E15A	4.5 in. dia. 1.5 in. thick	75, 100, 150, 250
			45E20A	4.5 in. dia. 2.0 in. thick	250
160M50A	160 mm dia. 50 mm thick	150, 250	65E15A	6.5 in. dia. 1.5 in. thick	50
			65E20A	6.5 in. dia. 2.0 in. thick	75, 100, 150, 250, 400, 500
			75E15A	7.5 in. dia. 1.5 in. thick	50
			75E20A	7.5 in. dia. 2.0 in. thick	75, 100, 150, 250, 400, 500

D.3 Elbow Load Cell

www.sensotec.com

Donut Shaped Load Cells

Model D

THRU-HOLE DESIGN

150 g - 30,000 lb.

FLEXIBLE DESIGN

Model D (Compression Only)

The Model D Donut Shaped Load Cell features a smooth thru-hole design perfect for applications which require the load structure to pass directly through the cell. Such applications include bolt force measurements, clamping forces, and monitoring overloads. Load ranges as low as 150 grams and as great as 30,000 pounds can be measured within a maximum full scale non-linearity and hysteresis of ±0.5% F.S. These models are used in compression applications and are available in multiple hole sizes. For optimum performance, these cells must be mounted between load surfaces which are flat and parallel. The Model D miniature load cell is designed to have a minimum thickness.

		Model D (Compression Only)
PERFORMANCE	Load Ranges	150 g to 30,000 lb.
	Non-linearity and Hysteresis (max)	±0.5% F.S.
	Non-repeatability (max)	±0.1% F.S.
	Output	20mV/V (gram units) 2mV/V (5 lb. and above)
	Resolution	Infinite
ENVIRONMENTAL	Temperature, Operating	-65° F to 250° F
	Temperature, Compensated	60° F to 160° F
	Temperature Effect	
	- Zero (max)	0.005% F.S./° F (5 lb. and above); 0.01%/° F (gram units)
	- Span (max)	0.010% Rdg./° F (5 lb. and above); 0.02%/° F (gram units)
ELECTRICAL	Strain Gage Type	Semi conductor (gram units) Bonded foil (5 lb. and above)
	Excitation (calibration)	Semi conductor 5V Bonded foil 10V
	Bridge Resistance	500 ohms (gram units) 350 ohms (5 lb. and above)
	Wiring Code (std)	#1 (See Pg. AP-8)
	Electrical Termination (std)	Teflon cable (5 ft.)
MECHANICAL	Overload, Safe	50% over capacity
	Casing Material	Stainless Steel

Dimensions

Model D (Order Code BL912)

Selection Guide-~~1~~50 g to 100 lb. units

Available Ranges	O.D."	I.D."	H"	Excitation
150; 250; 500; 1000 g	0.50	0.10	0.15	5VDC
5; 10 lb.	1.00	0.20	0.28	10VDC
25; 50; 100 lb.	1.00	0.20	0.28	10VDC

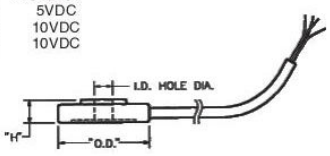

Options (See Appendix)

Temperature compensated 1b, 1c, 1f; Special calibration 9a, 9b

Premium Options: 1g (≥5 lb. only); 12b

Honeywell Sensotec Sensors

1-888-282-9891

www.honeywell.com/sensing

LO-32

Selection Instructions for Larger Capacity Units-30,000 lb.

Shown below are three separate outline drawings for the Model D Load Cell. The frame size selection guide below indicates that with a single shell size (outside diameter), different "donut holes" are available. For example, in the small frame size (A) it is possible to select a 250 lb. load cell with a nominal hole size of 1/8" (P), 3/16" (Q), 1/4" (R), or 3/8" (S) diameter. We manufacture the actual hole dimensions to provide some clearance; for example the 1/8" (P) diameter dimension, the actual dimension is 0.128".

HOW TO ORDER: SPECIAL ORDER INSTRUCTIONS

1. Specify the **order code** (See frame size A, B or C)
2. State the **load range** required in pounds and range code.
3. State the nominal **hole diameter** letter.

e.g. Model D: BL914CN R (1/4 inch) [250 lb.]

Frame Size Selection Guide

Hole Letters	P	Q	R	S	T	V	W	Y	Z
Nominal Hole Dia.	1/8"	3/16"	1/4"	3/8"	1/2"	5/8"	3/4"	1"	1 -1/4"
Actual Hole Dia.	0.128"	0.193"	0.266"	0.391"	0.532"	0.656"	0.781"	1.032"	1.281"
100 lb.	A	A	A	A					
250 lb	A or B	A or B	A or B	A or B	B	B			
500 lb.	A or B	A or B	A or B	A or B	B	B			
1,000 lb.	A or B	A or B	A or B	B	B	B			
2,000 lb.	A, B or C	A, B or C	A, B or C	B or C	B or C	B or C	C	C	C
3,000 lb.	B or C	B or C	B or C	B or C	B or C	C	C	C	C
5,000 lb.	B or C	B or C	B or C	B or C	B or C	C	C	C	C
7,500 lb.	B or C	B or C	B or C	B or C	B or C	C	C	C	C
10,000 lb.	B or C	B or C	B or C	B or C	B or C	C	C	C	C
15,000 lb.	C	C	C	C	C	C	C	C	C
20,000 lb.	C	C	C	C	C	C	C	C	C
30,000 lb.	C	C	C	C	C	C	C	C	C

LOAD DONUT

Options

(Dimensions in inches)

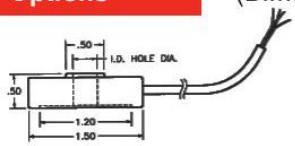

FRAME SIZE A
ORDER CODE BL913

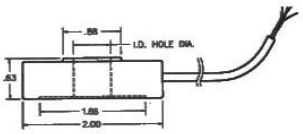

FRAME SIZE B
ORDER CODE BL914

***Choose Hole Dia. from Selection Guide above.**

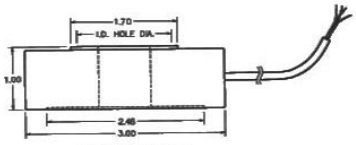

FRAME SIZE C
ORDER CODE BL915

REACTION TORQUE CELLS
NON-ROTATING SHAFT MOUNT
LOW TORQUE RANGE

TQ201 Series
Reaction Torque
0-25 oz-in to 0-1000 in-lb
0-0.18 N-m to 0-110 N-m

Starts at **$795**

TQ201-100, $795, shown slightly larger than actual size.

- **All Stainless Steel Case for Long-Term Reliability in Industrial Environments**
- **High Accuracy**
- **Shielded Cable for Precise Low-Noise Measurements**
- **Heavy-Duty Mounting for Positive, Non-Slip Connection**

OMEGA's TQ201 Series comprises in-line mount reaction torque sensors. They are designed to be mounted to the torque-producing element for measuring the starting torque of motors.

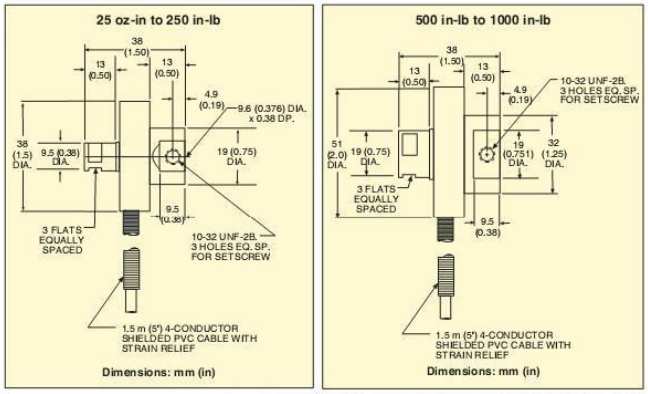

MOST POPULAR MODELS HIGHLIGHTED!

SPECIFICATIONS
Output: 2 mV/V
Excitation: 10 Vdc, 15 V max
Input Resistance: 350 Ω min
Output Resistance: 350 Ω min
Accuracy Class: ±0.2% FSO
Linearity: ±0.15% FSO
Hysteresis: ±0.10% FSO
Repeatability: ±0.03% FSO
Zero Balance: ±2% FSO
Operating Temp Range: -54 to 107°C (-65 to 225°F)
Compensated Temp Range: 16 to 71°C (60 to 160°F)
Thermal Effects:
Zero: ±0.005% FSO/°F
Span: ±0.005% rdg/°F
Safe Overload: 150% of capacity
Ultimate Overload: 300% of capacity
Construction: Stainless steel
Protection Class: IP65
Electrical (TQ201): 1.5 m (5') 4-conductor shielded PVC cable with strain relief

To Order *(Specify Model Number)*

RANGE	MODEL NO.	PRICE	COMPATIBLE METERS*
0 to 25 oz-in	**TQ201-25Z**	**$895**	DP41-S, DP25B-S
0 to 30 oz-in	**TQ201-30Z**	**895**	DP41-S, DP25B-S
0 to 100 oz-in	**TQ201-100Z**	**795**	DP41-S, DP25B-S
0 to 120 oz-in	**TQ201-120Z**	**795**	DP41-S, DP25B-S
0 to 150 oz-in	**TQ201-150Z**	**795**	DP41-S, DP25B-S
0 to 200 oz-in	**TQ201-200Z**	**795**	DP41-S, DP25B-S
0 to 25 in-lb	**TQ201-25**	**795**	DP41-S, DP25B-S
0 to 50 in-lb	**TQ201-50**	**795**	DP41-S, DP25B-S
0 to 100 in-lb	**TQ201-100**	**795**	DP41-S, DP25B-S
0 to 250 in-lb	**TQ201-250**	**795**	DP41-S, DP25B-S
0 to 500 in-lb	**TQ201-500**	**795**	DP41-S, DP25B-S
0 to 1000 in-lb	**TQ201-1K**	**795**	DP41-S, DP25B-S

Comes with 5-point calibration.
** See section D for compatible meters.* *Metric ranges available – consult Engineering.*
Ordering Examples: TQ201-30Z**, 30 oz-in range reaction torque sensor, **$895.
TQ201-250**, 250 in-lb range reaction torque sensor, **$795.

ACCESSORY

MODEL NO.	PRICE	DESCRIPTION
OP-17	$15	Reference Book: Measure for Measure

D.5 Incremental Encoder

Technical Specification

Resolution

Resolution A is defined as the smallest angular value which is still detected by the evaluating electronics (display, control) when the grating disk is turned relative to the EPIFLEX measuring module.

The resolution can be calculated using the following formula:

$A = Z \cdot i \cdot N$ [increments/revolution]

$A = \frac{360°}{Z \cdot i \cdot N}$ [degrees]

Z the number of lines on the grating disk

i interpolation factor of the connector board (5x, 10x, 25x or 50x)

N factor for evaluation mode in the counter

N = 1 for single-edged evaluation
N = 2 for double-edged evaluation
N = 4 for quad-edged evaluation

Elektrical data

Scanning frequency	max. 500 kHz
Output interfaces	
– voltage output	1 V_{pp} with integrated line driver
– current output	11 μA_{pp}
– square-wave output	RS 422; optionally with internal signal interpolation 5/10/25/50x
Supply voltage	5 V ± 10%
Power consumption	
– voltage output	< 60 mA
– current output	< 30 mA
– square-wave output (RS 422)	< 180 mA
Cable length – connecting cable (round cable)	1 m with connector; other lengths on request; for greater lengths use extension cable
Permissible cable lengths (with extensions)	max. 18 m for current output 11 μA_{pp} max. 100 m for voltage output 1 V_{pp} max. 100 m for square-wave output RS 422

Accuracy

Accuracy (extremes of direction deviations) is affected by

- graduation errors of the grating disk
- eccentricity of the graduation relative to the axle bearing
- radial eccentricity of the axle bearing
- deviations in the positions of the grating disk and the EPIFLEX measuring module (installation tolerance)
- interpolation error in signal processing

The accuracy is largely determined by the eccentricity of the graduation relative to the axle bearing and the radial eccentricity of the axle bearing.
The error resulting from these factors is calculated using the following formula:

$\Delta\varphi = \pm 412 \frac{e}{D}$

$\Delta\varphi$ angular error [seconds of arc]

e eccentricity of the graduation relative to the axle of rotation including the radial eccentricity of the axle bearing [µm]

D graduation diameter of the grating disk [mm]

Ambient conditions

Operating temperature range	0°C ... +55°C
Storage temperature range	–20°C ... +70°C
Vibration (50 Hz ... 2000 Hz)	≤ 200 ms^{-2}
Shock (11 ms)	≤ 400 ms^{-2}

The way the EPIFLEX measuring module is designed (optoelectronic function elements on a glass substrate) it is alone not immune against electromagnetic radiation (EMC).

Mechanical data

Grating disks	see ordering key page 6
Dimensions of EPIFLEX measuring module	8 x 20 x 2.6 mm^3
EPIFLEX measuring module fixed in the frame	see page 7
Maximum numbers of revolution as a function of the counter	see table page 9 below

(The table already takes into account any limitation of the number of revolution due to signal tolerances.)

Z: number of lines of the grating disk

Interpolation	none	5x	10x	25x	50x
max. speed (rpm)	$\frac{30.000.000}{Z}$	$\frac{30.000.000}{Z}$	$\frac{21.600.000}{Z}$	$\frac{8.640.000}{Z}$	$\frac{4.320.000}{Z}$
min. edge separation of output signals at max. speed	0.33 µs	28 ns	28 ns	28 ns	28 ns
min. counting frequency (clock frequency) of counter at max. speed	3 MHz	36 MHz	36 MHz	36 MHz	36 MHz

Safety factor without interpolation: 1.5 Safety factor with interpolation: 2.5

http://numerik.cycro-project.de

Ordering Key

Components for measurement of rotary motions

Kit R	1	2	2	B	40/3600	L	4	–	F	Z

(Designation example)

Version – Measuring head

Kit R	with signal processing
EMR	without signal processing

Type of sensor

1	dimensions 20 x 8 x 2.6

Flexible tape – length

1	25 mm
2	55 mm

Frame – versions for fixing

0	none
1	through boring Ø 2,2
2	thread M 2,5

Type of frame

A	without frame
B	standard/steel (passivated)
C	standard/aluminium (cromated)
D	customized frame on request
...	other frames

Disks

Optical diameter of graduation	Number of lines
30.0 [3]	1000 [4]
40.4 [3]	1800 [4]
40.4 [3]	2048 [4]
40.4 [3]	3600 [4]
64.4 [3]	2048 [4]
64.4 [3]	9000 [4]
64.4 [3]	10000 [4]
92.4 [3]	3600 [4]
92.4 [3]	9000 [4]
92.4 [3]	1800 [4]
142.4 [3]	5400 [4]
142.4 [3]	18000 [4]

Signal processing in the connector

Y[1,2]	9-pin; D-Sub; electronic unit inside the connector (1 V_{pp})
Z[1,2]	15-pin; D-Sub; electronic unit inside the connector (RS 422, 1 V_{pp})

Cable Kit R for signal processing in the connector

Cable Ø 5.1 mm	
A[1]	0.3 m
B[1]	0.5 m
F[1]	1.0 m
E[1]	1.5 m
G[1]	2.0 m
K[1]	3.0 m

Cable Ø 3.7 mm	
R[1]	0.3 m
S[1]	0.5 m
T[1]	1.0 m
P[1]	1.5 m
V[1]	2.0 m
W[1]	3.0 m

Version – measuring system

–	standard

Speed factor

X	Costumized value, depending of max. speed and max. input frequency of the counter; please contact NUMERIK Jena

Output signals

B	sinusoidal signal 11 μA_{pp}
C	sinusoidal signal 1 V_{pp}
K	square wave signal RS 422 without interpolation
L	square wave signal RS 422 with interpolation 5x
M	square wave signal RS 422 with interpolation 10x
I[4]	square wave signal RS 422 with interpolation 25x
N[4]	square wave signal RS 422 with interpolation 50x

1 *Only necessary if the electronic unit is inside the connector*

2 *Standard lengths: 0.3 m; 0.5 m; 1.0 m; 1.5 m; 2.0 m; 3.0 m; greater lengths with extension cable; other lengths on request*

3 *For ordering please round the diameter of the disks to a whole number*

4 *Electronic adjustment recommend; requires adjustment kit*

For ordering key of grating disks see page 6

D.6 Absolute Encoder

Gurley Model A37
Absolute Encoder

Motion Type:
Rotary

Usage Grade:
Industrial

Output:
Absolute

Max Resolution:
12 Bit

Small Encoder - High Resolution

The model **A37** mini encoder is a single-turn absolute rotary encoder with opto-electronic technology. This encoder is used in a wide variety of position-sensing applications for the measuring of angles and distances in relatively small envelopes. Mechanical features include a 37-mm aluminum housing, a 3 - 5 mm (or 1/8" - 1/4") dia stainless steel solid or blind hollow shaft, and precision ball bearings.

ingenuity@work®

ISO 9001 Certified

Gurley Precision Instruments
514 Fulton Street
Troy, NY 12180 U.S.A.
(800) 759-1844, (518) 272-6300, fax (518) 274-0336,
Online at www.gurley.com, e-mail: info@gurley.com

GPI

SPECIFICATIONS

	Units	Limiting Values	See Note
Mechanical Specifications			
Moment of Inertia	in-oz-s^2 (g-cm^2)	2.3 x 10^{-5} (1.7)	
Starting Torque	in-oz (Nm)	0.14 (0.001)	
Radial Shaft Load	lb (N)	1 (5)	
Axial Shaft Load	lb (N)	1 (5)	
Bearing Arrangement		2 pre-loaded bearings	
Bearings		Grease-lubricated and sealed	
Code Disk Type		etched chrome on glass	
Non-Operating Slew	RPM	10,000	
Acceleration	rad/s^2	3 x 10^6	
Shock 11 (ms)	g	50	
Vibration (0-2000Hz)	g	15	
Sealing		IP64	2
Recommended Coupling	SCA		
Environmental Specifications			
Operating Temperature	°F (°C)	32 to 158 (0 to 70)	
Storage Temperature	°F (°C)	0 to 160 (-18 to 71)	
Relative Humidity	%	98	1
Electrical Specifications			
Supply Voltage	VDC	4.75 to 5.25, 5.00 nominal	
Current Consumption	mA	≤ 100	
LED Life	hours	≥ 100,000	
Output Code		Gray code or Natural binary	
Output Format		12 bit parallel, multiplexed bite-wide or serial	
Output Device		TTL, RS, OC	
Accuracy		+/- 0.5 LSB	
Step Frequency LSB		standard 25 kHz (valid code) 100 kHz option @ 6,000 RPM (call for details)	

Notes

1. Non-condensing
2. Per CEI / IEC 529 - Degrees of protection provided by enclosures (IP Code)

As part of our continuing product improvement program, all specifications are subject to change without notice.

Gurley Precision Instruments
514 Fulton Street
Troy, NY 12180 U.S.A.
(800) 759-1844, (518) 272-6300, fax (518) 274-0336,
Online at www.gurley.com, e-mail: info@gurley.com

Output Options

Parallel Output without Output Enable (Gray Code)

Electrical Signal	Pin	Color
D0	1	Yellow
D1	2	Brown
D2	3	Green
D3	4	Yellow-white
D4	5	Blue
D5	6	White
D6	7	Violet
D7	8	Gray
D8	9	White-green
D9	10	Red-blue
D10	11	Pink
D11	12	Yellow-brown
0V	13	Black
+5V	14	Red
Case	15	Shield

Time Diagram

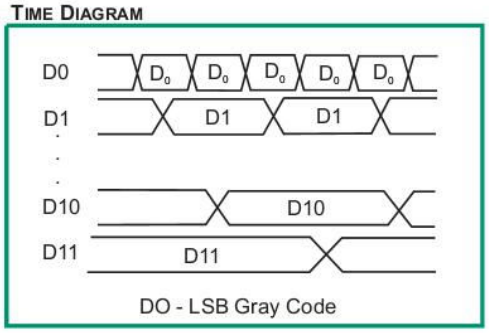

Parallel Output with Output Enable (Gray Code or Binary)

Electrical Signal	Pin	Color
D0	1	Yellow
D1	2	Brown
D2	3	Green
D3	4	Yellow-white
D4	5	Blue
D5	6	White
D6	7	Violet
D7	8	Gray
D8	9	White-green
D9	10	Red-blue
D10	11	Pink
D11	12	Yellow-brown
0V	13	Black
+5V	14	Red
CASE	15	Shield
OE	16	Brown-green

Time Diagram

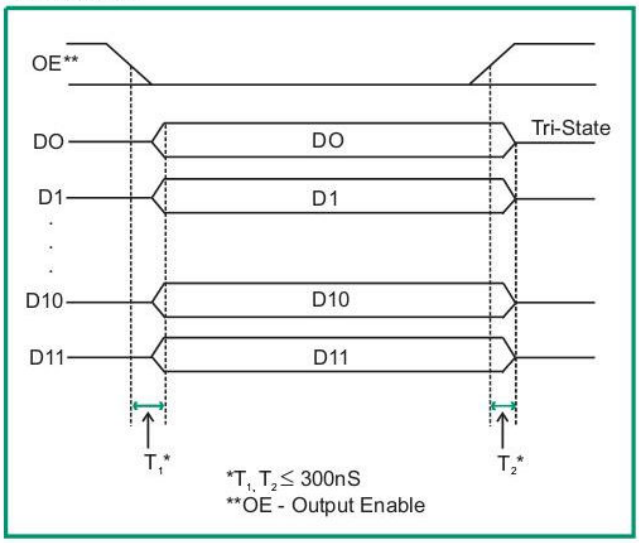

A37
PAGE 3 OF 8
V1006

Gurley Precision Instruments
514 Fulton Street
Troy, NY 12180 U.S.A.
(800) 759-1844, (518) 272-6300, fax (518) 274-0336,
Online at www.gurley.com, e-mail: info@gurley.com

Output Options

Multiplexed (byte-parallel) Gray code or Binary

Electrical Signal	Pin	Color
D0	1	Yellow
D1	2	Brown
D2	3	Green
D3	4	Yellow-white
D4	5	Blue
D5	6	White
D6	7	Violet
D7	8	Gray
OE1	10	Red-blue
OE2	11	Pink
0V	13	Black
+5V	14	Red
CASE	15	Shield

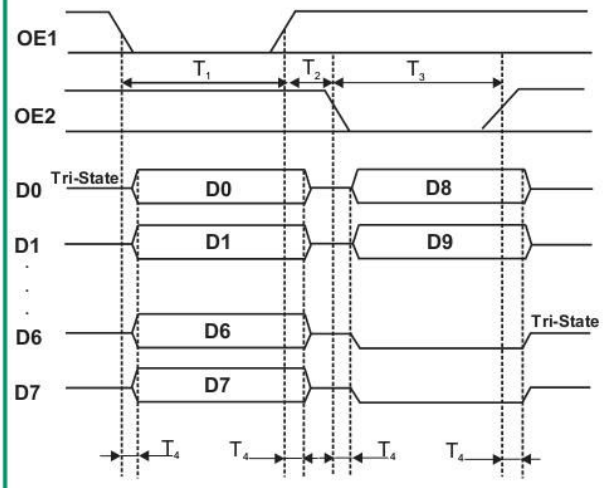

$T_1, T_2, T_3 > 300nS$
$T_4 \leq 300nS$

On falling edge of OE1 - output code is fixed.
On logic low of OE1 - D0 -D7 are output.
On logic low of OE2 - D_8 - D_{msB} are output.

Serial Output - Gray code or Binary

Electrical Signal	Pin	Color
Case	1	Shield
Clock	2	Yellow
/ Clock	3	Brown
Data	6	Green
/ Data	7	Orange
0V	9	Black
+5V	5	Red

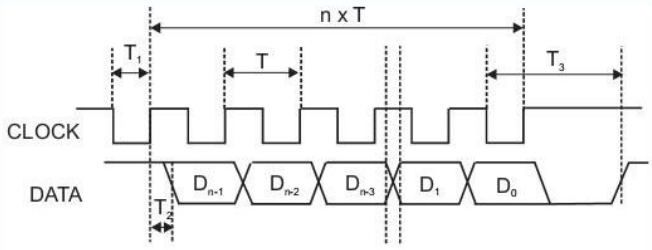

T = 0.9-11µs
T_1 > 0.45 µs
T_2 < 0.4 µs
T_3 = 12-35 µs

Gurley Precision Instruments
514 Fulton Street
Troy, NY 12180 U.S.A.
(800) 759-1844, (518) 272-6300, fax (518) 274-0336,
Online at www.gurley.com, e-mail: info@gurley.com

Outline Dimensions

MODEL A37S WITH BASE CODE A
SIDE EXIT

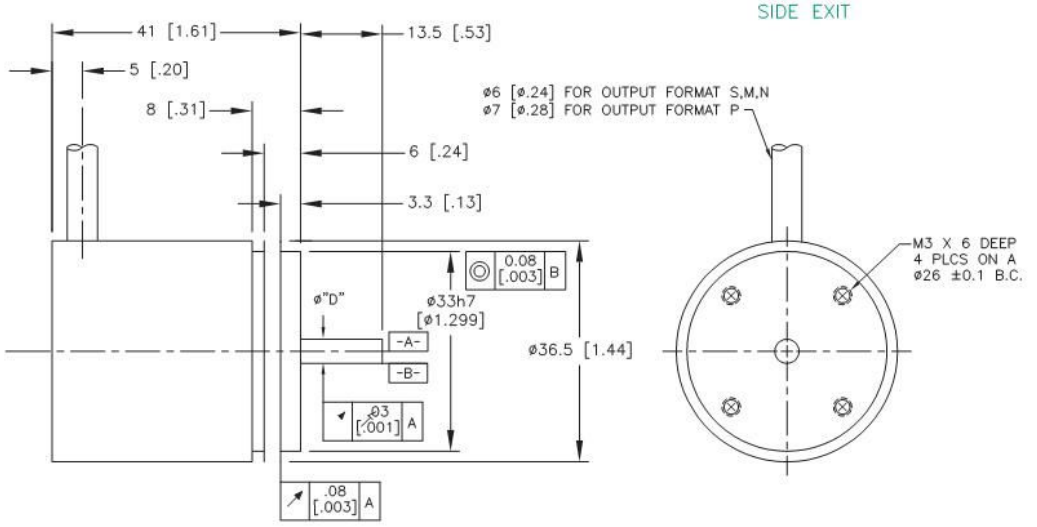

ø "D" TABLE		
DIA	A37S	A37B
03M	ø3mm	ø3mm
04M	ø4mm	ø4mm
05M	ø5mm	N/A
02E	ø0.125"	ø0.125"

MODEL A37S WITH BASE CODE A
TOP EXIT

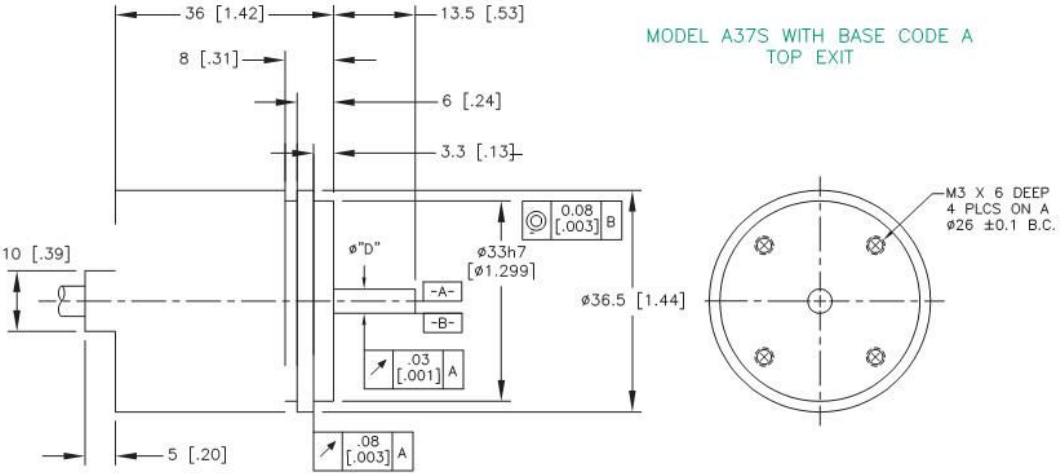

ALL DIMENSIONS IN mm [INCHES]

Gurley Precision Instruments
514 Fulton Street
Troy, NY 12180 U.S.A.
(800) 759-1844, (518) 272-6300, fax (518) 274-0336,
Online at www.gurley.com, e-mail: info@gurley.com

Outline Dimensions

MODEL A37B WITH BASE CODE B
SIDE EXIT

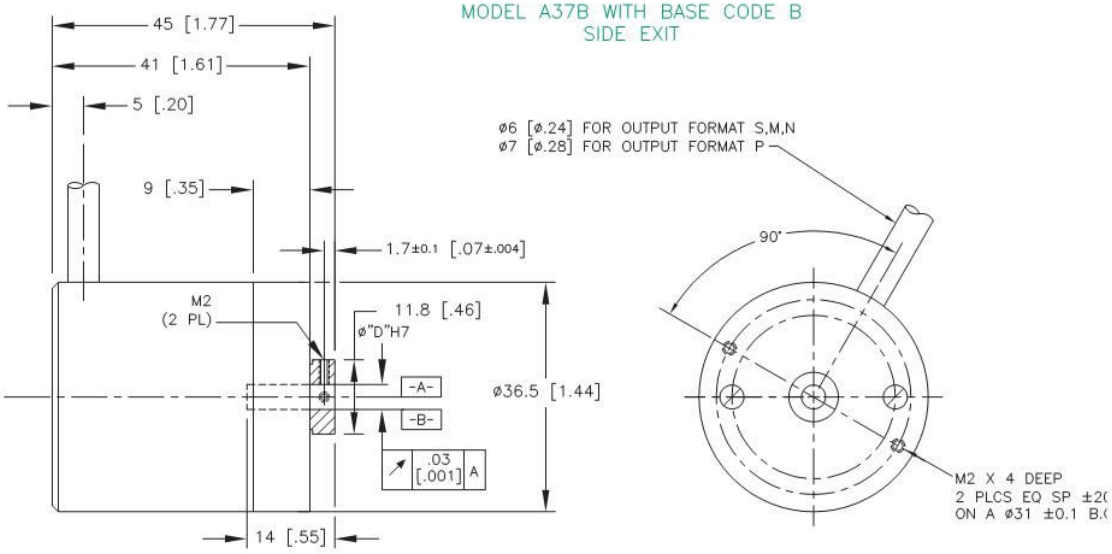

ø "D" TABLE		
DIA	A37S	A37B
03M	ø3mm	ø3mm
04M	ø4mm	ø4mm
05M	ø5mm	ø5mm
02E	ø0.125"	ø0.125"

ALL DIMENSIONS IN mm [INCHES]

MODEL A37B WITH BASE CODE B
TOP EXIT

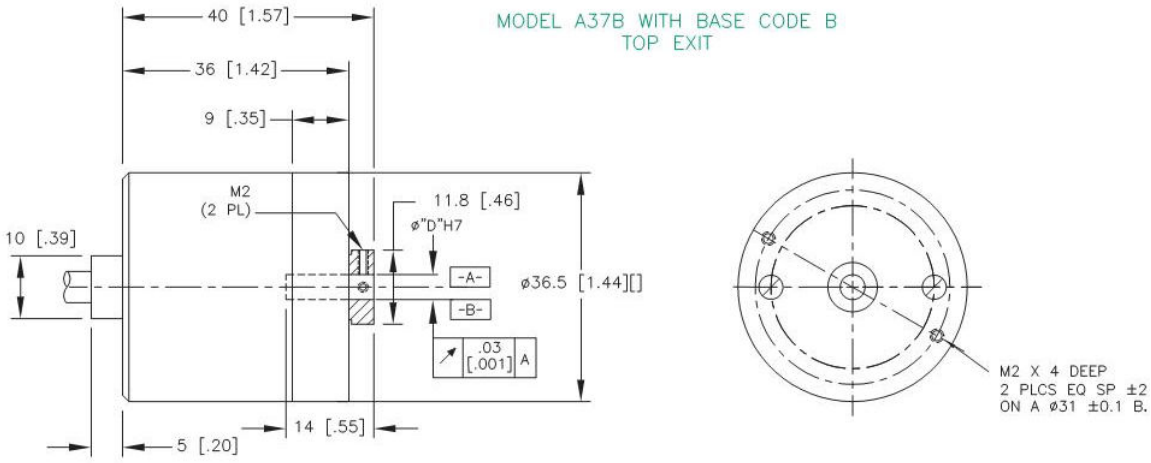

Gurley Precision Instruments
514 Fulton Street
Troy, NY 12180 U.S.A.
(800) 759-1844, (518) 272-6300, fax (518) 274-0336,
Online at www.gurley.com, e-mail: info@gurley.com

Output Signals and Recommended Circuit Interface

TTL:

V0<0.5V @ I≤20mA
WITH +5V POWER SUPPLY

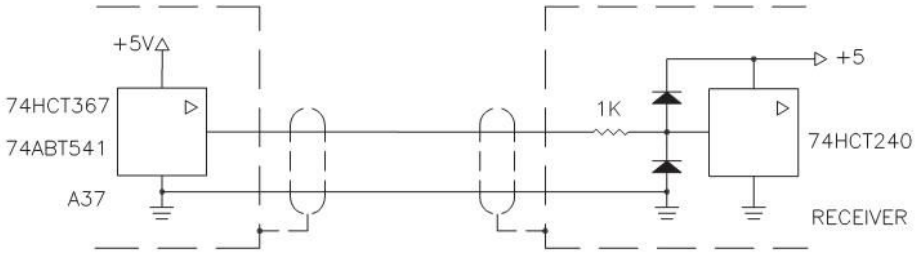

OC (OPEN COLLECTOR):

V=+5V
VEXT=50V MAX
IEXT=50mA MAX

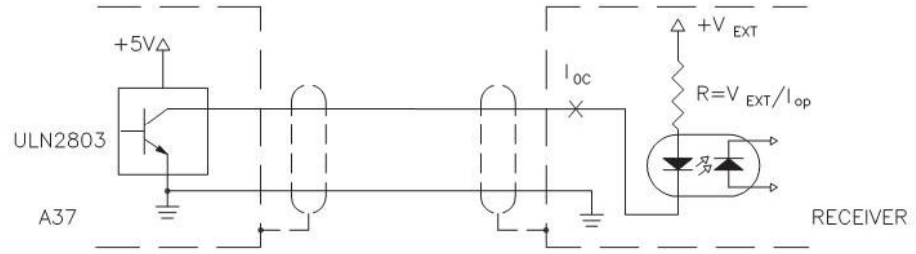

SSI (RS485):

V=+5V

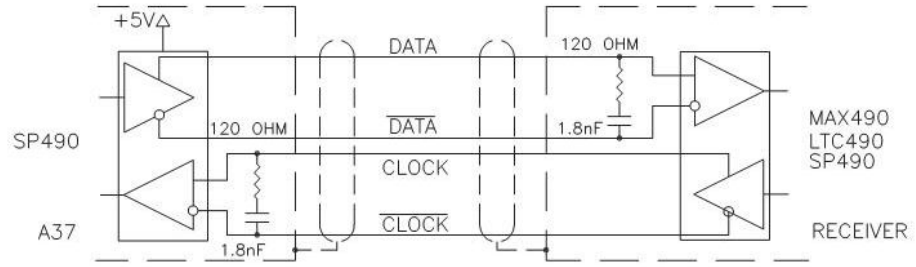

Gurley Precision Instruments
514 Fulton Street
Troy, NY 12180 U.S.A.
(800) 759-1844, (518) 272-6300, fax (518) 274-0336,
Online at www.gurley.com, e-mail: info@gurley.com

ORDERING INFORMATION

A37 Ordering Combinations

RES	OF	OC	OD	VOLT	CONN
12	S	B, G	RS	5	P, S
	P	B, G	TT, OC	5	P, T
	N	G	TT, OC	5	P, Q, R
	M	B, G	TT, OC	5	P, Q, R

MODEL	SHAFT	RES	OF	OC	OD	VOLT	TEMP	BASE	EXIT	CAB	CONN	SHAFT	SPEC
☐	☐	☐	☐	☐	☐	☐	☐	☐	☐	☐	☐	☐	☐

MODEL
A37

SHAFT - Shaft type
S Solid shaft
B Blind Hollow Shaft

RES – Resolution
12 12Bit resolution

OF – Output Format
S SSI
P Parallel, Output Enable
N Paralled, no Output Enable
M Multiplexed Output Enable

OC – Output Code
B Binary
G Gray code

OD – Output Device
TT TTL (74HCT367, 74ABT541)
OC Open Collector (ULN 2803)
RS RS Differential (SP 490)

VOLT – Voltage
05 5VDC Power Supply

TEMP – Temperature Range
S Standard (0 - 70 C)

BASE
A Combination Synchro flange/face mount base
B Blind hollow shaft with external tether

EXIT – Cable Exit
S Side exit cable
T Top exit cable

CAB – Cable length, inches
39 Standard (1M)
XX 02" – 99"

CONN – Conector
P Pigtail
Q DA-15P
R DE-15P
S DE-9P
T DA-26P

SHAFT
03M 3 mm
04M 4 mm
05M 5 mm ("S" shaft only)
02E 1/8 inch
04E ¼ inch

SPEC – Special features
N No Special Features

SPECIAL CAPABILITIES

For special situations, we can optimize catalog encoders to provide higher frequency response, greater accuracy, wider temperature range, reduced torque, non-standard line counts, or other modified parameters. In addition, we regularly design and manufacture custom encoders for user-specific requirements. These range from high-volume, low-cost, limited-performance commercial applications to encoders for military, aerospace and similar high-performance, high-reliability conditions. We would welcome the opportunity to help you with your encoder needs.

WARRANTY

Gurley Precision Instruments offers a limited warranty against defects in material and workmanship for a period of one year from the date of shipment.

Gurley Precision Instruments
514 Fulton Street
Troy, NY 12180 U.S.A.
(800) 759-1844, (518) 272-6300, fax (518) 274-0336,
Online at www.gurley.com, e-mail: info@gurley.com

D.7 Harmonic Drive

CSF Rating Table

Table 1

Size	Ratio	Rated Torque at 2000 T_r rpm Nm	Rated Torque at 2000 T_r rpm in-lb	Limit for Repeated Peak Torque Nm	Limit for Repeated Peak Torque in-lb	Limit for Average Torque Nm	Limit for Average Torque in-lb	Limit for Momentary Peak Torque Nm	Limit for Momentary Peak Torque in-lb	Maximum Input Speed rpm Oil	Maximum Input Speed rpm Grease	Limit for Average Input Speed rpm Oil	Limit for Average Input Speed rpm Grease	Moment of Inertia $x10^{-4}kg \cdot m^2$	Moment of Inertia $x10^{-5}kgf \cdot m \cdot s^2$
8	30	0.9	8	1.8	16	1.4-	12	3.3	29	14000	8500	6500	3500	0.003	0.0031
	50	1.8	16	3.3	29	2.3-	20	6.6	58						
	100	2.4	18	4.8	42	3.3-	29	9.0	80						
11	30	2.2	19	4.5	40	3.4-	30	8.5	75	14000	8500	6500	3500	0.012	0.012
	50	3.5	31	8.3	73	5.5-	49	17	150						
	100	5.0	44	11	97	8.9-	79	25	221						
14	30	4.0	35	9.0	80	6.8	60	17	150	14000	8500	6500	3500	0.033	0.034
	50	5.4	48	18	159	6.9	61	35	310						
	80	7.8	69	23	204	11	97	47	416						
	100	7.8	69	28	248	11	97	54	478						
17	30	8.8	78	16	142	12	106	30	266	10000	7300	6500	3500	0.079	0.081
	50	16	142	34	301	26	230	70	620						
	80	22	195	43	381	27	239	87	770						
	100	24	212	54	478	39	345	108	956						
	120	24	212	54	478	39	345	86	761						
20	30	15	133	27	239	20	177	50	443	10000	6500	6500	3500	0.193	0.197
	50	25	221	56	496	34	301	98	867						
	80	34	301	74	655	47	411	127	1124						
	100	40	354	82	726	49	434	147	1301						
	120	40	354	87	770	49	434	147	1301						
	160	40	354	92	814	49	434	147	1301						
25	30	27	239	50	443	38	336	95	841	7500	5600	5600	3500	0.413	0.421
	50	39	345	98	868	55	487	186	1646						
	80	63	558	137	1212	87	770	255	2257						
	100	67	593	157	1389	108	956	284	2513						
	120	67	593	167	1478	108	956	304	2690						
	160	67	593	176	1558	108	956	314	2779						
32	30	54	478	100	885	75	664	200	1770	7000	4800	4600	3500	1.69	1.72
	50	76	673	216	1912	108	956	382	3381						
	80	118	1044	304	2690	167	1478	568	5027						
	100	137	1212	333	2947	216	1912	647	5726						
	120	137	1212	353	3124	216	1912	686	6071						
	160	137	1212	372	3292	216	1912	686	6071						
40	50	137	1212	402	3558	196	1735	686	6071	5600	4000	3600	3000	4.50	4.59
	80	206	1823	519	4593	284	2513	980	8673						
	100	265	2345	568	5027	372	3292	1080	9558						
	120	294	2602	617	5460	451	3991	1180	10443						
	160	294	2602	647	5726	451	3991	1180	10443						
45	50	176	1558	500	4425	265	2345	950	8408	5000	3800	3300	3000	8.68	8.86
	80	313	2770	706	6248	390	3452	1270	11240						
	100	353	3124	755	6682	500	4425	1570	13895						
	120	402	3558	823	7284	620	5487	1760	15576						
	160	402	3558	882	7806	630	5576	1910	16904						
50	50	245	2168	715	6328	350	3098	1430	12656	4500	3500	3000	2500	12.5	12.8
	80	372	3292	941	8328	519	4593	1860	16461						
	100	470	4160	980	8673	666	5894	2060	18231						
	120	529	4682	1080	9558	813	7195	2060	18231						
	160	529	4682	1180	10443	843	7461	2450	21683						
58	50	353	3124	1020	9027	520	4602	1960	17346	4000	3000	2700	2200	27.3	27.9
	80	549	4859	1480	13098	770	6815	2450	21683						
	100	696	6160	1590	14072	1060	9381	3180	28143						
	120	745	6593	1720	15222	1190	10532	3330	29471						
	160	745	6593	1840	16284	1210	10709	3430	30356						

Table 2

Size	Ratio	Rated Torque at 2000 T_r rpm		Limit for Repeated Peak Torque		Limit for Average Torque		Limit for Momentary Peak Torque		Maximum Input Speed rpm		Limit for Average Input Speed rpm		Moment of Inertia	
		Nm	in-lb	Nm	in-lb	Nm	in-lb	Nm	in-lb	Oil	Grease	Oil	Grease	$\times 10^{-4}$kg·m^2	$\times 10^{-5}$kgf·m·s^2
65	50	490	4337	1420	12567	720	6372	2830	25046	3500	2800	2400	1900	46.8	47.8
	80	745	6593	2110	187	1040	9204	3720	32922						
	100	951	8416	2300	20355	1520	13452	4750	42038						
	120	951	8416	2510	22214	1570	13895	4750	42038						
	160	951	8416	2630	23276	1570	13895	4750	42038						
80	50	872	7717	2440	21594	1260	11151	4870	43100	2900	2300	2200	1500	122	124
	80	1320	11682	3430	30356	1830	16196	6590	58322						
	100	1700	15045	4220	37347	2360	20886	7910	70004						
	120	1990	17612	4590	40622	3130	27701	7910	70004						
	160	1990	17612	4910	43454	3130	27701	7910	70004						
90	50	1180	10443	3530	31241	1720	15222	6660	58941	2700	2000	2100	1300	214	218
	80	1550	13718	3990	35312	2510	22214	7250	64163						
	100	2270	20090	5680	50268	3360	29736	9020	79827						
	120	2570	22745	6160	54516	4300	38055	9800	86730						
	160	2700	23895	6840	60534	4300	38055	11300	100005						
100	50	1580	13983	4450	39383	2280	20178	8900	78765	2500	1800	2000	1200	356	363
	80	2380	21063	6060	53631	3310	29294	11600	102660						
	100	2940	26019	7350	65048	4630	40976	14100	124785						
	120	3180	28143	7960	70446	5720	50622	15300	135405						
	160	3550	31418	9180	81243	5720	50622	15500	137175						

CSG Rating Table

Table 3

Size	Ratio	Rated Torque at 2000 Tr rpm		Limit for Repeated Peak Torque		Limit for Average Torque		Limit for Momentary Peak Torque		Maximum Input Speed rpm		Limit for Average Input Speed rpm		Moment of Inertia	
		Nm	in-lb	Nm	in-lb	Nm	in-lb	Nm	in-lb	Oil	Grease	Oil	Grease	$\times 10^{-4}$kg·m^2	$\times 10^{-5}$kgf·m·s^2
14	50	7.0	62	23	204	9	80	46	407	14000	8500	6500	3500	0.033	0.0034
	80	10	89	30	266	14	124	61	540						
	100	10	89	36	319	14	124	70	620						
17	50	21	186	44	390	34	301	91	805	10000	7300	6500	3500	0.079	0.081
	80	29	257	56	496	35	310	113	1000						
	100	31	274	70	620	51	451	143	1266						
	120	31	274	70	620	51	451	112	991						
20	50	33	292	73	646	44	389	127	1124	10000	6500	6500	3500	0.193	0.197
	80	44	389	96	850	61	540	165	1460						
	100	52	460	107	947	64	566	191	1690						
	120	52	460	113	1000	64	566	191	1690						
	160	52	460	120	1062	64	566	191	1690						
25	50	51	451	127	1124	72	637	242	2142	7500	5600	5600	3500	0.413	0.421
	80	82	726	178	1575	113	1000	332	2938						
	100	87	770	204	1805	140	1239	369	3266						
	120	87	770	217	1920	140	1239	395	3496						
	160	87	770	229	2027	140	1239	408	3611						
32	50	99	876	281	2487	140	1239	497	4399	7000	4800	4600	3500	1.69	1.72
	80	153	1354	395	3496	217	1920	738	6531						
	100	178	1575	433	3832	281	2487	841	7443						
	120	178	1575	459	4062	281	2487	892	7894						
	160	178	1575	484	4283	281	2487	892	7894						
40	50	178	1575	523	4629	255	2257	892	7894	5600	4000	3600	5000	4.50	4.59
	80	268	2372	675	5974	369	3266	1270	11240						
	100	345	3053	738	6531	484	4283	1400	12390						
	120	382	3381	802	7098	586	5186	1530	13541						
	160	382	3381	841	7443	586	5186	1530	13541						

Figure 9

Efficiency Compensation Coefficient

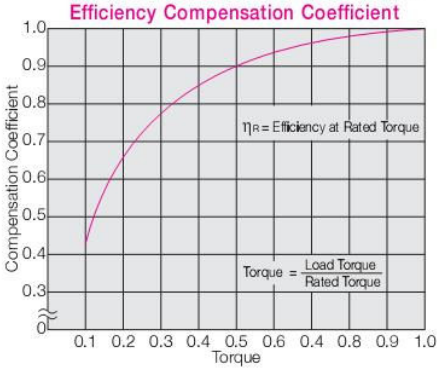

COMPONENT SET 17~100

Harmonic drive grease SK-1A, SK-2

Ratio 30

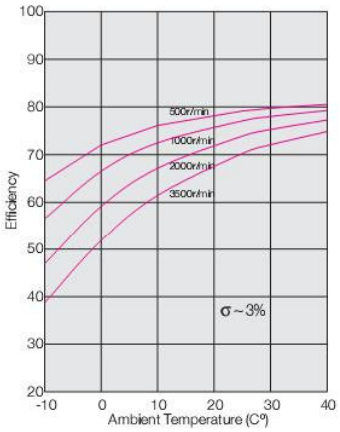

Ratio 50

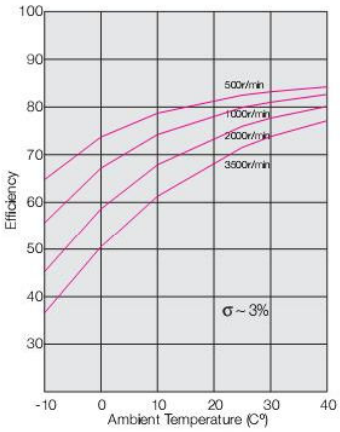

Ratio 80, 100

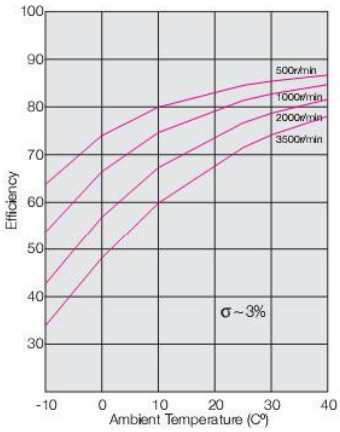

Ratio 120

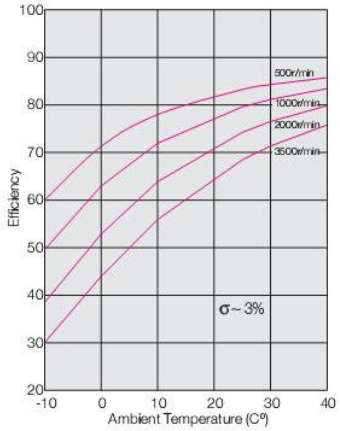

Ratio 160

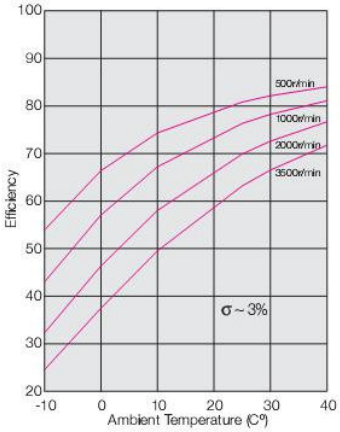

Starting Torque

Starting torque is the torque required to commence rotation of the input element (high speed side), with no load being applied to the output. The table below indicates the maximum values. The lower values are approximately 1/2 to 1/3 of the maximum values.

Component Type Backdriving Torque

Backdriving torque is the torque required to commence rotation of input element (high speed side) when torque is applied on the output side (low speed side). The table below indicates the maximum values. The typical values are approximately 1/2 to 1/3 of the maximum values. The backdriving torque should not be relied upon to provide a holding torque to prevent the output from backdriving. A failsafe brake should be used for this purpose.

Measurement condition: Ambient temperature 20ºC

Values shown below vary depending on condition. Please use values as a reference.

Starting Torque for Component Sets (Ncm) Table 36

Size		8	11	14	17	20	25	32	40	45	50	58	65	80	90	100
30	CSF	1.3	2.7	4.3	6.5	11	19	45	-	-	-	-	-	-	-	-
	CSG	-	-	4.7	7.2	12	21	50	-	-	-	-	-	-	-	-
50	CSF	0.8	1.6	3.3	5.1	6.6	12	26	46	63	86	130	180	320	450	590
	CSG	-	-	3.6	5.6	7.3	13	29	51	-	-	-	-	-	-	-
80	CSF	-	-	2.4	3.3	4.1	7.7	16	29	41	54	82	110	200	280	380
	CSG	-	-	2.6	3.6	4.5	8.5	18	32	-	-	-	-	-	-	-
100	CSF	0.59	1.1	2.1	2.9	3.7	6.9	15	26	36	48	73	98	180	250	340
	CSG	-	-	2.3	3.2	4.1	7.6	17	29	-	-	-	-	-	-	-
120	CSF	-	-	-	2.7	3.3	6.3	13	24	33	45	67	92	170	230	310
	CSG	-	-	-	3.0	3.6	6.9	14	26	-	-	-	-	-	-	-
160	CSF	-	-	-	-	2.9	5.5	12	21	29	39	58	80	140	200	270
	CSG	-	-	-	-	3.2	6.1	13	23	-	-	-	-	-	-	-

Back Driving Torque for Component Sets (Nm) Table 37

Size		8	11	14	17	20	25	32	40	45	50	58	65	80	90	100
30	CSF	0.65	1.3	2	3.2	5.5	10	21	-	-	-	-	-	-	-	-
	CSG	-	-	2.2	3.5	6.1	11	23	-	-	-	-	-	-	-	-
50	CSF	0.5	1	1.4	2.5	4	7.5	16	28	37	52	80	110	200	270	360
	CSG	-	-	1.5	2.8	4.4	8.3	18	31	-	-	-	-	-	-	-
80	CSF	-	-	1.4	2.5	4.2	7.7	16	28	39	53	81	120	200	270	370
	CSG	-	-	1.5	2.8	4.6	8.5	18	31	-	-	-	-	-	-	-
100	CSF	0.7	1.4	1.7	2.8	4.5	8.4	18	31	42	57	88	130	220	300	400
	CSG	-	-	1.9	3.1	5.0	9.2	20	34	-	-	-	-	-	-	-
120	CSF	-	-	-	3.1	4.9	9.2	19	34	47	63	97	140	240	330	440
	CSG		-	-	3.4	5.4	10	21	37	-	-	-	-	-	-	-
160	CSF	-	-	-	-	5.8	11	23	40	57	77	120	170	290	390	540
	CSG	-	-	-	-	6.4	12	25	44	-	-	-	-	-	-	-

Starting Torque for Housed Units (Ncm) Table 38

Size		14	17	20	25	32	40	45	50	58	65
30	CSF	6.4	9.3	15	25	54	-	-	-	-	-
	CSG	7.0	10	17	28	59	-	-	-	-	-
50	CSF	4.1	6.1	7.8	15	31	55	77	110	160	220
	CSG	4.5	6.7	8.6	17	34	61	-	-	-	-
80	CSF	2.8	4	4.9	9.2	19	35	49	66	98	140
	CSG	3.1	4.4	5.4	10	21	39	-	-	-	-
100	CSF	2.5	3.4	4.3	8	18	31	43	58	88	120
	CSG	2.8	3.7	4.7	8.8	20	34	-	-	-	
120	CSF	-	3.1	3.8	7.3	15	28	39	52	80	110
	CSG	-	3.4	4.2	8.0	17	31	-	-		
160	CSF	-	-	3.3	6.3	14	24	33	45	68	93
	CSG	-	-	3.6	6.9	15	26	-	-	-	-

Back driving Torque for Housed Units (Nm) Table 39

Size		14	17	20	25	32	40	45	50	58	65
30	CSF	2.4	3.8	6.2	11	23	-	-	-	-	-
	CSG	2.6	4.2	6.8	12	25	-	-	-	-	-
50	CSF	1.6	3	4.7	9	18	33	47	62	95	130
	CSG	1.8	3.3	5.2	9.9	20	36	-	-	-	-
80	CSF	1.6	3	4.8	9.1	19	33	48	63	96	140
	CSG	1.8	3.3	5.3	10	21	36	-	-	-	-
100	CSF	1.8	3.3	5.1	9.8	20	36	51	68	110	150
	CSG	2	3.6	5.6	11	22	40	-	-	-	-
120	CSF	-	3.5	5.5	11	22	39	55	73	110	160
	CSG	-	3.9	6.1	12	24	43	-	-	-	-
160	CSF	-	-	6.4	13	26	46	64	85	130	180
	CSG	-	-	7	14	29	51	-	-	-	-

CSD Rating Table

Table 1

CSD Size	Gear Ratio R	Rated Torque at 2000 T, rpm Nm	Rated Torque at 2000 T, rpm in-lb	Limit for Repeated Peak Torque Nm	Limit for Repeated Peak Torque in-lb	Limit for Average Torque Nm	Limit for Average Torque in-lb	Limit for Momentary Peak Torque Nm	Limit for Momentary Peak Torque in-lb	Maximum Input Speed rpm Oil	Maximum Input Speed rpm Grease	Limit for Average Input Speed rpm Oil	Limit for Average Input Speed rpm Grease	Moment of Inertia I $x10^{-4}kg\cdot m^2$	Moment of Inertia J $x10^{-4}kgf\cdot m\cdot s^2$
14	50	3.7	33	12	106	4.8	42	24	212	14000	8500	6500	3500	0.021	0.021
	100	5.4	48	19	168	7.7	68	31	274						
17	50	11	97	23	204	18	159	48	425	10000	7300	6500	3500	0.054	0.055
	100	16	142	37	327	27	239	55	487						
20	50	17	150	39	345	24	212	69	611	10000	6500	6500	3500	0.090	0.092
	100	28	248	57	504	34	301	76* (65)	673* (575)						
	160	28	248	64	566	34	301	76* (65)	673* (575)						
25	50	27	239	69	611	38	336	127 (135)	1124 (1195)	7500	5600	5600	3500	0.282	0.288
	100	47	416	110	974	75	664	152* (135)	1345* (1195)						
	160	47	416	123	1089	75	664	152*	1345*						
32	50	53	469	151	1336	75	664	268 (331)	2372 (2929)	7000	4800	4600	3500	1.09	1.11
	100	96	850	233	2062	151	1336	359* (331)	3177* (2929)						
	160	96	850	261	2310	151	1336	359*	3177*						
40	50	96	850	281	2487	137	1212	480 (580)	4248 (5133)	5600	4000	3600	3000	2.85	2.91
	100	185	1637	398	3522	260	2301	694* (580)	6142* (5133)						
	160	206	1823	453	4009	316	2797	694*	6142*						
50	50	172	1522	500	4425	247	2186	1000 (1315)	8850 (11638)	4500	3500	3000	2500	8.61	8.78
	100	329	2912	686	6071	466	4124	1440 (1315)	12744 (11638)						
	160	370	3275	823	7284	590	5222	1577*	13956*						

Note: The moment of inertia : $I=1/4GD^2$, measured at the input

The momentary peak torque is limited by tightening torque on the flexspline.

The values in parenthesis are values in the case of the Big Bore option on the flexspline.

Efficiency

The efficiency depends on the conditions shown below. Efficiency depends on gear ratio, input speed, load torque, temperature, quantity of lubricant and type of lubricant.

Measurement Condition for Efficiency Graphs

Installation: Based on recommended tolerance
Load Torque: Rated Torque
Lubricant: Harmonic grease SK-1A (size 20 and up)
Harmonic grease SK-2 (size 14, 17)
Harmonic grease 4B No.2 (SHD Output Bearing)

Grease quantity: Recommended quantity

Please contact us for details pertaining to recommended oil lubricant for CSD.

CSD Series

Ratio 50

Size 14

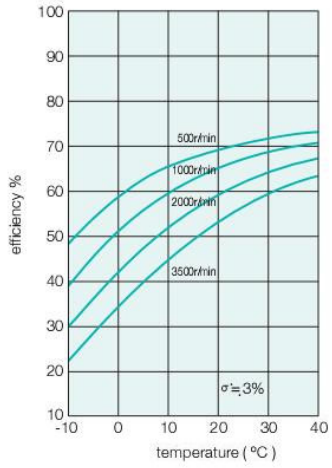

Size 17, 20

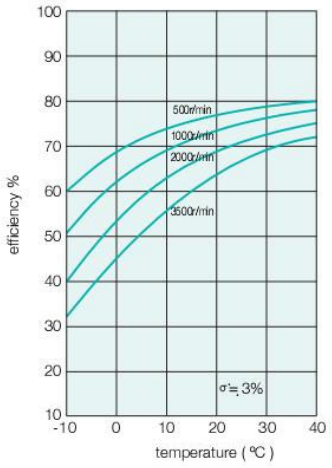

Size 25, 32, 40, 50

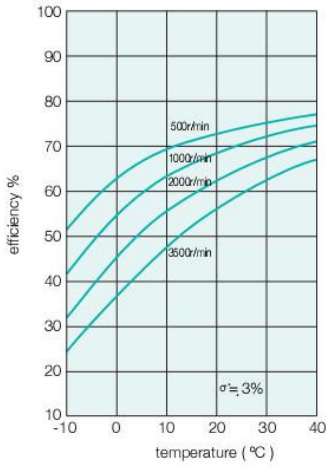

Ratio 100

Size 14

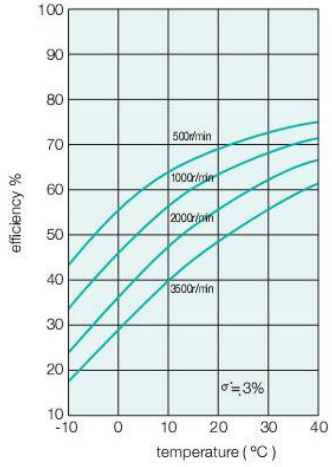

Size 17, 20, 25, 32, 40, 50

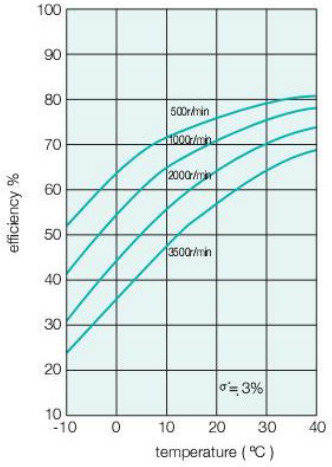

Ratio 160

Size 20, 25, 32, 40, 50

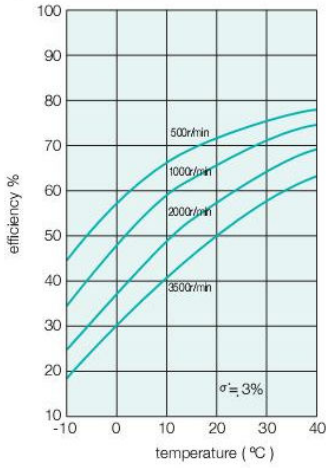

Efficiency (@ Torque ≠ Rated Torque) = Efficiency (from graph) x Compensation Coefficient (from graph page 36)

Starting Torque and Backdriving Torque

Starting Torque

Starting torque is the torque required to commence rotation of the input element (high speed side), with no load being applied to the output. The table below indicates the maximum values. The lower values are approximately 1/2 to 1/3 of the maximum values.

Component Type Backdriving Torque

Backdriving torque is the torque required to commence rotation of input element (high speed side) when torque is applied on the output side (low speed side). The table below indicates the maximum values. The typical values are approximately 1/2 to 1/3 of the maximum values. The backdriving torque should not be relied upon to provide a holding torque to prevent the output from backdriving. A failsafe brake should be used for this purpose.

Measurement condition: Ambient temperature 20ºC

Values shown below vary depending on condition.
Please use values as a reference.

Starting Torque for Component Sets (Ncm) Table 25

Ratio	Size	14	17	20	25	32	40	50
50	CSD	3.7	5.7	7.3	14	28	50	94
	SHD	6.2	19	25	39	60	95	-
100	CSD	2.4	3.3	4.3	7.9	18	29	56
	SHD	4.8	17	22	34	50	78	-
160	CSD	-	-	3.4	6.4	14	24	44
	SHD	-	-	22	33	47	74	-

Backdriving Torque for Component Sets (Nm) Table 26

Ratio	Size	14	17	20	25	32	40	50
50	CSD	2.5	3.8	4.4	8.3	17	30	57
	SHD	3.7	11	15	24	36	57	-
100	CSD	3.1	4.1	5.2	9.6	21	35	67
	SHD	5.8	21	27	41	60	94	-
160	CSD	-	-	6.6	12	28	45	85
	SHD	-	-	42	64	91	143	-

Bibliography

[1] L. Aksman, "Force Estimation Based Compliance Control of a Two Link Harmonically Driven Robotic Manipulator," Master's Thesis, University of Maryland, Dec. 2006.

[2] *Anthropometric Source Book Volume II: A Handbook of Anthropometric Data*, NASA reference publication 1024, Yellow Springs, Ohio: Webb Associates, 1978

[3] M. Bergamasco, B. Allotta, L. Bosio, L. Ferretti, G. Parrini, G. Prisco, F. Salsedo, and G. Sartini, "An arm exoskeleton system for teleoperation and virtual environments applications," in *Proc. of the IEEE Intl. Conf. on Robotics and Automation*, San Diego, 1994, pp. 1449–1454.

[4] M. Bergamasco, G.M. Prisco, "Virtual Surfaces Contour Following: An Experimental Approach Exploiting an Arm Exoskeleton as Haptic Interface," in *Proc. of the ASME Dymanic Systems and Control Division*, vol.57-2, 1995, pp.681-687.

[5] M.A. Buckley, G.R. Johnson, "Computer simulation of the dynamics of human arm and orthosis linkage mechanism," in *Proc. Inst. Mech. Engrs.* Part H, vol. 211, 1997, pp.349-357.

[6] G.C. Burdea, *Force And Touch Feedback For Virtual Reality*. New York: John Wiley and Sons, 1996.

[7] D.G. Caldwell, C. Favede, and N. Tsagarakis, "Dextrous exploration of a virtual world for improved prototyping," in *Proc. of the IEEE Intl. Conf. on Robotics and Automation*, Leuven, Belgium, May 1998, pp.298–303.

[8] D.G. Caldwell, N. Tsagarakis, D. Badihi, G.A. Medrano-Cerda, "Pneumatic Muscle Actuator Technology: a light weight power system for a Humanoid Robot," in *Proc. of the IEEE Int. Conf. on Robotics & Automation*, Leuven, Belgium, May 1998, pp.3053-3058.

[9] N. Chernov, C. Lesort, "Fitting circles and lines by least squares: theory and experiment," preprint, available at http://www.math.uab.edu/cl/cl1

[10] W. Chou, T. Wang, J. Xiao, "Haptic interaction with virtual environment using an arm type exoskeleton device," in *Proc. of the IEEE Intl. Conf. on Robotics and Automation*, New Orleans, USA, Apr. 2004, pp.1992–1997.

[11] H.P.V. Cottande, Robert G. Kinkade, *Human Engineering Guide to Equipment Design*, rev. ed. New York: McGraw-Hill, 1963.

[12] J.J. Craig, *Introduction to Robotics Mechanics and Control*, 3rd ed. Upper Saddle River, NJ: Prentice Hall, 2005.

[13] A. Frisoli, F. Rocchi, S. Marcheschi, A. Dettori, F.Salsedo, and M. Bergamasco, "A new force-feedback arm exoskeleton for haptic interaction in virtual environments," in *Proc. of the First Joint Euro-haptics Conference and Symposium on Haptic Interfaces for Virtual Environment and Teleoperator Systems*, 2005.

[14] J. He, E. Koeneman, H. Huang, D. Herring, T. Sugar, R. Herman, and J. Koeneman, "Design of a robotic upper extremity repetitive therapy device," in *Proc. Int. Conf. on Rehabilitation Robotics (ICORR)*, Chicago, 2005.

[15] *Human Factors Design Standard: For Acquisition of Commercial-Off-The-Shelf Subsystems, Non-Developmental Items, and Developmental Systems*, FAA Technical Center, Atlantic City International Airport, NJ, 1996.

[16] S.C. Jacobsen, F.M. Smith, and D.K. Backman, "High performance, dextrous telerobotic manipulator with force reflection," in *Intervention/ROV '91 Conference and Exposition*. Hollywood, Florida: Marine Technology Society, May 1991, pp.213–218.

[17] S.C. Jacobsen, F.M. Smith, D.K. Backman, and E.K. Iverson, "High performance, high dexterity, force reflective teleoperator II," In *ANS Topical Meeting on Robotics and Remote Systems*, Albuquerque, N.M. 1991, pp.393-402.

[18] G.R. Johnson, D.A. Carus, G. Parrini, S.S. Marchese, and R. Valeggi, "The design of a five-degree-of-freedom powered orthosis for the upper limb," in *Proc. Instn. Mech. Engrs.* Part H, vol. 215, 2001, pp.275–284.

[19] S. Marcheschi, "Progettazione e realizzazione di un sistema di controllo per uninterfaccia aptica a 7 gradi di libert," Master's thesis, Universita Degli Studi Di Pisa, Apr. 2001.

[20] T.B. Moeslund, C.B. Madsen, and E. Granum, "Modelling the 3d pose of a human arm and the shoulder complex utilizing only two parameters," in *Proc. of the Intl. Conference on Model-based Imaging, Rendering, Image Analysis and Graphical Special Effects*, INRIA Rocquencourt, France, 2003.

[21] A. Nakai, Y. Kunii, H. Hashimoto, F. Harashima, "Arm Type Haptic Human Interface: Sensor Arm", in the *7th Int. Conf. on Artificial Reality and Tele-existence*, University of Tokyo, Tokyo, Japan, 1997, pp.77-84.

[22] A. Nakai, T. Ohashi, and H. Hashimoto, "7 dof arm type haptic interface for teleoperation and virtual reality systems," in *Proc.of the IEEE/RSJ Intl. Conf. on Intelligent Robots and Systems*, Victoria, B.C., Canada, Oct. 1998, pp.1266–1271.

[23] E. Oberg, F.D. Jones, H.L. Horton, H.H. Ryffel, *Machinery's Handbook*, 26th ed. New York: Industrial Press Inc., 2000

[24] K. Ogata, *Descrete-Time Control Systems*, Englewood Cliffs, NJ: Prentice Hall, 1987.

[25] L. Peterson, P. Renstrom, *Sports Injuries – Their Prevention and Treatment*, 3rd ed. Champaign, IL: Human Kinetics, 2001

[26] S. Plagenhoef, F.G. Evans, T. Abdelnour, "Anatomical data for analyzing human motion," in *Research Quarterly for Exercise and Sport*, 1983, 54(2), pp.169-178.

[27] D.W. Repperger, S.J. Remis, and G. Merrill, "Performance measures of teleoperation using an exoskeleton device," in *Proc. of the IEEE Intl. Conf. on Robotics and Automation*, Cincinnati, May 1990, pp.552–557.

[28] D.P. Romilly, C. Anglin, R.G. Gosine, C. Hershler, S.U. Raschke, "A Functional Task Analysis and Motion Simulation for the Development of a Powered Upper-Limb Orthosis," in *Transactions on Rehabilitation Engineering*, vol. 2, no. 3, 1994, pp.119-129.

[29] J. Rosen, B. Hannaford, and S. Burns, "Neural control of an upper limb powered exoskeleton system – grant report," in *Proc. of the First NSF Robotics and Computer Vision (RCV) Workshop*, Los Vegas, Oct. 2003.

[30] A. Schiele and G. Visentin, "The ESA human arm exoskeleton for space robotics telepresence," in *Proc. 7th Int. Symposium on Artificial Intelligence, Robotics and Automation in Space (iSAIRAS)*, Nara, Japan, 2006.

[31] N. Tsagarakis, D.G. Caldwell, and G.A. Medrano-Cerda, "A 7 dof pneumatic muscle actuator (pma) powered exoskeleton," in *Proc. of the IEEE Intl. Workshop on Robot and Human Interaction*, Pisa, Italy, Sep. 1999, pp.327–333.

[32] R.L. Williams, M.A. Murphy, D. North, J. Berlin, and M. Krier, "Kinesthetic force/moment feedback via active exoskeleton," in *Proc. of the Image Society Conference*, Scottsdale, Arizona, 1998.